Final Report

Adaptive Regional Airliner

Group 23

TU Delft

Final Report

Adaptive Regional Airliner

by

Group 23

Anique Altena	4554345
Sybren Bootsma	4535154
Rik Bouwmeester	4445996
Lisa Kestens	4548248
Ahmad Mahmoud	4562658
Niels Maseland	4540832
Coen Minderhoud	4545338
Stijn van Selling	4561619
Daan Snijders	4484150
Chee Wai Thong	4471520

Supervised by:
Dr.ir. W.J.C. Verhagen
S. Luesutthiviboon, PhD candidate
B.R. Cheneka, PhD candidate

in partial fulfillment of the requirements for the degree of

Bachelor of Science
in Aerospace Engineering
AE3200 Design Synthesis Exercise

at the Delft University of Technology
July 2, 2019

TU Delft Delft University of Technology

Contents

Nomenclature

α	Absorption coefficient	$[dB/m]$
α	Angle of attack	$[^\circ]$
α	Model parameter	$[-]$
β	Prandtl-Glauert compressibility correction factor	$[-]$
ΔP	Pressure difference	$[Pa]$
$\Delta(LC)$	Increment in life cycle cost	[$]
δ_f	Flap deflection	$[^\circ]$
$\dot{M}_{fuel}$	Fuel flow	$[kg/s]$
ϵ_t	Wingtwist angle	$[rad]$
η_s	Shock absorber efficiency	$[-]$
η_t	Tire absorption efficiency	$[-]$
$\frac{C_{D_L}}{C_L^2}$	Induced drag parameter	$[-]$
$\frac{t}{c}$	Thickness over chord ratio	$[-]$
γ	Climb angle	$[rad]$
λ	Taper ratio	$[-]$
$\Lambda_{c/2}$	Sweep angle half chord	$[rad]$
$\Lambda_{c/4}$	Sweep angle quarter chord	$[rad]$
Λ_{LE}	Sweep angle leading edge	$[rad]$
μ	Friction coefficient	$[-]$
ν	Poisson's ratio	$[-]$
ϕ	Azimuthal directivity angle	$[^\circ]$
π_{oo}	Pressure ratio	$[-]$
σ	Stress	$[Pa]$
θ	Polar directivity angle	$[^\circ]$
A	Area	$[m^2]$
A	Aspect ratio	$[-]$
ab	Age based replacement	$[-]$
b	Span	$[m]$
b_m	Distance between the c.g. and main landing gear	$[m]$
b_n	Distance between the c.g. and nose landing gear	$[m]$
c	Airfoil chord length	$[m]$
c'	Flapped airfoil chord length	$[m]$
C_c	Cost of corrective repair	[€]
C_i	Cost of inspection	[€]
c_j	Specific fuel consumption	$[kg/Ns]$
C_p	Cost of preventive repair	[€]
C_{ail}	Chord length of aileron	$[m]$
$C_{D_{0_w}}$	Zero lift drag coefficient of the wing	$[-]$
C_{D_L}	Lift induced drag coefficient	$[-]$
C_{elev}	Chord length of elevator	$[m]$
C_{f_w}	Turbulent flat plate friction coefficient	$[-]$
C_{L_α}	Derivative lift coefficient aircraft	$[-]$
$C_{L_{\alpha_c}}$	Derivative lift coefficient canard	$[-]$
$C_{L_{\alpha_h}}$	Derivative lift coefficient horizontal tail	$[-]$
C_{L_α}	Lift curve slope	$[1/rad]$
$C_{L_{A-h}}$	Lift coefficient aircraft minus tail	$[-]$
C_{L_c}	Lift coefficient canard	$[-]$
C_{L_h}	Lift coefficient horizontal tail	$[-]$
$C_{L_{max}}$	Maximum wing lift coefficient	$[-]$
$C_{l_{max}}$	Maximum airfoil lift coefficient	$[-]$
C_L	Lift coefficient	$[-]$
$C_{m_{ac}}$	Moment coefficient around a.c. main wing	$[-]$
C_{rud}	Chord length of rudder	$[m]$
C_{splr}	Chord length of spoiler	$[m]$
$CAROC$	Cash Airplane-Related Operating Costs	[$]
ci	Constant interval replacement	$[-]$
Cr	Root chord	$[m]$
Ct	Tip chord	$[m]$
D	Drag	$[N]$
$d\epsilon/d\alpha$	Downwash gradient	$[-]$
d_f	Fuselage diameter	$[m]$
D_p	Total mass of NO_x	$[g]$
D_{mlg}	Diameter main landing gear wheel	$[m]$
D_{nlg}	Diameter nose landing gear wheel	$[m]$
$de/d\alpha$	Downwash gradient	$[-]$
E	Young's Modulus	$[Pa]$
EI	Emission Index	$[g/kg]$
$EPNL$	Effective Perceived Noise Level	$[EPNdB]$
F	Force	$[N]$
f	Frequency	$[Hz]$
F_m	Force on the main landing gear	$[N]$
F_n	Force on the nose landing gear	$[N]$
F_{engine}	Thrust generated by the engine	$[N]$
F_{oo}	Rated output	$[kN]$
FF	Fuel flow	$[kg/s]$
g	Gravitational constant	$[\frac{m}{s^2}]$
h	Height	$[m]$
H_e	Energy height	$[m]$
I	Area Moment of Inertia	$[m^4]$
i	Angle of incidence	$[^\circ]$
ib	Inspection based replacement	$[-]$
k_1	Model parameter	$[-]$
k_2	Model parameter	$[-]$
L'	Airfoil thickness location parameter	$[-]$
L_c	Lift generated by the canard	$[N]$
l_c	Absolute distance between a.c. wing and canard	$[m]$
l_f	Fuselage length	$[m]$
L_h	Lift generated by the horizontal tail	$[N]$
l_h	Absolute distance between a.c. wing and tail	$[m]$
L_w	Lift generated by the main wing	$[N]$
LTO	Landing and Take-Off Cycle	$[-]$
M	Moments	$[N \cdot m]$
M_{ac}	Moment around the a.c. of the wing	$[Nm]$
$M_{c.g.}$	Moment around the c.g. of the aircraft	$[Nm]$
M_{fuel}	Fuel Mass	$[kg]$
$M_{payload}$	Payload Mass	$[kg]$
MAC	Length mean aerodynamic chord	$[m]$
MLW	Maximum Landing Weight	$[N]$
$MTOW$	Maximum Take-Off Weight	$[N]$
N	Total Noy value	[Noy]

n	Load factor	[−]	SF	Safety factor	[−]
n	Noy value	[Noy]	SL	Sea level	[−]
n_s	Number of main landing gear struts	[−]	SPL	Sound Pressure Level	$[dB]$
N_{pax}	Number of passengers	[−]	T	Thrust	$[N]$
OEM	Operational Empty Mass	$[kg]$	t	Thickness	$[m]$
OEW	Operational Empty Weight	$[N]$	T/W	Thrust loading	[−]
$OSPL$	Overall Sound Pressure Level	$[dB(A)]$	t_p	Time between two preventive repairs	[hours]
$P_{m_{strut}}$	Maximum load on the main strut	$[N]$	TEC	Total expected cost per unit time	[%]
PBL	Pressure Band Level	$[dB(A)]$	TFU	Theoretical First Unit Cost	[$]
pdf	Probability density function	[−]	TOM	Take-off Mass	$[kg]$
PNL	Perceived Noise Level	$[PNdB]$	V	Airspeed on the main wing	$[m/s]$
$Price_{ref}$	Price of reference aircraft	[$]	v, w	Wingtwist correction factors	[−]
R	Leading edge suction parameter	[−]	V_c	Airspeed on the canard	$[m/s]$
r	Radius	$[m]$	V_h	Airspeed on the horizontal tail	$[m/s]$
R_{LS}	Lifting surface correction factor	[−]	W	Weight of the aircraft	$[N]$
R_{wf}	Wing-fuselage interference factor	[−]	W/S	Wing loading	$[N/m^2]$
$Range$	Design Range	$[km]$	w_t	Vertical landing speed	$[ft/s]$
$Range_{ref}$	Range reference aircraft	$[km]$	x_{ac}	X-location a.c. of the main wing	$[m]$
ROC	Rate of climb	$[m/s]$	$x_{c.g.}$	X-location of the c.g.	$[m]$
S	Wing surface area	$[m^2]$	x_c	X-location of the a.c. of the canard	$[m]$
s	Distance	$[m]$	x_h	X-location of the a.c. of the horizontal tail	$[m]$
S_c	Canard area	$[m^2]$	x_{MAC}	X-location mean aerodynamic chord	$[m]$
S_h	Horizontal tail area	$[m^2]$	x_w	X-location of the a.c. of the wing	$[m]$
s_t	Maximum tire deflection	$[inch]$	y_{MAC}	Y-location mean aerodynamic chord	$[m]$
S_{wet}	Wetted surface area	[−]	z_h	Z-location horizontal tail	$[m]$
$Seats$	Passenger Capacity	[−]	$z_{c.g.}$	Z-location of the c.g.	$[m]$
$Seats_{ref}$	Reference Passenger Capacity	[−]	z_{engine}	Z-location of the engine	$[m]$

Executive Overview

Modern aircraft are typically designed for a certain design point, that is defined in terms of passenger capacity and range. This makes these aircraft optimal and very efficient for a particular flight profile, but overdesigned for or incapable of flying other profiles. The goal of this design project is to design a state-of-the-art aircraft, that is able to cover a variety of ranges and passenger capacities. The aim is to have a regional airliner that is able to efficiently fly different flight profiles. This would reduce waste for airlines and enable them to have one aircraft that serves the full functionality of an aircraft family.

Market and requirement analyses

To begin with, a thorough market analysis was performed as well as a requirement analysis, in order to come up with a set of requirements and design points that would guide the rest of the design process. The market analysis looked into more profitable design points, and explored the opportunities in the market. Whereas, the requirement analysis looked into the technical feasibility of the requirements, and formulated new requirements that are essential to the safe and reliable operation of the aircraft. Three design points were chosen, that the aircraft should be able to adapt to. The three configurations are presented below.

- Configuration 1: 90 passengers over a range of 4,000 km (base configuration)
- Configuration 2: 120 passengers over a range of 2,000 km
- Configuration 3: 120 passengers over a range of 4,000 km

Design options

With the requirements defined, it was possible to come up with conceptual ideas, that could fulfil the purpose of the design. During a brainstorm session, a number of straw-man concepts were generated by all team members, and a design option tree was constructed. This helped in the elimination of several concepts that were deemed non-feasible, or not useful in addressing the requirements. All the remaining ideas were reconsidered and elements of each were chosen to form three complete concepts, that would enter the trade-off process.

The first concept is distinguished by having a removable fuselage section that could be used to increase the passenger capacity of the aircraft. In addition to that, a removable canard is fixed to the removable section, to help with the stability and control of the aircraft, along with providing extra lift to support the section. The concept also made use of external fuel pods under the wings to increase fuel capacity, and consequently range.

The second concept relies on having a fixed external fuselage structure, but having a partially transformable interior. This is facilitated by having a large hatch aft of the aircraft, similar to those found in cargo aircraft. Through this hatch, a module is loaded, fitted with the 30 extra seats required whenever needed. The extra space is otherwise filled with cargo or fuel tanks. A belly that could be added under the fuselage was also considered, in order to increase the fuel capacity of the aircraft when required. The concept also used detachable flaps to increase wing surface area when necessary.

The third concept, comprises of a fully changeable fuselage. Where the whole fuselage, excluding the cockpit, slides out from under the high wing, and a different fuselage, with a different passenger seating capacity can be placed instead. The cockpit is connected to the high wing and a T-tail using an external structure. An external fuel tank is also used in this concept, when required, and is placed at the connection of the wing with the fuselage. This concept would also be fitted with detachable wing tips, in order to increase wing surface area, and consequently lift, whenever required.

Trade-off and chosen design

With the concepts set, the team was divided into different groups, each responsible for a different discipline. Each discipline set their own trade-off criteria, based on the set requirements. The criteria were weighted according to their importance for the design goal. To be able to give scores to each of the concepts, each discipline group performed analyses of the chosen concepts, to assess how well they are able to meet the requirements and

fulfil the purpose of the design. Finally, all the scores were compiled into a final trade-off, that can be seen in Table 1.

Table 1: Trade-off table

Criterion / Option	Stability and Control (3)	Operations (5)	Structures (4)	Sustainable Engineering (5)	*Score*
Concept 1	Difficult stability and control (3.05)	Difficult maintainability and conversion (2.12)	Larger MOI for multiple load carrying structure (4.00)	Low noise, good mass efficiency (3.48)	3.13
Concept 2	Good stability and control (4.19)	Good certification and easy conversion (3.65)	High fuel tank mass, permanent modular mass (2.45)	High noise, low fuel consumption , low mass efficiency (2.33)	3.07
Concept 3	Difficult landing gear (3.29)	Easy conversion but high costs (2.55)	Reinforcement at the top part of fuselage (1.91)	High noise, neutral fuel consumption, good mass efficiency (2.56)	2.54

Excellent | Good | Neutral | Deficient | Unacceptable

As the results of the trade-off were close to each other, a sensitivity analysis was performed, and a requirement analysis on how well the concepts are able to meet the requirements, or adjusted to meet them. It was proven that concept 1 was most fit for the purpose of this design project, and for meeting the set requirements. However, it should be noted that this concept scored as deficient in operations. This was due to a more difficult and lengthy conversion method, that did not meet the '8-hour conversion time' requirement, which presented a complication that had to be dealt with in the detailed design phase.

Detailed design

To begin the detailed design phase, an outline was constructed of all the interfaces between the different disciplines, defining the inputs and outputs of each discipline. A complete class-I estimation and a class-II weight estimation were performed as the first steps in sizing the aircraft. The results from the class-I and II estimations, along with historical and statistical data were set to be used as the inputs to the first iterations of all the disciplines. The analyses of each discipline were done separately and then compiled in a main Python file. This was done to be able to manage the interfaces and the iterations were run till the Operational Empty Weight (OEW) changes reached a value of less than 1%. The disciplines analysed throughout this phase were: 'Aerodynamics', 'Stability and Control', 'Performance and Propulsion', 'Structures, Manufacturing and Materials', 'Sustainable Development', 'Operations', and 'Cost'. The analyses done in each of the disciplines are discussed below.

Aerodynamics

To begin the aerodynamic analysis, it was necessary to have an initial sizing of the High-Lift Devices (HLDs) to be used. This was done based on the $\Delta C_{L_{max}}$ calculated in the class-I estimation, and it was decided to use double slotted flaps for the trailing edge, and Kreuger flaps for the leading edge. Then the analysis was performed, based on the Roskam series on aircraft design [83]. Firstly, the lift was estimated for the airfoil, for both flaps up and down cases. This was then extended to the whole wing and finally to the whole aircraft. The drag was calculated using a Class-II method. Two types of drag were calculated for each component, namely zero-lift drag, C_{D_0}, and lift-induced drag, C_{D_L}, and then summed up to find the total drag of the aircraft. The aerodynamic moments were also calculated similarly to the lift. The moments were calculated first for the airfoil and then extended to find the aerodynamic moment of the whole wing.

Stability and control

To begin with the stability and control analysis, a loading diagram had to be constructed, in order to examine the c.g. range that could be experienced during flight. With this, it was possible to begin sizing the horizontal tail. The horizontal tail was sized for configuration 1, by constructing a scissor plot for stick-fixed stability and

control. Using the scissor plot, the wing location was also fixed, at a location that would ensure the minimum horizontal tail surface area. However, rotation during take-off proved to be a more critical case and the horizontal tail was sized accordingly. The vertical tail was sized for the critical case of take-off with one engine inoperative. The canard was placed as forward as possible in the removable section, in order to have a large moment arm, and was also sized using a scissor plot. Furthermore, the moment and force equilibrium were analysed for steady flight and the required loads were calculated for all configurations. Finally, the landing gear location was updated to reflect the changes in c.g., in order to ensure ground equilibrium, and compliance with certain safety angles.

Performance and propulsion

The performance analysis was done in the order of the different flight phases. First, the take-off performance was analysed for both normal conditions, to find the required field length and decision speed, and in the one engine inoperative condition, to find the balanced field length. This was done using the method from Ruijgrok [88]. Next, the climb performance was assessed and the climb phase was optimised for the maximum rate of climb. This was done using energy heights, as the climb phase is always a trade-off between climbing and accelerating. After the cruise phase was analysed, the descent was investigated in the same manner as the climb, and the landing in the same manner as take-off. The landing field length was also analysed for normal conditions, and for an engine failure. From the take-off and landing field lengths, the number of serviceable airports was calculated and is visualised in Figure 1. With all the flight phases analysed, the fuel consumption for each phase was calculated, which is later used in other departments. Finally, the flight envelope was constructed to be able to find the most critical loads to be encountered during flight, which is then used for the structural analysis of the aircraft.

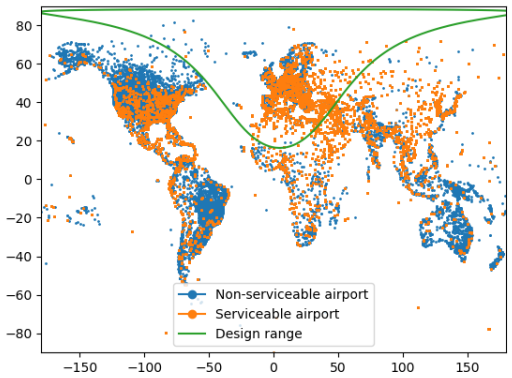

Figure 1: Serviceable airports configuration 3

Structures, manufacturing and materials

Before the structural analysis could be started, the different materials to be used throughout the aircraft had to be determined. Different materials were explored. Metal alloys such as aluminium, steel and titanium alloys were considered, as well as composites such as polymer matrix composites and fibre metal laminate. The materials were selected to be used throughout the structure based on their mechanical properties, costs, manufacturability, and end-of-life characteristics. The choice of materials was done in close cooperation with the sustainability department. The structural analysis was done similarly for the different components analysed. The wing analysis was performed based on the critical load cases, to determine the size, number, and location of stiffening elements in order to prevent buckling. The wing analysis was also similarly applied for the vertical and horizontal tails, as well as the canard. The fuselage analysis was done in a similar manner, and was extended to size the joints responsible for connecting the cut sections to each other. The joints were analysed for three different failure modes. The landing gear's tires, struts, and shock absorbers were also sized to be able to withstand the static and dynamic loads encountered during operation. Finally, the manufacturing process was outlined for different components. It was also decided that the assembly process would be done in an assembly line that utilises different stations, for increase of efficiency of production.

Sustainable development

The sustainability department aims to have an overall sustainable approach towards the design of the aircraft, by employing measures to decrease the environmental footprint of the aircraft throughout its lifetime. To begin with, measures were taken to reduce the noise emissions during approach and take-off. Those included using chevrons and acoustic liners to reduce noise during take-off. By using porous materials, landing gear fairing, and optimising slat settings, airframe noise during approach can be reduced. The airframe noise was analysed using the ANOPP model from NASA. Next, the greenhouse gas emissions were analysed. The NO_x and CO_2 emissions were both found to be directly related to fuel consumption. Hence, electrical taxiing was used to reduce fuel consumption during ground operations. Additionally, multiple measures were used to reduce drag and weight to further reduce fuel consumption and reduce emissions. The NO_x emissions were measured against the CAEP/6 standards, while the CO_2 emissions were compared to other aircraft that would compete with the adaptive regional airliner. Finally, the manufacturing and recycling of the materials used was analysed, and a retirement strategy was developed for the aircraft.

Operations

The main challenge for the operations department was coming up with a new conversion method, since the one analysed in the preliminary design did not meet the conversion time requirement. A new conversion method was established, that relies on using lasers that work in a feedback loop with lifts to align the sections. Automated fasteners that lock in the sections are also installed. This makes the process mostly automated and able to meet the requirement. A Markov chain was also constructed, with all possible failures during conversion, to be able to estimate a probability of the conversion meeting the required time. Next, based on maintenance data, it was possible to analyse the checking and maintenance procedures. Checking of the aircraft is needed each time the conversion has been performed. For maintenance, three different strategies were analysed based on probability data, and it was found that age-based replacement is the most cost effective for the Auxiliary Power Unit (APU) system. For the certification procedure, a new process had to be outlined for the authorities to approve. This included the aircraft getting a type certificate first, followed by a conversion certificate, and finally, a conversion checking certificate. Additionally, the turn around time was also analysed, as well as the probability of completing the turn around in a set amount of time. Finally, the operational concept was outlined as a guideline to airlines using the aircraft, with the transponder of the aircraft being able to communicate with Air traffic control (ATC) to indicate which configuration is approaching the airport.

Cost

Finally, the different costs associated with the life cycle of the aircraft were analysed. This included development cost, manufacturing costs, and operational costs. A learning curve was applied to the manufacturing costs to account for the learning effects experienced during production. Moreover, a new unit cost was proposed, which helped in projecting an estimated market share. This was all used to find an estimate of the Return on Investment (ROI) of the program after 5 years of production.

Risk analysis

The aircraft being designed, is mostly similar to conventional aircraft, and therefore carry all the risks that a normal aircraft would be prone to. However, two risks arise that are specific to the aircraft being designed. The first risks arises at the connection points of the fuselage, where several systems have to go through, and have to be reattached during every conversion. This risk is mitigated by having the systems having one to two redundant systems to prevent catastrophic failure. The second risk arises from the use of Epoxy/HS carbon for the fuselage and lifting surfaces' skins. A problem with Epoxy/HS carbon, is that the detection of the cracks in the structure is more difficult than for aluminium. This risk is alleviated by having regular visual and non-visual inspections.

Final design

Finally, all subsystem calculations were compiled into one interface, and the design was iterated until the Operational Empty Mass (OEM) and Maximum Take-off Mass (MTOM) converged. The variation of the MTOM and OEM with iterations is shown in Figure 2 and Figure 3, respectively.

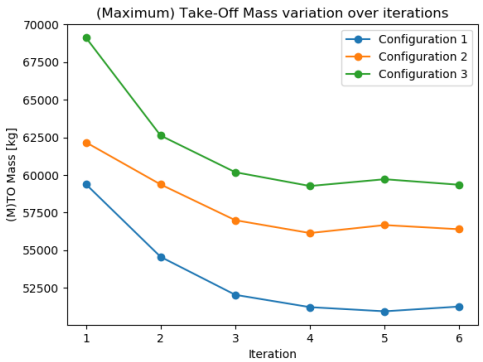

Figure 2: Variation of (M)TOM over the iterations

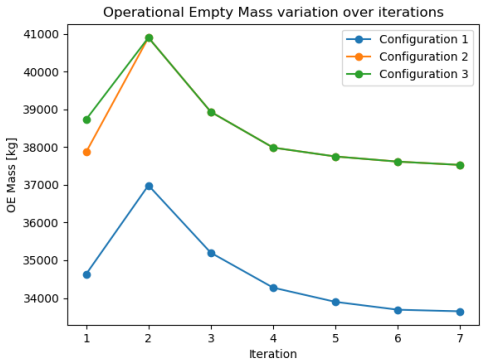

Figure 3: Variation of the OEM over the iterations

The sudden increase in OEM between iterations 1 and 2, could be explained by the fact that the values from the first iteration were from a class-I weight estimation, while the second iteration already used a class-II estimation, which calculated a more accurate and noticeably heavier mass. The final design parameters after iterations were stopped are shown in Table 2.

Table 2: Final design main parameters

	T/W [−]	W/S $[N/m^2]$	OEM $[kg]$	$MTOM$ $[kg]$	S $[m^2]$	S_h $[m^2]$	S_v $[m^2]$	S_c $[m^2]$	X_{lemac} $[m]$	L_{cutout} $[m]$
Config. 1	0.288	4,173	33,649.12	51,213.9	120.5	29	26.5	0	14.1	0
Config. 2	0.2995	4,173	37,526.3	56,301.0	120.5	29	26.5	37.1	19.8	5.7
Config. 3	0.2995	4,173	37,526.3	59,249.3	120.5	29	26.5	37.1	19.8	5.7

From the parameters, it can be noticed that the idea of having a removable canard between configurations 2 and 3 was not desirable, due to the fact that stability and control were the restricting factors when sizing the canard, and the difference between required areas was very small. It was also found that external fuel tanks were not required, as the wing had more than sufficient volume to store all the fuel needed for all configurations. Finally, the internal and external layouts for the longer configurations are shown in Figure 4 and Figure 5, respectively.

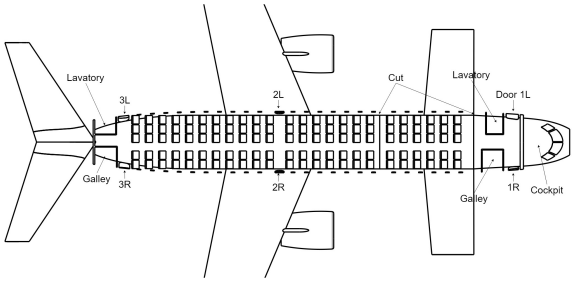

Figure 4: Internal lay-out of configurations 2 & 3

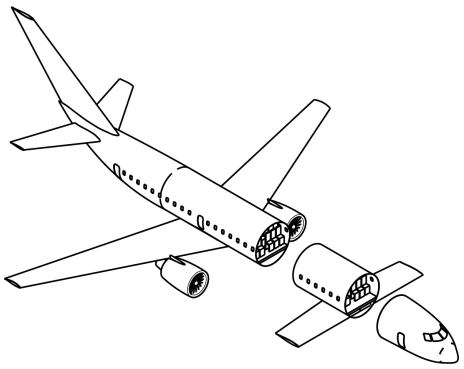

Figure 5: Isometric view of the external layout of configurations 2 & 3

Further recommendations

Finally, upon assessing all the set requirements, it was noted that three requirements were not met. These were the requirements on NO_x emissions, noise, and unit cost. Some recommendations on further developments will be presented. For the NO_x requirement, the goal was to have 55% less emissions compared to the CAEP/6 standard, the design ended up having a reduction of 49.8%, compared to the same standard, which is still a huge improvement. However, more analysis should be done into the climb and descent phases, as to optimise them for minimum fuel consumption and consequently less NO_x emissions. For the noise requirement, the aim was to reach a noise level of 90 $EPNdB$, while the aircraft initially had a noise level on approach of 105 $EPNdB$. Several measures were taken to reduce noise levels, which led to a noise reduction of 6.2 dB. However, further research should go in to those techniques in order to meet the ambitious requirement. For the unit cost requirement, the requirement of a unit cost of $60 million was not met, as the unit cost was changed to $62.15 million. Nonetheless, this was done to maximise the ROI for the manufacturer, and it is believed that the aircraft would still be competitive. Finally, the canard is currently required to have a C_L of 1.4, which is not achievable with the current symmetric airfoil used. Further research must go into the sizing of the canard and the possibility of using different airfoils that would ensure the canard is able to deliver the required lift. Disregarding the canard and using another method of increasing lift, is also a possibility that should be further investigated.

1 Introduction

Airliners are passengers aircraft, made for a fixed amount of passengers and a fixed range. Passengers, however, want airlines to offer a large amount of destinations on flexible moments. This results in aircraft that are not optimally used. Seats are empty and aircraft are overdesigned, which means their operational costs are higher than needed. It is the task of DSE group 23 to tackle this problem. Their goal is therefore to design an adaptive regional airliner which can be adapted such that it can fly in optimal configuration for different design points. It follows from the executed market analysis in previous design phases that the design points are as follows:

- Configuration 1: 90 passengers over a range of 4,000 km (base configuration)
- Configuration 2: 120 passengers over a range of 2,000 km
- Configuration 3: 120 passengers over a range of 4,000 km

The design is currently in its fourth phase. In the first phase, the project team was set up and an overview was made of all the steps that had to be done in the different design phases. This was done in a structured way, with the help of a work breakdown structure and a work flow diagram. This was converted to a Gantt chart, which is a timeline of the project, together with an estimation of the duration and a responsible person per task. During the second phase of the design, a more technical aspect of the project was discussed. A functional breakdown structure and functional flow diagram were set up to determine the systems functions. After that, brainstorm sessions were organised to come up with as many ideas as possible to fulfil the mission need statement. A design option tree was made to structure the options and point out all aspects of the system. Non-feasible options were eliminated and finally three possible options were chosen for further analysis. Concept 1 had a extendable fuselage to deal with larger passenger demands. Concept 2 consisted of compartments with seats inside the fuselage, which could be added or removed for different configurations. Concept 3 had different fuselages that could be slid into an airframe consisting of the wings and cockpit. During the third phase of the design, the three conceptual ideas were worked out in more detail. Basic analysis on different technical aspect were executed. These engineering disciplines were aerodynamics, performance and propulsion, structures, manufacturing and materials, stability and control, operations, and sustainable engineering. This design phase was concluded with a trade-off, in which all disciplines had set-up a set of criteria with different weights. Together with the help of a sensitivity analysis and requirement analysis, it was decided to continue the fourth design phase with concept 1.

The purpose of this report is to provide the reader with a complete overview of the project tackled by the group. The final design continued on the initial sizing that was executed in the previous phase of the design. This was again done for the different engineering disciplines as mentioned before. The result of these analyses were put together and iterated to improve the design even more. This resulted in a final design, which is visualised with CATIA. After finalising the design, system characteristics such as the hydraulic and electrical system were designed.

The structure of the report is as follows: first, in chapter 2 a detailed market analysis which analyses the requirements given by the customer is discussed. chapter 3 continues with presenting the full list of requirements. After that, chapter 4 gives an overview of the initial design option tree, the three conceptual ideas and the trade-off done to choose one. Then, chapter 5 presents the methodology used during the final phase of the design. chapter 6 presents the initial sizing of the aircraft. After that, the aerodynamic analysis is presented in chapter 7 and chapter 8 presents the stability and control analysis. Subsequently, chapter 9 discusses the performance and propulsion analysis and the structures, manufacturing and materials aspect of the design is discussed in chapter 10.The sustainable development of the design is discussed in chapter 11, followed by chapter 12 which presents the design's operational aspect. chapter 13 discusses extensively the cost analysis of the design. In chapter 14, a risk assessment is executed on the fuselage connection, aircraft structure and other systems. To give a good overview of the final design, chapter 15 sums up the iterations ,shows the internal and external lay-out and presents the requirement compliance matrix. To finish the design, chapter 16 presents the subsystems of the adaptive airliner like the fuel and electrical system. Finally, chapter 17 gives an overview of activities that should be done after the project is finished, before the aircraft enters service, which is followed by the conclusion and recommendations in chapter 18.

2 Market Analysis

A market analysis is the one of the first steps in any design process. A market analysis gives designers a general idea on how the demand is in the market, and what products are profitable to design. Additionally, a market analysis aims to identify market gaps and problems that are not addressed by competitors.

In the market analysis, first the SWOT analysis is discussed, in which the strengths, weaknesses, opportunities and threats of the current and future market are analysed. Secondly, the customer requirements were reevaluated. Finally, the chosen design points are presented as a result of the market analysis.

2.1. SWOT analysis

In this section the SWOT analysis is discussed of the large regional aircraft market. The strengths, weaknesses, opportunities and threats are analysed.

Strength: Regional aircraft enable operations on new routes, enabling direct flights [4]. Flights can operate on routes with less demand more efficiently. The initial range required by the customer, 3,500 km, is enough to enable travel to a large number of destinations within a region.

Weakness: The initial weakness of the requirements set by the customer is the low indicated unit cost, which was set at $40 million. The aircraft would not be able to compete with new generation regional jets. These aircraft are mostly equipped with new highly efficient engines, such as the PW1000G family with a unit price of $12 million each [91][1]. Secondly, the series magnitudes are relatively low, making it more difficult to have a high Return On Investment(ROI). Additionally, the demand for single-aisle aircraft (e.g. Boeing 737) is increasing, while the demand for regional aircraft is stagnant, as can be seen in Figure 2.2.

Opportunity: There are two big opportunities. Firstly, the adaptability of the aircraft is able to cover a market gap for medium-haul medium capacity (90-120), while still being able to serve smaller airports due to it small external dimensions. Secondly, there is no focus on cargo in the regional airliner industry. Later, a more in-depth analysis is presented on cargo possibilities.

Threats: There is a lot of competition in the booming 75-100 passengers market. Bombardier and Embraer offer highly efficient aircraft in the same passenger range as the adaptive aircraft.

To conclude, a market gap is discovered in the large regional aircraft segment (90-120 passenger capacity). However, the competition is very strong in the 75 to 100 passenger capacity segment, that is why the adaptive regional airliner needs to be distinctive to cope with this competition.

2.2. Requirement analysis

The purpose of this section is to reevaluate the given customer requirements, based on a thorough market analysis, and to propose, when necessary, new requirements that are believed to be more profitable to the customer. This will be done based on current market demand, as well as on projected market demand, as the aircraft being designed is set to enter service in the year 2035.

2.2.1. Passenger capacity

The first aspect to be analysed was the passenger capacity of the aircraft. The current requirements stipulate a baseline configuration with a 75 passenger seating capacity. However, upon analysis of similar aircraft, and their average number of orders per year, over the whole duration they have been in production for, it was found that there is a peak in orders around a seating capacity of 90 passengers, and that was thus chosen as the seating capacity for the baseline configuration. This data is visualised in Figure 2.1.
Additionally, upon analysing the projected market demand from aircraft manufacturers, it was noted that there is an increasing demand for single-aisle aircraft, especially with their increasing capability to fly longer ranges more efficiently [12]. On the other hand, there is a stagnant projected demand for regional aircraft, with most

[1] URL: `https://www.bloomberg.com/news/articles/2011-12-14/jetblue-to-buy-pratt-whitney-engines` [cited 2 May 2019]

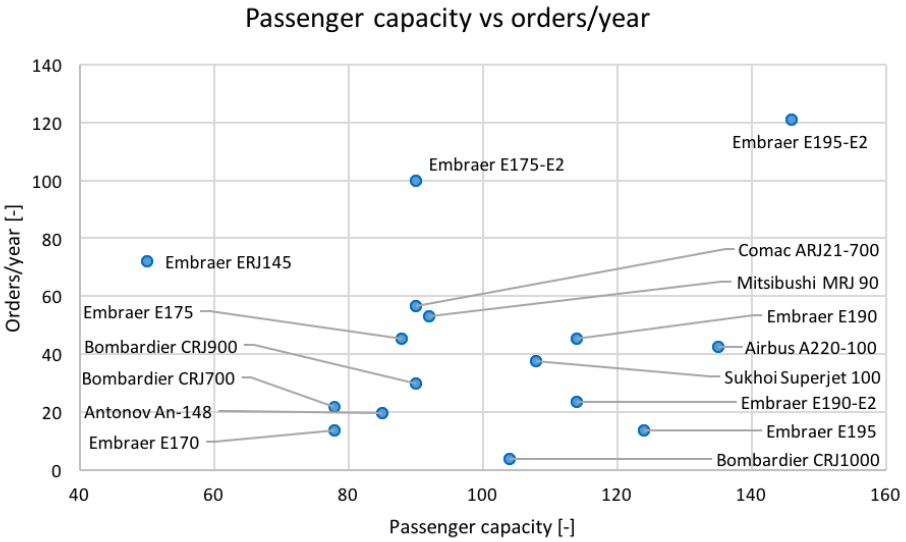

Figure 2.1: Orders per year against passenger capacity for comparable aircraft

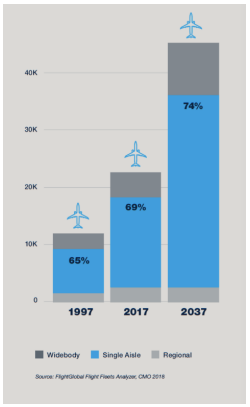

Figure 2.2: Change of market segment [12].

sales representing replacements rather than growth [12]. However, most single-aisle aircraft are not fully utilised during operation, with 45% of single-aisle aircraft in North America flying with less than 130 passengers [28]. For those reasons, it was decided that the adaptive regional airliner would have a maximum capacity of 120 passengers. This also represents a market that is untouched by the aircraft industry, the market between regional airliners and single-aisle aircraft [34].

2.2.2. Range

The second requirement to be analysed was the range requirement. For analysing this requirement, it was interesting to analyse the increasingly popular point-to-point model. Using this model, airlines fly directly to destinations without stopping at a large hub. Since the number of passengers on those routes are less, this trend requires that aircraft with relatively low passenger capacities are able to fly over longer ranges, to serve direct routes, which is becoming more feasible with the introduction of newer, more efficient engines, like the PW1000G family [2][2]. With this in mind, the competitors were again analysed, and a graph of the passenger capacity against range was plotted, as can be seen in Figure 2.3. From this figure, it can be noticed that at a passenger capacity of 90, the range of comparable aircraft is around 4,000 km. However, at the maximum capacity of 120 passengers, the range is around 5200 km. However, in operation, these aircraft are usually not utilised to their full range capability, as for longer routes, even larger aircraft than single aisle are usually more profitable [28]. Therefore, the maximum range of the aircraft was chosen at 4,000 km.

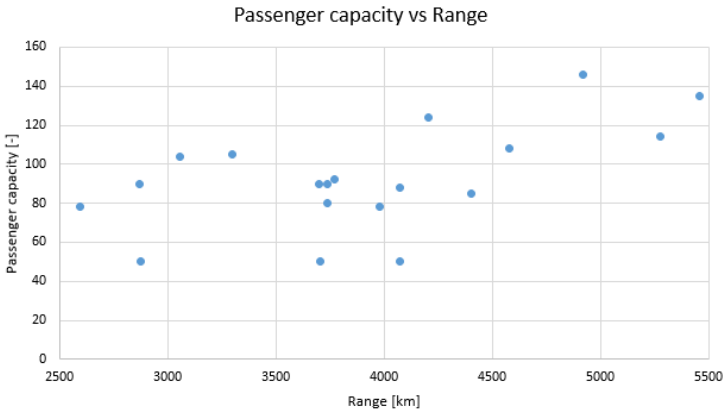

Figure 2.3: Passenger capacity against Range in kilometres for comparable aircraft

[2]URL: https://www.mtu.de/engines/commercial-aircraft-engines/narrowbody-and-regional-jets/gtf-engine-family/ [cited 13 June 2019]

While it is beneficial to have a long range, it is important to note that some of the most popular routes in the world are relatively short, and airlines are forced to fly these routes with overdesigned aircraft [81][3]. For that reason, it was decided that the aircraft should be able to adapt to have a range of 2,000 km.

2.2.3. Proposed unit cost

As was mentioned before, newer aircraft are able to achieve large ranges thanks to newer and more efficient engines, those engines are equipped on almost all new regional airliners. However, an engine such as those in the PW1000G family come at a unit cost of $12 million each, those would consume more than half the initial proposed unit cost. Therefore, it is deemed as more profitable to increase the unit cost to $60 million, in order to have a more efficient aircraft, that would show great savings in operational costs on the long run. The operational costs are analysed in more detail in section 13.3.

2.2.4. Cargo capability

Analysing the cargo profitability of the aircraft was also done to check whether requirements had to be set in terms of the aircraft's cargo capability. It was noticed that belly cargo is becoming more and more popular, especially for smaller packages, that do not pose a problem with being stored in the cargo hold of a passenger aircraft. Airlines make a lot of extra profit from cargo, it is loaded after the plane has been fully boarded and helps increase the profit per flight for airline. On average, 50% of international fights are only profitable due to cargo's contribution [97][4]. However, cargo is not usually something that passenger planes are designed for, but more of a secondary outcome, after the fuselage and cabin are designed. However, the cargo hold, as designed at this point, does already allow for more cargo volume than would be required for passenger luggage, and the aircraft will be capable of carrying the mass of a full cargo hold.

2.2.5. Seasonal fluctuations

In the aviation industry, there is a big fluctuation in demand due to seasonal effects. The seasonal fluctuation is needed to estimate the amount of times the aircraft would have to convert in a year. Therefore, data from the government of the United States is used [69]. Unfortunately, no data was found of every region in the world. This type of data is usually very expensive. The data that was obtained was first processed, after which the average load factor of every flight during a certain month was obtained, the load factor is the occupancy rate. For example, with a load factor of 100% all seats are occupied. Firstly, the average load factor was calculated over one year. Secondly, every load factor was divided by the average of the year to see if it was below or above the average load factor. Thirdly, all the months were averaged as is depicted in Figure 2.4.

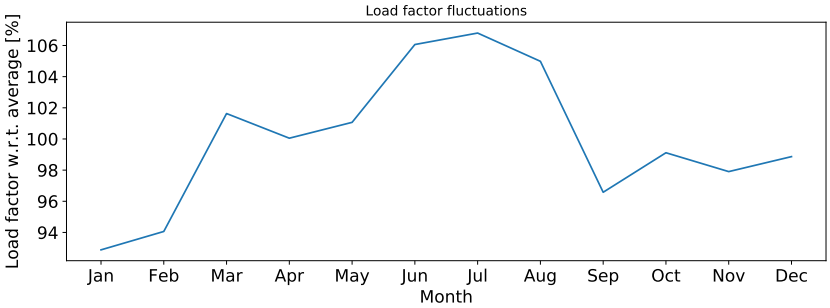

Figure 2.4: Seasonal fluctuations of the load factor [69]

In Figure 2.4[5], two major peaks can be seen. A peak in march and a peak during summer. Furthermore, two small peaks in October and December can be seen. These peaks are due to recesses that schools and universities usually have in the United States. These peaks are however below 100%. This would initiate that an adaptation is not needed here. However, since these recess periods are usually short, only one or two weeks, the load factor will increase to above 100%. These load factors will average down because of the low load factor during the rest of the month. All in all, in the United States, four peaks can be seen and therefore 8 adaptation times per year can be expected. Since the aircraft will adapt around 8 times per year, the requirement of 8 hours conversion time, without checking, is the right duration.

[3]URL: https://www.forbes.com/sites/ericrosen/2019/04/02/the-2019-list-of-busiest-airline-routes-in-the-world/#22ea1aac1d48 [cited 13 June 2019]
[4]URL: https://thepointsguy.com/news/how-airlines-make-big-bucks-from-cargo/ [cited on 28 May 2019]
[5]URL: https://www.transtats.bts.gov/osea/seasonaladjustment/?PageVar=ASM [cited on 3 June 2019]

2.3. Design points

In the market analysis, it is important to decide on a number of specific design points, that would be the driving factor for the design process, rather than covering an entire range of targeted ranges and passenger capacities. It was decided that the aircraft would have 3 different configurations with one as the baseline configurations. The design points chosen can be seen in Figure 2.5. The baseline configuration will be adaptable in terms of passenger capacity and range.

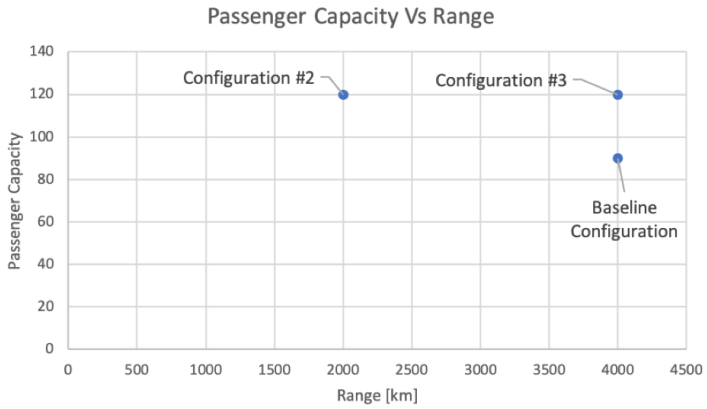

Figure 2.5: Design points in terms of passenger capacity against range in kilometres

The point shown vertically above the baseline configuration, at 4,000 km and 120 passengers, represents the adaptation in passenger capacity while maintaining the same range. This point was chosen as it provides the maximum passenger capacity, while still maintaining a high range able to cover a large number of destinations. The point configuration 2, shows the second adaptable configuration. This point is horizontally to the left of the previous configuration, at 2,000 km and 120 passengers. This represents a reduction in range while maintaining the high passenger capacity. This configuration is meant to be able to cover a high number of short-haul popular destinations with a high passenger capacity, while having the aircraft be optimised for that configuration rather than have excess fuel or structures that are not used. These 3 points are considered the driving design points.

3 Requirement Analysis

This chapter presents the requirement analysis which is used to design the adaptive aircraft. In section 3.1 the initial requirements set by the customer are discussed. Next, in section 3.2 the sustainability requirements are presented. The functional flow and breakdown are presented in section 3.3 and section 3.4 respectively. To conclude this chapter, section 3.5 lists all requirements which is used in the design procedure.

3.1. Customer requirements

This section presents the requirements which have been given initially by the customer. These are presented in the following list. In the following sections of this report these requirements will be analysed for feasibility and challenged whenever possible and agreed upon in negotiations with the customer.

- The aircraft shall provide space for two pilots and a flight attendant.
- The aircraft should be capable of carrying 75 passengers over a range of 3,500 km.
- The aircraft should be flying at 37,000 ft with a cruise speed of Mach 0.75
- The aircraft should be compliant with CS-25 regulations.
- The aircraft maximum take-off mass shall not exceed 23,000 kg.
- The unit cost shall not exceed $40 million.
- Environment emission should be reduced with 50% in CO_2 and 25% in NO_x.
- The aircraft shall have a 50% reduction in acoustic emissions.

The first requirement is related to CS-25 regulations, covered in subsection 3.5.4. The passenger capacity and range of the aircraft are further analysed in the market analysis presented in chapter 2. From analysis it turned out that the service ceiling and cruise speed will be kept the same. The maximum take-off weight is seen as an output value of this project and will be minimised. Using this approach, the requirement on maximum take-off weight can be removed. The unit cost price was discussed in the market analysis chapter as well.

3.2. Sustainability requirements

This section will present the sustainable elements considered in the requirements, namely the CO_2, NO_x, and noise emissions. The requirements set by the customer are analysed by comparing them to reference aircraft such as the E175, E175-E2, E190 and E190-E2. The CO_2 emission is directly related to the fuel burned and the mission fuel consumption from [5] has been analysed. From this data it was concluded that the adaptive regional airliner should aim to be 30.8% more efficient compared to the Embraer E175 and E190 first generation.

The NO_x analysis has been performed according to the CAEP/6 procedure. This procedure will be elaborated on in chapter 11. Reference material is analysed from [29][1], and a 55% reduction in NO_x is determined to be achievable.

Finally, the noise emission were analysed. For reference, the E190 and E190-E2 have been taken into account and the analysis is performed using the obtained noise certification from [26][2]. It was determined that the take-off and landing phases are most critical in noise production. During take-off the engine noise dominates and during approach the airframe is the main source of noise. As the engine needs to be selected in this stage with current technology, the noise level of recent comparable aircraft has been selected and determined to be 86 $EPNdB$. The noise requirement for approach is determined by extrapolating current data to the year 2035, in which the aircraft goes into service. As a result, this noise shall not exceed 90 $EPNdB$.

[1] URL: https://www.mtu.de/fileadmin/EN/7_News_Media/2_Media/Brochures/Engines/MTU-19-013_Prod_PW1000G.pdf [cited 1 May 2019]

[2] URL: https://www.easa.europa.eu/easa-and-you/environment/easa-certification-noise-levels [cited 1 May 2019]

3.3. Functional flow

Apart from the requirements which have been generated in the previous section, it is important to extensively research the functions which an aircraft needs to fulfil. This section will present the functional flow diagram, which can later be used to determine additional requirements in terms of aircraft functions. The following life-time phases of an aircraft have been identified [45]:

1. Market analysis
2. Design
3. Manufacture
4. Certification
5. Market launch / distribution
6. Aircraft system operation
7. Retirement

The market analysis has been discussed in chapter 2. The design phase is mostly related to the allocation of resources, this will be done in the beginning of each project. The manufacturing phase of this project does not impose any specific requirements but is developed as a result of the design phase. It is expected that the adaptive airliner will undergo a challenging certification procedure, therefore this phase is reflected on in the CS-25 requirements. Additionally, the customer has established a few requirements for the market launch and distribution of the aircraft. The aircraft system operation introduces a lot of requirements, which will be a result of the functional flow. Finally, retirement requirements are taken into consideration when determining the material selection for the aircraft. In the flight operational phase, the following phases have been identified [45]:

1. Perform pre-flight operations
2. Perform take-off preparations
3. Perform flight operations
4. Perform post-landing operations

The presented phases have been worked out in more detail in the functional flow diagram which is presented in Figure E.1.

3.4. Functional breakdown

From the functional flow diagram discussed earlier, the functional breakdown structure can be set up. This diagram goes one level deeper and visualises the dependencies of tasks to one-another. The functional breakdown structure is presented in multiple figures in Appendix E.

3.5. Full list of requirements

Finally, in this section the full list of requirements is presented. It should be noted that the requirements hold for all configurations unless otherwise stated. The mission requirements is comprised of customer, passenger and pilot requirements. The system and (sub)-system requirements were identified with the use of a requirement discovery tree and the functional analysis. Finally, the CS-25 requirements are implemented.

3.5.1. Mission requirements

For the mission requirements, the stakeholders whose requirements would influence the design were identified. These requirements are as follows:

Customer requirements

The underlined identifiers indicate that the stated requirement will drive the actual design of the product more than other requirements presented.

- **SYS-MI-CU-01** The aircraft in its base configuration shall have a range of 4,000 km.
- **SYS-MI-CU-02** The aircraft in its base configuration shall have a capacity of 90 passengers.
- **SYS-MI-CU-03** The aircraft shall adapt from its baseline configuration to a configuration with a range of 4000 km and a passenger capacity of 120.
- **SYS-MI-CU-04** The aircraft shall adapt from its baseline configuration to a configuration with a range of 2,000 km and a passenger capacity of 120.
- **SYS-MI-CU-05** The aircraft shall be able to change its configuration within 8 hours without regulation checks.
- **SYS-MI-CU-06** The regulation checking time will not be higher than 7 hours after an adaptability has been performed.
- **SYS-MI-CU-07** The aircraft shall cruise at a minimum speed of Mach 0.75.

- **SYS-MI-CU-08** The aircraft shall have a minimum service ceiling of 37,000 ft.
- **SYS-MI-CU-09** The aircraft shall be compliant with CS-25 regulations.
- **SYS-MI-CU-10** The aircraft shall have a CO_2 emissions reduction of 30.8% in comparison to the first generation Embraer 175 and 190 aircraft.
- **SYS-MI-CU-11** The aircraft shall have a NO_x emissions reduction of 55% in comparison to the CAEP/6 regulations.
- **SYS-MI-CU-12** The aircraft shall have a reduction in noise of 1.5 $EPNdB$ during the approach phase compared to the E190-E2.
- **SYS-MI-CU-13** The aircraft shall have a maximum lateral noise of 86 $EPNdB$.
- **SYS-MI-CU-14** The aircraft shall not exceed a total unit cost of $60 million.
- **SYS-MI-CU-15** The aircraft development program shall have a ROI of 5% after 5 years.
- **SYS-MI-CU-16** The aircraft shall enter into service in the year 2035.
- **SYS-MI-CU-17** One cabin crew member shall be responsible for a maximum of 50 passengers.
- **SYS-MI-CU-18** The aircraft in its base configuration shall be able to fly a range of 4,300 km when only 70 passengers are on board.

Passengers

- **SYS-MI-PA-01** The cabin shall have at least one lavatory for every 50 passengers.

Pilots

- **SYS-MI-PI-01** The pilots shall be able to see at least the first 0.5 meters of each wing tip from the cockpit.

3.5.2. System requirements

In this subsection the requirements of the system are listed. These requirements are not stated by the stakeholders, however are deemed required in order to fulfil the stakeholders needs.

- **SYS-S-01** The aircraft shall be statically stable.
- **SYS-S-02** The aircraft shall be able to touchdown and stop on a runway with an available runway length of 1,300 meters (ISA and at sea level).
- **SYS-S-03** The aircraft shall be able to take-off from a runway with a take-off run available of 2,000 meters (ISA and at sea level).
- **SYS-S-04** The wingspan of the aircraft shall not exceed 36 meters.
- **SYS-S-05** The wheel base of the aircraft shall not exceed 9 meters.
- **SYS-S-06** The aircraft shall have a life time of 55,000 cycles.
- **SYS-S-07** The aircraft shall have a life time of 231,000 flight hours.
- **SYS-S-08** The aircraft shall have a life time of 30 years.

3.5.3. Subsystem requirements

In this subsection the requirements of the different subsystems are listed. The subsystems covered are listed in Table 3.1 including their unique code used to group the different requirements according to the subsystem they represent.

Table 3.1: Subsystems with respective codes

Avionics	**AV**
Cabin Environment	**CE**
Electronics	**EL**
Flight Control	**FC**
Fuel System	**FS**
Guidance, Navigation & Control	**GNC**
Hydraulics	**HD**
Ice Protection	**IP**
Landing Gear	**LG**
Propulsion	**PP**
Structures	**ST**
Auxiliary Power Unit	**APU**

- **SYS-AV-01** The avionics shall be able to determine the attitude of the aircraft.
- **SYS-AV-02** The avionics shall be able to determine the altitude above sea level of the aircraft.
- **SYS-AV-03** The avionics shall be able to determine the airspeed of the aircraft.
- **SYS-AV-04** The avionics shall be able to determine the ground speed of the aircraft while taxiing on the ground.
- **SYS-AV-05** The avionics shall be able to determine the heading of the aircraft.
- **SYS-AV-06** The avionics shall be able to determine the angle of attack of the aircraft.
- **SYS-AV-07** The avionics shall be able to determine the rate of climb of the aircraft.
- **SYS-AV-08** The avionics shall allow the aircraft to communicate with the ground.
- **SYS-AV-09** The avionics shall provide the ground with flight information.
- **SYS-CE-01** The cabin shall provide a back-up system for oxygen supply.
- **SYS-EL-01** The electronics shall distribute electric power to other subsystems.
- **SYS-FC-01** The flight control system shall provide control system inputs.
- **SYS-FS-01** The fuel system shall provide the required amount of fuel to the engines.
- **SYS-FS-02** The fuel system shall be able to pump fuel between different fuel tanks.
- **SYS-GNC-01** The aircraft shall be able to determine its position at any point in time.
- **SYS-HD-01** The hydraulics shall provide hydraulic power to other subsystems.
- **SYS-IP-01** The ice protection system shall prevent ice forming on the aircraft.
- **SYS-LG-01** The landing gear shall be strong enough to carry a load of 184 kN.
- **SYS-LG-02** The landing gear shall be able to steer the aircraft on the ground.
- **SYS-LG-03** The landing gear shall be able to brake the aircraft on the ground.
- **SYS-LG-04** The landing gear shall be extendable.
- **SYS-LG-05** The landing gear shall be retractable.
- **SYS-ST-01** The aircraft structure shall be able to handle the loads during all phases of flight.

- **SYS-APU-01** The auxiliary power unit shall provide electrical power on the ground.
- **SYS-APU-02** The auxiliary power unit shall provide hydraulic power on the ground.
- **SYS-APU-03** The auxiliary power unit shall provide back-up electrical power during flight.
- **SYS-APU-04** The auxiliary power unit shall provide back-up hydraulic power during flight.

3.5.4. CS-25 requirements

CS-25 is the certification specification for turbine powered large aeroplanes which covers requirements on structures, control systems, electrical systems, engines and flight performance, that the aircraft must comply with. The CS-25 document is detailed and the relevance of many stated requirements are beyond the scope of this project. Hence, analysis was carried out on CS-25 and lower level requirements for SYS-SH-07 are formulated to guide the design of the adaptable aircraft. All information presented below is taken from [23].

- **SYS-MI-CU-09-01** The cabin shall provide a maximum cabin pressure altitude of 2,438 m at the maximum operating altitude of the aeroplane.
- **SYS-MI-CU-09-02** The loads in the aircraft shall not exceed the limits at which the structure is proven.
- **SYS-MI-CU-09-03** The climb gradient in landing configuration shall not be less than 3.2%.
- **SYS-MI-CU-09-04** The climb gradient in take-off configuration shall be more than 1.2%.
- **SYS-MI-CU-09-05** The aircraft shall be able to yaw into the operative engine and to safely make a sudden change in heading of up to 15° in the direction of the critical inoperative engine.
- **SYS-MI-CU-09-06** The aircraft shall make a 20° bank turn, with and against the inoperative engine.
- **SYS-MI-CU-09-07** The aircraft shall have no uncontrollable tendency to nose over in any expected operation condition.
- **SYS-MI-CU-09-08** The aircraft shall be stable for the short period oscillation.
- **SYS-MI-CU-09-09** The aircraft shall be stable for the Dutch roll.
- **SYS-MI-CU-09-10** Integral fuel tanks shall accommodate the facilities for interior inspection and repair.
- **SYS-MI-CU-09-11** A factor of safety of 1.5 shall be applied to the prescribed limit load which are considered external loads of the structure.
- **SYS-MI-CU-09-12** A factor of safety shall not be applied to ultimate loads which are considered external loads of the structure.
- **SYS-MI-CU-09-13** The flight crew shall be able to perform the basic workload such as flight path control, collision avoidance, navigation, communications, command decisions, operations and monitoring of aircraft and systems.
- **SYS-MI-CU-09-14** The structure shall be able to support ultimate loads without failure for at least 2 seconds.
- **SYS-MI-CU-09-15** The aircraft shall have a maximum rudder force of 1,335 N.
- **SYS-MI-CU-09-16** The aircraft shall have maximum aileron stick force of 445 N.
- **SYS-MI-CU-09-17** The aircraft shall have minimum aileron stick force of 178 N.
- **SYS-MI-CU-09-18** The aircraft shall have maximum elevator stick force of 1,112 N.
- **SYS-MI-CU-09-19** The aircraft shall have minimum elevator stick force of 445 N.
- **SYS-MI-CU-09-20** The aircraft shall have minimum rudder force of 578 N.
- **SYS-MI-CU-09-21** The aircraft shall withstand unsymmetrical loads resulting from the failure of the critical engine.

- **SYS-MI-CU-09-22** The structure shall withstand the flight loads combined with pressure differential loads from zero up to maximum relief valve setting.
- **SYS-MI-CU-09-23** The aircraft shall maintain stability when aircraft's centre of gravity is most aft or forward or critical vertically or laterally.
- **SYS-MI-CU-09-24** Removable bolt, screw, nut, pin or other removable fastener shall incorporate two separate locking devices.
- **SYS-MI-CU-09-25** Self locking nut shall not be used on any bolt subjected to rotating in operation.
- **SYS-MI-CU-09-26** The cabin shall have minimum of 2 Type I and 1 Type II exits for each side of the fuselage.
- **SYS-MI-CU-09-27** The aisle width shall be more than 51 cm.
- **SYS-MI-CU-09-28** The cabin shall have a maximum of 3 seats abreast at each side of the aisle in any row.
- **SYS-MI-CU-09-29** The cabin environment subsystem will provide backup oxygen for at least 15 minutes.
- **SYS-MI-CU-09-30** The cabin environment subsystem will provide backup oxygen for a pressure altitude of 8,000 feet.

4 Design options

This chapter presents the design options for the adaptive regional airliner and the three conceptual ideas that were in the trade-off. Additionally, the trade-off methodology is presented, as well as the final trade-off which was used to select the concept for the detailed design phase.

4.1. Conceptual ideas

In this section the wide variety of design options for the adaptive regional airliner are presented. These were narrowed down to three conceptual ideas that were analysed in the trade-off, which are discussed in detail.

4.1.1. Design option tree

Once the full list of requirements was generated, a brainstorm session was held to come up with all the possible design options for the adaptive regional airliner. This resulted in approximately 50 different design options, which were gathered in a design option tree, including every design possibility. In this phase of the design, feasibility was not a criteria. However, this had to be narrowed down to three concepts which would enter a more detailed analysis and trade-off in the build-up to the final design phase. This was done in a systematic way, first of all by sketching straw-man concepts for each of the design proposals and eliminating those for which of the proposals no concept could be generated. Secondly, the designs which were certainly deemed to be non-feasible were eliminated. This approach resulted in 5 design options for each of the adaptability measures, namely extended passenger capacity and extended range. All of the combinations between these were listed and again had to be narrowed down. This was done by initially removing all the conflicting combinations and analysing the (dis)advantages of each option quantitatively. Finally, the concepts were scored and 3 final concepts were selected to enter the midterm phase of the project.

4.1.2. Concept 1

The first concept increases its passenger capacity by having a removable fuselage section. In order to keep the range of the extended version according to the requirements, external fuel tanks are used below the wing. The design points of this concept are met by having the following configurations:

- Extended fuselage version, excluding external fuel tanks with a capacity of 120 passengers and a range of 2,000 km.
- Non-extended fuselage version, including external fuel tanks with a capacity of 90 passengers and a range of 4,000 km.
- Extendable fuselage version, including external fuel tanks with a capacity 120 passengers and a range of 4,000 km.

The extension of the fuselage will consist of a prebuilt fuselage section, which can be added between the cockpit and the cabin. This section can be removed or added, dependent on the passenger capacity demand. However, when in extended version, the wing surface area will need to be increased as the mass increases. In order to create additional lifting area, a canard wing was fixed to the prebuilt fuselage section.

In order to cover the design range of the different configurations, external fuel tanks will be mounted under the wing in this concept. This range adaptability measure was investigated in more detail in the trade-off phase. It remained possible to interchange range adaptability methods between concepts after the trade-off in order to have the most optimum combination of passenger and fuel adaptability.

The aircraft design was kept conventional on purpose, in order to focus more on the adaptability concept and the correlated complications. Therefore, a conventional low wing was chosen at this point in the design. A low wing does not interfere with the adaptability feature in this design, as well as it provides advantages for integration of the landing gear. Additionally, its good accessibility is a benefit for maintenance and installation of the fuel pods under the wing. An overview of this concept is presented in Figure 4.1.

A turbofan was chosen as the propulsion system. This is mainly the result of the range requirement. As it is quite large, it is more feasible with a turbofan, as they can reach a higher cruise speed than turboprops can. For

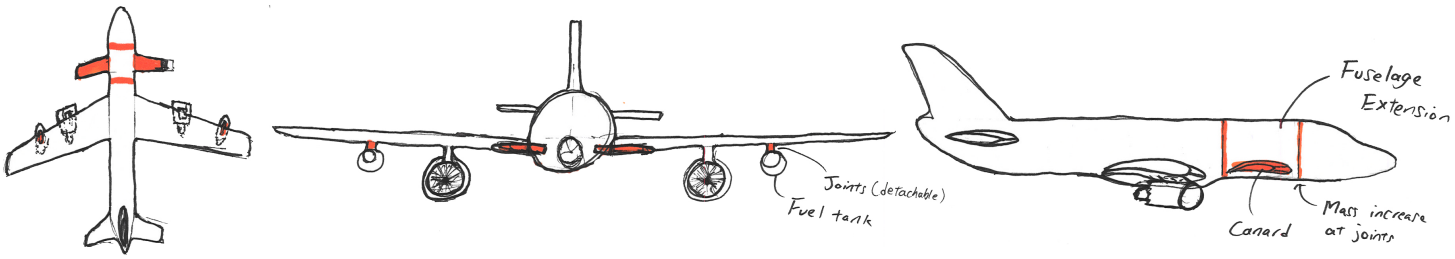

Figure 4.1: Concept 1 sketch

accessibility purposes, the engines are positioned underneath the wing. Additionally, when there is a passenger capacity of over 110, the regulations state that two Type-I doors are required [23]. Therefore, fuselage mounted engines could possibly introduce a safety risk. As a low wing is considered for this concept, it is safe to select a conventional empennage.

A few control complicates arose for this concepts, due to the removal of the prebuilt fuselage section. This makes the wiring and piping systems and their connections a challenge. In order to solve this, a conceptual system was designed, which would make use of magnetic pins in the circumference of the fuselage. This would consist of all the connections needed for the control system, hydraulics and power distribution.

4.1.3. Concept 2

The second concept considered in the trade-off phase uses modular sections for the internals of the aircraft. Therefore, the length and volume of the fuselage do not differ. The design points of this concept are met by having the following configurations:

- Passenger module, without fuel extensions with a capacity of 120 passengers and a range of 2,000 km.
- Fuel module, without fuel extensions with a capacity of 90 passengers and a range of 4,000 km.
- Passenger module with fuel extensions with a capacity of 120 passengers and a range of 4,000 km.

An internal passenger module is used to make the aircraft adaptable in terms of passenger capacity. The baseline configuration consists of 90 passengers and therefore the first 90 seats are fixed. The additional 30 seats are implemented in the passenger module. When only a passenger capacity of 90 is demanded, the passenger module can be replaced and used for other purposes, such as fuel. When the range has to be extended, this modular section can be used to insert a fuel module. In case of the 3rd configuration, the additional fuel is stored in an extension of the wing-fuselage fairing. An overview of the second concept is presented in Figure 4.2.

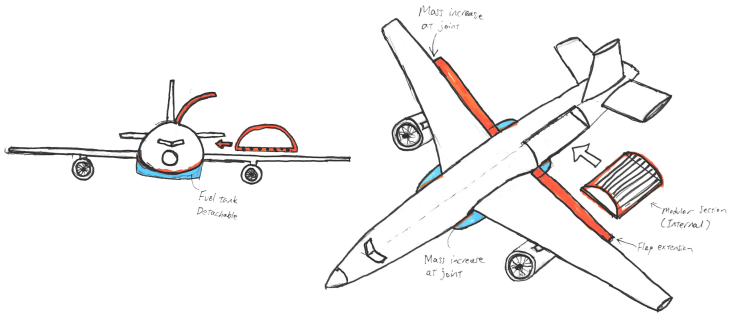

Figure 4.2: Concept 2 sketch

The general layout of the aircraft, such as the wing position, engine type, engine placement and empennage will be the same as with concept 1 for the same reasons.

4.1.4. Concept 3

The third and last concept uses a completely detachable cabin, which allows different versions of the cabin to be installed. The design points of this concept are met by having the following configurations:

- A large cabin without fuel extensions with capacity of 120 passengers and a range of 2,000 km.

- A smaller cabin, combined with fuel extensions, with a capacity of 90 passengers and a range of 4,000 km.
- A large cabin, combined with fuel extensions, with a capacity of 120 passengers and a range of 4,000 km.

The cabin is completely detachable,to make it adaptable for the number of passengers. This makes it possible to attach a shorter version with fewer seats whenever the passenger demand is lower. In order to make the aircraft adaptive in terms of range, external fuel tanks were used. These were positioned between the fuselage and the wing, which was chosen to be a high wing as this would have no interference with the detachable fuselage, which slides in from the bottom. A schematic overview of this concept is presented in Figure 4.3.

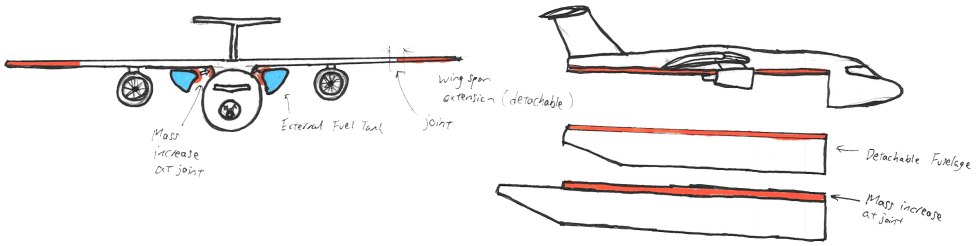

Figure 4.3: Concept 3 sketch

Similar to the previously described concepts, turbofan engines are considered. A T-tail is necessary to avoid the horizontal tail being in the wake of the main wing.

4.2. Trade-off methodology

In order to select one of the concepts as a final design, a trade-off had to be performed between all proposed concepts for the adaptive regional airliner. The main trade-off criteria consisted of several engineering disciplines. However, within every engineering discipline several trade-off criteria were identified. Therefore, the final trade-off table consists of trade-off criteria and scores which are the results of trade-offs within the engineering disciplines.

Initially, the trade-off criteria for every performed trade-off had to be identified. These were ranked according to their relative importance in the design, and were considered as 'critical', 'important' and 'relevant'. The corresponding trade-off criteria weights are presented in Table 4.1.

The performance of each of the concepts to the trade-off criteria translated in a score, of which the system is shown in Table 4.2. The scoring of the concepts in each trade-off criteria is dependent on whether or not the requirements of the aircraft are met. However, in the case that there is no actual requirement set for a specific trade-off criteria, the scoring will be done in terms of relative performance of the concepts.

Table 4.1: trade-off criteria weights

Critical	Important	Relevant
5	4	3

Table 4.2: Scoring system

Excellent	Good	Neutral	Deficient	Unacceptable
5	4	3	2	1

As mentioned before, the final trade-off table is a result of trade-off performed on a lower level for each of the final trade-off criteria. In order to translate the scores in a sub trade-off to a level higher trade-off the weighted-average score is used as an output of the trade-off. This average score of each concept is then used in the further trade-offs, such that the pure score of the concepts is maintained and remains comparable.

4.3. Final trade-off

In this section the final trade-off is discussed. Firstly, the trade-off table and used trade-off criteria are discussed. This is followed by a sensitivity analysis to determine the final concept, which is taken into the detailed design phase.

4.3.1. Summarising trade-off table

The trade-off tables were generated in a systematic manner. The proposed design concepts are placed on the left side of the table, whereas the trade-off criteria are positioned at the top of the columns. The relative weight of

the trade-off criteria is represented by the column width. For clarity to the reader, the weights are also presented next to the trade-off criterion itself. A colour code is used to represent the scoring of the concept to the trade-off criteria, which is backed-up by presenting the scoring between brackets in case the colour system cannot be used.

In Table 4.3 the final trade-off table is presented. The final trade-off criteria were set to be the following engineering disciplines: 'sustainability', 'operations', 'structures', and 'stability and control'. Not all engineering disciplines were considered to be final trade-off criteria, as their analysis was used in their outcomes are analysed in the sustainability criteria. This was done to consider the different aspect of the design only once in the trade-off.

Sustainability and operations were considered to be 'critical' in the design of the adaptive airliner. This was done as most of the driving requirements reflect on these engineering disciplines. Structures was ranked to be 'important' as this analysis shows the efficiency and feasibility of the adaptability measures and method. Lastly, the control and stability aspect of the design was determined to be 'relevant', as this is a crucial aspect in aircraft design but additional measures can be taken further into the design.

Table 4.3: Trade-off table

Criterion / Option	Stability and Control (3)	Operations (5)	Structures (4)	Sustainable Engineering (5)	*Score*
Concept 1	Difficult stability and control (3.05)	Difficult maintainability and conversion (2.12)	Larger MOI for multiple load carrying structure (4.00)	Low noise, good mass efficiency (3.48)	3.13
Concept 2	Good stability and control (4.19)	Good certification and easy conversion (3.65)	High fuel tank mass, permanent modular mass (2.45)	High noise, low fuel consumption , low mass efficiency (2.33)	3.07
Concept 3	Difficult landing gear (3.29)	Easy conversion but high costs (2.55)	Reinforcement at the top part of fuselage (1.91)	High noise, neutral fuel consumption, good mass efficiency (2.56)	2.54

Excellent | Good | Neutral | Deficient | Unacceptable

4.3.2. Sensitivity analysis

From Table 4.3, it is observed that concept 1 has the overall highest average score and therefore is the concept that should be taken into the final design phase according to the trade-off. However, the difference with concept 2 is very small. In order to further investigate the performance difference between the two, a sensitivity analysis is performed. This consisted of a requirement analysis, a sensitivity trade-off of the final trade-off, and a test of robustness of the design.

First of all, it was investigated whether the driving requirements are met by both concepts. From analysis it resulted that concept 1 currently did not meet the 8 hour conversion time requirement, whereas concept 2 did. However, in terms of noise and climate emissions, concept 1 shows potentially better performance.

The final trade-off was tested in terms of sensitivity by changing the weights of the trade-off criteria or deleting them individually in order to examine the influence on the outcome. It could be concluded that concept 2 is the favourable concept in terms of operations and control & stability, whereas concept 1 is favourable when sustainability and structures is considered to be more important in the design.

Lastly, both concepts were tested in terms of their robustness to changes in the driving requirements. For each requirement, it is determined what the effect is on concept 1 and concept 2, if the requirements are made more challenging.The results are summarised in Table 4.4. The sign next to each requirement, shows how easy that concept can adapt to that requirement. - indicates that the concept cannot adapt to a requirement easily, and

+ indicates that the concept is still able to fulfil a different requirement where no big changes to the design are needed. The requirement codes can be found in section 3.5.

Table 4.4: Results of the sensitivity analysis on driving requirements

	Concept 1	Concept 2		Concept 1	Concept 2
SYS-MI-CU-01	-	-	SYS-MI-CU-10	-	-
SYS-MI-CU-02	-	-	SYS-MI-CU-11	-	-
SYS-MI-CU-03	+	-	SYS-MI-CU-12	+	-
SYS-MI-CU-04	+	-	SYS-MI-CU-13	+	-
SYS-MI-CU-05	- -	+	SYS-MI-CU-14	-	-
SYS-MI-CU-09	+	±			

In general, it can be concluded that concept 1 is in general a more robust design. However, the only killing requirement at the moment is the 8 hour conversion time, which is deemed to be infeasible with the current adaptability method of concept 1. However, concept 1 performs clearly better in terms of sustainability. Finally, it was determined that the sustainable aspect of the design was the most important and therefore concept 1 was chosen to be taken into the detailed design phase. A new adaptability method will be design such that the driving requirements will be fulfilled.

5 Detailed Design Methodology

In this chapter, the design methodology is presented. This consists of the interface definition between the different (sub-)systems of the adaptive regional airliner and the engineering disciplines involved in the design, which is discussed in section 5.1. Furthermore, in section 5.2 the developed numerical model is presented and the iterative process of the design is discussed. Lastly, the general verification and validation procedures used throughout the design are presented in section 5.3.

5.1. Interface definition

In the detailed design phase of the adaptive regional airliner several inter-dependencies between the involved engineering disciplines arose. In order to visualise and manage these encountered interfaces between the different engineering departments, an N2-chart was generated. This is presented in Figure 5.1. All the involved engineering disciplines in the design were placed on the diagonal of the N2-chart. The work packages 'Class-I weight estimation', 'Initial sizing', and 'Class-II estimation' were positioned on this main diagonal, although they do not directly represented an engineering discipline. These work packages were also included here as they are actively involved in the design as they were needed to start the technical analysis of each department and are included in the design iterations.

The interfaces can be identified from Figure 5.1. The main interfaces between the different disciplines are the following. The aerodynamics department produces and analyses the aerodynamic characteristics of the design. However the input required to these values were the specific geometry of all the structural components of the aircraft, which was partly analysed by the department of Control and Stability and Structures. However, here the interface difficulty arises as these departments are highly influenced by the aerodynamic characteristics to determine the required loads and structural reinforcements needed. Additionally the Power and Performance analysis was required as an input in order to evaluate the noise and gas emissions of the aircraft, however the performance analysis again required the aerodynamic characteristics. Lastly, the structures and operational departments collaborated on the joints required at the cut-out fuselage section, as the type and amount of joints influenced the adaptability time significantly.

In order to manage these interfaces, an iterative design process was used. This makes sure that every department can use the outputs of the previous iteration until the results converge to a value smaller than the set threshold of 1%. This process will be specified in more detail in the upcoming sections of this chapter.

5.2. Numerical model

This section presents the outline and the working process of the numerical model which was developed to design the adaptive regional airliner in detail. A visual illustration of the numerical model is presented under the form of a flowchart. This is followed by a discussion on the iterative process followed during the detailed design phase.

5.2.1. Flowchart

In Figure 5.2, a visual presentation of the numerical model used to design the aircraft in detail is shown. The illustration is made under the form of a flowchart, such that the sequence of the program and the different in- and outputs needed can be tracked easily.

5.2.2. Iterative process

It can be noticed from the numerical model flowchart presented in Figure 5.3, that several outputs are required earlier on in the model as an input to a certain module. This can be tackled by assuming an initial value by means of historical or statistical data for the first input. The actual calculated value can then again be used as in input, which is repeated until the input and output values converge. In order to visualise this iterative process, Figure 5.3 is presented.

The main values which needed to be exchanged from output to input in the process are the aerodynamic coefficients, the landing and take-off conditions, the fuel fractions, the Operational Empty Mass (OEM) or Weight (OEW) and the empennage, canard, and landing gear sizes. The aerodynamic coefficients, combined with the

take-off and landing conditions are needed to determine the wing (W/S) and thrust loading (T/W) of the aircraft, but these are only determined in the detailed sizing module. Secondly, the fuel fractions and the OEM are needed to update the mass estimates of the aircraft. These are computed in the class-II mass estimation and sub-module Power and Performance. Lastly, after the detailed sizing has determined the needed sizes of the empennage, canard, and landing gear, this should be updated in the class-II mass and c.g. estimation.

specific fuel consumption L/D OEW/MTOW									
Class I weight estimation	OEW Fuel Fractions								
	Mass & Sizing	MTOW MZFM Geometry & sizes	MTOW			Geometry of wing	Wing planform size and geometry	General sizing and geometry	Position/length of main components
	OEW	**Class II weight & CG estimation**			Component masses			Component masses	Structural component masses CG locations
	Fuel Fractions		**Propulsion**	Fuel consumption		Fuel consumption Engine selection Thrust level	Fuel volume	Fuel volume & mass	
	Rate of climb Take-off and landing field length Fuel fractions	Dive speed Maximum load factor	Rate of climb Take-off and landing field length	**Performance**		Take-off thrust Approach speed		Load factors	Flight profile * velocities
					Operations			Conversion time	
			Noise emissions Greenhouse gas emissions			**Sustainability**			
	Lift Drag		Drag Wing fuel storing capacity	Lift Drag		Drag HLD sizing	**Aerodynamics**	Lift Drag Lift Distribution	Lift of the planforms aerodynamic moments
		Mass of reinforcement Material selections			Type of joints	Material choice Landing gear wheel sizing	Wing fuel tank volume & mass Landing gear diameter	**Structures**	
		Wing postion sizing of the empennage & canard				Control surfaces Landing gear length	Landing gear length	CG shifts Planform shape empennage landing gear placements	**Control and stability**

Figure 5.1: N2 chart of the interfaces between the engineering disciplines

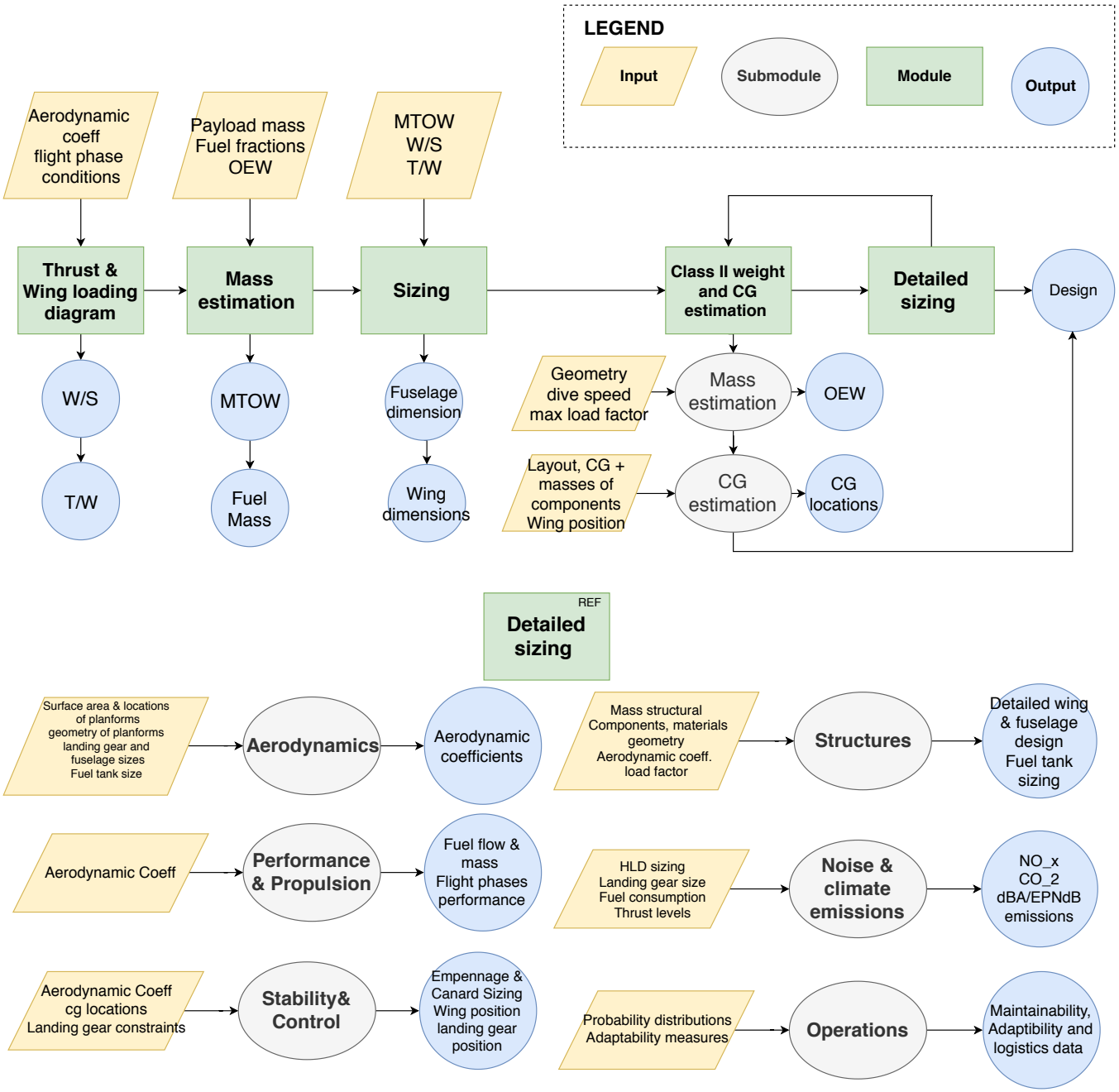

Figure 5.2: Flowchart Numerical Model

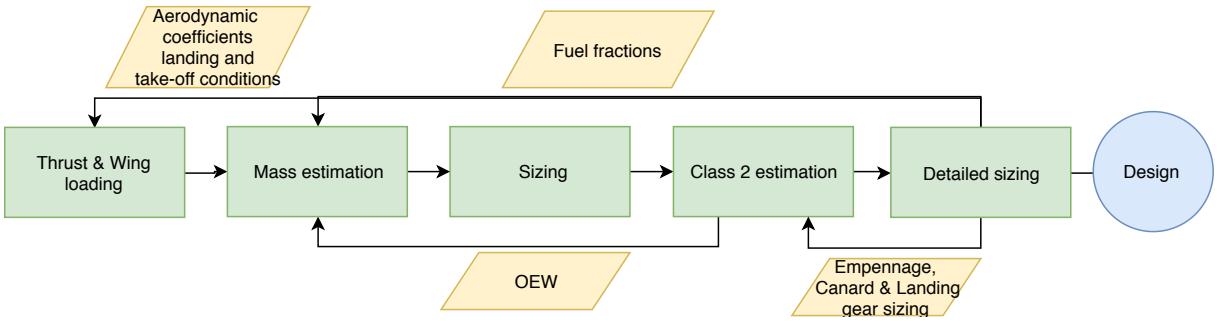

Figure 5.3: Iteration in the numerical model

5.3. Verification and validation

The numerical model developed should be verified and validated. This should be done to control whether the written model performs the calculations correctly and represents reality accurately. This section will describe the general approach towards verification and validation.

The general verification method will consist of unit tests and system tests. Additionally, when available, additional material is used to verify the solution of the numerical model. In unit testing, the output of each of the different functions is checked whether the correct output is returned. This was implemented in the numerical model as it was written in separate functions which combine in a final function, which allows to test the functions separately and trace the faults of the model efficiently. Once the individual functions are tested, the module can be verified by means of a module test, which again tests the output, but of the entire module. Additionally, system testing was also adopted to verify the models. This type of tests controls whether the integration of the different functions and modules has been done completely and correctly. The verification tests should cover the entire numerical model, and therefore is executed per module. The final integration of the modules was verified separately by means of (sub-)system testing.

In order to test the influence of the made assumptions and test whether the numerical model represents reality accurately, validation needs to be performed. The main validation approach consists of using data from reference aircraft to validate the output of the results. Additionally, statistical data from the aviation industry can be used as well. By comparing the output from the numerical model to the data, the results can be validated and the influence of the made assumptions can be investigated.

6 Sizing Method

In this chapter, the initial sizing method used in the design of the adaptive regional airliner is presented. First of all, a class-I weight estimation that has been performed is presented in section 6.1, which includes a correction for adaptability measures of the design. This is followed by the initial sizing of the aircraft in section 6.2. Finally, in section 6.3, a more accurate class-II estimate is presented.

6.1. Class-I estimation

A class-I weight estimation is based upon statistical data, the desired range and passenger capacity [86]. As no specific information about the aircraft layout were yet known, reference aircraft have been used to set up a relation between the operational empty weight and the maximum take-off weight. The reference aircraft were chosen to be as close to the desired range and passenger capacity to get a reliable relation. Linear regression ($R^2 = 0.968$) is done in Equation 6.1, relating the $MTOW$ and OEW of reference aircraft.

$$OEM = 0.582 \cdot MTOM - 1{,}000 \tag{6.1}$$

To determine the fuel weight which is carried by the aircraft, the method of fuel fractions has been used. In this method the different flight phases are separated from each other and for each phase a fuel fraction is determined using statistical data. An overview of the considered flight phases is presented in Figure 6.1.

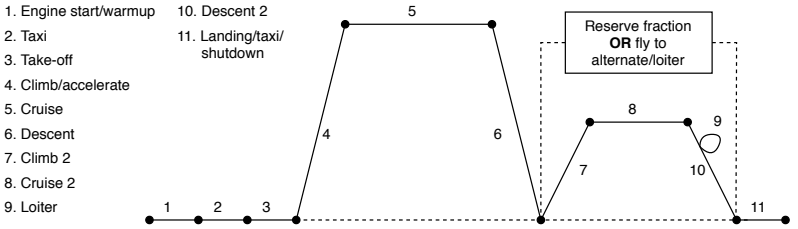

Figure 6.1: Different flight phases analysed for the fuel fraction method [86, 107]

For each configuration it was now determined what the $MTOM$ and OEM are. The class-I weight estimation is however limited in reliability when applying to an adaptive aircraft. The wing thickness, engine weight, empennage design and landing gear layout will remain unchanged between configurations. The class-I estimation however does not take this into account. To solve this problem, the highest operational empty weight was taken and between different configurations the mass of the removable items were subtracted. In addition to that, the increase in mass due to its adaptability was taken into account, by quantifying the additional mass due to joints and structural reinforcement. This includes the fuselage extensions, the addition of the canard, and the fuel tank mass. From this process the final OEM and $MTOM$ were established for all three configurations. An overview of the initial estimations is presented in Table 6.1

Table 6.1: Class-I operational empty mass and maximum take-off mass

	OEM [kg]	*MTOM [kg]*
Configuration 1	34,632	58,723
Configuration 2	38,223	67,394
Configuration 3	38,730	68,264

6.2. Sizing

The first step in the initial sizing is constructing the wing and thrust loading diagram. This analysis takes into consideration all important flight phases and their restrictions on the ratio of weight over wing surface area, W/S, and thrust over weight, T/W. In the wing/thrust loading diagram the requirements reflecting on the following flight phases have been taken into consideration: The cruise condition, the climb rate and gradient, and take-off and landing restrictions. The resulting diagram is presented in Figure 6.2.

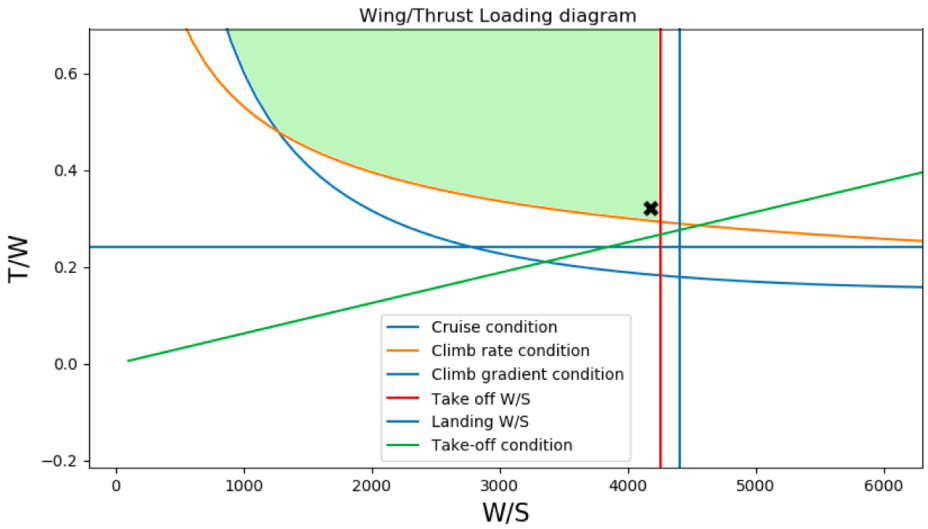

Figure 6.2: Wing and thrust loading diagram

An optimal design point is then chosen to minimise the surface area and to minimise the thrust required. In the presented figure, this corresponds to the bottom right point in the shaded region.

The sizing of the wing planform has been done according to the ADSEE-I method [107]. This method allows to express the wing parameters in terms of basic geometry values. The fuselage design is done according to the amount of passengers which it should carry. This is done using the Roskam method [82]. From this is was determined to have 5 seats abreast with a seat pitch of 32 inch, seat width of 20 inch and finally an armrest width of 2 inch. In this design phase it was determined that the average weight of each passenger is equal to 83.8 kg.

The empennage is designed to provide longitudinal stability to the aircraft during flight. In order to determine the size and location of this system it is needed to have a general overview of the centre of gravity locations throughout the aircraft. For the aircraft masses were lumped into two groups: the wing group and the fuselage group. The fuselage group consist of the fuselage itself, the empennage and fixed equipment. The engine, nacelle and wing weight are accommodated in the wing group. Using statistical group mass data, the c.g. location can be estimated and the empennage designed.

The initial sizing of the undercarriage outputs the size, location and amount of wheels needed. In order to have acceptable load distribution on the ground it was assumed that at least 8% of the weight shall be on the nose wheel. The configuration of the gear can now be determined for the configurations. The next step is to come up with the location of the gear. This is done by incorporating constraint angles. The turnover angle, tip-back angle, scrape angle and wingtip clearance angle are taken into consideration. It is chosen to have the retraction system fit within the wings. During further analysis the gear placement will be analysed in more detail as the current output is different for each configuration, while in reality all configurations will have the same landing gear.

From the thrust over weight estimate which is presented earlier, the required thrust is determined. The required thrust was determined to be equal to 204.3 kN for the third configuration. To simplify maintenance procedures and with increasing efficiency of aircraft engines, it was established that the aircraft will have two engines. The PW1525G engine which could deliver up to 108.54 kN per engine was determined to be most suitable for the aircraft [24]. The output values of the initial sizing are summarised in Table 6.2.

Table 6.2: Results initial sizing

	$S\ [m^2]$	$b[m]$	$d_f\ [m]$	$l_f\ [m]$	$T_{req}\ [kN]$	$x_{LEMAC}[m]$	$x_{c.g._{empty}}$	$S_h[m^2]$	$S_v[m^2]$
config. 1	135.4	38.6	3.68	29,335	169.9	11.8	12.9	49.4	38.8
config. 2	155.4	41.3	3.68	35,815	195	18.3	17.4	55.2	43.4
config. 3	157.4	41.6	3.68	35,815	197.4	18.3	17.4	56.2	44.2

6.3. Class-II estimation

The class-II weight estimation consisted of a more accurate computation of the aircraft's mass and centre of gravity location. The followed method is the Torenbeek method for 'Commercial Transport Airlines', described in *Airplane Design part V: Component Weight Estimation*' from *J.Roskam* [85]. Additionally, once the material selection was performed for the different structural parts of the aircraft, this effect was incorporated in the class-II mass estimation. This was done by calculating the fraction of mass difference between using the selected material and aluminium, which is the base material of the class-II estimation.

The result of the initial sizing is needed in order to perform the class-II weight estimation, as well as the load factors encountered during flight, presented in detail in chapter 9. The class-II weight estimation calculates the masses of the individual main structural components, the mass of the powerplant group and the mass of the fixed equipment of the aircraft. The structure mass estimation generated the mass of the wing, canard, fuselage, landing gears, nacelle and empennage. In the powerplant mass estimation the engines, fuel system and propulsion system masses are estimated separately. Finally the fixed equipment consists of mass estimations for the hydraulics, avionics, electrical system, furnishing, etc.

Initially, a detachable and interchangeable canard was considered for configuration 2 and 3. This resulted in differing initial class-II mass estimates for these configurations. The centre of gravity of each of the structural components is estimated based on their individual centre of gravity, retrieved from [85], and their position on the aircraft. In Table 6.3 and 6.4 the initial results of the class-II c.g. and mass estimation, respectively, are presented for each configuration. The c.g. locations are expressed in the main coordinate system of the aircraft, presented in Figure 6.3.

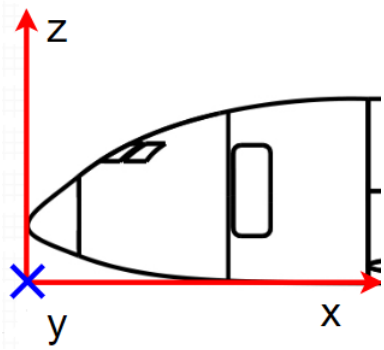

Figure 6.3: Coordinate system used

Table 6.3: Initial results of class-II centre of gravity estimation

	$x_{c.g.}$ $[m]$	$y_{c.g.}$ $[m]$	$z_{c.g.}$ $[m]$
Config.1	12.4	0.0	0.59
Config.2	16.8	0.0	0.66
Config.3	16.7	0.0	0.66

Table 6.4: Initial results of class-II mass estimation

	$M_{structures}$ $[kg]$	$M_{powerplant}$ $[kg]$	$M_{fixedeq}[kg]$	OEM $[kg]$
Config.1	22,656.7	4,875.9	8,295.9	35,828.4
Config.2	24,705.8	4,855.7	9,667.1	39,228.6
Config.3	24,965.9	4,889.4	9,667.1	39,522.3

7 Aerodynamics

In this chapter the aerodynamic analysis executed in the final phase of the project is elaborated upon. First, the initial sizing of the high lift devices (HLD) is pointed out in section 7.1, since this is needed for the detailed aerodynamic design. After that, the drag coefficient, lift coefficient and moment coefficient calculations are explained in section 7.2-7.4. This is followed by Table 7.5, which presents the results. After that, section 7.6 shows the verification and validation of the aerodynamics analysis. The chapter is concluded with a sensitivity analysis, presented in section 7.7.

7.1. High lift devices

The purpose of high lift devices is to provide enough lift and postpone stall during landing and take-off. The trailing edge (TE) devices are mainly used for the lift provision, whereas the leading edge (LE) devices are used for better stall characteristics. From this, it flows that the trailing edge devices will be sized based on the maximum lift coefficient ($C_{L_{max}}$) that must be achieved during take-off and landing. From class-I estimations used in earlier phase of the project, the $C_{L_{max}}$ values for clean flight, take-off and landing were determined to be 1.5, 1.9 and 2.4 respectively. Since initial sizing of HLDs usually takes place during this initial phase of design, these values will be used to do this. As the TE devices are used for the increase in $C_{L_{max}}$, the maximum possible increase must be used to size them. Therefore a $\Delta C_{L_{max}}$ of 0.9, the difference between clean and landing, will be used. After the detailed calculations for the lift and drag coefficient, these values will be updated in order to prevent overdesigning of the HLDs. Sizing the trailing edge devices starts with choosing a specific type of TE device. Based on the HLDs given in the ADSEE-II slides [72], and their expected $\Delta C_{L_{max}}$, the double slotted flaps were chosen. Furthermore, some assumptions were made on the placing of the flaps. A typical location for the spars is 15% and 60% for the front spar and rear spar respectively. Next to this, about 5% of the chord length must be kept free between the spar and a HLD. Therefore, it was decided that the double slotted flaps will have a chord of 35% of the total chord length. A basic outline of the double slotted flaps can be seen in Figure 7.1 [54][1]. For further calculations on the lift increment due to the flaps, a more detailed geometry of the HLD is needed. In this phase of aircraft design, it is not possible to determine this according to an engineering method. Therefore, at this stage it is estimated in such a way that the results are the most optimum for the design. For the double slotted flaps the chord of both flaps had to be determined. The first flap length, C1, was estimated to be 0.2 times the chord and the second flap length, C2, was estimated to be 0.17 times the chord. The maximum deflection was fixed on 20° for take-off and 50° for landing. Lastly, the total chord length with extended flaps, C', was estimated to be 1.2 times the chord length [51].

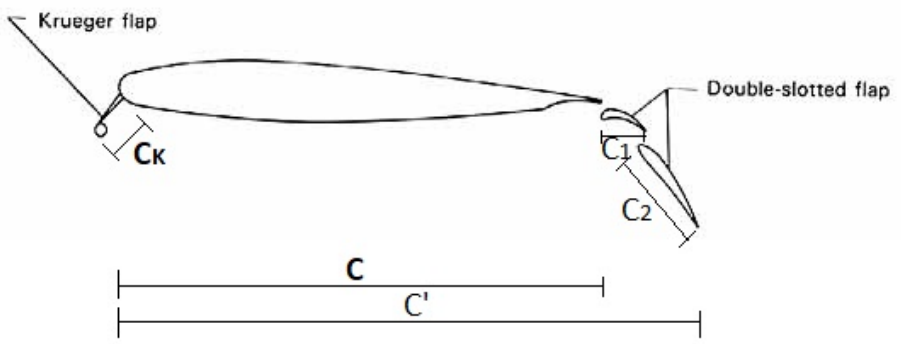

Figure 7.1: Cross section of the airfoil including the double slotted flaps and Krueger flaps [54]

As mentioned before, the leading edge devices are added in order to prevent stalling at an early angle of attack. This is because the LE HLDs energise the flow, which results in a renewed thin and stable boundary layer over the airfoil. This postpones flow separation, which means a higher stall angle. Again, before sizing, a choice must be made on what type of leading edge HLD will be used. This choice is also based on the ADSEE-II lectures [72]. It was determined that the Krueger flap will be used, due to its easy shape and low level of complexity. For this device, a length of 0.1 of the chord was chosen and a maximum deflection of 60°. For further sizing of the HLDs,

[1] https://history.nasa.gov/SP-468/ch10-5.htm [cited on 17 June 2019]

the increment in lift during flap extension must be known as well. Leading edge HLDs typically have a $\Delta C_{L_{max}}$ of 0.1, which will be used here as well [72].

During sizing of the HLDs the span of the flaps will be determined. This is done with the help of the so-called reference wing flapped surface (Swf), which is the area of the wing affected by the HLDs. This can be calculated with the help of Equation 7.1. The sweep of the hinge line, Λ_{hinge_line}, is based on an estimate for the location of the hinge line, which is determined with the help of the flaps chord length. Rewriting the equations leads to Swf for both trailing edge and leading edge HLDs. Assuming that the trailing edge devices start at 0.1 m from the fuselage its span is 16.5 m. The leading edge device starts at a distance of 0.5 m from the fuselage. The reason they start further from the fuselage is because due to the lack of LE devices the wing root will stall earlier than the wing tip, which is preferable. The wing span of the leading edge HLDs is 25.7 m.

$$\Delta C_{L_{max}} = 0.9 C_{l_{max}} \frac{Swf}{S} cos\Lambda_{hinge\_line} \tag{7.1}$$

7.2. Lift

The lift calculations are done first for the airfoil, after which the different parameters are calculated for the wing and after that for the total aircraft. This will be done for both flaps up and flaps down. The most important parameters that will be determined are the maximum lift coefficient, $C_{L_{max}}$, the lift curve slope C_{L_α} and the zero angle of attack lift coefficient C_{L_0} as well as the zero lift angle of attack, α_{0_L}. Furthermore, for flaps down a $\Delta C_{L_{max}}$ and ΔC_{L_α} will be determined. Next to that, for flaps up these parameters will be determined for both subsonic and transonic flight conditions. Since the flaps are only needed for landing and take-off, these parameters are only calculated in subsonic flight only. One note must be made for the calculations for the flaps down. For improving both stall and lift characteristics it was chosen to have trailing edge and leading edge HLDs. The total difference in $C_{L_{max}}$ and C_{L_α} must be calculated per HLD and after that they are added together. However, after combining them on one wing they will influence each others performance. In preliminary design it is acceptable to add the increments due to both HLDs, however this will lead to a small, negligible, over-prediction of the lifting capabilities of the wing [83].

Airfoil lift flaps up

An airfoil for the design was chosen in the initial stage of the project. It was determined that the NACA65-615 airfoil will be used from the root up to the mean aerodynamic chord, and the NACA66-615 airfoil will be positioned from the MAC to the wing tip [35]. From Javafoil, the parameters of the airfoils were determined, such as the slope of the lift curve C_{l_α}, the maximum lift coefficient $C_{l_{max}}$, the maximum lift angle of attack $\alpha_{C_{L_{max}}}$, the zero lift angle of attack $\alpha_{L=0}$, and the range in which the lift curve is linear α^*. The found parameters for the NACA 65-615 airfoil are without the correction for the mach number, and are used for the wing and airplane lift calculations.

Airfoil lift flaps down

For flaps down an increment for the different characteristics are determined, for both LE (Krueger flap) and TE (double slotted flap) high lift devices. To do this for the double slotted flap the chord length of both flap extensions are needed as well as some values on how long the chord is with the extensions. These values were estimated in this phase of the design, as mentioned in section 7.1. Equation 7.2 to Equation 7.6 show the equations with which the different increments can be calculated.

$$\Delta c_l = \eta_1 (c_{l_{\delta_{f_1}}})(\delta_{f_1})(c'_a/c) + \eta_2 \eta_t (c_{l_{\delta_{f_2}}})(\delta_{f_2})\Big(1 + (c' - c'_a)/c\Big) \tag{7.2}$$

$$\Delta c_l = c_{l_\delta} \delta_f (c'/c) \tag{7.3}$$

$$(c_{l_\alpha})_\delta = (c'/c) c_{l_\alpha} \tag{7.4}$$

$$\Delta c_{l_{max}} = k_1 k_2 k_3 (\Delta c_{l_{max}})_{base} \tag{7.5}$$

$$\Delta c_{l_{max}} = (c_{l_{\delta_{max}}}) \eta_{max} \delta_f (c'/c) \tag{7.6}$$

Equation 7.2 gives the increment in c_l due to the double slotted flaps. The numbers 1 and 2 refer to the extended flaps, as can be seen in Figure 7.1. Furthermore, η and $c_{l_{\delta_{f_{1,2}}}}$ are constants picked from graphs based on chord extension and deflection angle. Lastly, c'_a is the chord extension if both flaps were deflected as if it was one flap. Equation 7.3 is the increment in C_{l_0} due to the Krueger flap. The c_{l_δ} is the leading edge flap effectiveness parameter, which is based on the chord extension due to the Krueger flap. Furthermore, a special note must be made here. The flapped chord length c' is different than for the TE high lift device, because it is now the chord

length with Krueger flap extended and the double slotted flaps not extended. The increment in C_{l_α}, as can be seen in Equation 7.4, is based on the lift curve slope from the airfoil as determined during flaps up calculations. Finally, the increase in maximum lift coefficient can be calculated with Equation 7.5 and Equation 7.6 for the TE and LE high lift devices respectively. For the TE HLDs, $k1$, $k2$ and $k3$ are factors that account for flap geometry and deflection, based on statistical data [83]. $(\Delta c_{l_{max}})_{base}$ is a reference increment based on flap type and thickness to chord ratio. For the LE HLD, $c_{l_{\delta_{max}}}$ is a theoretical maximum lifting effectiveness for the Krueger flap and η_{max} is a factor that accounts for the geometry of the flap, also based on statistical data [83].

Wing lift flaps up

For the wing, the same parameters as for the airfoil are determined. This is mainly done by taking the airfoil parameter and correcting it for the wing parameters. It is assumed that the linear range of the airfoil lift curve is the same for the wing lift curve.

$$\alpha_{0_{L_w}} = \left[\alpha_{0_l} + \frac{\Delta\alpha_0}{\epsilon_t}\epsilon_t\right]\frac{(\alpha_{0_l})_{\text{at M}}}{(\alpha_{0_l})_{\text{at M=0.3}}} \tag{7.7}$$

$$C_{L_{\alpha_w}} = \left[2\pi A\right]/\left[2+\sqrt{(4+\left(\frac{A\beta}{k}\right)^2\left(1+\left(\frac{tan(\lambda_{c/2})^2)}{\beta^2}\right)\right)}\right] \tag{7.8}$$

The angle of attack for the maximum lift coefficient $\alpha_{C_{L_{max}}}$ is found from the spanwise distribution of section maximum lift coefficient, and the wing lift distribution. The wing lift distribution for various angles of attack is found from [44]. If the spanwise distribution of section maximum lift coefficient is tangent to the wing lift distribution for a certain angle of attack, that angle of attack will be the maximum lift angle of attack for the wing. The produced figure can be seen in Figure 7.2. When decreasing the step size of α, it can be found that the angle of attack of maximum lift of the wing is 9.75°. This leads to a wing maximum lift coefficient of 2.003 in clean configuration. A wing twist angle of −3° is added to move the maximum lift coefficient to a lower spanwise location, in order to make sure the wing stalls more towards the root of the wing instead of the tip [83]. This is desired, as wing tip stall may lead to an uncontrollable aircraft.

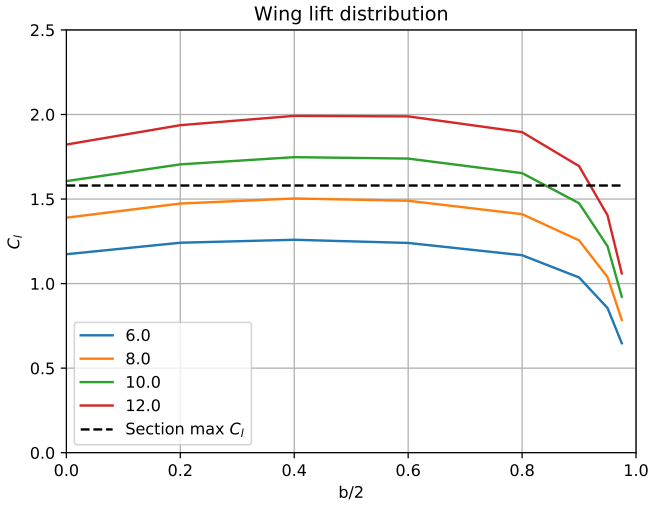

Figure 7.2: Wing lift distribution for configuration 1

Wing lift flaps down

For the wing lift with flaps down, mostly the parameters from the airfoil flaps down are used. ΔC_{L_w} is the extra lift at zero angle of attack provided by the flaps. $(C_{L_{\alpha_w}})_\delta$ is the new lift curve slope of the lift curve with flaps. The $\Delta C_{L_{max_w}}$ calculated in Equation 7.11 and 7.12 is the change in maximum lift coefficient due to the trailing and leading edge HLDs, respectively.

$$\Delta C_{L_w} = K_b(\Delta C_l)(C_{L_{\alpha_w}}/C_{l_\alpha})\frac{(\alpha_\delta)_{C_L}}{(\alpha_\delta)_{C_l}} \tag{7.9}$$

$$(C_{L_{\alpha_w}})_\delta = C_{L_{\alpha_w}}\left(1+(c'-1)\frac{S_{w_f}}{S}\right) \tag{7.10}$$

$$\Delta C_{L_{max_w}} = \Delta c_{l_{max}}\frac{S_{w_f}}{S}K_\Delta \tag{7.11}$$

$$\Delta C_{L_{max_w}} = 7.11\frac{c_f}{c}\left(\frac{b_{LE}}{b_e}\right)^2(cos(\lambda_{c/4}))^2 \tag{7.12}$$

Airplane flaps up

The total airplane lift has three contributions: wing lift, canard lift and horizontal tail lift and builds on lift calculations for the airfoil and the wing. Two important parameters that will come back often during the upcoming calculations are lift curve slopes of the horizontal tail and the canard, $C_{L_{\alpha_h}}$ and $C_{L_{\alpha_c}}$ respectively. These values can be calculated with Equation 7.8, by filling in the correct geometry for the different components. During the airplane flaps up calculations Equation 7.13 to Equation 7.16 are used to determine all needed values. The final goal is being able to plot a $C_L - \alpha$ curve.

$$\alpha_{0_L} = (-C_{L_0}/C_{L_\alpha}) \tag{7.13}$$

$$C_{L_0} = C_{L_{0_{wf}}} + C_{L_{\alpha_h}} \eta_h (S_h/S)(i_h) + C_{L_{\alpha_c}} \eta_c (S_c/S)(i_c) \tag{7.14}$$

$$C_{L_\alpha} = C_{L_{\alpha_{wf}}} + C_{L_{\alpha_h}} \eta_h (S_h/S)(1 - de/d\alpha) + C_{L_{\alpha_c}} \eta_c (S_c/S)(1 - de_c/d\alpha) \tag{7.15}$$

$$\begin{aligned} C_{L_{max}} = C_{L_{max_w}} - (C_{L_{\alpha_{wf}}})\Delta\alpha_{w/c} + \\ (C_{L_{\alpha_h}})(S_h/S)\Big((\alpha_{C_{L_{max}}})(1 - de/d\alpha) + i_h\Big) + (C_{L_{\alpha_c}})(S_c/S)\Big((\alpha_{C_{L_{max}}})(1 + de_c/d\alpha) + i_c\Big) \end{aligned} \tag{7.16}$$

Most parameters mentioned throughout these equations are already mentioned for previous calculations. However, there are some important characteristics that need special attention. The first one is η_h. This is the ratio between the dynamic pressure of the horizontal tail and the wing. Due to downwash this is not the same. The velocity over the horizontal tail is usually smaller than the one over the wing. As an estimate 0.9 is chosen here [92][2]. For the canard, in early phase of the design it is acceptable to assume η_c is zero, based on Roskam [83]. Next to this, $C_{L_{0_{wf}}}$ and $C_{L_{\alpha_{wf}}}$ are the zero angle of attack lift coefficient and the lift curve slope for the wing-fuselage combination. This depends on the values for the wing, however an interference factor is taken into account. Lastly, $\Delta\alpha_{w/c}$ is the difference in stall angle of the canard and the wing. In preliminary design, Roskam suggests to use 3°. At this point, all values are available to perform the calculations.

Airplane flaps downs

To finalise the lift calculations, the different parameters must be calculated for the airplane with flaps down. These calculations again continue on previous calculations. The equations that are needed are the following:

$$\Delta C_L = k_{cw}\Delta C_{L_W} + k_{cw}(S_c/S)\Delta C_{L_c} + k_{wh}(S_h/S)\Delta C_{L_h} - C_{L_{\alpha_h}} \eta_h (S_h/S)\Delta\epsilon_f \tag{7.17}$$

$$(C_{L_\alpha})_\delta = k_{wf}(C_{L_{\alpha_w}})_\delta + C_{L_{\alpha_h}} \eta_h (S_h/S)\Big(1 - (de/da)_\delta\Big) + C_{L_{\alpha_c}} \eta_c (S_c/S)\Big(1 - (de_c/da)_\delta\Big) \tag{7.18}$$

$$\Delta C_{L_{max}} = k_{cw}\Delta C_{L_{max_w}} - (C_{L_{\alpha_w}})_\delta \Delta\alpha_{w/c} + (S_c/S)\Delta C_{L_{max_c}} + (S_h/S)C_{L_{\alpha_h}}\Big((1 - de/d\alpha) + i_h - \Delta\epsilon_f\Big) \tag{7.19}$$

Again, most values are already calculated in earlier aerodynamic calculations, however some new parameters need special attention here. The first is k_{cw}. This is the interference factor between the canard and the wing. It is only possible to determine this with advanced finite element aerodynamic tools. Roskam [83] suggests to take $k_{cw} = 1$, for a canard which is sufficiently small and sufficiently far forward. However, it is assumed that this is not valid for the current canard. Therefore, only a rough estimation is made and the value is set at 0.95. Because only estimations can be made at this point, this factor will be used in the sensitivity analysis, as can be seen in section 7.7. Furthermore, $\Delta\epsilon_f$ is the increase in downwash angle due to the flap deflection and has to be estimated from a graph, based on aircraft geometry. Finally, k_{wf} is the interference factor between wing and fuselage. It is based on the wing span and fuselage diameter. With these final calculations, it is possible to plot the $C_L - \alpha$ curve for the flaps extended configuration as well.

[2]URL: https://www.fzt.haw-hamburg.de/pers/Scholz/HOOU/AircraftDesign_11_EmpennageSizing.pdf [cited on 22-06-2019]

7.3. Drag

For the drag, a class-II estimation will be done in this phase of the project. The drag of the different aircraft parts will be estimated with the use of Roskam part VI [83], for both subsonic and transonic flight. The subsonic drag is the drag during take-off or landing and the transonic drag is the drag during cruise flight. For now it is assumed that the drag of the different components consists of two types. The first type is called zero-lift drag, C_{D_0}, and the second type is lift induced drag, C_{D_L}. For transonic flight wave drag is added to C_{D_0}. This is a type of drag that arises during transonic and supersonic flight due to shock waves on the wing. These shock waves are present because the local Mach number over the wing is higher than one, due to its high cruise Mach number of 0.75. Furthermore, due to the calculations for both subsonic, incompressible flow, and transonic, compressible flow, the compressibility effects are also taken into account.

Wing

When determining the wing drag coefficient, the flaps extension is assumed to be zero. The drag caused by the flaps is determined by a different approach, which will be explained in a later section. Included in the wing drag, is the wing-fuselage interference, which is represented by R_{wf}. This is determined by the Reynolds number of the fuselage and is part of the zero lift drag $C_{D_{0_w}}$. Furthermore, the zero lift drag consist of a lifting surface correction factor R_{LS}, the turbulent flat plate friction coefficient C_{f_w}, the airfoil thickness location parameter L', the thickness over chord ratio $\frac{t}{c}$, and the wetted surface area over the surface area $\frac{S_{wet}}{S}$, as can be seen in Equation 7.20. When flying in the transonic region, the wave drag component is added to the zero lift drag. This drag parameter is found from the Roskam VI book, and is estimated to be 0.002.

$$C_{D_{0_w}} = R_{wf} R_{LS} C_{f_w} \left(1 + L' \frac{t}{c} + 100\left(\frac{t}{c}\right)^4\right) \frac{S_{wet}}{S} \quad (7.20) \qquad C_{D_{L_w}} = \frac{C_{D_L}}{C_L^2} C_{L_w}^2 \quad (7.21)$$

Next to the zero lift drag, the induced drag is calculated. This is dependent on the velocity of the aircraft. During cruise, the aircraft flies in the transonic regime, and therefore the transonic induced drag is used for this flight phase. For the subsonic flight region, the corresponding induced drag is used. The transonic and subsonic drag are determined by using Equation 7.21 and Equation 7.22 respectively.

$$C_{D_{L_w}} = \frac{C_{L_w}^2}{\pi A e} + 2\pi C_{L_w} \epsilon_t v + 4\pi^2 (\epsilon_t)^2 w \quad (7.22) \qquad e = 1.1\left(\frac{C_{L_{a_w}}}{A}\right) / \left(R\left(\frac{C_{L_{a_w}}}{A}\right) + (1-R)\pi\right) \quad (7.23)$$

The subsonic induced drag is dependent on the lift coefficient of the wing, the Oswald factor e, the aspect ratio A, the wings twist ϵ_t, and two wing twist correction parameters v and w. The Oswald factor is dependent on the lift curve slope $C_{L_{a_w}}$, the aspect ratio, and the leading edge suction parameter R, as can be seen in Equation 7.23. The $C_{L_{a_w}}$ is determined from the DATCOM method found in section 7.2. The transonic induced drag is only dependent on the induced drag parameter C_{D_L}/C_L^2 and the lift coefficient itself, where the induced drag parameter is found as a function of transonic similarity parameters in the Roskam book [83]. To determine the entire wing drag component during subsonic flight, the $C_{D_{0_w}}$ and the $C_{D_{L_w}}$ for subsonic flight are added together. For transonic flight, $C_{D_{0_w}}$, $C_{D_{wave}}$, and $C_{D_{L_w}}$ for transonic flight are added together.

Fuselage

The zero-lift drag depends on a few characteristics, such as fuselage length l_f, fuselage diameter d_f, and the fuselage wetted area $S_{wet_{fus}}$. This is the area of the fuselage that is in contact with the airflow and therefore the area that is responsible for C_{D_0}. This is compared by a reference area, which is the wing area S. By doing this for all components, the drag coefficients are normalised. With Equation 7.24, the $C_{D_{0_{fus}}}$ can be calculated. A special factor here is R_{wf}, which is the interference factor between the wing and fuselage. Due to this factor, the fuselage is not analysed as a single part, but as a component of a larger system. $C_{f_{fus}}$ is the turbulent flat plate skin-friction, which is a function of the Mach number and the Reynolds number. Finally, $C_{D_{b_{fus}}}$ is the fuselage base-drag coefficient, which is a drag coefficient due to an abrupt, not smooth, cut-off at the end of the fuselage.

$$C_{D_{0_{fus}}} = R_{wf} C_{f_{fus}} (1 + 60/(l_f/d_f)^3 + 0.0025(l_f/d_f)) S_{wet_{fus}}/S + C_{D_{b_{fus}}} \quad (7.24)$$

After this, the lift induced drag of the fuselage was calculated. For this the cruise angle of attack was needed, because this angle determines how far the lift vector on the wing is tilted backwards. The further it is tilted, the higher the drag component. This angle can be calculated with Equation 7.25.

$$\alpha = (\frac{W}{qS} - C_{L_0})/C_{L_\alpha} \tag{7.25}$$

The values for the zero angle lift coefficient C_{L_0} and lift curve slope C_{L_α} come from the aircraft lift calculations as mentioned in section 7.2. The dynamic pressure and weights are chosen to be those during cruise. This is done because the aircraft will mainly fly at this angle and therefore this will result in the most accurate value for the drag. The lift induced drag can be calculated with Equation 7.26.

$$C_{D_{L_{fus}}} = 2\alpha^2 S_{b_{fus}}/S + \eta c_{d_c} \alpha^3 S_{plf_{fus}}/S \tag{7.26}$$

Here $S_{b_{fus}}$ is the fuselage base area, η is ratio for the drag of a finite cylinder to the drag of an infinite cylinder and c_{d_c} is estimate for the cross-flow drag. Finally, $S_{plf_{fus}}$ is the fuselage planform area, which is the area as seen from a top view of the aircraft.

Lastly, the wave drag must be added for transonic flight. The wave drag depends on the Mach number and the fuselage fineness ratio, l_f/d_f. Based on these values it is estimated to be 0.005. Because wave drag is very hard to predict and this value is only an estimate, it will be part of the sensitivity analysis, discussed in section 7.7.

Empennage

The empennage drag calculation consists of three parts: canard drag, horizontal tail drag, and vertical tail drag calculation. The calculations for these three components are similar to the drag calculations of the wing, because it has the same shape. C_{D_0} is determined with Equation 7.20, by replacing some main wing parameters by parameters of the empennage. These are mainly parameters concerning the geometry. For the C_{D_L} only the horizontal tail and canard are taken into account. Special cases in which the aircraft is flying with a sideslip are not considered in this phase of the design and therefore the lift induced drag of the vertical tail is assumed to be zero.

For both the canard and the horizontal tail the lift coefficient needs to be calculated. This can be done with Equation 7.27, where x can be either h for horizontal tailplane or c for canard. The lift curve slope followed from the lift calculations. The angle of the empennage can be determined with Equation 7.28. Here, α is the angle of attack as calculated for the fuselage and $\frac{de}{d\alpha}$ is the downwash gradient. Furthermore, i is the angle of incidence, which is the angle under which the wing or other surface is placed on the aircraft. Lastly, α_{0_L} is the zero lift angle of attack, which also follows from the lift calculations.

$$C_{L_x} = C_{L_{\alpha_x}}(\alpha_x - \alpha_{0_{L_x}}) \tag{7.27}$$

$$\alpha_x = \alpha(1 - \frac{de}{d\alpha}) + i_x \tag{7.28}$$

with the lift coefficient of the horizontal tail and the canard it is possible to calculate C_{D_L}. This can be done with Equation 7.29, where the geometric properties of the empennage surfaces are needed as well. Next to this, their Oswald efficiency factors are needed. For this, Roskam gives an estimate of 0.75 for e_h and 0.5 for e_c [83]. With all the information given, $C_{D_{i_{emp}}}$ for both the horizontal tail and canard can be determined.

$$C_{D_{L_{emp}}} = (\frac{C_{L_h}^2}{\pi A_h e_h})\frac{S_h}{S} + (\frac{C_{L_c}^2}{\pi A_c e_c})\frac{S_c}{S} \tag{7.29}$$

The last step is accounting for transonic flight conditions. Roskam estimates the wave drag coefficient for all empennage surfaces to be 0.002. For the lift induced drag, Equation 7.21 can be used after changing the lift coefficient of the wing for the canard and the horizontal tail.

Other drag components

Next to the before mentioned drag components, some other components are responsible for drag. However, their calculations can be based on equations mentioned previously or have a smaller contribution. Therefore they are mentioned only briefly here.

Nacelle/pylon: In this stage of the design, the pylon is not taken into account. More information is needed to be able to size these parts. Therefore only the nacelle drag will be determined. To do this, it is assumed that the nacelle is a small fuselage and therefore, the steps taken for the fuselage can be used here again. For the zero lift drag C_{D_0} Equation 7.24 was used and for the lift induced drag Equation 7.26 was used. The geometry of the fuselage was changed to the geometry of the nacelle. Special attention must be made to the angle of attack of the nacelle. This was calculated as shown in Equation 7.30. Here, ϵ_n is the nacelle downwash angle as can be seen in Equation 7.31. This can be calculated with equations used during lift calculations.

$$\alpha_n = \alpha_w + i_n + \epsilon_n \tag{7.30}$$

$$\epsilon_n = (\frac{d\epsilon_n}{d\alpha}))\alpha \tag{7.31}$$

For the transonic calculations the same equations as for fuselage transonic calculations will be used. This means adding a wave drag component. However, for the nacelle this turned out to be zero.

Flaps: Since flaps are only used during take-off and landing, the flap's drag will be calculated for subsonic flight only. The drag consists of three parts: flap profile drag, lift induced drag and interference drag. The first one is due to the flap itself and could therefore be seen as the zero lift drag of the flap. The lift induced drag is due to the extra lift that is created because of the presence of the flap. Finally, the interference drag is drag due to the airflow over the wing and airflow over the flaps mixing up. The drag was calculated for both take-off and landing, due to different flap deflection and furthermore it was calculated for the trailing edge double slotted flaps and the leading edge Krueger flaps.

Landing gear: The drag of the landing gear only plays minor role in the entire flight profile of the aircraft, as the landing gear will only be deployed during take-off and right before landing. It can therefore be assumed that the landing gear drag is only in the subsonic regime. The drag consists of a summation of the zero lift drag plus a correction factor for the nose and main landing gear. The drag coefficient is scaled by the ratio between the area of the gear and the wing surface area.

$$C_{D_{gear}} = \sum_{i=1}^{n} \left[\left((C_{D_{gear_{C_L=0}}})_i + p_i C_L \right) \frac{(S_{gear})_i}{S} \right] \tag{7.32}$$

Wind shield: Following the procedure in [83], the drag from the wind shield can be found. The cockpit is streamlined, meaning that no edges are present in the windshield. Therefore, the delta drag in Equation 7.33 is assumed to be 0.002 [83]. With S_{ws} being the frontal area, the drag caused by the wind shield can be found.

$$C_{D_{ws}} = \Delta_{C_{D_{ws}}} \cdot \frac{S_{ws}}{S} \tag{7.33}$$

$$\Delta C_{D_{trim_{lift}}} = ((\Delta C_{L_h})^2/(\pi A_h e_h)) \frac{S}{S_h} \tag{7.34}$$

Trim drag: Trim drag is a result of the lift produced by the horizontal stabiliser needed to trim the aircraft. The canard is not equipped with control surfaces, so it does not generate trim drag. The trim drag consists of two components, the trim drag due to lift generated on the trimming surface and the profile drag generated by the trimming surface due to a control surface deflection. The trim drag due-to-lift is determined by Equation 7.34, which is similar to the wing lift induced drag, but instead for the trim condition of the horizontal stabiliser, scaled by the ratio between the wing surface area and the horizontal stabiliser surface area.

$$\Delta C_{D_{trim_{prof}}} = \Delta C_{D_{p_{\lambda_{c/4=0}}}} cos(\lambda_{c/4}) \left(\frac{S_{elev}}{S_h} \right) \left(\frac{S_h}{S} \right) \tag{7.35}$$

The profile drag due to the deflection is determined by Equation 7.35. Here, $\Delta C_{D_{p_{\lambda_{c/4=0}}}}$ is calculated using the same procedure as for the drag of the flaps. In this calculation, the elevator is assumed to be a plain flap, and the parameters for the horizontal stabiliser are used instead of the wing parameters. Adding the profile drag and the drag due to lift together finally yields the total trim drag.

Spoilers: The drag of the spoilers is determined by Equation 7.36, where $\Delta C_{D_{sp_i}}$ is the change in drag due to the spoiler and where S_{sp_i} is the flat plate area of each spoiler. For the first estimate, the flat plate area of each spoiler is assumed to be 12 m^2. From this, the additional drag is calculated when the spoilers are activated for aerodynamic braking.

$$\Delta C_{D_{sp}} = \sum_{i=1}^{n} \left[\Delta C_{D_{sp_i}} \left(\frac{S_{sp_i}}{S} \right) \right] \tag{7.36}$$

Surface roughness: The methods for determining the friction and profile drag for the aircraft wing and fuselage (as presented in the beginning of this section) only hold for smooth surfaces. If the surface of the wing or fuselage is rough, the actual level of turbulent boundary layer friction drag may be higher. For determining if the C_{f_w} in Equation 7.20 and $C_{f_{fus}}$ in Equation 7.24 must be adjusted, l/k is calculated, where l is the reference length and k the equivalent sand roughness. From Roskam [83], k is found to be 0.00000167 ft. With the average chord and fuselage length in feet, l_f/k and $\bar{c}_w/k$ are determined. This is used to find the cut-off Reynolds number. This Reynolds number is compared to the actual Reynolds number for both the wing and fuselage. If the cut-off Reynolds number would be lower than the actual Reynolds number, C_{f_w} and $C_{f_{fus}}$ would have to be determined based on the cut-off Reynolds number instead of the actual Reynolds number. However, the actual Reynolds

number is found to be lower than the cut-off Reynolds number, so C_{f_w} and $C_{f_{fus}}$ does not have to be corrected for surface roughness.

7.4. Aerodynamic moment

The calculations of the moment coefficients can be compared with the calculations for the lift coefficients. First the airfoil will be analysed for flaps up and down and after that the same will be done for the wing. The total aircraft is not analysed here, because only the wing moment coefficient will be used for designing for control and stability in chapter 8. For the calculations a reference point on the airfoil must be chosen. This can be any point and for the output values that are given in the next section, 0.5c is chosen as reference.

Airfoil flaps up

The moment coefficient for the airfoil flaps up come from the basic simulation program used in the previous phase of the design, which was Javafoil. With this program, the moment coefficient at zero lift c_{m_0} can be determined for the chosen airfoils, both of them are -0.123. This will therefore be the c_{m_0} with which the upcoming calculations are executed. Furthermore, it is assumed that the aerodynamic centre is at the quarter chord point. This is the point around which the aerodynamic moment does not change if the angle of attack changes. The value of this is c_{m_0}. Lastly, with Equation 7.37 the moment coefficient can be calculated at any point on the airfoil.

$$c_m = c_{m_0} + c_l(x_{ref} - x_{ac})/c \tag{7.37}$$

$$\Delta c_m = \Delta c_l\Big(x_{ref}/c - (x_{cp}/c')(c'/c)\Big) \tag{7.38}$$

Airfoil flaps down

For flaps down, again increments will be calculated. This must be done for both the leading edge and trailing edge HLDs. Equation 7.38 gives the increment due to the TE HLDs and Equation 7.39 gives the increment due to LE HLDs. Most parameters come from earlier (lift) calculations.

$$\Delta c_{m_{le}} = (c_{m_{\delta le}})'(c'/c)^2\delta_{fle} + \Big((x_{ref}/c) + (c'-c)/c\Big)\Delta c_{l_{le}} + c_m\Big((c'/c)^2 - 1\Big) + 0.75c_l(c'/c)\Big((c'/c) - 1\Big) \tag{7.39}$$

The x_{cp} is the centre of pressure, which is the point where the resultant force, which is caused by the pressure distribution over the airfoil, acts on. Furthermore, x_{cp}/c' and $c_{m_{\delta le}}$ are based on the flapped chord length and come from graphs.

Wing flaps up

The zero lift moment coefficient for the wing, $C_{m_{0_w}}$ is given by Equation 7.40. As can be seen, it depends on the geometry. Furthermore, $c_{m_{0_r}}$ and $c_{m_{0_t}}$ are the zero lift moment coefficient for the root and tip for the airfoil respectively. These values are determined with Javafoil. $\Delta C_{m_0}/\epsilon_t$ comes from a graph that depends on the quarter chord sweep angle. Finally, ϵ_t is the wing twist.

$$C_{m_{0_w}} = \Big((A\cos^2\Lambda_{c/4})/(A + 2\cos\Lambda_{c/4})\Big)(c_{m_{0_r}} + c_{m_{0_t}})/2 + (\Delta C_{m_0}/\epsilon_t)\epsilon_t \tag{7.40}$$

Wing flaps down

The last step in the aerodynamic analysis is the increment in zero lift moment coefficient due to flaps on the wing. The increment due to trailing edge flaps can be calculated with Equation 7.41 and the increment due to the leading edge flaps can be calculated with Equation 7.42.

$$\Delta C_{m_w} = (x_{ref} - 0.25)(C_{L_w})_\delta + K_\Lambda(A/1.5)(\Delta C_{L_{ref_w}})\tan\Lambda_{c/4} + K_p\Big((\Delta C'_m/\Delta C_{L_{ref_w}})\Delta C_{L_{ref_w}}(c'/c)^2\Big) - K_p[0.25C_{L_w}\Big((c'/c)^2 - (c'/c)\Big)] + K_p C_{m_w}\Big((c'/c)^2 - 1\Big) \tag{7.41}$$

$$\Delta C_{m_w} = \Big((c_{m_{\delta le}})'(c'/c) + (n_{ref} - n_{le})c_{l_\delta}\Big)(S_{wf}/S)\delta_f + [C_{m_w}\Big((c'/c)^2 - 1\Big) + 0.75C_{L_w}\Big((c'/c)(c'-c)/c)\Big)](b_{lef}/b) \tag{7.42}$$

Some new parameters appear. First, $\Delta C_{L_{ref_w}}$ is the lift increment for a reference wing with an aspect ratio of 6, full span flaps and zero half chord sweep. This can be calculated with equations from section 7.2. Then, K_p

and K_Λ are factors found in Roskam and as well as $\Delta C'_m/\Delta C_{L_{refw}}$. Next to this, n_{ref} and n_{le} are the location of the reference point and the MAC leading edge as seen from root chord leading edge. Finally, b_{lef} is the total flap chord of the leading edge flaps. Now all values are known and the calculations can be finished.

7.5. Results

This section elaborates on the input values used and output values calculated.

Input values

The main input parameters for the aerodynamic analysis, are the wing geometry parameters, atmospheric data, fuselage dimensions, and airfoil data, and can be seen in Table 7.1. These parameters are used to initiate the lift calculations. Following the lift calculations, the drag calculations are done. The extra parameters needed for the drag calculations can be seen in Table 7.2.

Table 7.1: Input parameters lift

Parameter	Config. 1	Config. 3
S	120.47 $[m^2]$	
A	9.5 $[-]$	
MAC	3.89 $[m]$	
λ	0.309 $[-]$	
$\Lambda_{c/4}$	25.97 $[^\circ]$	
ϵ	-3 $[^\circ]$	
i_w	0 $[^\circ]$	
x_{LEMAC}	13.55 $[m]$	19.24 $[m]$
SWF	67.36 $[m^2]$	
b_{flap}	8.23 $[m]$	
A_h	4.95 $[-]$	
A_c	6.0 $[-]$	
$\Lambda_{h_{c/2}}$	26.44 $[^\circ]$	
$\Lambda_{c_{c/2}}$	21.76 $[^\circ]$	
i_c	0 $[^\circ]$	
i_h	0 $[^\circ]$	
S_h	28.0 $[m^2]$	35.18 $[m^2]$
S_c	0 $[m^2]$	
l_f	30.13 $[m]$	35.82 $[m]$
$d_{f_{outer}}$	3.68 $[m]$	
ρ	0.348 $[kg/m^3]$	
ρ_0	1.225 $[kg/m^3]$	
V_{cruise}	221.30 $[m/s]$	
M_{cruise}	0.75 $[-]$	
V_{TO}	59.88 $[m/s]$	64.43 $[m/s]$
μ_{cruise}	$1.43{\cdot}10^{-5}$ $[Pa\cdot s]$	
μ_0	$1.79{\cdot}10^{-5}$ $[Pa\cdot s]$	

Table 7.2: Extra input parameters drag

Parameter	Config. 1	Config. 3
x_{nlg}	2.0 $[m]$	
z_{nlg}	-3.17 $[m]$	
w_{nlg}	0.20 $[m]$	
$D_{strut_{nlg}}$	0.15 $[m]$	
z_{mlg}	-3.17 $[m]$	
w_{mlg}	0.39 $[m]$	
$D_{strut_{mlg}}$	0.19 $[m]$	
S_{elev}	9.99 $[m^2]$	
$C_{L_{des}}$	0.472 $[-]$	0.547 $[-]$
$C_{L_{\alpha_h}}$	4.61 $[1/rad]$	
$C_{L_{\alpha_c}}$	5.15 $[1/rad]$	
$\alpha_{L=0}$	-3.97 $[^\circ]$	-3.25 $[^\circ]$
ΔC_{L_h}	0 $[-]$	
ΔC_{L_c}	0 $[-]$	
MAC_c	2.68 $[m]$	
C_{r_v}	5.94 $[m]$	
C_{t_v}	2.23 $[m]$	
C_{r_h}	3.42 $[m]$	
C_{t_h}	1.33 $[m]$	
S_v	25.03 $[m^2]$	
$d\epsilon/d\alpha$	0.445 $[-]$	0.566 $[-]$
$(d\epsilon/d\alpha)_c$	0 $[-]$	0.15 $[-]$
$l_{nacelle}$	3.50 $[m]$	
$d_{nacelle}$	2.21 $[m]$	
b_slat	12.85 $[m]$	
SWF_{slat}	89.75 $[m]$	

Output values

The results of the lift, drag and moment calculations are shown in Table 7.3 and Table 7.4. The first table shows the result of the lift calculations, for both flaps up and flaps down. The first five columns show the results for flaps up. α^*, is the region in which the $C_L-\alpha$ curve is linear. The other parameters are mentioned before. The last three columns show the results for the flaps down. In the second table, the first three columns give the results for the drag for cruise, take-off and landing. The last columns show the results for the moment calculations, which start with flaps up and then gives the results for flaps down. Some comments must be made about the results. For the drag calculations, specific flight conditions were chosen as discussed in section 7.3. However, the drag changes with changing lift and angle of attack. Before using these values in further design, the flight conditions must be checked to see if the values are relevant. For the moment calculations it is important to note that they are based on C_{m_0} of the airfoil determined by Javafoil. This is only a basic simulation program which does not take into account compressibility effects. During analysis, some more advanced simulation programs, like TSfoil and SU2_EDU, were consulted, however due to time constraints and a lack of CFD (Computational Fluid Dynamics)

knowledge, it was not possible to get them running and therefore Javafoil was again used. For a next phase of the design it is therefore advised to start with detailed flow analysis over the airfoil, wing and total aircraft, taking into account compressibility effects. The results are further discussed in section 7.6, where they will be validated.

Table 7.3: The results of the aerodynamic analysis for the lift

	C_{L_α}	α_{0_L}	$C_{L_{max}}$	$\alpha_{C_{L_{max}}}$	α^*	ΔC_L	ΔC_{L_α}	$\Delta C_{L_{max}}$
Config 1	7.27	-3.97	1.75	9.75	-7 to 3	1.19	8.02	0.94
Config 2	8.99	-3.21	2.04	9.75	-7 to 3	1.19	9.29	0.94
Config 3	8.88	-3.25	2.02	9.75	-7 to 3	1.19	9.18	0.94

Table 7.4: The results of the aerodynamic analysis for the drag and moment

	$C_{D_{cruise}}$	$C_{D_{land}}$	$C_{D_{TO}}$	$C_{m_{0_{sub}}}$	$C_{m_{0_{trans}}}$	$\Delta C_{M_{w_{flaps}}}$	$\Delta C_{M_{w_{Krueger}}}$
Config 1	0.038	0.197	0.121	-0.061	-0.076	0.080	0.072
Config 2	0.044	0.204	0.128	-0.061	-0.076	0.080	0.072
Config 3	0.046	0.206	0.130	-0.061	-0.076	0.080	0.072

The results for the lift calculations can be plotted in a $C_L - \alpha$ curve. This is needed to be able to determine the lift coefficient for the full range of possible angles of attack. Figure 7.3 shows the curve for both flaps up and flaps down. This plot is made with the results for configuration 1. The kink which can be observed in the graph, is due to the quadratic interpolation between the linear lift slope and the $C_{L_{max}}$. The lift curve is linear between -7° and 3°, and almost linear between 3° and $\alpha_{C_{L_{max}}}$.

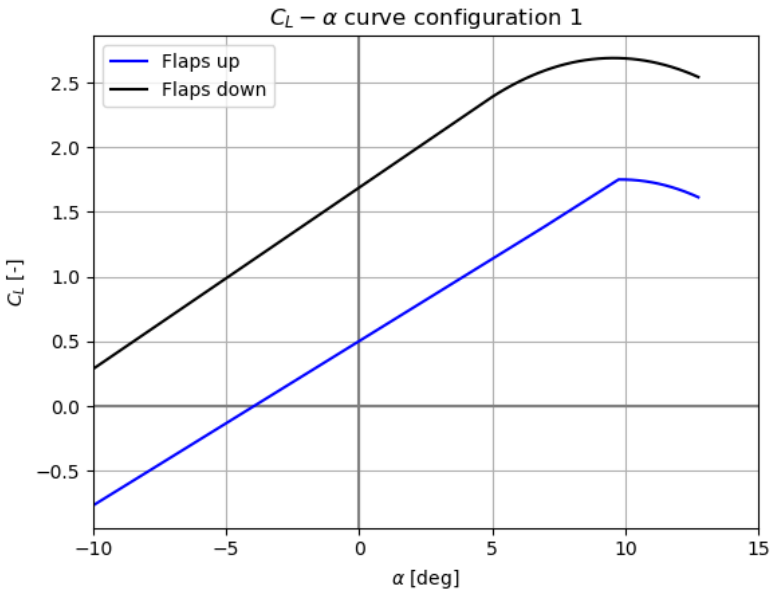

Figure 7.3: The $C_L - \alpha$ curve for the aircraft with flaps up and flaps down for configuration 1

Lastly, for the drag a breakdown structure can be created. This block diagram summarises the components that contribute to the drag and shows the corresponding values for the drag coefficients. In the case of the adaptive regional airliner, this can be done for all three configurations and for different flight conditions. Figure 7.4 presents the breakdown structure for the first configuration for the three flight phases mentioned in section 7.3. From this it can be seen that the wing contributes most to the drag during cruise. During take-off and landing, the flaps contribute most. Lastly, the drag of the spoilers is shown for landing. This drag component is however not taken into account in the total drag during landing, $C_{D,land}$. The reason for this is that the spoilers are not fully always fully deployed during approach. Because no data was available on how much they are deployed during this phase, it was decided not to use the spoiler drag in the landing drag calculations.

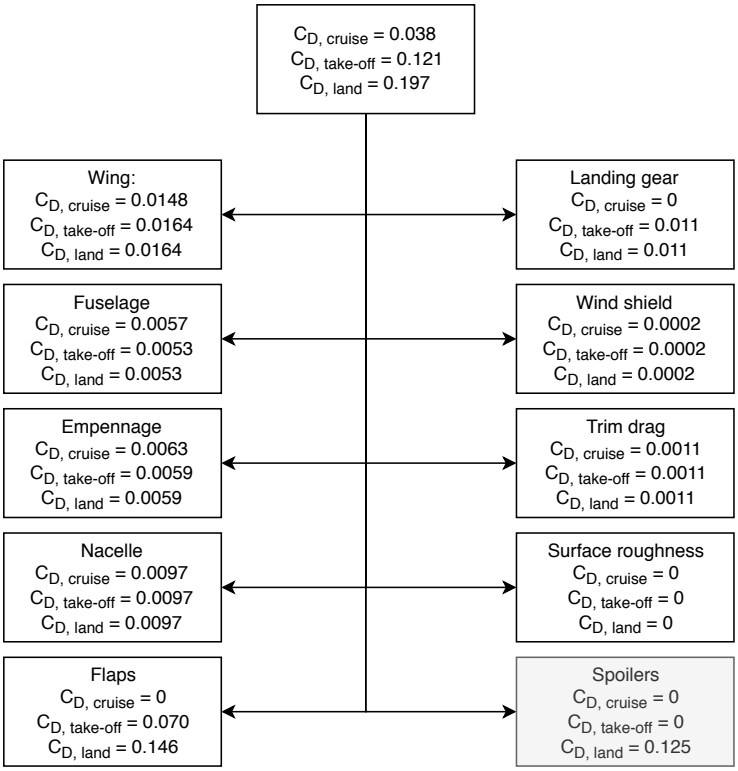

Figure 7.4: A drag breakdown structure for the drag of the first configuration for three different flight conditions

7.6. Verification and validation

For the aerodynamics department, verification must be executed on the code that was written and validation must be done for the results of the code. For the verification the code will be divided into different units and a unit test will be done for all units. A basic code map of the aerodynamics department can be seen in Figure 7.5. In this map the three obvious units of aerodynamics are specified: lift, drag and moment. The inputs are weights from class-I estimations, dimensions of the aircraft and wing following from initial sizing and flight conditions that specify altitude and speed. Furthermore, it becomes clear from the map that iterations will be done on the input values of the aerodynamics department to optimise the aircraft. The goal of the verification is to check if the calculations are correct.

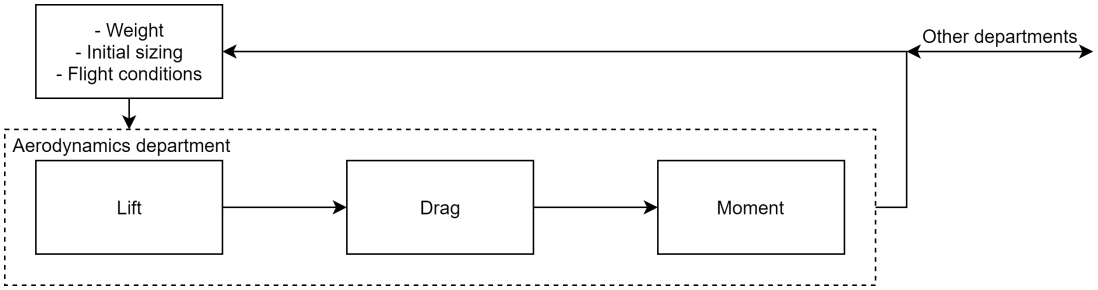

Figure 7.5: A visualisation of the aerodynamics code with its inputs

Unit 1: Lift

The lift calculations as explained in section 7.2 are part of the first unit. The lift unit consists of eight definitions. The first six perform the calculations as mentioned previously and the last two plot the $C_L - \alpha$ curve and read the plot for all values of angle of attack. The calculations for the wing coefficients continue on the calculations for the airfoil coefficients and the calculations of the aircraft coefficients continue on the wing coefficients. This means that minor errors could quickly lead to big differences in output. To prevent this all outputs of the definitions are printed and checked on their feasibility. This usually resulted in small errors that could be fixed easily, like forgetting inputs. Finally, the $C_L - \alpha$ curve was a way to check this unit as well. The curve had the desired shape and the lift curve slope C_{L_α} and maximum lift coefficient $C_{L_{max}}$ were as expected. However, the curve gave a

value for the zero-lift angle, α_{0_L} that was around $0°$. This was too high and after some research it was found out that conversion between radians and degrees was incorrect. After changing that, the calculations were assumed to be verified.

Unit 2: Drag
The drag calculations are elaborated upon in section 7.3. For this unit, the definitions are less dependent on each other. Therefore, errors in results are less amplified, which makes them harder to spot. When testing the program, the different drag coefficients for the components were all printed and checked on their feasibility. Here, again, some debugging had to be done. Furthermore, calculations were done by hand to check the correctness of the program. Small errors were again found and fixed, after which unit 2 was also verified.

Unit 3: Moment
The third unit was used for calculating the moment coefficients, as can be read in section 7.4. It is only a small unit, consisting of four definitions. Again, the results were printed per definition and the calculations were checked by hand. The results were as expected and therefore also this unit was verified.

Next to the unit test another way to verify the lift and drag calculations was found, which is plotting the drag polar. In this phase the drag is determined with Equation 7.43. As can be seen, this is a second order polynomial and therefore a parabola. If the result would be a parabola, the connection between the two units would be verified as well. To make the plot, the results for the first configuration were picked. The result is shown in Figure 7.6. As can be seen, the result is parabolic and therefore the connection is verified.

$$C_D = C_{D_0} + \frac{C_L^2}{\pi A e} \tag{7.43}$$

More realistic drag polars look like a bucket. This would be part of further detailed design, where flow simulations and wind tunnel test on models would be executed. At this point, however, it is beyond the scope of this phase of design.

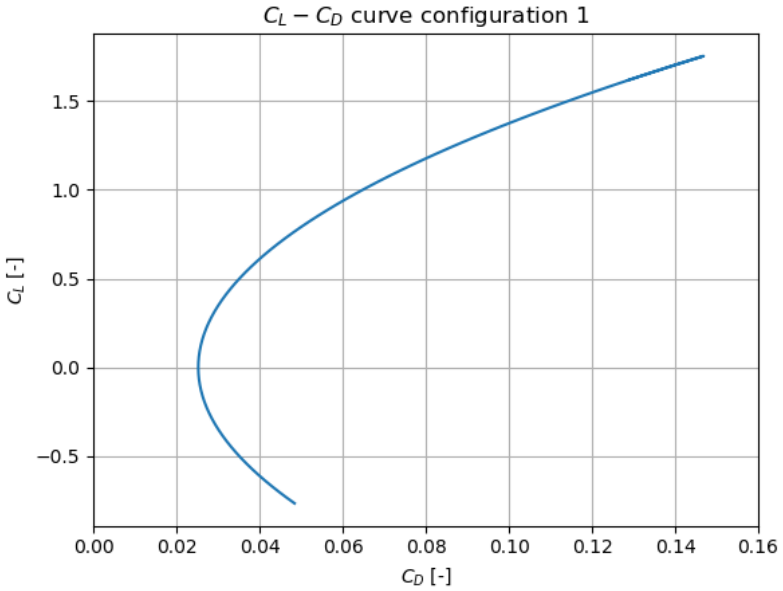

Figure 7.6: The drag polar of configuration 1

Now that the code is verified, it is time to do the validation. This means that the results must be checked on the feasibility. This can be done by comparing the results with reference values. The Embraer 190 is taken as a reference aircraft, and data is taken from [46][3] unless stated otherwise. The $C_{D_{0_{clean}}} = 0.020$ for the Embraer 190. For the adaptive airliner, it is 0.025. It is not strange that the $C_{D_{0_{clean}}}$ of the last one is slightly higher, because of its larger wing and tail. Therefore it is said to be validated.

[3]URL: https://www.sesarju.eu/sites/default/files/documents/sid/2018/papers/SIDs_2018_paper_75.pdf [cited on 24-06-2019]

Furthermore, the $\Delta C_{D,flap}$ is usually 0.12 for a $40° - 50°$ degree angle, and the adaptive airliner has a $\Delta C_{D,land} = 0.140$. Next to this, for take-off, the $\Delta C_{D,TO} = 0.070$, whereas the flaps are estimated to have a $\Delta C_{D,flap}$ of 0.04. Considering the basic approach Roskam provides, these results are deemed to be validated.
The $C_{L_{max}}/cos(\Lambda_{c/4})$ for double-slotted flaps with slats lies between 2.80 and 3.20 [102]. When calculating that for the adaptive airlines, it is found that $C_{L_{max}}/cos(\Lambda_{c/4}) = 2.99$, which perfectly fits within the expected range, which validates the calculations.

For the other parameters it was not possible to find relevant data. Therefore, in a next phase the calculations must be validated with data obtained from experimental analysis. Especially the moment calculations need special attention, since there is no validation done for that part. Possibilities for this are CFD and windtunnel testing.

7.7. Sensitivity analysis

Two major assumptions made during the analysis are the wave drag coefficients and the wing-canard interference factor. In this section, on both parameters a sensitivity analysis is executed.

Wave drag

The wave drag for the wing, nacelle and empennage is estimated to be $C_{D_{wave}} = 0.002$, and $C_{D_{wave}} = 0.005$ for the fuselage. It is a basic estimate from Roskam [83]. As it is not further investigated, it is assumed that the level of project definition for the wave drag coefficient, as defined in [18], is still class five. This means that the variation in actual wave drag can be between -50% and +100%. Therefore, the wave drag coefficient is varied by taking 50%, 75%, 150% and 200% of the current coefficient for the sensitivity analysis. When calculating the total drag during cruise, the following values are found, as can be seen in Table 7.5. It is advised to further investigate the flow behaviour over the wing and fuselage, and to perform a detailed boundary layer investigation. With that, the wave drag component can be further analysed. The implications of the change in wave drag coefficient is expected to be relatively low, as a 200% increase in wave drag coefficient will only lead to an increase in drag of 5%.

Table 7.5: Sensitivity analysis for aerodynamics

	50% $C_{D_{wave}}$	**75%** $C_{D_{wave}}$	**150%** $C_{D_{wave}}$	**200%** $C_{D_{wave}}$
$C_{D_{cruise}}$	0.0704	0.0714	0.0742	0.0760
Difference	-2.57%	-1.29%	2.57%	5.14%

Wing-canard interference

The wing-canard interference factor k_{cw} is a basic estimate from Roskam as well [83]. Whenever the canard is small relative to the wing and far enough forward, it can be assumed to be equal to 1. However, it is assumed that this is not the case. Roskam suggests that a finite element aerodynamic analysis should be done in order to get a better estimate for the k_{cw} factor. This is too detailed for the current design phase, so therefore an estimate is taken. This estimate is subjected to the sensitivity analysis. The first estimate used was $k_{cw} = 0.95$, and for the sensitivity analysis, k_{cw} = 0.75, 0.85, 1.05 are used. The implications of changing this parameter is very large. It can lead up to 30% less lift at flaps extended conditions, as can be seen in Table 7.6. It is therefore crucial in the next phase of the design to investigate the interference of the canard on the main wing.

Table 7.6: Sensitivity analysis for aerodynamics

	$k_{cw} = 0.75$	$k_{cw} = 0.85$	$k_{cw} = 1.05$
ΔC_L	0.867	1.002	1.270
Difference	-23.64%	-11.82%	11.82
$\Delta C_{L_{max}}$	0.660	0.800	1.080
Difference	-29.84%	-14.92%	14.92%

8 Stability and Control

In this chapter, the stability and control aspect of the aircraft will be elaborated upon for the detailed design. In section 8.1, the assumptions made for control and stability are listed, in section 8.2, the loading diagrams are explained, after which the empennage is sized in section 8.3. After this, the control surfaces are sized in section 8.4, followed by the canard sizing in section 8.5. The aircraft is checked for moment equilibrium in section 8.6, and the landing gear is redesigned in section 8.7. Finally, the verification and validation is done and presented in section 8.8 and the sensitivity analysis is elaborated upon in section 8.9.

8.1. Assumptions stability and control

In this section, the assumptions used for stability and control are listed. These will be revisited during the validation of the design.

- The passengers are assumed to place their carry on luggage directly above their seats with the same c.g. location from the nose. This is a valid assumption, since most passengers will put their luggage in a storage unit directly above them. Only a few bags will be placed in the cargo hold on full flights, and it can be assumed that the cargo volumes are not completely filled during most of the flights.
- The aircraft consist of two cargo holds wherein the cargo is assumed to be a point load. This is a valid assumption since the crew will position it such during loading that the c.g. will be controlled.
- The airfoils of the horizontal tail, vertical tail and canard are assumed to be symmetric. This causes the moment coefficient of these airfoils to be zero. This is valid, since it can be chosen during the design process as long as enough lift is being created.
- The arms of the drag caused by the horizontal tail, the vertical tail, the main wing and the canard are assumed to be zero. This is valid since they are small compared to the arms of the lift. The thrust and the lift on the main wing are however not neglected, since those forces are significantly higher and thus should be taken into account.
- The upward force of the engine is assumed to be zero. This is valid since the engine is position aligned with the body axis of the aircraft.
- Incidence angle of the main wing, canard and the horizontal tail are assumed to be zero. This is a valid assumption, since it is chosen during the design process and a small incidence angle will have minor effect on the lift created.
- Small angles are assumed, resulting in $C_L \approx C_N$ and $C_D \approx C_T$. This is valid, since the force and moment equilibrium is calculated for steady flight.

8.2. Loading diagram

In order to analyse stability and control, the c.g. range during flight is required. This is obtained by constructing three loading diagrams using the procedure presented in *AE3211-I Systems Engineering & Aerospace Design* [78] and are based on the class-II weight estimate for the OEW.

For the design of the empennage and canard, two load cases are considered. Namely the c.g. range during flight when the aircraft is fully loaded and the range during flight when no passengers and cargo are loaded. From these values, the maximum and minimum c.g. location is taken and designed for. Next to that, in terms of ground stability it is important that the aircraft does not tip over during loading and that during taxiing the aircraft is controllable. In order to achieve this, the landing gear should be positioned accordingly and the load fraction on the nose landing gear should stay within a predetermined range.

Lastly, loading diagrams are used for the placement of the main wing for configuration 1. The wing was initially placed during the initial sizing. During the sizing of the empennage, the wing will be repositioned, such that the minimal empennage size is required and the aircraft is both stable and controllable at the same time. In order to determine the c.g. range due to this wing shift, the leading edge of the wing is moved 10% forward and 10% aft in terms of the fuselage length. This provides three c.g. ranges from the loading diagram, which are used to interpolate between for different wing positions. This will be elaborated upon in section 8.3.

8.3. Empennage design

In order to design the empennage, first the wing needs to be positioned, so that afterwards the empennage can be sized and the loads required on the empennage can be calculated. This section will start with the elaboration of the wing placement, after which the horizontal tail and vertical tail are designed respectively. The empennage is designed for configuration 1, because for configuration 2 and 3 a canard is added, which will counteract the additional loads generated on the aircraft.

8.3.1. Horizontal tail

In order to size the horizontal tail, a scissor plot is constructed using the method provided during *AE3211-I Systems Engineering & Aerospace Design* [78]. The stability equation used is shown in Equation 8.1 and is based on stick-fixed static stability. The controllability equation used is shown in Equation 8.2. Both equations are rewritten to represent $\frac{S_h}{S}$ as function of $x_{c.g.}$, so that the optimal horizontal tail area ratio can be found.

$$x_{c.g.} = x_{ac} + \frac{C_{L_{\alpha_h}}}{C_{L_\alpha}}\left(1 - \frac{d\varepsilon}{d\alpha}\right)\frac{S_h l_h}{S}\left(\frac{V_h}{V}\right)^2 - 0.05 \cdot MAC \tag{8.1}$$

$$x_{c.g.} = x_{ac} - \frac{C_{m_{ac}}}{C_{L_{A-h}}} \cdot MAC + \frac{C_{L_h}}{C_{L_{A-h}}}\frac{S_h l_h}{S}\left(\frac{V_h}{V}\right)^2 \tag{8.2}$$

To construct the scissor plot, first, Equation 8.1 is plotted twice, since both the neutral point location and the neutral point location including a stability margin of $0.05 \cdot MAC$ m are plotted. The stability margin allows passengers and flight attendants to move through the cabin safely during flight and allow some other constraints, such as the minimum force on the stick to be satisfied [78]. Then, the controllability curve is plotted in the same graph, resulting in an X shaped plot. The stability line represents the maximum c.g. location for which the aircraft is stable and the controllability line represents the minimum c.g. location for controllability. The area between the three lines, for which these conditions are also satisfied, is the area that can be designed for in terms of the c.g., for this area the aircraft is both stable and controllable.

The last step is to find the optimum for the horizontal tail area and the longitudinal position of the wing. Since both plots have the same x-axis, they can be combined in one plot, as shown in Figure 8.1. The maximum and minimum c.g. positions need to lie within the stable and controllable region. This can be optimised by making sure that the distance between the maximum and minimum c.g. location equals the distance between the stability and controllability lines, resulting in a minimum horizontal tail area.

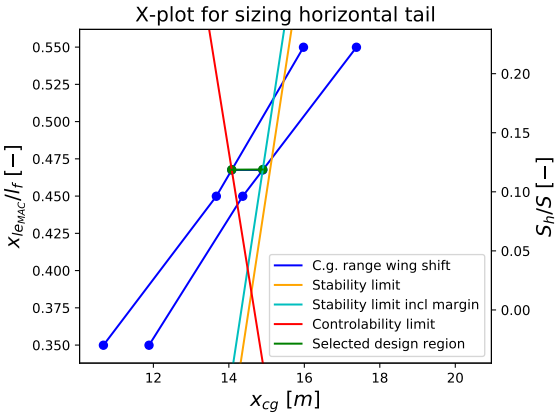

Figure 8.1: Scissor plot of configuration 1, used for the empennage sizing

Table 8.1: Horizontal tail parameters

Parameter	Value	Parameter	Value
A_h	4.95 [−]	MAC_h	2.58 $[m]$
λ_h	0.39 [−]	y_{MAC_h}	2.56 $[m]$
b_h	11.98 $[m]$	x_{MAC_h}	26.47 $[m]$
Cr_h	3.48 $[m]$	Λ_{LE_h}	0.593 $[rad]$
Ct_h	1.36 $[m]$	$\Lambda_{c/4_h}$	0.530 $[rad]$
z_h	2.76 $[m]$	$\Lambda_{c/2_h}$	0.461 $[rad]$
S_h	29.00 $[m]$	t/c_h	0.10 [−]

However, not only does the horizontal tail need to provide stability during flight, it should also be able to rotate the aircraft during the take-off roll in order to obtain the required angle of attack for lift-off. Therefore, the force the horizontal tail must be able to generate, should be large enough to lift the nosewheel off the ground. This was included in the calculations after the third iteration. The generated moment was calculated using the $MTOW$ at the most forward c.g. location. This was considered to be the limiting case in which the horizontal tail needs to counteract the largest moment. The required wing surface area is calculated using the required force, the rotation speed, air density at sea level, and the maximum C_l of the NACA 63-010 airfoil, which is 0.86. This resulted in a more strict requirement than the stability requirement and hence the horizontal tail is sized using

the take-off requirement. This was initially forgotten in the analysis, however realised and implemented after the third iteration, as can be seen in Figure 8.3. It can be seen that the increase only has a minor negative influence on the canard area.

After the tail area is determined, the other horizontal tail parameters can be established. The aspect ratio is found to be a company trade mark [14][1], thus the value obtained during the initial sizing is used in the detailed design. The same holds for the taper ratio, the sweep angle and the thickness over chord ratio. The span, mean aerodynamic chord length and position, root chord length, tip chord length, half chord sweep angle, and quarter chord sweep angle are then calculated using above mentioned parameters in combination with the found horizontal tail area. The final parameters are shown in Table 8.1.

After these values were determined, an elevator trim curve was constructed for the three configurations, as shown in Figure 8.2. It can be seen that C_{m_α} is negative, as is desired, however there is no trim point for a positive angle of attack. The trim point for configuration 1 is located at an angle of attack of $-1.76°$, for configuration 2 at $-1.86°$ and for configuration 3 at $-1.75°$. It can be concluded that for all configurations, the angle of attack for which the aircraft is trimmed is negative. There can be a number of reasons for this, such as that the equations for constructing an elevator trim curve are not applicable to a three surface aircraft, or that the coefficients found by the aerodynamics department are not applicable for the canard. This is something that has to be looked into in the next stage of the design, as discussed in chapter 17.

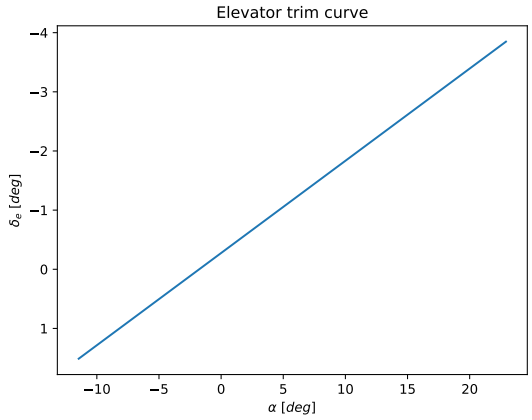

Figure 8.2: Elevator trim curve for configuration 1

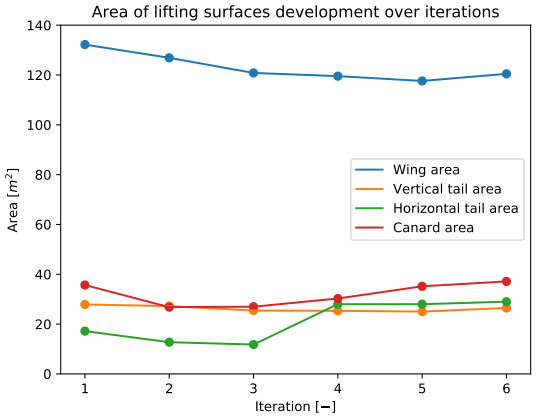

Figure 8.3: Canard area, horizontal tail area and vertical tail and wing area development over the iterations.

8.3.2. Vertical tail

In this section the sizing of the vertical tail is elaborated upon. In order to determine the size of the vertical tail, the most critical phase of flight was determined for which the tail must be designed. The one engine inoperative condition at the decision speed was considered the most critical flight phase for the vertical tail. Since the aircraft flies at a low speed with take-off thrust applied to the operating engine, the tail needs to be large enough to counteract the moment caused by the engine and stop the aircraft from yawing.

$$F_{v_{max}} = C_{l_{v_{max}}} \cdot \frac{1}{2}\rho V_1^2 \cdot S_v \tag{8.3}$$

Using Equation 8.3, the maximum force that the vertical tail can generate before stalling without using the rudder is calculated ($F_{v_{max}}$). Then by using the maximum thrust and the y-location with respect to the c.g. of the engine , the moment caused by the engine can be calculated. This moment needs to be counteracted by the vertical tail. Using this as a condition that has to be satisfied in combination with a tail volume of 1.1 based on reference aircraft, the surface area of the vertical tail is determined [84]. This resulted in a tail that was not able to satisfy the engine inoperative condition on its own, however by the use of deflecting the rudder to the operating engine, the rudder will be able to increase its $C_{l_{max}}$ and the required force needed will be sufficient to counteract the moment caused by the operating engine. The parameters obtained are shown in Table 8.2 and the NACA 63-012 is used.

[1] URL: `https://booksite.elsevier.com/9780340741528/appendices/data-a/default.htm` [cited 19 June 2019]

Table 8.2: Vertical tail parameters

Parameter	Value	Parameter	Value
A_v	1.5 [−]	MAC_v	4.49 $[m]$
λ_v	0.375 [−]	z_{MAC_v}	5.02 $[m]$
b_v	6.30 $[m]$	x_{MAC_v}	25.99 $[m]$
Cr_v	6.11 $[m]$	Λ_{LE_v}	0.977 $[rad]$
Ct_v	2.29 $[m]$	$\Lambda_{c/4_v}$	0.868 $[rad]$
y_v	0.0 $[m]$	$\Lambda_{c/2_v}$	0.720 $[rad]$
S_v	26.47 $[m]$	t/c_v	0.12 [−]

Table 8.3: Control surfaces fractions

Parameter	Value
C_{elev}/C_h	0.3 [−]
C_{rud}/C_v	0.3 [−]
C_{ail}/C	0.22 [−]
C_{splr}/C	0.22 [−]

8.4. Control surfaces

In this section, the sizing of the control surfaces is elaborated upon. The control surfaces will be sized based on statistical data [84]. Using this data, the chord length of the control surfaces can be determined. Also the location along the span can be estimated using this approach. The elevator and rudder will have control surfaces that span the whole horizontal and vertical tail, respectively. The aileron however will only have a movable control surface from 75% until 95% of $\frac{b}{2}$. They are positioned at the wingtips in order to have the largest moment arm with respect to the y-location of the c.g. such that the aileron is most effective. The same approach is used for the spoilers on the wing which help the aircraft brake in the air and during landing or a rejected take-off. These are positioned on the wings just in front of the HLDs at 40% to 65% of $\frac{b}{2}$. In order to determine the chord length and surface area of the control surfaces, the fractions shown in Table 8.3 are used.

Due to the changing chord length along the span of the wings, the chord of the control surfaces will also change along the span. Therefore a tip and root chord is also calculated for the control surfaces. This resulted in the parameters shown in Table 8.4.

Table 8.4: Control surfaces parameters

Elevator	Value	Rudder	Value	Aileron	Value	Spoiler	Value
Cr_{elev}	1.04 $[m]$	Cr_{rud}	1.83 $[m]$	Cr_{ail}	0.59 $[m]$	Cr_{splr}	0.55 $[m]$
Ct_{elev}	0.41 $[m]$	Ct_{rud}	0.69 $[m]$	Ct_{ail}	0.41 $[m]$	Ct_{splr}	0.42 $[m]$
b_{elev}	11.98$[m]$	b_{rud}	6.30 $[m]$	b_{ail}	3.55 $[m]$	b_{splr}	4.23 $[m]$

8.5. Canard sizing

In this section, the canard sizing and placement will be elaborated upon. The canard is positioned at the front of the modular section, since a larger arm will result in a smaller area required to generate the same moment with respect to the aerodynamic centre of the main wing. In order to size the canard, a scissor plot is constructed for both configuration 2 and 3. The equations used for the sizing of the horizontal tail, presented in subsection 8.3.1, are modified such that they can be used to size the canard. The stability region is calculated using Equation 8.4 and for the controllability region Equation 8.5 is used, both with $l_c = x_{c.g.} - x_c$. The airfoil used for the canard is the NACA 63-010.

$$x_{c.g.} = x_{ac} + \frac{C_{L_{\alpha_h}}}{C_{L_\alpha}}\left(1 - \frac{d\varepsilon}{d\alpha}\right)\frac{S_h l_h}{S}\left(\frac{V_h}{V}\right)^2 - \frac{C_{L_{\alpha_c}}}{C_{L_\alpha}}\frac{S_c l_c}{S}\left(\frac{V_c}{V}\right)^2 - 0.05 \cdot MAC \tag{8.4}$$

$$x_{c.g.} = x_{ac} - \frac{C_{m_{ac}}}{C_{L_{A-h}}} \cdot MAC + \frac{C_{L_h}}{C_{L_{A-h}}}\frac{S_h l_h}{S}\left(\frac{V_h}{V}\right)^2 - \frac{C_{L_c}}{C_{L_{A-h}}}\frac{S_c l_c}{S}\left(\frac{V_c}{V}\right)^2 \tag{8.5}$$

The scissor plot is shown in Figure 8.4. The wing position is not variable in this scissor plot, since this was fixed after the sizing of the empennage. This results in only one loading diagram and thus one forward and aft c.g. location. These c.g. locations both have to fall within both the stable and controllable region of the scissor plot, while also minimising the canard area, as can be seen in Figure 8.4. After the area of the canard is known, the additional parameters can be determined, as is done for the horizontal and vertical tail in section 8.3. The parameters for the canard are shown in Table 8.5. In order to fit the c.g. range in the scissor plot of the canard, a C_L value of 1.4 was required on the canard. This is not feasible at this moment with a symmetrical airfoil, so this requires additional investigation in a later phase of the design.

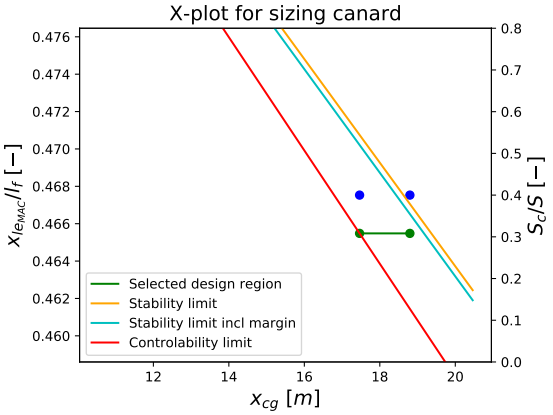

Figure 8.4: Scissor plot of configuration 3, used for the canard sizing

Table 8.5: Canard parameters

Parameter	Value	Parameter	Value
A_c	4.95 [−]	MAC_c	2.75 [m]
λ_c	0.80 [−]	y_{MAC}	3.26 [m]
b_c	13.56 [m]	x_{MAC}	6.81 [m]
Cr_c	3.04 [m]	Λ_{LE_c}	-0.002 [rad]
Ct_c	2.43 [m]	$\Lambda_{c/4_c}$	-0.047 [rad]
z_c	0.18 [m]	$\Lambda_{c/2_c}$	-0.047 [rad]
S_c	37.13 [m]	t/c_c	0.10 [−]

8.6. Force and moment equilibrium

In the previous section it is shown that the aircraft is designed to be both stable and controllable. In this section the loads on the canard and tail will be calculated for steady flight, for which it is important that both a force equilibrium and a moment equilibrium are satisfied. The forces and moments acting on the aircraft are shown in Figure 8.5. From this, the vertical equilibrium and moment equilibrium can be derived to be Equation 8.6 and Equation 8.7 respectively. Since the equations are derived for steady flight, it is valid to use the small angle approximation. It is important to note that other assumptions are made in order to simplify the equations, as listed in section 8.1, so that the equations can be solved.

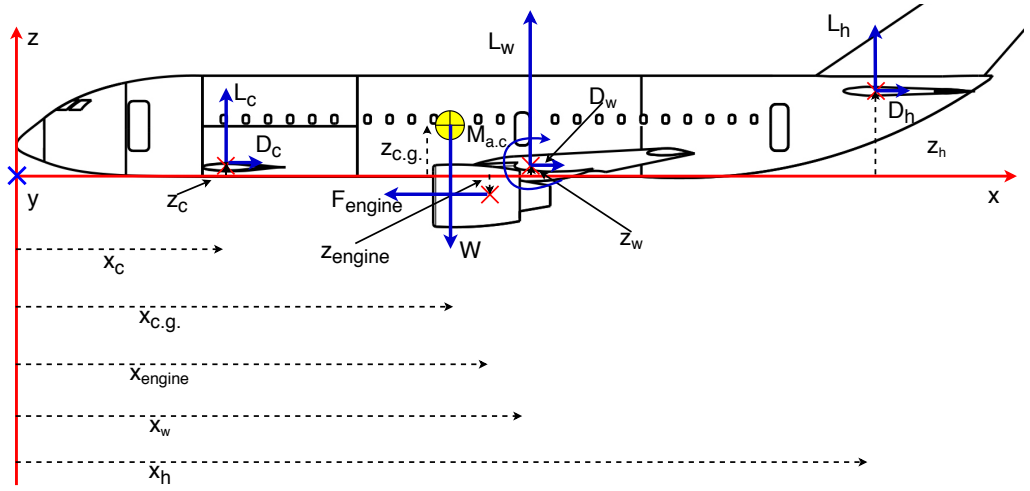

Figure 8.5: Forces taken into account for moment equilibrium

$$W = L_w + L_h + L_c \tag{8.6}$$

$$M_{c.g.} = M_{a.c.} + F_{engine}(z_{c.g.} - z_{engine}) + L_c(x_{c.g.} - x_c) - L_w(x_w - x_{c.g.}) - L_h(x_h - x_{c.g.}) = 0 \tag{8.7}$$

It is important that the equations above are satisfied for all configurations. For configuration 1, all terms including L_c are neglected. First L_w and L_h were calculated for configuration one, but when designing the canard, an additional unknown, L_c, was imposed. This required the group to make a decision on fixing either the lift generated on the main wing, or the lift generated on the horizontal tail. Both methods were used to calculate the required lift generated on the canard. It was found that by keeping L_h constant, a small percentile difference of only 4.4% was achieved between the maximum and minimum lift on the main wing instead of a 36% difference on the tail by keeping L_w constant. By keeping L_h constant, the aircraft is prevented from being overdesigned for one of the configurations.

8.7. Ground equilibrium design

This section elaborates upon the landing gear position and the load fractions on the landing gears. Initially the landing gear was positioned based on the initial sizing, however due to the c.g. shift, the landing gear position needs to be updated as explained below.

When positioning the landing gear, first the main landing gear is positioned after which the nose landing gear is placed. There are a few constraints regarding the main landing gear position as can be seen in Figure 8.6 and Figure 8.7. These constraints are the tip-back angle, scrape angle and wing-tip/engine clearance angle. Satisfying these constraints will result in the safe operation on landing and take-off.

The scrape angle ensures safe rotation of the aircraft without the tail hitting the ground. This angle is set to the angle of attack at which the aircraft would stall. The tip-back angle should then be at least larger than the scrape angle as it ensures that the c.g. position will not fall behind the axis of rotation on take-off or landing, as that would make the aircraft unstable. Therefore this angle was set to 15 degrees opposed to the 12.75 degree scrape angle. This resulted in an x-location of 15.34 metres in configuration 1 and 21.03 metres in configuration 2/3, since the length of the cutout has to be taken into account. Its z-location is negative, with respect to the reference system presented in Figure 8.5, as it is under the belly of the aircraft and its magnitude is 3.11 metres.

The wing-tip/engine clearance angle ensures that on landing, the wing or engines do not hit the ground in case the aircraft is not able to land with its wings level. Therefore the wing tip/engine clearance angle was set to at least 5 degrees. Using this constraint in combination with the overturn angle, which will prevent lateral tip over when manoeuvring on the ground, the minimum y-location of the main landing gear was determined. This however resulted in a position of the gear which would not allow to retract the gear into the fuselage, as the z-length was larger than the y-length. Therefore the landing gear was positioned more outward to 3.8 metres which also allowed the gear structure to be integrated more easily with the wing.

With the placement of the main landing gear, the nose landing gear can be placed. Its y-location will be 0 metres and its z-location will be the same as for the main landing gear in order to have a level cabin floor when the aircraft is on the ground. Its position along the length of the fuselage is determined by the percentage of weight that will have to be carried by the nose landing gear. Since the nose landing gear position with respect to the nose will not change for the different configurations, the placement of the nose wheel will have to be checked for all configurations. By checking all configurations, the nose landing gear was placed at 2 metres from the nose.

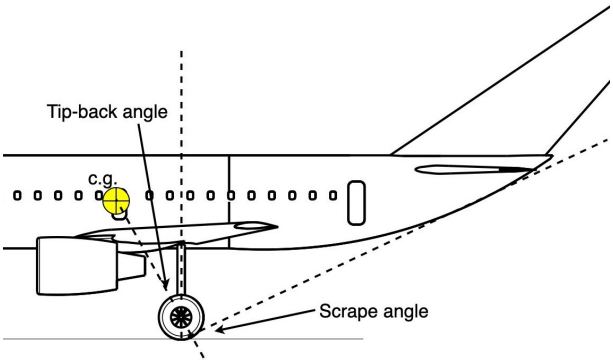

Figure 8.6: Scrape and tip-back angle definition

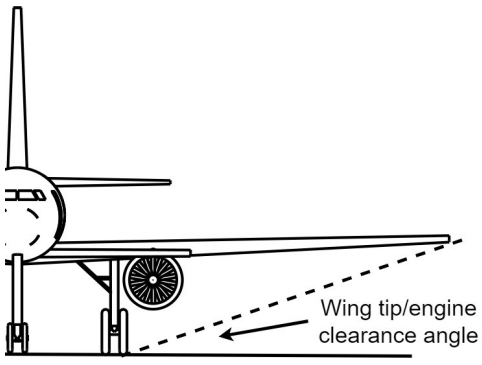

Figure 8.7: Wing/engine clearance angle definition

In order for the aircraft to be steerable on the ground, a minimum and maximum fraction of the weight is set to be carried by the nose landing gear. These fractions are calculated for all points in the loading diagrams using the vertical force equilibrium and moment equilibrium around the c.g. locations for these points using Equation 8.8 and Equation 8.9 respectively. These fractions are required to fall between 0.08 and 0.20 for all configurations [78]. The aircraft complies with this requirement since the minimum fraction is found to be 0.088 for configuration 1 and the maximum fraction is found to be 0.183 for configuration 3. Another check that is done for both the main landing gear and the nose landing gear is if the load due to the maximum loading fraction does not exceed the maximum tire pressure, if this is the case an update is required during the iterations. This requirement is met for all three configurations. The sizing of the wheels and struts is presented in chapter 10.

$$W = 2F_m + F_n \tag{8.8}$$

$$2F_m b_m - F_n b_n = 0 \tag{8.9}$$

8.8. Verification and validation

In this section the verification process will be discussed first and after that the approach will be validated. The assumptions made for stability and control are already validated in section 8.1 and in this section, the approach used will be discussed. The stability program can be divided into different units, all for which verification is applied. A flow diagram of the stability and control code can be seen in Figure 8.8.

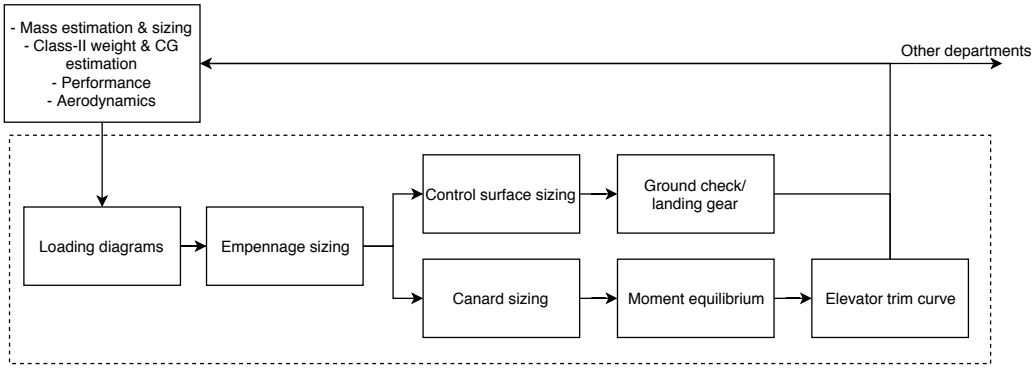

Figure 8.8: Schematic overview of the stability and control program

Unit 1: Loading diagrams

The construction of the loading diagrams was initially done in excel in order for the process to be graphically visible. In a later design stage, it was necessary to convert this construction to Python, so that the program could be linked to other disciplines. This took some additional time, however it also provided the possibility to verify the used program. The loading diagrams constructed by the different programs have the same shape, but consist of different values, which can be explained by the different input in this later design phase.

Unit 2: Empennage sizing

For the horizontal tail sizing, initially statistical values were used to check whether the program performed the calculations correctly. This was done because the program was developed simultaneously with the program that is calculating the aerodynamic coefficients needed. In the code that calculates the c.g. location for different wing positions, initially a mistake was found. The program mixed the class-I inputs with the class-II inputs when calculating the c.g. range, but this error was fixed right away. Once the aerodynamic coefficients were known, the x-plot needed to be matched with the c.g. locations of the aircraft due to different wing positions. This required an interpolation to be implemented in order to prevent reading errors from the graphs, which would have resulted in a less optimal tail area. For the other parameters, basic formulas have been used, so aside of unit testing no additional tests were required.

Unit 3: Control surface sizing

The control surfaces are sized purely based on statistical data [84], this was coded as fractions of the wings. This was then checked by the use of manual calculation of the fraction of the wings and for the span checking if the length does not exceed the length of $\frac{b}{2}$ as this would not be physically possible. Also the surface area was checked by multiplying the span by the average chord. This ensured that the calculations that were supposed to be done were indeed implemented correctly.

Unit 4: Ground check/ landing gear

In order to check if the landing gear was placed correctly, the constraints that had to be met were checked again to make sure that they were satisfied. Next up, the weight fractions on the nose landing gear were checked, in order to not exceed 20% or subceed 8% of the aircraft weight on the nose wheel. Another important criterion was that the position of the main landing gear should allow the gear to be mounted to the wings and retract into the wings and fuselage. This resulted in some small adjustments with respect to the y-location of the main landing gear. Lastly, the landing gear wheel base should not exceed 9 metres (SYS-S-05 requirement), which was also checked at last. This way the landing gear is positioned such that all the constraints are taken into account, checked and comply with the set requirements.

Unit 5: Canard sizing
For the canard sizing, the equations had to be rewritten. Initially a mistake was made regarding the term l_c, the distance between the a.c. of the canard and the c.g. location. This distance was assumed to be positive, however an additional minus sign had to be added to make this term negative. This resulted in the expected x-plot for the canard stability and controllability. Futhermore, as was done for the empennnage sizing, an interpolation was needed and checking the right outputs of this interpolation was required. Additional constraints had to be added to the program after the first tests, in order to make sure that the right canard area ratio was taken from the plot.

Unit 6: force and moment equilibrium
For the verification of the moment equilibrium, assert functions were used. The forces on the canard, main wing and horizontal tail were calculated for all configurations and afterwards the sum of these forces and moments were added up. If one of those summations was bigger than $1 \cdot 10^{-8}$, the program stopped working and printed an error message. This way equilibrium is always satisfied for steady flight.

Unit 7: Elevator trim curve
The last unit is the elevator trim curve construction. It is known that C_{m_α} is required to be negative, which it is. However it is desired that the trim point is located at a positive angle of attack. Whereas it is currently at a small negative angle of attack. Initially the same mistake, regarding the sign of l_c, was made, however this came to light during the unit testing.

Now that the program is verified, its validation can be discussed. Validating the program can first of all be done by looking at the surface areas of the canard, wing, horizontal tail, and vertical tail in Figure 8.3. It can be seen that as the number of iterations gets higher, the differences in area between the iterations get smaller. This means that the model converges to one final value. Validating the dimensions and approach of the empennage sizing can also be done by comparing the aircraft to reference aircraft [14][2] for configuration 1 and by comparing the shape of the scissor plots to that of other aircraft. The horizontal tail and vertical tail are bigger than on reference aircraft, however this is to be expected since the aircraft is heavier due to the additional weight induced by the reinforced structure due to additional load presented by the modular section. Validating the approach regarding stability and control for a three surface aircraft is very difficult at this stage, since no data is available of comparable aircraft of the same size. The Piaggio Avanti P180 II is one of the few three surface aircraft ever build, which is only able to carry 11 passengers including crew [100][3]. This aircraft is therefore not considered to be comparable to the regional airliner, as the regional airliner is a lot larger. Therefore, in order to size the canard an identical approach is used as for the sizing of the tail, however this needs to be confirmed in a later design phase. The same holds for the elevator trim curve, which has a negative angle of attack of around $-1.8°$ for the trim point. As the approach for this plot is extrapolated from the design of a conventional aircraft, it is recommended to investigate the stability, controllability, sizing for the canard, and the elevator trim curve further in the next phase of the design. Another recommendation would be to perform scaled wind tunnel tests and perform CFD analysis on the model to investigate the stability and controllablility of the aircraft in more detail. Finally, in order to fit the c.g. range of configuration 2 and 3 in the stable and controllable region of the scissor plot for the canard, a C_{L_c} value of 1.4 was required. This is not feasible at this moment for a symmetrical airfoil, so this requires additional investigation.

8.9. Sensitivity analysis

In this section, a technical sensitivity analysis is presented for the stability and control of the aircraft. The stability and control department combines parameters from different disciplines. For this section the aim of this sensitivity analysis is to determine whether small changes in the input data obtained by other disciplines also relates to small changes in the outputs of the program regarding stability and control. It is important that the aircraft stays both stable and controllable for these inputs.

The sensitivity of the program was checked by multiplying the coefficients in Table 8.6 and Table 8.7 all by 1.1 and 0.9 to check the robustness of the program. This resulted in the fact that the aircraft was still both stable and controllable for all configurations, however it results in different empennage and canard sizes, which will have to be iterated again in a further design phase.

In Table 8.6 and Table 8.7, the maximum absolute difference found during the sensitivity analysis, thus by mul-

[2]URL: `https://booksite.elsevier.com/9780340741528/appendices/data-a/table-8/table.htm` [cited 22 June 2019]
[3]URL: `http://www.smartcockpit.com/docs/P180_Avanti-Specification_and_Description.pdf` [cited 22 June 2019]

tiplying the input value with 0.9 and 1.1, is shown. It can be seen that for most of the coefficients, the area of the canard changes slightly, but for all coefficients the difference is lower than 25%. The area of the horizontal tail stays constant, which is to be expected, since the limiting factor was not obtained from the scissor plot, but from the rotation speed of the aircraft required on take-off. For the vertical tail, the area only changes for a change of the c.g. location, which is to be expected, since this changes the moment created by the one engine inoperative case.

Table 8.6: Difference in values during the sensitivity analysis (1)

Initial	Δ	η_h	$C_{L_{h_\alpha}}$	$C_{L_{A-h_\alpha}}$	$d\epsilon/d\alpha$	V_h/V	$C_{m_{ac}}$	$C_{L_{A-h}}$	$x_{c.g.}$	C_{L_h}
$S_h = 29.00\ [m^2]$	ΔS_h	0.0	0.0	0.0	0.0	0.0	0.0	0.0	0.0	0.0
$S_v = 26.47\ [m^2]$	ΔS_v	0.0	0.0	0.0	0.0	0.0	0.0	0.0	2.7	0.0
$S_c = 37.13\ [m^2]$	ΔS_c	0.0	0.6	0.6	0.5	4.0	0.4	5.8	0.0	2.5

Table 8.7: Difference in values during the sensitivity analysis (2)

Initial	Δ	C_{L_c}	$C_{L_{c_\alpha}}$	$C_{L_{w_\alpha}}$	$C_{L_{h_\delta}}$	V_c/V	$V_{critical}$
$S_h = 29.00\ [m^2]$	ΔS_h	0.0	0.0	0.0	0.0	0.0	0.0
$S_v = 26.47\ [m^2]$	ΔS_v	0.0	0.0	0.0	0.0	0.0	0.0
$S_c = 37.13\ [m^2]$	ΔS_c	4.1	0.0	0.0	0.0	8.7	0.0

9 Performance and Propulsion

In this chapter, the performance of the aircraft and the engine's fuel consumption will be assessed. First, analyses of all flight phases, from take-off to landing, are done in section 9.1 through section 9.4. Next, in section 9.5, the percentage of airports that the adaptive airliner can service is determined. In section 9.6, the flight profile is elaborated upon, including an analysis of requirements on fuel reserves. In section 9.7, the fuel consumption of the entire flight profile is analysed. Section 9.8 and section 9.9 show the payload-range diagrams and flight envelope of the final configurations, respectively. In section 9.10, the methods used in this chapter are verified and validated. Finally, in section 9.11, a technical sensitivity analysis is done. Results are for $MTOM$ at take-off, design range mission, unless mentioned otherwise.

9.1. Take-off performance

The take-off procedure can be split up into three phases. The ground run phase, in which the aircraft accelerates over the ground up to take-off velocity. Secondly, the transition phase, in which the aircraft rotates into a climb. And finally, the climb-out phase, in which the aircraft climbs up to screen height, as set by airworthiness requirements. The take-off performance is analysed for both nominal and engine failure conditions, to assess whether requirement **SYS-S-03** is fulfilled and at what minimum field length the aircraft can be operated, respectively.

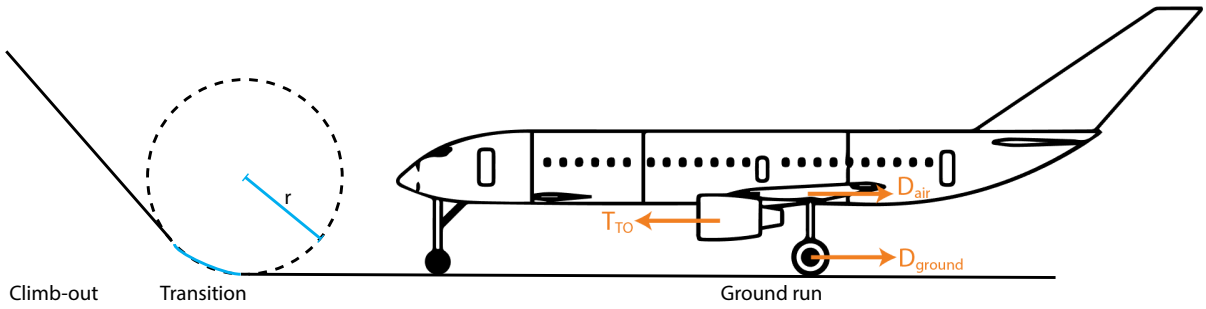

Figure 9.1: Visualisation of take-off phases

Several assumptions were made for analysis of the take-off performance. There is assumed to be no wind; taking off into the wind would shorten the take-off field length, this leads to an overestimation of the take-off field length in windy conditions. The runway is assumed to be dry and icing conditions are neglected. These assumptions lead to an underestimation of the take-off field length. The ground effect has a positive influence on the lift and drag of the aircraft, but climb must be continued as the ground effect fades, so it is not possible to take-off at lower velocity. Hence, the ground effect is neglected.

9.1.1. Ground run

The ground run distance is determined using Equation 9.4, following from the derivation in Equation 9.1 through Equation 9.3, where the acceleration is assumed to be constant. The average acceleration, $\overline{a}$, is found using Equation 9.5. The sum of forces, $\overline{F}$ is taken at an average airspeed, $\overline{V}$. During the ground run the aircraft accelerates from standstill to rotation speed, V_R. The factor to calculate the rotation speed from stall speed, V_{stall}, using Equation 9.8, follows from *CS-25* [23]. The take-off thrust setting is assumed to be at *100%*.

$$dt = \frac{ds}{V},\ a = \frac{dV}{dt} \tag{9.1}$$

$$\int_0^{V_R} V dV = \int_0^s a ds \tag{9.3}$$

$$a = \frac{dV}{\frac{ds}{V}} \tag{9.2}$$

$$\frac{1}{2} V_R^2 = \overline{a} s \tag{9.4}$$

$$\overline{a} = \overline{F}/m \tag{9.5}$$

$$\overline{F} = T_{TO} - \overline{D}_{air} - \overline{D}_{ground} \tag{9.6}$$

$$\overline{V} = \frac{V_R}{\sqrt{2}} \tag{9.7}$$

$$V_R = 1.05 \cdot V_{stall} \tag{9.8}$$

$$V_{stall} = \sqrt{\frac{mg}{\frac{1}{2}\rho S C_{L_{TO}}}} \tag{9.9}$$

$$\overline{D}_{air} = \frac{1}{2}\rho \overline{V}^2 S C_{D_{TO}} \tag{9.10}$$

$$\overline{D}_{ground} = \mu_{MLG}(mg - \overline{L}) \tag{9.11}$$

$$\mu_{MLG} = \frac{(\frac{F_{NLG}}{mg} - 1)l_m + \frac{F_{NLG}}{mg} l_n}{h_{cg}(1 - \frac{F_{NLG}}{mg})} \tag{9.12}$$

$$\overline{L} = \frac{1}{2}\rho \overline{V}^2 S C_{L_{TO}} \tag{9.13}$$

9.1.2. Transition

Dividing Equation 9.14 [88] by W, and assuming $cos\gamma_{climb} \approx 1$, gives Equation 9.15. Rewriting to Equation 9.16, gives the radius of the transition manoeuvre. The load factor, n, is assumed to be 1.15 during the transition [43]. It is assumed that the aircraft does not accelerate throughout the transition. The climb gradient at the end of the transition is calculated using Equation 9.17. Using 9.18 and 9.19, the transition distance and the height achieved during transition are calculated. Similar to the ground run, the thrust setting is at 100%. The aircraft is assumed not to accelerate during the transition, and V is fixed at V_R.

$$\frac{W}{g} V \frac{d\gamma_{climb}}{dt} = \frac{W}{g}\frac{V^2}{r} = L - W\cos\gamma_{climb} \tag{9.14}$$

$$\frac{V^2}{gr} = \frac{L}{W} - 1 = n - 1 \tag{9.15}$$

$$r = \frac{V^2}{g(n-1)} \tag{9.16}$$

$$\gamma_{climb} = \frac{T - D_{air}}{W} \tag{9.17}$$

$$s_{transition} = r(sin\gamma_{climb}) \tag{9.18}$$

$$h_{transition} = r(1 - \cos\gamma_{climb}) \tag{9.19}$$

9.1.3. Climb-out

The screen height for take-off, after which the take-off is considered completed, is set at 35 ft as determined by *CS-25* [23]. This screen height can already be achieved during the transition phase. If the screen height is not yet attained, a climb-out phase must follow. The distance covered during climb-out can be calculated using Equation 9.20.

$$s_{climb\_out} = \frac{h_{screen} - h_{transition}}{\tan\gamma_{climb}} \tag{9.20}$$

9.1.4. Take-off field length

Combining the ground run, transition and climb-out distance gives the total take-off field length,as seen in Equation 9.21. The take-off field length is assessed from OEM to $MTOM$ and at different airport altitudes. Note that the aircraft can not take-off at OEM, as it completely excludes fuel. Table 9.1 shows the take-off field length at $MTOM$, sea level for all three configurations. Figure 9.2 shows the take-off field length as a function of mass and altitude for configuration 3, which is the most critical configuration for take-off performance, as it is the heaviest configuration.

$$s_{take\_off} = s_{ground\_run} + s_{transition} + s_{climb\_out} \tag{9.21}$$

After the currently limited number of iterations, the aircraft is clearly overdesigned for take-off. Lift during take-off may be reduced by downsizing the flaps, and/or a less powerful engine should be selected. For an elaboration on future iterations and design phases, please refer to section 17.1.

Table 9.1: Take-off field length

	Config. 1	Config. 2	Config. 3
Take-off field length $MTOM$, ISA, SL [m]	1,346.18	1,538.74	1,658.98

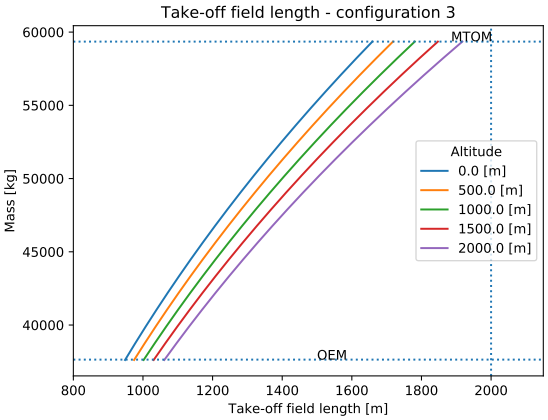

Figure 9.2: Take-off field length of configuration 3

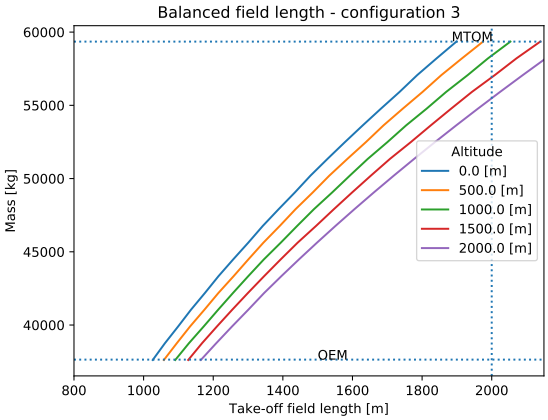

Figure 9.3: Balanced field length of configuration 3

9.1.5. Balanced field length

The calculated field length in section 9.1 neglects the possibility of an engine failure during take-off. In this section, this critical case is covered. First, the decision speed, V_1, must be determined. After attaining this airspeed, the take-off procedure will be completed, even in case of an engine failure. Aborting take-off after V_1 must be avoided, as the aircraft will not be able to decelerate fast enough to prevent runway excursion. With an engine failure at V_1, the field length required to continue take-off, and the field length required to decelerate to a stop, are equal. The take-off field length required to complete/abort take-off with an engine failure at V_1 is called the *balanced field length*, and is a critical value in determining what airports are serviceable by the aircraft.

V_1 is determined by making an initial guess, assessing the take-off field length and accelerate-stop distance for engine failure at V_1, and calculating the difference between the two. Deceleration is discussed in section 9.4. Next, the decision is incremented depending on the sign of the difference. A variable step size, depending on the magnitude of the difference, is used. The loop is terminated as soon as the magnitude of the difference drops under 5 m (0.25% of 2,000 m, requirement **SYS-S-03**). This logical flow is visualised in Figure 9.4. Using the methods of subsection 9.1.1, 9.1.2 and 9.1.3, splitting the ground run into a nominal and engine-failure part, the balanced field length can be calculated. The most critical balanced field length, of configuration 3, is plotted in Figure 9.3. The balanced field lengths of all configurations at $MTOM$ and sea level can be found in Table 9.2.

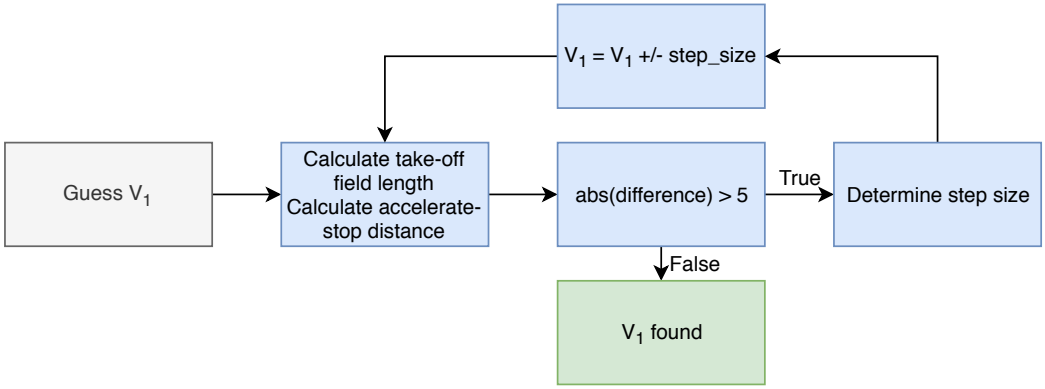

Figure 9.4: Decision speed determination flow

9.2. Climb and descent performance

The climb gradient, γ_{climb}, is calculated using Equation 9.17. The rate of climb, ROC, is calculated using Equation 9.22. During the climb flight phase, the altitude and airspeed increase to cruise altitude and cruise speed,

Table 9.2: Balanced field length

	Config. 1	Config. 2	Config. 3
Balanced field length $MTOM$, ISA, SL [m]	1,514.05	1,752.66	1,898.56

respectively. The concept of energy height, H_E, can be used to assess the performance of a combined climb and acceleration.

$$ROC = \frac{(T-D)V}{W} \tag{9.22}$$

$$H_e = H + \frac{V^2}{2g_0} \tag{9.23}$$

A number of assumptions were made in the analysis of the climb performance. Most importantly, the effects of wind have been neglected. Depending on the wind direction this can lead to an over- or underestimation of parameters. Vertical gradients in wind velocity could, similarly, be advantageous or disadvantageous. Furthermore; the fuel mass burned during engine start-up has been neglected in the analysis of the climb performance, this leads to an overestimation of the fuel burned during climb, and an underestimation of γ_{climb} and ROC. This assumption was made to ensure sufficient climb performance, even in case of a more efficient engine start-up. Cabin pressurisation speed and human adaptation to pressure differences have been neglected; no limitations were placed on ROC. The fuel burnt during climb is neglected in calculations, this leads to an underestimation of the ROC and γ_{climb}.

9.2.1. Climb optimisation

Optimisation of the climb phase is complex and related to optimisation of the entire flight profile. In the current design phase, the climb performance is primarily used to estimate the fuel mass burned in this phase, as there is no constraining requirement on rate of climb nor on climb gradient. More conventional methods to assess climb performance are minimising fuel burned in climb, minimising climb time, or maximising climb gradient. Note that minimising fuel burned in climb does not necessarily mean a more fuel efficient flight, as this might result in a very short cruise phase. Minimising climb time was chosen to maximise cruise time. Proper flight profile optimisation should follow, please refer to section 9.6 for an elaboration on flight profile optimisation.

Equation 9.24, 9.25, and 9.26, derived in *'Elements of aircraft performance'* [88], relate energy height and ROC, climb time t_{climb}, and climb distance s_{climb}, respectively.

$$\frac{dH_e}{dt} = ROC \tag{9.24}$$

$$t_{climb} = \int_{H_{e_1}}^{H_{e_2}} \frac{dH_e}{ROC} \tag{9.25}$$

$$s_{climb} = \int_{H_{e_1}}^{H_{e_2}} \frac{dH_e}{tan\gamma_s} \tag{9.26}$$

To minimise t_{climb}, the ROC must be maximised for all energy heights. This is true when the derivative of ROC with respect to H_e is zero, in other words, where ROC and H_e are tangent. The solution is visualised in Figure 9.5. By climbing through the points of maximum rate of climb, up to the desired energy height, the minimum time to climb is achieved. By minimising the step size between lines of constant rate of climb, a more accurate result is achieved.

As the ROC must be calculated at varying altitudes and airspeeds, the altitude and velocity effects on thrust (Equation 9.22) must assessed. As there is no test data on altitude effects available for the selected engine, these effects are estimated using Equation 9.27 [88]. Velocity effects are engine specific and can not be estimated without more detailed information on mass flows or test data; these are thus neglected in the current design phase. Typically, turbofan thrust decreases with airspeed. By neglecting its effects, the climb rate is overestimated. Table 9.3 shows the climb time from sea level to cruise altitude at $MTOM$ per configuration.

$$\frac{T}{T_0} = \frac{\rho}{\rho_0} \tag{9.27}$$

Table 9.3: Climb time per configuration, sea level to cruise altitude

	Configuration 1	Configuration 2	Configuration 3
Climb time [s]	1,317.84	1,496.37	1,809.69

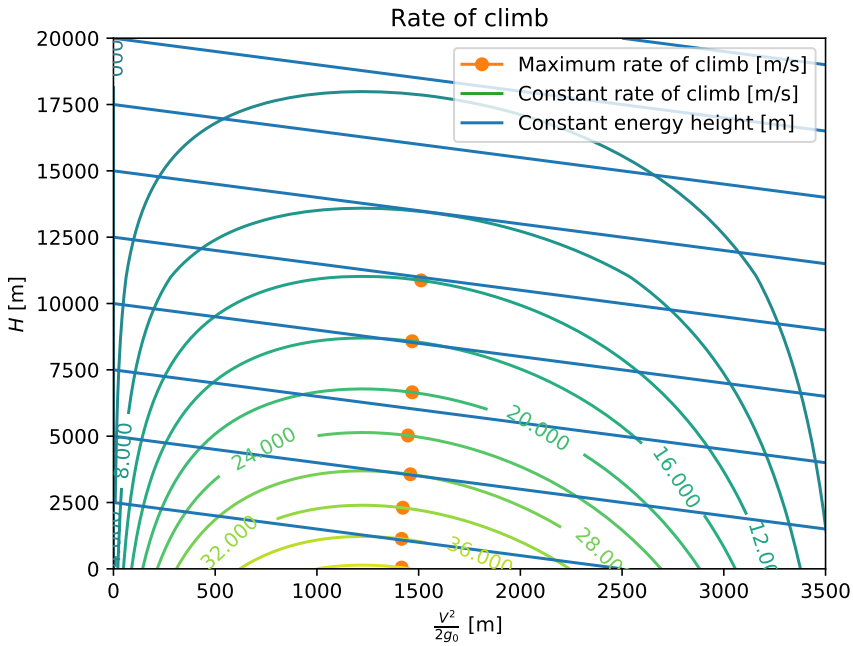

Figure 9.5: Rate of climb optimisation

9.2.2. Descent

Analysing descent performance follows the same method as in section 9.2, optimising for minimum descent time. For the descent phase the thrust is set at idle, which is at 7% of T_{max} [40]. By minimising both climb and descent time, the longest time is spent in cruise flight

9.3. Cruise performance

Rewriting the Breguet equation, Equation 9.28, the fuel consumed during cruise can be determined, where m_1 and m_2 represent the aircraft mass at the initiation and termination of cruise, respectively. The specific fuel consumption, c_j, is found in section 9.7. Following from mission requirements, presented in subsection 3.5.1; the cruise velocity, V_{cruise}, is set at 0.75 Mach (International Standard Atmosphere), cruise altitude is set at 37,000 ft, the aircraft's service ceiling. During the cruise flight, fuel is burnt and a slight decrease in lift is allowed, hence changing $\frac{L}{D}$. To obtain a more accurate result, the Breguet equation is applied incrementally, by dividing the total flying range into several parts.

$$R = \frac{V_{cruise}}{c_j}\left(\frac{L}{D}\right)_{cruise} ln\left(\frac{m_1}{m_2}\right) \tag{9.28}$$

9.4. Landing performance

The landing procedure is split up into similar phases as presented in section 9.1. Firstly the descent phase, which is similar to the climb-out phase.Subsequently the flare phase, which similar to the transition phase during take-off. This is followed by a rotation, where the nose of the aircraft is brought down to the ground. Finally, a ground run is performed in which the aircraft decelerates to standstill.

The assumptions made for take-off also apply to the landing analysis. The ground effect, however, has a negative impact on the landing field length. By neglecting it, the field length is underestimated. Several additional assumptions need to be made.The brakes are assumed to have a constant friction coefficient, μ_{brakes}, of 0.45 [80]. The engines are assumed to provide a reverse thrust of $0.4T_{max}$ [80]. The load factor, n, is assumed to be 1.10 and the time to rotate, $t_{rotation}$, is assumed to be 2 seconds [42].

The maximum weight at which the aircraft needs to be able to land within the required landing field length can be lowered by assessing how much of the fuel can be jettisoned and subtracting this from the $MTOW$ to find the MLW, the maximum landing weight. As currently, the landing requirements are easily met, fuel jettison is not required.

$$V_{approach} = 1.23 V_{stall} \tag{9.29}$$

$$\gamma_{approach} = \arcsin \frac{C_{D_{landing}}}{C_{L_{landing}}} \tag{9.30}$$

$$s_{descent} = \frac{h_{screen} - h_{flare}}{tan\gamma_{approach}} \tag{9.31}$$

$$s_{flare} = r(\sin\gamma_{approach}) \tag{9.32}$$

$$h_{flare} = r(1 - \cos\gamma_{approach}) \tag{9.33}$$

$$s_{rotation} = t_{rotation} V_{approach} \tag{9.34}$$

$$\overline{F} = -T_{reverse} - \overline{D}_{air} - \overline{D}_{ground} \tag{9.35}$$

$$s_{landing} = s_{descent} + s_{flare} + s_{rotation} + s_{ground\_run} \tag{9.36}$$

Table 9.4: Landing field length

	Config. 1	Config. 2	Config. 3
Landing field length $MTOM$, ISA, SL $[m]$	1,087.62	1,185.11	1,242.59

Table 9.5: Landing field length, 1 engine inoperative

	Config. 1	Config. 2	Config. 3
Landing field length engine failure $MTOM$, ISA, SL $[m]$	1,280.40	1,389.05	1,453.00

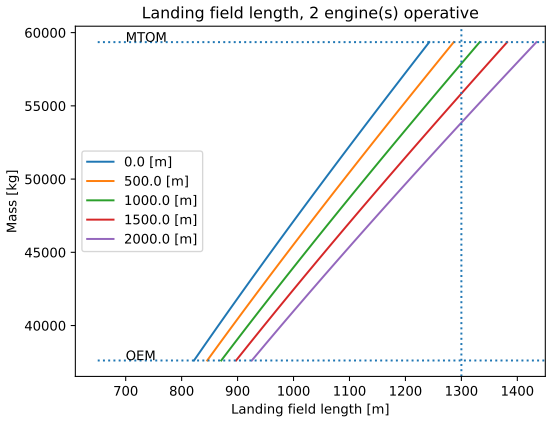

Figure 9.6: Landing field length of configuration 3

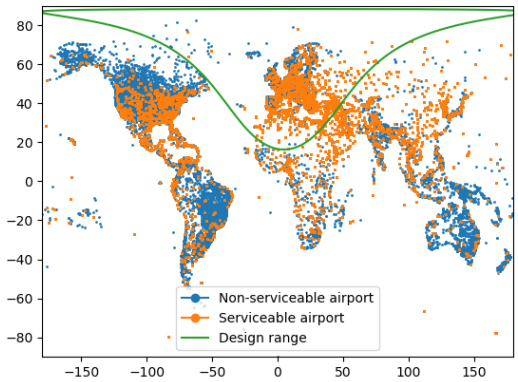

Figure 9.7: Serviceable airports configuration 3

9.5. Serviceable airports

Using the calculated take-off and landing field length, an assessment of the serviceable airports can be made. Only airports with a runway longer than the balanced field length at $MTOM$ and where landing at MLW with engine failure is possible are considered serviceable. This analysis only looks at serviceability in terms of performance, and ignores availability of ground operations. Note that, currently, the balanced field length exceeds the landing field length in all cases.

The balanced field lengths and landing field lengths at varying altitudes, calculated in 9.1.5 and 9.4, can be used to filter out serviceable airports from a large database [62]. Table 9.6 shows the percentage of aircraft in the database that are serviceable. Note that many airports in the database are relatively small. To get a better overview of what airports can be serviced, the result for configuration 3 are visualised in Figure 9.7. The flying range of the aircraft is plotted in green around *AMS* with a correction for latitude/longitude to correct for the map projection.

Table 9.6: Serviceable airport

	Config. 1	Config. 2	Config. 3
Airports serviceable	18.86%	14.34%	12.17%

9.6. Flight profile

The flight profile is split up into pre-flight, trip and contingency phases. These phases are presented in Table 9.7. Requirements for loiter (e.g. waiting for landing clearance) and diversion to an alternative destination (starting from take-off 2, which succeeds a failed landing attempt at the first destination) follow from *Standards and Recommended Practices: Annex 6* by *ICAO* [74]. E.g., loiter 2 requires a minimum of 30 minutes of flight at holding speed, at 450 m above the alternate aerodrome. Holding speed is set at the *ICAO's* maximum of 230 kts, aerodrome height is assumed to be 2000 ft. No hard requirement is set on the alternate destination range, based on section 9.5 an alternate range of 200 km was deemed to be sufficient.

Table 9.7: Flight profile phases

Pre-flight					
Engine start-up	Taxi				
Trip					
Take-off	Climb	Cruise	Descent	Loiter	Landing
Contingency					
Take-off 2	Climb 2	Cruise 2	Descent 2	Loiter 2	Landing 2

In future design phases, the flight profile should be optimised. Currently, flight phases are optimised independently, but due to the many dependencies between phases, this does not result in the optimisation of the profile as a whole.

9.7. Fuel economy

It is important to estimate the fuel consumption throughout the design process. Not only is it a large mass component that affects the sizing of all systems, but it also serves as a direct input to the sustainability analysis. To properly assess the fuel consumption in all flight phases, as defined in 9.6, the fuel flow as a function of thrust must be found. From *ICAO* tests on the *Pratt & Whitney PW1525G* [40], a linear relation between thrust and fuel flow is found, see Equation 9.37. The specific fuel consumption, c_j, can be found using Equation 9.38 and is used in section 9.3. The thrust setting during take-off and landing is fixed, the fuel mass burned during these flight phases can be found using Equation 9.40, where s is the take-off/landing field length and $\overline{V}$ the average velocity. As electrical taxiing will be used (subsection 12.6.1), taxi is assumed to not consume fuel. Fuel fractions, FF per phase can be calculated using Equation 9.39. Table 9.8 shows fuel characteristics per flight phase of configuration 3, whereas Table 9.9 shows the total fuel fractions per configuration.

$$\dot{m}_{fuel} = 7\times10^{6}\cdot T_0 + 0.1047 \qquad (R^2 = 0.9981) \tag{9.37}$$

$$c_j = \dot{m}_{fuel}/T \tag{9.38}$$

$$FF = 1 - m_{fuel}/MTOW \tag{9.39}$$

$$m_{fuel} = s/\overline{V}\cdot\dot{m}_{fuel} \tag{9.40}$$

9.8. Payload-range diagram

Figure 9.8, 9.9, and 9.10 show the payload range diagrams for configuration 1, 2, and 3 respectively. The zero-payload range is calculated using the Breguet range equation, Equation 9.28.

9.9. Flight envelope

To find the maximum loads the aircraft will encounter during utilisation, a flight envelope diagram can be generated. Figure 9.11 has been created following the method of *Airplane design - Part V* by *J. Roskam* [85].The ultimate load factor *n_ultimate* serves as an input for the structural analysis of the aircraft, covered in chapter 10.

Table 9.8: Fuel characteristics configuration 3

	$\dot{m}_{fuel}\ [kg/s]$	$m_{fuel}\ [kg]$	$FF\ [-]$
engine_startup	NaN	593.5	0.9900
take_off	1.534	30.8	0.9995
climb	1.396	1,840.4	0.969
cruise	0.309	2,191.9	0.963
descent	0.136	1,313.3	0.978
loiter	0.376	203.2	0.997
landing	0.622	14.7	0.9995
take_off_2	1.534	28.4	0.9995
climb_2	1.396	515.0	0.991
cruise_2	0.304	274.5	0.995
descent_2	0.068	681.9	0.989
loiter_2	0.376	677.0	0.989
landing_2	0.622	14.5	0.9998

Table 9.9: Total fuel fraction per configuration

	Configuration 1	Configuration 2	Configuration 3
$FF_{total}\ [-]$	0.8690	0.9093	0.8588

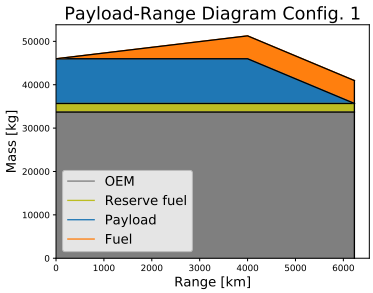

Figure 9.8: Payload-range diagram for configuration 1

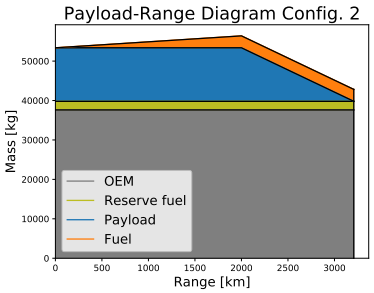

Figure 9.9: Payload-range diagram for configuration 2

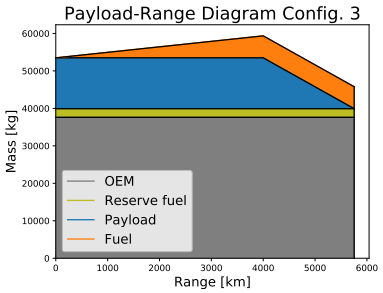

Figure 9.10: Payload-range diagram for configuration 3

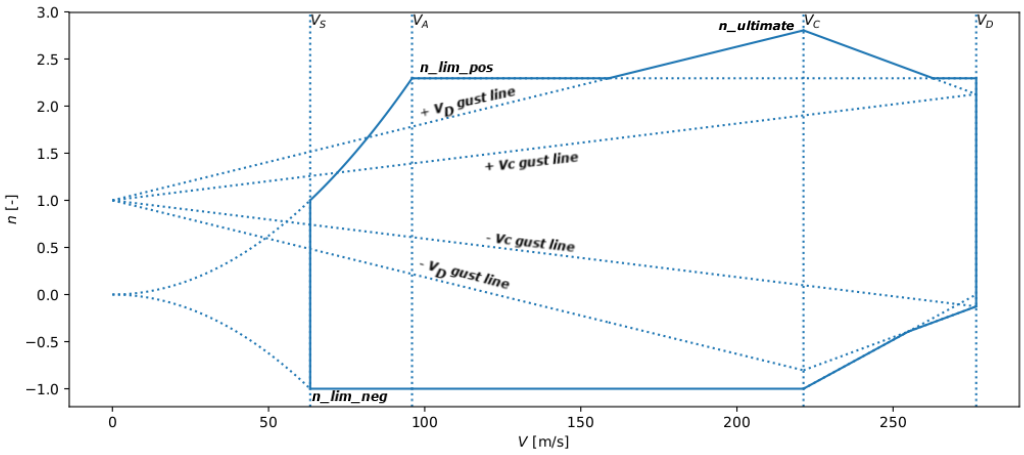

Figure 9.11: Flight envelope configuration 1

9.10. Verification and validation

Similar to other departments, the performance and propulsion calculations were written in code, split into several units, in turn built up out of definitions. The code structure is visualised in Figure 9.12.

The take-off and landing analysis consists of a rather complex code, built up out of 12 individual functions. Each

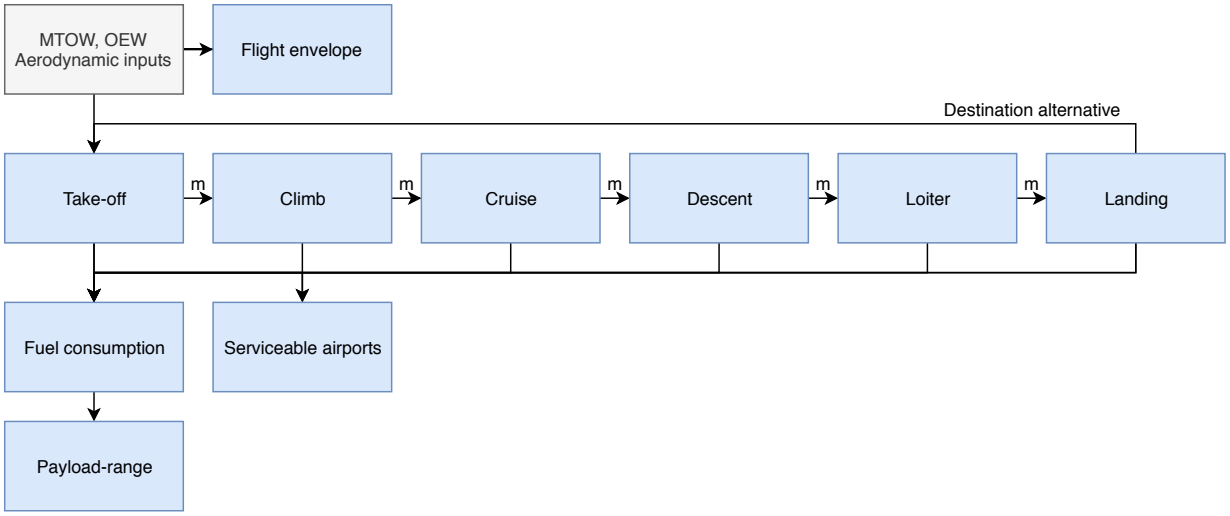

Figure 9.12: Visualisation of performance and propulsion code structure and flow

function's output was checked for correctness. A sensitivity analysis is applied as a sanity check. It is checked that an increase in $MTOW$ indeed increases the take-off field length required, also an engine failure will negatively affect the field length and V_1 must be asserted to be less than take-off velocity.

The climb/descent performance has been plotted in figures similar to Figure 9.5, to verify if the correct points were chosen. A sensitivity analysis, like for the take-off/landing analysis, can be used to check for sanity. Decreasing step size between energy heights should converge the solutions.

The cruise/loiter analysis is not very prone to code errors,as errors will likely follow from other units. Fuel consumption between phases were compared, used to test whether the results were logical considering the thrust setting and flight time per phase. As the payload-range diagram does not introduce any new definitions, all used definitions have been verified before, and it only needed to be checked if these were implemented correctly. For the flight envelope the following assertions that follow from *Airplane design - Part V* by *J. Roskam* [85] were implemented: $V_S < V_A < V_C < V_D$, the positive gust line must intersect the positive limited load, n_lim_pos, between V_A and V_D, and $n\_lim\_neg < -1.0$. Lastly, to avoid errors, only SI units were used. Alternative units from e.g. reference data were converted before use.

Because the aircraft is not built yet, nor has a simulation or physical model been made, validation data is limited to comparison with existing reference aircraft. All checked outputs are compared with the *Embraer E-195 LR*[1], *E-195-AR*[1], *E-175-LR*[2] and *E-175-AR*[2]. Take-off field lengths and landing field lengths are compared in Figure 9.13 and Figure 9.14, respectively. In both cases the aircraft performs equally well or even better at higher mass. The values are in reasonable range from the reference aircraft, however, and are bound to change with iterations. A likely cause of the differences would be the limited detail in the structural mass estimations and flap design done so far.

Climb time for the reference aircraft is available for a 500 nautical mile take-off weight, with a climb from sea level to FL350. By setting these requirements as inputs to the performance calculations, the required fuel mass for such a mission can be determined and the climb time can be found and compared. As a change in required fuel mass for the change of mission influences the fuel consumption, a few internal iterations, leaving all aerodynamic parameters fixed, must be done to converge to a new fuel mass. Results are presented in Table 9.10. The climb time for configuration 2 and 3, which are almost identical configurations in case of an equal flight mission, are very similar to the reference aircraft. Configuration 1 has a significantly shorter climb time, this can be explained by the fact that configuration 1 has equal thrust to the other configurations, but lower structural mass and drag.

Fuel consumption validation is covered in chapter 11. No reference information is available on descent, nor fuel

[1]URL: `https://www.embraercommercialaviation.com/wp-content/uploads/2017/02/Embraer_spec_175_web.pdf` [cited on 25 May 2019]
[2]URL: `https://www.embraercommercialaviation.com/wp-content/uploads/2017/02/Embraer_spec_195_web.pdf` [cited on 25 May 2019]

consumption per flight phase.

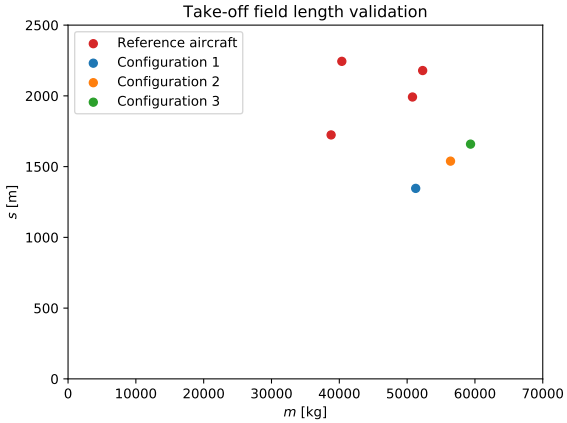

Figure 9.13: Take-off field length validation

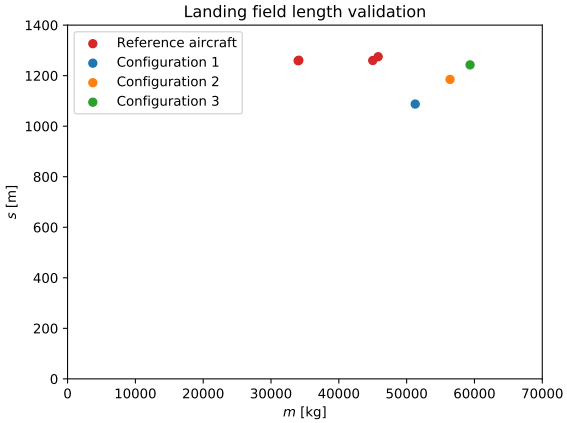

Figure 9.14: Landing field length validation

Table 9.10: Climb time validation

	E-175 LR/AR	E-195 LR/AR	Configuration 1	Configuration 2	Configuration 3
Climb time $[s]$	1,080	1,080	791.4	1,028.5	1,036.8

9.11. Sensitivity analysis

To assess how a change in input values affects the results obtained in the performance and propulsion calculations, a sensitivity analysis is performed. Several input values are altered by 10% [18]. Table 9.11 shows the sensitivity analysis for configuration 3. Only the landing field length requirement is at risk of not being met, indicated with the cells marked in red. A decrease in lift at take-off can be rather easily averted. A mass increase may not be avertable, but could be compensated for by an increase in lift by reselecting the airfoil or redesigning the high lift devices. For configuration one and two, all requirements, for all input variations, are met.

Table 9.11: Sensitivity analysis configuration 3

	Take-off field length $[m]$	Decision speed $[m/s]$	Take-off velocity $[m/s]$	Landing field length $[m]$	Approach velocity $[m/s]$	Fuel mass total $[kg]$
Nominal	1,658.977	57.9	62.86481	1,242.594	66.57867	8,381.739
C_L take-off -10%	1,808.703	61.1	66.26533	1,242.594	66.57867	8,226.688
C_L take-off +10%	1,538.471	55.1	59.93924	1,242.594	66.57867	8,380.209
C_L landing -10%	1,658.977	57.9	62.86481	1,323.98	70.18008	7,847.33
C_L landing +10%	1,658.977	57.9	62.86481	1,173.664	63.48027	8,450.501
C_L cruise -10%	1,658.977	57.9	62.86481	1,242.594	66.57867	8,664.438
C_L cruise +10%	1,658.977	57.9	62.86481	1,242.594	66.57867	7,995.159
$MTOM, OEM$ -10%	1,430.896	54.7	59.63879	1,123.118	63.16207	8,027.397
$MTOM, OEM$ +10%	1,915.584	61	65.93317	1,364.735	69.82829	8,263.392

10 Structures, Manufacturing and Materials

This chapter elaborates on the processes used to determine the structure of the adaptive aircraft, the materials used for each component, and the manufacturing processes. In section 10.1, materials that have been considered into the design are explained. It is followed by section 10.2, detailing the analysis conducted to size the components. Verification and validation procedures are elaborated upon in section 10.3. The manufacturing process is further explained in section 10.4 and the technical sensitivity analysis is described in section 10.5

10.1. Materials

The materials used in the aircraft must not only possess high strength and low density; they must also have sufficient stiffness against buckling instabilities and deformation. The long service life also demands resistance against fatigue, since the aircraft undergoes repeated loading and has to endure harsh environmental conditions. Moreover, it should also possess fracture toughness against impact by foreign debris. Metal alloys and composites are common materials used in the aerospace industry and are elaborated upon in subsection 10.1.1 and subsection 10.1.2, respectively. The rationale behind the material selection for major components of the aircraft is explained in subsection 10.1.3.

10.1.1. Metal alloys

Metal alloys have been used since 1920 and large demands for better performing aircraft have led to their significant developments [67]. Aluminium, steel, and titanium alloys have been widely applied in the majority of airframe structures. The performance of these materials can be enhanced by the shaping of the material grain, as well as by tempering.

Aluminium

Aluminium alloys are categorised in groups according to their composition. The groups 2000 series and 7000 series alloys are principal materials used for airframe structures, and contain copper and zinc as their major alloying element, respectively. The group 2000 series has a higher specific stiffness and ratio of fatigue to tensile strength than the 7000 series. Hence, it is an ideal material for fatigue critical components. The group 7000 series has greater yield strength and is preferred when static strength and stability are dominant [36]. Aluminium is anodic, and has negative galvanic potential, making it incompatible with cathodic materials, such as stainless steel and carbon fibre composites. When an anodic and cathodic material are in contact, galvanic corrosion occurs. This can be avoided by applying surface coating.

Steel

Steel is an iron-carbon alloy that has higher mechanical properties compared to aluminium, but at the expense of higher density. There are two major groups of steels, namely plain carbon steels and stainless steel. Plain carbon steel contains only carbon as an alloying element, whereas stainless steel contains additional alloying elements, such as nickel and molybdenum. Due to the high availability of iron ores, material cost is significantly lower. It is a common material used in landing gear struts, actuators and fasteners.

Titanium alloys

Titanium alloys are strong and lightweight. They are used not only for high strength applications, but also in high temperature environments because of their resistance against creep. Furthermore, titanium alloys are not susceptible to corrosion and have good fatigue properties. They are ideal materials, used in fatigue critical areas, where space is limited for the use of aluminium, or as firewalls between the engine and structure.

10.1.2. Composites

Composites are increasingly applied to many structural parts. Their continuous development has led to improved mechanical and physical properties that are competitive with metal alloys. Their properties are dependent on their composition of matrices and fibres, which can be varied to obtain optimum characteristics.

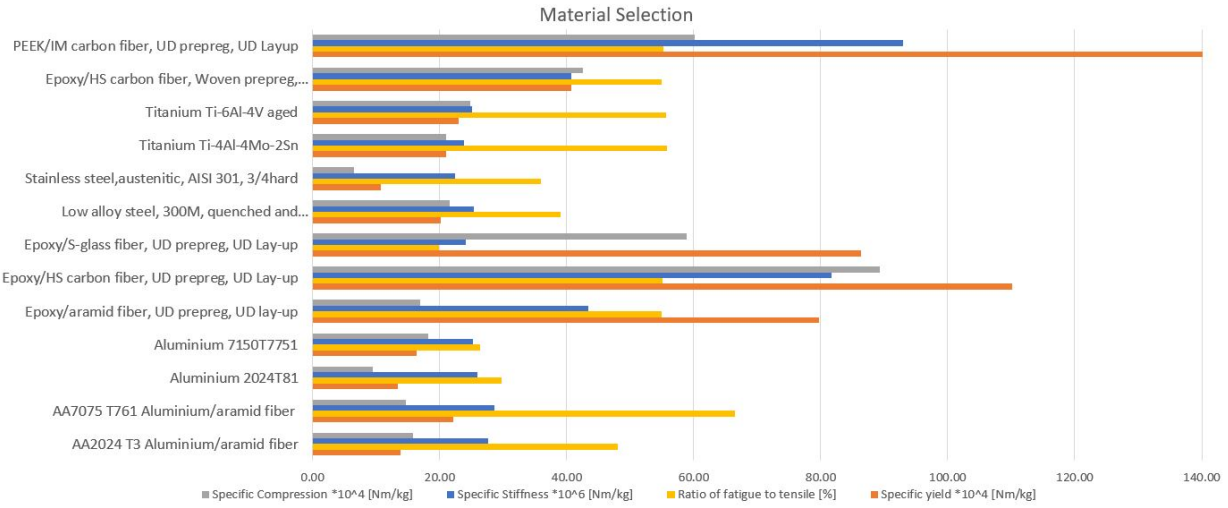

Figure 10.1: Bar graph of the materials and its specific material properties

The matrices are responsible for the binding of fibres together, and for the transfer and distribution of loads to it. There are many different types of matrices available. Matrices can be made from metal, polymer or ceramic. The composites that are being considered in the design of the aircraft are fibre reinforced polymer and fibre metal laminate. Fibres are mainly responsible for the composites' structural strength. They exist in different lengths, and can be woven into fabrics. The ones being considered are glass fibres, carbon fibres and aramid fibres. The fibres' directions can also be oriented to obtain a load tailored structure design.

Polymer matrix composites

Polymer matrix composites are commonly used in aerostructures, such as the skin of the wing, fuselage and empennage. Thermosets such as epoxy are large in quantity and easy to manufacture, making them cost effective and widely applied. Complex shapes could also be moulded. However, assembly and manufacture of composite components differs from metals, as the curing temperature, pressure and the materials' composition, as well as ply orientation, all have an influence on the resulting structural properties. Furthermore, it is also more challenging to design for and analyse given its non-isotropic nature, including imperfections in the actual manufacturing process. Thermoplastic matrices have also been considered. Unlike thermoset composites, thermoplastics offer the possibility to be re-melt and re-processed, reducing the environmental burden, improving the aircraft's performance in the aspect of sustainability. They can also be repaired by heating the local damaged area. The polymer matrix composites that are being considered are as follows:

- **Glass fibre reinforced polymer**
- **Carbon fibre reinforced polymer**
- **Aramid fibre reinforced polymer**

Fibre metal laminate

A fibre metal laminate is composed of multiple, alternating layers of fibre polymer composites and metal sheets. This hybrid material possesses not only strong mechanical strength and low density, but also long fatigue life, high residual strength and durability. The possibility to specify fibre orientation during the manufacturing process, allows for the strengthening of the components in specific directions. The alternating layers of composites also act as crack stoppers, improving the damage tolerance of the components. Aluminium aramid fibre epoxy laminate is considered into the design of the aircraft, as it is useful for fatigue critical parts, with relatively thin skinned structures.

10.1.3. Material selection

Different materials are selected that are best fitted for each component's specific purpose. Selecting the materials based on their static strength is not adequate; their density has to be considered as well. Hence, the specific stiffness (the ratio of young's modulus to density) and the specific strengths (ratio of strength to density) of the materials were evaluated as well. Additionally, the resistance of the material against fatigue was also an important aspect of the material selection. The ratio of fatigue strength to tensile strength was also taken into account.

The fatigue strength is the maximum cyclic stress for which the un-notched sample material survives 10^7 cycles. Furthermore, while some materials may be lighter and more advanced, they may be too expensive to attain, or expensive to manufacture. All material properties shown in Figure 10.1 have been obtained from the software CES Edupack 2018. The selection procedure was thorough and iterative, aiming to end up with the most efficient materials, while avoiding conflicts.

The criteria used for selection were:

- Material costs
- Static mechanical properties
- Specific mechanical properties
- Recycling and end of life characteristics
- Fabrication characteristics
- Compatibility with other materials

Fuselage

The skin of the fuselage is a fatigue critical area, as it experiences repeated compressive and tensile loading due to bending and pressurisation. The fuselage structure has to be stiffened, which can be done by selecting materials that have high specific stiffness. Aluminium 2024T81 has the highest specific stiffness compared to the other aluminium alloys. Furthermore, it has a good ratio of tensile to fatigue strength. Hence, it was chosen for the stringers. Epoxy/HS carbon fibre composites were selected for the skin due to their high specific strength properties. An insulation layer will be applied in between the aluminium alloy and carbon fibre composites, to prevent galvanic corrosion. The aluminium alloy and composite has thermal expansion coefficient of $23.8\mu_{strain}/^{\circ}C$ and $17.4\mu_{strain}/^{\circ}C$ respectively, which are different and generate stress. This can be reduced by adding an interlayer between the dissimilar materials [114]. Aluminium was chosen for the stringers, because it is able to yield and absorb the energy in the event of a crash landing, whereas composites exhibit brittle crush. Thermoplastic composites such as PEEK/IM carbon fibre, were considered for the fuselage skin. However, they are three times more expensive and have a lower specific compression strength than the thermoset carbon fibre composites. Furthermore, they are difficult to manufacture as they require a high temperature for compression and injection moulding. Therefore, they were not selected for the primary structures. However, thermoplastic composites could be applied to secondary structures and to the interiors of the fuselage. The materials properties can be seen in Table 10.1.

Components	**Materials**	**Cost** $[USD/kg]$	**Density** $[kg/m^3]$	**Young-modulus** $[GPa]$	**Yield Strength** $[MPa]$	**Compressive Strength** $[MPa]$
Fuselage skin	Epoxy/HS carbon fibre,Woven prepreg, Biaxial Lay-up	58.70	1,540	62.70	627	655
Fuselage stringers and web frames	Aluminium 2024T81	2.32	2,780	72	372	262

Table 10.1: Material properties of the fuselage components

Fuselage extension joints

The joints at the fuselage extension are critically loaded and experience a large stress concentration. The material selected must not only be very strong but must also possess strong resistance to fatigue. Furthermore, the fasteners at the joints are removable which makes them prone to abrasion and removal of protective surface coating, which can lead to fretting and surface corrosion. Titanium Ti-6Al-4V aged is an ideal material for both the joint fittings and removable fasteners. Its high strength and stiffness allow the joints to be small and fit in tight spaces. Furthermore, it is highly resistant against corrosion. The materials properties can be seen in Table 10.2.

Components	**Materials**	**Cost** $[USD/kg]$	**Density** $[kg/m^3]$	**Young-modulus** $[GPa]$	**Yield Strength** $[MPa]$	**Compressive Strength** $[MPa]$
Joints	Titanium Ti-6Al-4V aged	21.50	4,430	111	1,020	1,100

Table 10.2: Material properties of the joints

Wing/empennage/canard

The wing, empennage, and canard have to withstand the bending loads and vibrations during flight. The majority of the load will be carried by the box like structure inside them. AA7075 T761 Aluminium/aramid fibre was chosen for the skins of the lifting surfaces, as they are fatigue critical components. The spars and stringers will be made from Aluminium 7150 T7751, as it has the highest yield strength amongst the aluminium alloys, and has a relatively low cost. Furthermore, the replacement of damaged stringers is simpler with metal alloys than composites. As the fuel is stored inside the wing box, the material chosen for the wingbox structure must be non-flammable and non-reactive when in contact with organic solvents. Moreover, both materials have a similar galvanic potential. The materials properties can be seen in Table 10.3.

Components	**Materials**	**Cost** $[USD/kg]$	**Density** $[kg/m^3]$	**Young-modulus** $[GPa]$	**Yield Strength** $[MPa]$	**Compressive Strength** $[MPa]$
Skin	AA7075 T761 Aluminium/ aramid fibre	415	2,360	67.60	524	345
Spars, stringers, ribs	Aluminium 7150 T7751	4.43	2,810	71	462	510

Table 10.3: Material properties of the lifting wing, empennage and canard

Landing gear

Low alloy steel 300M, is an ideal material when quenched and tempered for the landing gear struts, as it has a high specific compression strength and stiffness. The materials properties can be seen in Table 10.4.

Components	**Materials**	**Cost** $[USD/kg]$	**Density** $[kg/m^3]$	**Young-modulus** $[GPa]$	**Yield Strength** $[MPa]$	**Compressive Strength** $[MPa]$
Landing gear Strut	Low alloy steel, 300M, quenched and tempered	0.91	7,870	200	1,590	1,700

Table 10.4: Material properties of the landing gears

10.2. Structure

This section elaborates on the methods that were used for the preliminary structural design of the aircraft. Figure 10.2 illustrates the general iterative process of the structural analysis which covered the wing, fuselage, empennage, canard and the joints. As stipulated in the CS-25 regulations, safety factor of 1.5 was applied to the limit load.

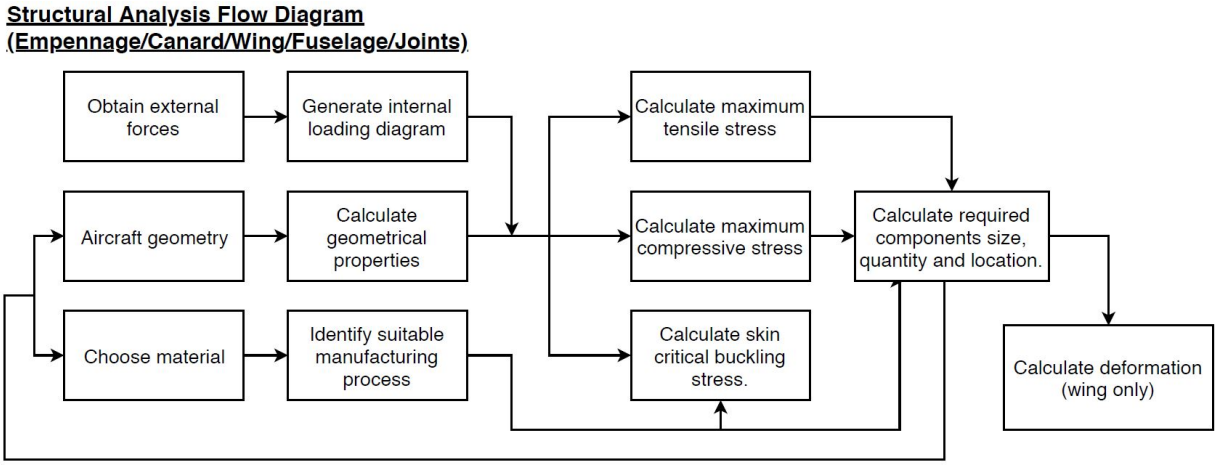

Figure 10.2: Structural analysis flow diagram

10.2.1. Fuselage

This section aims to explain the method used to analyse and size the fuselage. This analysis aimed to model all the forces that the fuselage experiences, and to model the fuselage as a beam in bending, in order to be able to find the required skin thickness and number of stringers throughout the fuselage length. The loads due to the pressurisation of the cabin were also considered.

First, the fuselage length was discretised into 10,000 sections. The fuselage was then modelled as a beam. The weight of each component, as calculated from the class-II weight estimation, and later from newer iterations, was modelled as a point load, at its respective centre of gravity. The lift from the tail and canard were modelled as point load. Additionally, the lift created by the main wing was modelled as linearly distributed loads over the wingbox length. The fuel mass was also grouped with the wing group mass. The payload weight was distributed over the cabin length. Finally, the moments exerted by the main wing were also added. A load factor, n, of 3.00 was applied, which was the maximum load factor to be experienced during flight, as was calculated in section 9.9.

First, the skin thickness was calculated, so that the skin can carry the hoop stress induced by the pressurisation of the cabin. The hoop stress, as calculated using Equation 10.1, should not exceed the yield stress of the skin's material. The stress is multiplied by a safety factor, to account for uncertainties. This resulted in a skin thickness of 0.31 mm. However, to avoid buckling of the skin, the skin thickness was increased to 1.5 mm, as is explained later on.

$$\sigma_{hoop} = \frac{\Delta P \cdot r}{t} \tag{10.1}$$

Next, the number of stringers had to be calculated. This was done in an iterative manner for each section. To begin with, the internal shear and bending moments diagrams of the fuselage were generated based on the applied forces. The internal load diagrams can be seen in Figure 10.3, Figure 10.4, Figure 10.5, and Figure 10.6.

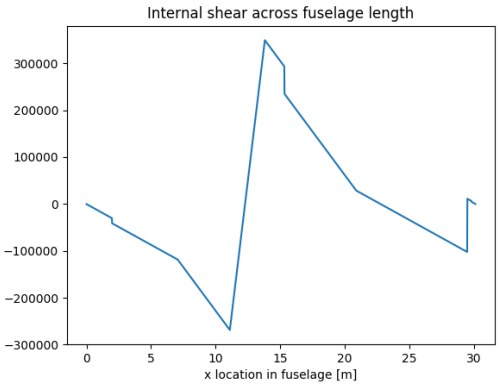

Figure 10.3: Internal shear against fuselage length for configuration 1 at ultimate load

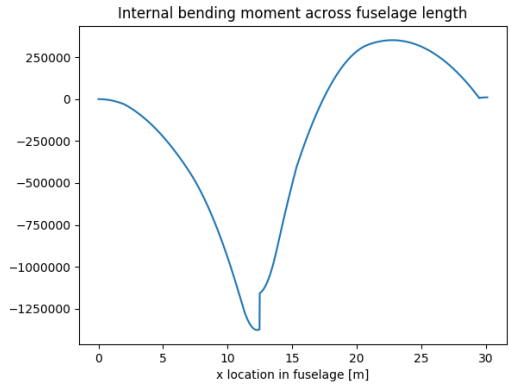

Figure 10.4: Internal bending moments against fuselage length for configuration 1 at ultimate load

The stringer type chosen was extruded J-stringers, as they have two joining points, and thus provide good fail-safe characteristics [6]. The stringer cross-sectional area was set at 200 mm^2. Next, for each discretised section, the area moment of inertia was calculated using the area of the stringers. This was used to calculate the maximum stress in the stringers, using Equation 10.2, which is caused by both the pressurisation and the bending moment. The maximum stress, after being multiplied by the safety factor, had to be lower than the yield stress of the stringers' material. When the stress exceeded the yield stress, a stringer was added and the calculation is repeated, until the number of stringers required for each discrete section is determined.

$$\sigma_{normal} = -\frac{M \cdot y}{I} + \frac{\Delta P \cdot \pi \cdot r^2}{A} \tag{10.2}$$

After the number of stringers required to prevent yielding due to axial stress was calculated, the number of stringers required to prevent buckling in the fuselage skin had to be calculated. However, since buckling would not cause a disastrous failure of the aircraft, the maximum load factor that was analysed for buckling was the limit load, without the application of the safety factor. As this is the maximum expected load on the structure in its lifetime, the occurrence is rare and the buckling load set was valid. Additionally, the stringers are designed to

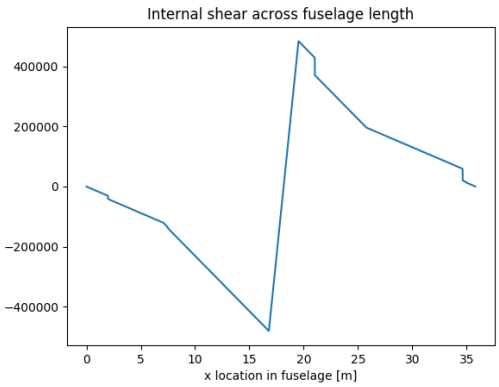

Figure 10.5: Internal shear against fuselage length for configurations 2 and 3 at ultimate load

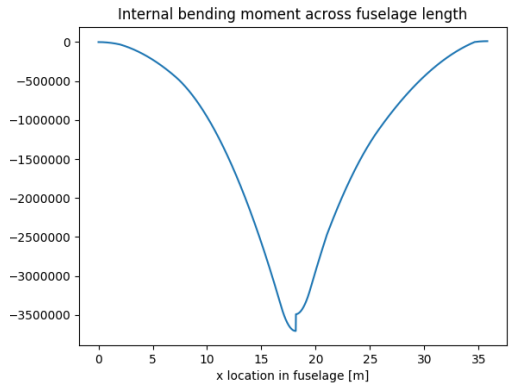

Figure 10.6: Internal bending moments against fuselage length for configurations 2 and 3 at ultimate load

be able to carry all the axial loads in case of a skin failure. The stresses that would cause buckling are compressive stresses, the maximum compressive stress can be calculated using Equation 10.2, as the most negative stresses.

For the buckling analysis, the skin is treated as a thin plate, with side lengths a and b. Where a is equal to the frame spacing, and b is equal to the stringer pitch. Using the same discretisation method as explained above, the compressive stress experienced in the skin was compared to the compressive strength of the material, as well as to the critical buckling load, σ_{cr}. When the stress experienced was higher, a stringer was added and the calculation was repeated again, until a sufficient number of stringers was found for each section. The critical buckling stress is calculated using Equation 10.3. As the buckling analysis of composites is complicated, it was assumed that the composite skin has isotropic characteristics similar to metals. Composite buckling analysis will be addressed in the next phase.

$$\sigma_{cr} = \frac{\pi^2 \cdot k_c \cdot E}{12(1-\nu^2)} \cdot \left(\frac{t}{b}\right)^2 \tag{10.3}$$

In this equation, ν is the Poisson ratio of the material used, equal to 0.058, and k_c is a constant that depends on ratio $\frac{a}{b}$ and the type of support along the unloaded edges. The plate was considered to be clamped along the unloaded edges, due to the use of adhesives in addition to fasteners, to join the stringers to the skin . Additionally, the lowest value for k_c, which corresponds to the highest $\frac{a}{b}$ ratio was chosen, in order to have a more conservative design. Because the $\frac{a}{b}$ ratio would be different for each section, depending on the number of stringers. At the first iteration of this method, it was realised that the number of stringers required would be disproportionately large. Hence, it was decided that increasing the skin thickness to 1.5 mm, is a reasonable solution to that problem, and showed a great improvement in the required number of stringers.

Finally, it was decided that the number of stringers would stay constant between web frames. Additionally, it was decided that the frame spacing would be constant throughout the fuselage length, at 0.5 m between frames [67]. However, at the cut section, a frame is added exactly at the section, to diffuse the stresses and transfer them to the joints. The highest number of stringers required between two frames, due to buckling or tensile yielding, was then chosen to be the number of stringers between those two frames. The whole analysis was done for configurations 1, 2, and 3. The highest number of stringers required was also taken at each location to come up with the final distribution. The final stringer number distribution is shown in Figure 10.7 and Figure 10.8, for the 90 passenger and the 120 passenger configuration respectively.

10.2.2. Wing

The wing's bending load and torque, generated by the aerodynamic forces, is mainly carried by the wingbox. This analysis aimed to model all the forces that the wingbox experiences, and to find the required skin thickness, number of stringers throughout the span, the size of the spars and the location of the ribs.

The front spar and rear spar of the wing are positioned at 15% and 65% of the chord, respectively. Due to the aerodynamic factors, the spars are positioned so that sufficient space is available in the wing to accommodate the high lift devices such as slats and flaps. Furthermore, it was aimed that the spars are placed at the location

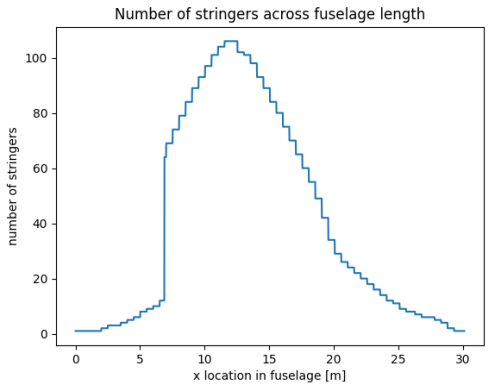

Figure 10.7: Stringer number distribution for configuration 1

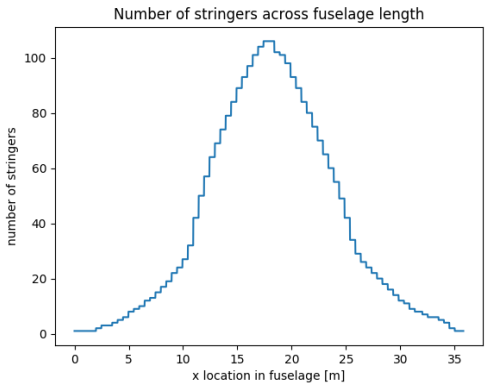

Figure 10.8: Stringer number distribution for configurations 2 and 3

where the wing has the highest thickness to chord ratio, in order to have a larger area moment of inertia. Moreover, the enclosed area of the wing box is also maximised, to provide structural strength against torsion. Stringers and ribs are used, to improve the wing skin's resistance against buckling.

Table 10.5: Load cases

Case	Load factor	Engine thrust	Fuel Weight
1	3.0	Maximum	Maximum
2	3.0	Minimum	Maximum
3	3.0	Maximum	Minimum
4	3.0	Minimum	Minimum
5	-1	Maximum	Maximum
6	-1	Minimum	Maximum
7	-1	Maximum	Minimum
8	-1	Minimum	Minimum

Since, the wing box has to be designed to withstand the critical loading conditions, different load cases had to be analysed, which are presented in Table 10.5. The internal shear, bending moment and torque have to be calculated at every point of the wing, to generate internal loading diagrams. The external forces considered in the analysis were wing lift and drag, engine's weight and thrust, and the main landing gear's weight and drag. Some assumptions were made for the analysis. The aerodynamic forces such as the lift and drag were assumed to be a distributed load on the quarter chord point across the span of the wing. The structure and fuel weights act at the neutral point of the wing box. External loads by the main landing gear and engine were assumed to be point loads acting on the wing. The shear centre of the cross-section was assumed to be at the same location as the neutral point. Furthermore, the analysis was carried out on steady, horizontal flight conditions.

The wing on each side is discretised into 1000 sections. The structural weight at each section is obtained by multiplying the cross sectional area by the discretised step size and the density of the material. The fuel weight at each section is obtained by multiplying the enclosed area with the discretised step size and the density of fuel (840 kg/m^3) [32][1]. The magnitude of aerodynamic forces generated at each section is directly proportional to the surface area of the section. The forces are calculated using the following Equation 10.4.

$$\begin{aligned} L_i &= S_i \cdot q \\ q &= \frac{MTOW_{config1} \cdot LF}{S} \end{aligned} \tag{10.4}$$

For the internal shear and bending moment diagrams, Macaulay's method was used. The reaction moment and shear at the root were calculated. Then, the internal shear force was calculated using Equation 10.5 and the internal bending moment was calculated using Equation 10.6.

$$\begin{aligned} V(y) &= \sum_{i=0}^{N} F_i(y-y_i) \cdot n \\ F_i(y-y_i)_{>0} &= F_i(y_i) \\ F_i(y-y_i)_{<0} &= 0 \end{aligned} \tag{10.5}$$

$$\begin{aligned} M(y) &= \sum_{i=0}^{N} F_i(y-y_i) \cdot (y-y_i) \cdot n \\ (y-y_i)_{>0} &= y-y_i \\ (y-y_i)_{<0} &= 0 \end{aligned} \tag{10.6}$$

As all the external forces do not act on the shear centre of the structure, the forces will induce an internal torque within the structure. The internal torque was calculated using Equation 10.7.

[1] URL: https://www.exxonmobil.com/en/aviation/products-and-services/products/jet-a-jet-a-1 [cited 24 June 2019]

$$T(y) = \sum_{i=0}^{N} \left(F_{i_x}(y - y_i) \cdot (z_i - \overline{z_i}) \cdot n + F_{i_z}(y - y_i) \cdot (x_i - \overline{x_i}) \cdot n + \frac{1}{2} \cdot \rho \cdot V_{air}^2 \cdot C_m \cdot S_i \cdot c \right) \tag{10.7}$$

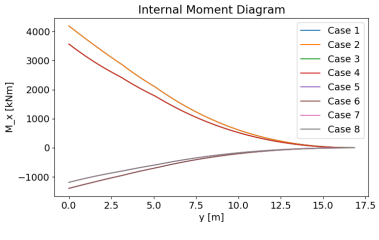

Figure 10.9: Internal bending moment diagram of the wing

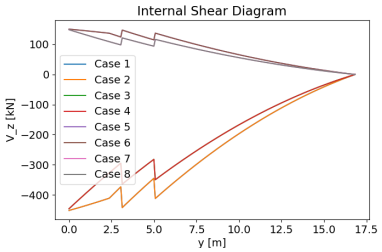

Figure 10.10: Internal shear diagram of the wing

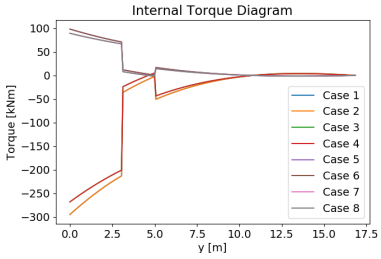

Figure 10.11: Internal torque diagram of the wing

The critical buckling stress of the skin had to be calculated, in order to determine the optimum number and location of the stringers and the ribs, together with the thickness of the spars and skin. The critical skin buckling stress is calculated using Equation 10.3, where b is the stringer spacing, and k_c depends on the ratio $\frac{a}{b}$, and the type of support along the unloaded edges. As clamped edges increase the critical buckling stress, the stringers will not only be fastened to the skin, but a layer of adhesives will also be used for joining. The magnitude of stresses at the upper skin has to be below the critical skin buckling stress as well as the maximum compressive stress of the material.

As the spars have to endure large shear stress that could lead to buckling at the webs, critical shear buckling stress was included into the analysis. It is calculated using Equation 10.8 [13]. The supports at the edges of the web panel were considered clamped. The shear centre was assumed to coincide with the neutral point of the cross-section. Shear stress at the web was calculated with Equation 10.9

$$\tau_{cr} = \frac{\pi^2 \cdot k_s \cdot E}{12 \cdot (1 - \nu^2)} \left(\frac{t_{web}}{b} \right)^2 \tag{10.8}$$

$$\tau = \frac{V(y) \cdot Q(y)}{I(y) \cdot t_{spar}} \cdot SF \tag{10.9}$$

$$\delta = \Sigma_{i=0}^{N} \frac{M_i \cdot L_i^2}{EI} \tag{10.10}$$

It was calculated that the wing spar has a constant web thickness of 15 mm, and that the wingbox's upper and lower skins have a thickness of 3.5 mm. The stringers used are J-stringers, and have a cross-sectional area of 630 mm^2. There are 11 ribs at each side of the wing. The number of stringers at each ribs location is in Table 10.6. The stringers are equally distributed in each section of the wing. The wing deflection is calculated using Equation 10.10 [63]. The normal stress at the upper skin, the shear stress at the spar webs, and the wing deflections can be visualised in Figure 10.12, Figure 10.13, and Figure 10.14, respectively.

Table 10.6: Number and location of stringers and ribs

Ribs	1	2	3	4	5	6	7	8	9	10	11
Ribs location [m]	0	0.85	1.69	3.38	5.07	6.77	8.46	10.57	12.69	14.80	16.92
No. of stringers at upper skin	28	28	25	23	20	17	14	11	8	5	2
No. of stringers at lower skin	20	20	18	17	15	12	10	8	6	3	1

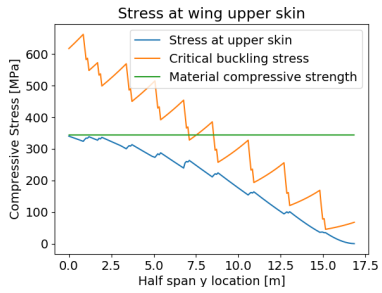

Figure 10.12: Compressive stress at the wing upper skin

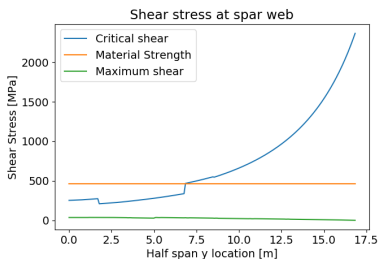

Figure 10.13: Shear stress at the spar webs

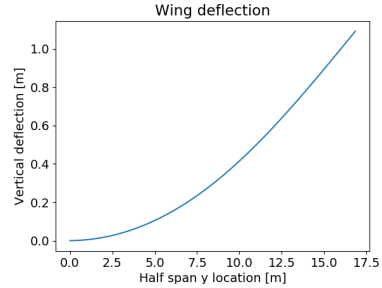

Figure 10.14: Wing deflections

10.2.3. Canard and empennage

For the vertical tail, horizontal tail and canard, the spars will be located at 15% and 65% of the chord. The analysis of these structures was carried out using the same method as in subsection 10.2.2. The structure differs due to the different magnitudes of aerodynamic forces that each experiences: the canard carries the additional lift needed for configuration 3, the horizontal tail carries the force needed to maintain longitudinal stability and the vertical tail carries the force needed to maintain lateral stability when one engine is inoperative. Table 10.7 shows the number of stringers and rib locations at each section of the canard and empennage.

Table 10.7: Number and location of stringers and ribs at the canard and the empennage

Ribs	1	2	3	4	5	6	7	8	9	10	11
Ribs location/half span [%]	0	5	10	20	30	40	50	62.5	75	87.5	100
No. of stringers at upper skin	16	16	16	14	13	12	10	8	6	4	2
No. of stringers at lower skin	12	12	12	10	9	9	7	6	4	3	1

Each stringers cross-sectional area is 300 mm^2. As the lifting surfaces experience different forces, the structures differ in skin thickness and spar thickness, as shown in Table 10.8

Table 10.8: Skin and spar thickness of the canard and the empennage

Structure	Vertical Tail	Horizontal Tail	Canard
Skin Thickness [mm]	2.5	1.5	2.3
Spar Thickness [mm]	5.0	3.0	4.5

10.2.4. Joint

For the adaptation method chosen, joints have to be used to connect the two fuselage sections together. The design of those joints is thus one of the most important aspects of the design at hand, as it is one of the few components that have to be designed specifically for this concept, and is not found in conventional aircraft. The joints were modelled as double shear lugs with two lugs on one side and one lug on the other fuselage side, with a bolt running through them. The detailed fastening method is elaborated on in subsection 12.1.2. The loads on the joint analysed, were the loads due to the bending moments, as calculated in subsection 10.2.1.

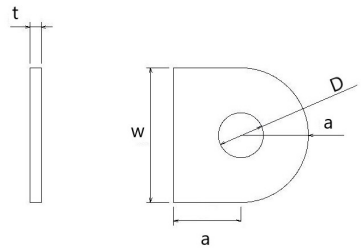

Figure 10.15: Lugs of fuselage-connecting joints

To begin sizing, the number of unknowns had to be reduced. For that, the dimensions of the lug were fixed as ratios of each other, with the thickness being the only variable. The ratios are $\frac{D}{t} = 4$, $\frac{a}{D} = 1.5$, and $\frac{W}{a} = 2$. This fixed the shape of the lug as visualised in Figure 10.15. Thus, changing the thickness would scale all of the other lug dimensions.

Three different failure modes were analysed for the lug in axial loading: shear-bearing failure, tension failure, and yield shear-bearing failure. The first failure mode is a shear tear-out, which assumes all the load to be transmitted on "40 degree planes" [67]. The ultimate load for shear-bearing failure is given by Equation 10.11.

$$F_{bru} = K_{br} \cdot A_{br} \cdot \sigma_{ult} \tag{10.11}$$

Where K_{br} is the shear-bearing efficiency factor, which depends on the ratios $\frac{a}{D}$ and $\frac{D}{t}$, and A_{br} is the projected bearing area equivalent to $D \cdot t$. The second failure mode is tension failure. The allowable ultimate load for tension failures is given by Equation 10.12.

$$F_{tu} = K_t \cdot A_t \cdot \sigma_{ult} \tag{10.12}$$

Where K_t is an efficiency factor for tension, which is dependant on the ratio $\frac{W}{D}$, and A_t is the minimum net section for tension, equivalent to $(W - D) \cdot t$. The final failure mode is yield due to shear-bearing. The yield axial load due to shear-bearing is given by Equation 10.13.

$$F_y = C \cdot \frac{\sigma_y}{\sigma_{ult}} \cdot (F_u)_{min} \tag{10.13}$$

Where C is a yield factor, which is dependant on the ratio $\frac{(F_u)_{min}}{A_{br} \cdot \sigma_{ult}}$, and $(F_u)_{min}$ is the smaller value of the two calculated before, F_{bru} and F_{tu}. The least of those three forces is taken to be the maximum allowable axial force on the joint, after being divided by a fitting factor of 1.15 [23].

Next, the number of joints was set at 12, to provide improved fail safe characteristics and adequate space for actuators. Furthermore, a thickness of 0.1 *mm* was assumed, and was used to calculate the area moment of inertia of the cross-section, which was used to calculate the stresses experienced by the lugs, using Equation 10.2, which translated finally into the forces experienced by the lug. When the forces experienced were higher than the allowable force, the thickness was increased by 0.1 *mm*, and the calculation was repeated until a suitable thickness, and thus size of the lug was determined. This was done for all configurations and for both cut sections, and the highest value was taken, since the same joints will have to be used at both location for compatibility. This led to a final thickness, t, of 9.3 *mm*, fastener diameter, D, of 37.2 *mm*, radius , a, of 55.8 *mm* and width, W, of 111.6 *mm*.

Further analysis was carried out to calculate the number of joints that are safe to fail, that will not lead to catastrophic failure of the fuselage extension. The analysis began with determining the critical failure stresses, after which the combinations of joint failures were iterated. The longitudinal stress due to pressurisation and bending increases as more joints fail. This leads to a maximum of 3 failed joints before a catastrophic failure.

10.2.5. Landing gear

In this subsection, the design of the landing gear will be presented. This consists of the sizing of wheels, the diameter of the strut, and the stroke of the shock absorbers.

Wheels

In order to size the wheels of the aircraft, the method from *Airplane Design part IV* from *J. Roskam* was followed[87]. From reference aircraft, it was determined that the main landing gear would be equipped with 4 wheels whereas the nose landing gear would consist of 2 wheels. The maximum loading acting on the wheels of the main and nose landing gears was determined. Following the FAR25 or CS-25 requirements, the wheels should be sized taking into account a safety factor of 1.07 on this maximum load, this is denoted as the ultimate load on the wheels. The determined wheel sizes are selected from a database of wheels from [87]. The wheels were chosen to be as small as possible while withstanding the maximum load, as the size of the wheels has a significant influence on the produced noise and drag. All landing gear parameters are shown in Table 10.9.

Table 10.9: Landing gear parameters

Landing gear	$N_{wheels}[-]$	$P_{max}[lbs]$	$P_{ult}[lbs]$	$P_{wheel}[lbs]$	$D[inch]$	$w[inch]$
Main	4	28,222	30,197.54	31,500	35.1	11.5
Nose	2	11,667	12,805	13,000	22.5	6.85

Strut

The strut at the nose and main landing gears should be designed to withstand the compression loads during take-off and especially landing. The strut should be equipped with shock absorbers to withstand the static and dynamic loads. The shock absorber stroke length and diameter were computed using the method from [87]. The sizing equation for the shock absorber stroke length is presented in Equation 10.14. The assumption here was made that the main landing gear is absorbing the complete kinetic energy during touch-down [87]. The type of shock absorbers selected were oleo-pneumatic. These have an efficiency of 0.8 according to [87], however, [67] reports that these shock absorbers have an increased efficiency up to 0.9.

Equation 10.14 is used to determine the length of the stroke. It should be designed for the length shown in this equation and by adding 1 $inch$ ($1/12$ ft). In Equation 10.14, w_t is defined by the FAR 25 and the s_t is the maximum deflection of the selected tires. All parameters aside from the Maximum Landing Weight and load acting on the main strut were retrieved from [87]. The maximum take-off mass was used for now to determine the landing weight, as it was determined in chapter 9 that this is possible with the current design. The resultant shock absorber stroke length was calculated to be 47.6 *cm*.

$$s_s = [(0.5(\frac{MLW}{g} \cdot w_t^2)/(n_s P_{m_{strut}} N_g)) - \eta_t \cdot s_t]/\eta_s + 1/12 \tag{10.14}$$

Table 10.10: Input values to determine the stroke of the shock absorber[87]

	MLW[lbf]	$P_{m_{strut}}$ $[lbs]$	n_s[−]	η_s [−]	N_g[−]	η_t [-]	s_t $[inch]$	w_t $[ft/s]$
$Strut_{main}$	130,667	56,444	2	0.8	2	0.47	2.85	12

In order to check whether the strut can withstand the compression loads, the failure in compression should be checked, using Equation 10.15. In addition, the strut should also have sufficient bending strength during side load condition as stipulated in CS-25.485.

$$\sigma_{compression} \geq \left(\frac{1.5 \cdot P_{m_{strut}}}{\pi \cdot D_{strut}^2/4} + \frac{0.8 \cdot P_{m_{strut}} \cdot l_{strut} \cdot r_{strut}}{\pi \cdot d^4/64}\right) \cdot SF \tag{10.15}$$

10.3. Verification and validation

The numerical analysis was performed with Python and has to be verified to ensure that the programme contains no code errors and that the underlying theory was correct.

The verification process began with unit testing of the individual components. The components were calculations of geometrical properties, force and moment equilibrium, internal loading, pressurisation and stress.

- Singularities check was performed, where the input values were set to zero to observe whether the results met the expectations.
- For the geometrical properties component, a CATIA model was made and compared with the numerical model. The difference in the wingbox cross-sectional area was 1.12%, in the z-neutral point 0.64%, and in the moment of inertia 2.04%. The difference in fuselage cross-sectional area was 0.92% and in area moment of inertia, 0.75%.
- The sum of forces and moments in the model was checked. Regardless of the input values, the forces and moments acting on the model should be in equilibrium. This was done by summing all the external forces and moments together and the resulting value should be zero.
- The internal loading diagrams were compared with an analytical model which was composed of standard beam deflection formulas. For example, the point loads and distributed loads were checked independently and the resulting diagrams should have the correct signs and values. The analytical model equations used for point load and distributed load are Equation 10.16, with reference to Figure 10.16, and Equation 10.17, with reference to Figure 10.17.
- Sizing of the lugs was verified by inputting values from the "Airframe Structural Design" book [67] and checking whether both answers were equal

Integration testing followed to check for faults in the interactions between individual units. The big bang approach was used, where all the units were combined and tested at one go. For example, the values used for the calculation of stress at a specific point of interest should be correctly obtained from the vast lists and arrays generated by the individual components. Furthermore, the results shown in the variable explorer were used to ensure input and output values were consistent and in SI units.

The system testing was carried out to ensure the programme met the desired specification. The verification of the calculation of the number of components and their size to meet the desired structural strength was done. Hand calculations were done to verify the stresses at the point. For the wing deflections, the standard beam deflection formula was used, shown in Equation 10.18 with reference to Figure 10.18. However, to compare both models, both cross-sections had to be constant. Hence, the inputs were changed to model a constant cross-section wing numerically, which was compared with the analytical model. The difference in the results was found to be 1.86%.

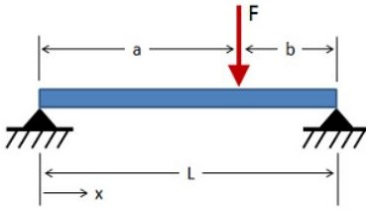

Figure 10.16: Analytical model of point load on a simply supported beam

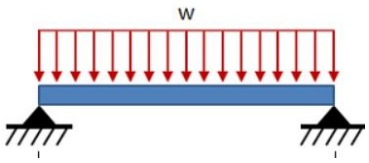

Figure 10.17: Analytical model of distributed load on a simply supported beam

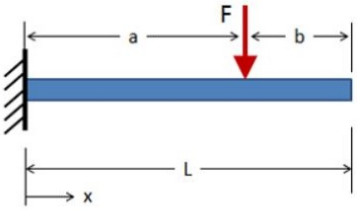

Figure 10.18: Analytical model of point load on a cantilever beam

$$M(y) = -\frac{F \cdot b \cdot y}{L} (0 \leq y \leq a)$$
$$M(y) = -\frac{F \cdot a \cdot b}{L} + \frac{F \cdot a \cdot (y-a)}{L} (a \leq y \leq b) \quad (10.16)$$

$$M(y) = \frac{1}{2} \cdot w \cdot y^2 \quad (10.17)$$

$$\delta_{max} = \Sigma_{i=0}^{N} \frac{F_i \cdot a_i^2}{6 \cdot E_i \cdot I_i} (3 \cdot L - a_i) \quad (10.18)$$

The aircraft of this specific design does not exist and there are no ready sources available to validate the structural analysis. Finite element method (FEM) modelling can be an alternative method for validation. However, due to the scope of this project, it was not carried out. Nevertheless, FEM is a useful method to check the accuracy of the results in the future.

10.4. Manufacturing

The manufacturing process plays an important role in the quality of the aircraft produced. It ranges from the fabrication process of individual components and the assembly of parts together to the integration of individual subsystems. In addition to that, the production process is also an important aspect to ensure that delays are minimised and the rate of production is maximised. In the light of sustainability, material wastage and energy consumption were also criteria for the selection of manufacturing processes.

10.4.1. Part manufacturing

The aircraft to be designed are composed of different materials. The shape of the components, as well as the material properties, dictate the fabrication process of the bulk materials to its final shape.

Stringers and fuselage web frames

Large quantities of continuous aluminium stringers are needed and its simple constant cross-section geometry make extrusion an ideal choice for fabrication. However, the extruded product is often not straight. A stretching machine or a three roll bending machine can be used to bend the stringers straight or to their required curvature. The metal grains in the extrusion are stretched during the process, introducing desired anisotropic behaviour [79]. The fuselage web frames can be manufactured with the same process, except with the three roll bending machine to bend it so that both ends meet together. The equipment and die cost are moderate and the automated process reduces labour cost.

Ribs

The ribs can be made from thin sheet of aluminium, by shearing away the parts that are not needed. It is important to allocate additional materials around the ribs for flanges, to provide means of attachment to the skin and spars [13]. The ribs also contain notches at the edges, to host the stringers and lightening holes to reduce the mass and provide access for inspections, wiring and fuel pipes. Rubber forming can be used to deform the sheet to its final component shape. The shape of the ribs differ spanwise and their relatively shallow drawing ratio makes rubber forming cheaper than die forming as only a male or female tool is needed.

Spars

The spars have a larger thickness and size than the stringers. Furthermore, the spar manufactured should be as long as possible to avoid joints, which contribute to additional weight. Extrusion is not a suitable process as the cross-section is large. Hot shape rolling is an ideal process to produce the spar as it can form long components. This process is often used to fabricate I-beams.

Skin

The manufacturing of the fuselage will be similar to the sector panel method used for the A350 [38][2]. It can be done by layup of continuous prepreg carbon fibre onto a mould. This process minimises wasted materials, further reducing material cost. Furthermore, the layup helps to achieve the desired fibre architecture. A layer of durable glass fibre epoxy will be added onto the CFRP to insulate it from the aluminium stringers. Like the fuselage, the skin of the wing, empennage and canard will be made from fibre metal laminate. This can be done by automatic tape layup of prepreg Aramid fibre onto the aluminium sheet. The skin will then be built from alternating layers of composites and aluminium.

Fuselage extension joints

Additional attention has to be given to the manufacturing of the fuselage extension joints. The lugs fittings and the bolts have to be forged in order to stretch the grain pattern of the titanium alloy to its desired shape. This process yields components with better strength and toughness, ideal in critical loading conditions. The non-uniform cooling of the part after hot forging, enhances the fatigue properties, where the outer section is under compressive stress and the inner section is under tensile stress [79].

10.4.2. Assembly process

In the previous section, the part manufacturing has been discussed. The next step is to bring all the components together into the final assembly. This would be done in an assembly line. This section will be split up in two parts. First of all, the development of an assembly line is presented. Secondly, the assembly line set up is presented along with the reasoning behind it. The development of the assembly line is schematically presented in Figure 10.19, and will be further elaborated on in the text.

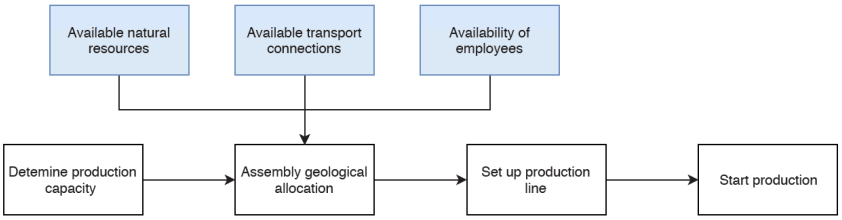

Figure 10.19: Schematic overview of assembly determination

The first thing to do in order to develop the assembly line, is to determine the desired production capacity. This is based on the market analysis which has been performed. A higher production capacity means that all factors mentioned below need to be scaled up.

The second aspect to consider in the procedure of setting up the assembly factory, is its geological location. These factories can consume lots of water and/or electricity. It is therefore important to have good access to resources at all times. It should also be taken into account that the resources should be made available in redundancy to avoid production delays, in case of a single point failure due to resource scarcity. The accessibility of the factory is also of major importance. Transportation facilities are vital, in order to have an efficient logistics process. Any incoming parts by either boat, train, airplane or truck should be easily and quickly transported to the factory. The assembly factory should also have direct access to an airstrip so that the produced planes can be flown to their customers directly. At last, it is important to also have the factory situated near a location which houses the desired working population. All aspects mentioned above need to be taken into account when selecting the geological location of the factory.

The next step is to set up the production line. This consists of designing the process itself, but also the building of the assembly line. Finally, the last step is to start producing aircraft.

The production assembly line will be split up into different stations. The advantages of this are as follows.

- Minimal transport
- Simple planning
- Good indication of progress

[2]URL: http://dx.doi.org/10.5772/intechopen.82353 [cited 20 June 2019]

- Maximal equal shaped products
- Maximal routine forming per crew [71]

For that reason, it was decided that the assembly line will be using stations. The aircraft will be moving through the stations very slowly. Each station is manned by the same crew. This means that the crew gets familiar with the tasks which they are performing over time, increasing the efficiency according to the learning curve [71]. In order to have the highest efficiency, each station should take the same amount of time. This ensures that the aircraft can successfully be moved on to the next station. An overview of the stations is presented in Figure B.1. In this figure, the blue boxes indicate external inputs. Dotted lines around boxes, indicate the current status, which is achieved from the previous station.

The first station will be responsible for collecting all individual part components. After this, the fuselage will be connected to both the nose and the tail sections as these are often individually produced at different locations. The alignment of these sections will be done using the laser alignment procedure presented in subsection 12.1.1. The fuselage is now completed but the wing still needs to be connected. This will be done in the second station. The horizontal and vertical stabiliser will also be installed in this stage. In the third station, all the interior items of the aircraft will be installed. This includes wires, but also chairs, lavatories and galleys. In parallel with this, the landing gear is installed. The aircraft assembly is now almost complete, and the first step of testing will start at the fourth station. This includes tests on the high lift devices, rudders, elevators, ailerons and the landing gear. In the fifth station, the engines will be installed onto the aircraft. In addition to that, fuel pipes, hydraulics and electric wiring to the engines need to be installed. The aircraft is now fully assembled and will be brought to the painting area, which is the sixth station. After the painting has been completed, the aircraft will undergo test flights to confirm it is working properly. The seventh station is closed with the delivery of the aircraft to the customer.

10.5. Sensitivity analysis

Material properties have an effect on the mass of the aircraft. The use of fibre metal laminate instead of aluminium alloys on the upper and lower panel of the wing box reduces the structural mass by 189.84 kg, a reduction of 3.38% of the wing mass. For the fuselage skin, the use of carbon fibre reinforced polymer contributes to a mass saving of 729.36 kg which is 7% of the fuselage mass. Therefore, the total mass reduction is approximately 2.42% of the operational empty mass. This indicates that the design is sensitive to a change in materials, in case the chosen materials could not be produced for other reasons.

Changes in the geometry of the aircraft, such as aspect ratio and taper ratio, like materials also have an influence on the structure, as well. An increase in aspect ratio of 30% results in an increase in mass of approximately 2,076 kg, which is an about 5.46% increase in operational empty mass and results in an increased wing deflection of 46.8%. An increase in taper ratio of 30% results in a mass increase of 456 kg which is an about 1.20% increase in operational empty mass. When the number of joints increases to 14, the total mass of the lugs decreases by 9%, and the additional space needed to accommodate the actuators reduces by 8.61%. The number of lugs that are safe to fail without catastrophic failure increases to 5, improving the fail safe characteristics. However, the accurate amount of space needed to fit the actuators and mechanisms can only be determined once the size of the actuators is determined.

11 Sustainable Development

In this chapter, the sustainable aspect of the design is analysed. Sustainability compromises of the impact of the design on the social, economic, and environmental aspect [101][1]. This chapter outlines how these aspects are taken into account in the design and what design measures were taken to develop an overall sustainable system. Firstly, the noise emissions of the aircraft are analysed in section 11.1. This is followed by the analysis of the emitted greenhouse gas emissions during operation in section 11.2. Subsequently the performed computations are verified and the outcomes validated as well as tested in their sensitivity to the inputs in section 11.3 and section 11.4 respectively. Lastly, the durability of the design in terms of material selection and retirement procedure is presented in section 11.5.

11.1. Noise emissions

The noise emissions of the aircraft reflect on the social aspect of sustainability. Aircraft noise emissions are becoming an increasingly important constraint posed by society, which is hindering airport expansion and thus growth of the aviation industry.

In the past, engine noise was the most prone source of aircraft noise. However, due to the technological developments over the past years, engine noise emissions decreased significantly. This revealed another major noise source of the aircraft, the airframe noise. During take-off, the major noise source remains the engine noise, as the engines are set at full power level during this flight phase. However, during approach and landing the airframe noise becomes the most prominent noise source as the thrust level of the engines is nearly idle in this phase. In chapter 3 two requirements were established in terms of the noise emissions of the aircraft, 1 for the take-off phase and 1 for the approach phase. These requirements and the point of measurements are based on the set noise requirements by The International Civil Aviation Organisation (ICAO). The noise reference point for take-off is set at a lateral distance of 450 m, and should be taken at the maximum noise level during take-off. The reference point for the noise emitted during approach is taken to be at 2,000 m from the start of the runway, which corresponds to an altitude of 120 m when an approach angle of 3 degrees is used. The point of reference is directly underneath the flight path of the aircraft [73].

11.1.1. Assumptions and implications

In order to estimate the noise emissions of the aircraft at take-off and approach, some assumptions had to be made. First of all, the aircraft was modelled to be a point source, such that the distance and directivity angles to the observer are the same for each of the aircraft's components. The aircraft is 120 m above the measurement point and the length of the fuselage is 35 m at its extended configuration, which would correspond to an angle of 8.38° between the observer and the nose/tail of the aircraft. Therefore, the small angle approximation (< 10 °) is considered to be valid. Additionally, it is assumed that the engine noise is the most dominant during take-off and the airframe noise is the dominant source on approach. This implies that these dominant noise sources determine the overall sound level during those flight phases. This could potentially lead to an underestimation of the noise emissions, as only the dominant sources of noise will be taken into account when assessing the noise levels at the required flight phases.

11.1.2. Airframe noise

In order to asses the airframe noise, which is the most dominant during the approach of the aircraft, the ANOPP model from NASA was used, which is a semi-empirical model [55]. From the course *'Advance noise modelling and measurement'* [98], the noise emissions of the major noise sources could be modelled: flaps, slats, trailing edge of the wing, landing gear and their struts. The model predicts the emitted noise level by computing the effective pressure using Equation 11.3. This is a function of the operational conditions, the acoustic pressure, P, the directivity function, D, and the spectrum function, F, which is a function of the Strouhal number, S. Figure 11.1 illustrates the used coordinate system in the ANOPP model, which is used in the calculation of the effective pressure and directivity function in Equation 11.3. The acoustic pressure, P, and Strouhal number, S, were calculated using Equation 11.1 and Equation 11.2. The directivity function, D, is a function of the polar directivity angle, θ, and the azimuthal angle, ϕ. The directivity function varies for each of the aircraft's airframe components and

[1] URL: `http://www.thwink.org/sustain/glossary/ThreePillarsOfSustainability.htm` [cited 17 June 2019]

can be found in the lecture slides of [98]. The same holds for the spectrum function,F, which is a function of the Strouhal number and it computational method varies for the different components.

$$P = KM^c G\left(\rho_\infty a^3 b^2\right) \tag{11.1}$$

$$S = \frac{fL(1-M\cos\theta)}{Ma} \tag{11.2}$$

$$p_e^2(f,\theta,\phi) = \frac{\rho_\infty a PD(\theta,\phi)F(S)}{4\pi r_{obs}^2(1-M\cos\theta)^4} \tag{11.3}$$

$$\mathrm{SPL} = 10\log\left(\frac{p_e^2}{p_{e0}^2}\right) \tag{11.4}$$

$$PBL = 10\log\left(\frac{p_e^2\Delta f}{p_{e0}^2}\right) = SPL + 10\log(\Delta f) \tag{11.5}$$

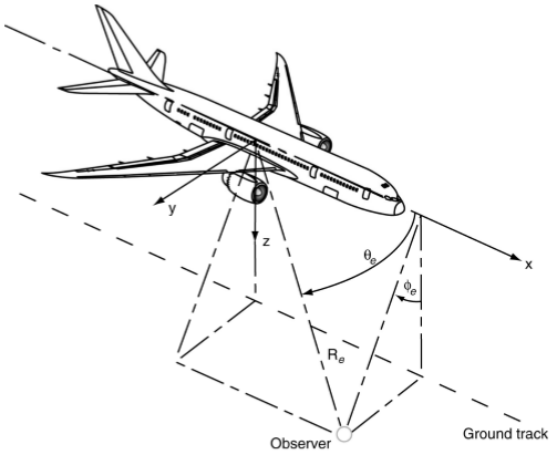

Figure 11.1: Coordinate system ANOPP method,[16]

The Strouhal number was calculated at 1/3 octave bands, which resulted in the effective pressure at each of these 43 centre frequencies. The effective pressure is converted to the Sound Pressure Level (SPL) using Equation 11.4, where p_{e_0} is equal to $2\cdot10^{-5}$. However, as only the centre frequencies are used to calculate the effective pressure, the SPL should be converted to the Pressure Band Level (PBL) by correcting for the width of the frequency band, as shown in Equation 11.5 [98]. The centre frequencies of the 1/3 octave bands were computed using Equation 11.6, where n denotes the number of the frequency band, which ranges from 1 to 43 for 1/3 octave bands. The width of each of the pressure bands is changing with increasing frequency and is computed using Equation 11.7 [98].

$$f_n = 10^{n/10} \tag{11.6}$$

$$\Delta f = f_U - f_L = \left(2^{1/6} - 2^{-1/6}\right) f_n = 0.23 f_n \tag{11.7}$$

In order to account for how humans perceive noise, the A-weighting method was adopted to the calculated PBL *dB* [98]. The change in PBL is again a function of the frequency at which the sound is produced, which can be computed using Equation 11.8. The Overall Sound Pressure Level (OSPL), with A-weightening *dBA*, is then computed using Equation 11.9.

$$\Delta L_\mathrm{A} = -145.528 + 98.262\log f - 19.509(\log f)^2 + 0.975(\log f)^3 \tag{11.8}$$

$$\mathrm{OSPL} = 10\log(\sum_{i=1}^{n} 10^{(\mathrm{PBL}(f)+\Delta L_A)/10}) \tag{11.9}$$

Lastly, in order to account for the Doppler effect, occurring between the aircraft and the observer, Equation 11.10 was used when the aircraft was moving towards the measuring points, whereas Equation 11.11 was used when the source is moving away. Additionally, the absorption of the sound by the atmosphere was accounted for, shown in Equation 11.12. This was evaluated at the standard atmospheric conditions of 20 degrees Celsius and 50% humidity.

$$f' = \frac{f}{1-\frac{V}{a}} \tag{11.10}$$

$$f' = \frac{f}{1+\frac{V}{a}} \tag{11.11}$$

$$PBL(f) = PBL(f) - \alpha(f)\cdot r_{observer} \tag{11.12}$$

However, the set requirement for approach is not expressed in *dBA*, but in $EPNdB$. This unit accounts for how the noise is perceived by humans and for the duration of the event. In order to convert *dB* to $EPNdB$, the different PBL for each of the 1/3 frequency bands had to be converted into the unit noy, which represented the noisiness of the PBL at the occurring frequency [98]. This is done using the noy graph, retrieved from the lecture slides of [98], which results in a noy value for every frequency. These are calculated into a total noy value, N, using Equation 11.13, which results in the Perceived Noise Level (PNL) using Equation 11.14, expressed in $PNdB$. Lastly, the Effective Perceived Noise Level (EPNL) is then calculated using Equation 11.15.

$$N = n_{\max} + 0.15\left(\left(\sum_{i=1}^{n} n_i\right) - n_{\max}\right) \tag{11.13}$$

$$\mathrm{PNL} = 40 + 33.3\log(N) \tag{11.14}$$

$$\mathrm{EPNL} \approx 10\log\left[\frac{\Delta t}{T_{10}}\sum_{k=t_1}^{t_2} 10^{\frac{L_{PN}(k)}{10}}\right] \tag{11.15}$$

the EPNL however has to be calculated accounting for the duration of the event, and therefore the PNL at multiple points from the observer had to be evaluated. This is illustrated in Figure 11.2. The second point is evaluated right above the observer, whereas point 1 and 3 are 5 seconds before and after the bypass of the aircraft. As discussed before, the requirement reference point is 2,300 m before touchdown, under an approach angle of 3°. This results in an altitude of 120.54 m at fly-over. Table 11.1 presents the calculated input conditions for the noise model at each of these measurement points. The used approach speed was the highest of all 3 configurations as speed has a very high influence on airframe noise. The resultant noise levels in dB as function of frequency are presented in Figure 11.3.

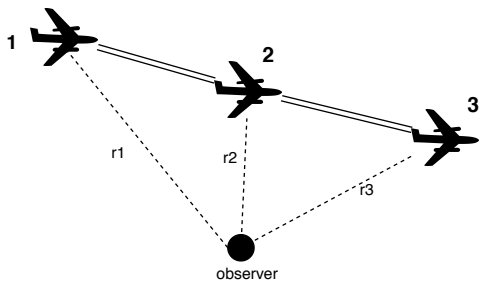

Figure 11.2: Points used to simulate fly-over

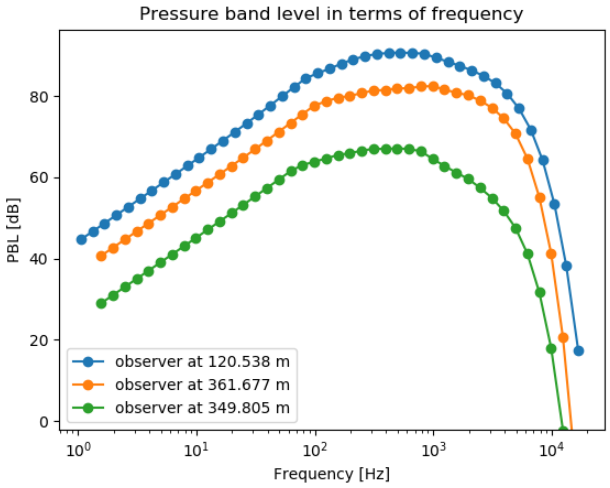

Figure 11.3: PBL values with frequency for different measurement points

Lastly, the results shown in Figure 11.3 were converted using the described approach to different units of noise. This is presented in Table 11.2. As expected, the noise levels are the highest for the second measurement point. The presented EPNL is 105 for the total fly-over of the aircraft, which is 15 $EPNdB$ above the set requirement. It was observed that the main airframe noise sources are mainly the flaps, slats and main landing gear.

Table 11.1: Inputs conditions for fly-over simulation at measurement point

	Point 1	Point 2	Point 3
$r_{obs}[m]$	361.67	120.53	349.8
$\theta[deg]$	22.44	90	162.87
$\phi[deg]$	0	0	0
$V_{appr}[m/s]$	66.95	66.95	66.95
$\delta_f[°]$	40	40	40

Table 11.2: Results of airframe noise model

	Point 1	Point 2	Point 3
PBL [dB]	93.01	101.05	77.42
PBL [dBA]	91.03	98.57	73.45
PNL [$PNdB$]	100.596	107.8	82.8
EPNL [$EPNdB$]		105	
Critical component	flaps/slats	flaps/mlg	flaps
PBL_{crit} [dB]	90/87	96	76

11.1.3. Engine noise

The engine noise needed to be assessed during take-off, as it is the most dominant source of noise during this flight phase. As mentioned under the listed assumptions, the engine noise will be the only source of noise considered during take-off.

In order to assess the noise level during take-off at the lateral position of 450 m described in the ICAO regulations [73], a certification database from EASA was used. This database contained the EPNL at the different certification points for a wide variety of jet aircraft [26]. Again the assumption was made that the level of noise of these reference aircraft at take-off was dominated by the engine noise. In this way the $EPNdB$ level of the selected engine could be determined. For the initially chosen engine, the PW1525G from Prandtl and Whitney resulted in a lateral noise level of 88 $EPNdB$, which is 2 $EPNdB$ over the set requirement [26].

11.1.4. Noise reduction measures

The engine does not meet the noise requirement for take-off currently. The increased bypass ratio is decreasing the exhaust noise of the engines, however, the fan noise is increased as its diameter increases with increasing bypass ratio. This can be partially reduced by using acoustic liners in the fan duct. These acoustic liners are made of noise absorbent material. Additionally, adding chevrons to the back of the engines show great potential in order to lower the engine noise even further. These improve the mixing of jet and ambient air to smoothen the transition between hot core air and cold bypass air. This technology has been applied to the Boeing 787 already [64]. The noise produced by the engines can be further decreased by optimising the speed at which the fan is rotating. In addition to that the engine noise can be reduced by introducing the zero splice concept, which is now possible with the latest manufacturing processes [49]. Combining this with the application of acoustic liners, can lead to a reduction of 5 dB. [56]. As these reductions occur at different parts of the engines, it is assumed that this noise reduction occurs over a wide variety of frequencies. This will reduce the overall noy values and thus the Perceived Noise Level (PNL). Therefore it is assumed that a reduction of 5 dB will translate in a reduction of 2 or more $EPNdB$. Therefore the requirement on a lateral noise level of 86 $EPNdB$ is achieved.

It was found that the flaps are the most prone sources of airframe noise of the adaptive airliner. Additionally, also the main landing gear and the slats were found to be the most dominant airframe components in terms of noise at one of the fly-over points. However if only one of these dominant noise sources is reduced, this will result in the fact that another component will become the most dominant. Therefore, all the three of these dominant airframe noise components need to be tackled. In order to reduce the flap noise, porous side edge devices are used on the flaps. Additionally, the settings of the slats could be optimised by reducing the gaps and increasing the overlap between the slat and the wing. Lastly, the landing gear noise could be reduced by applying a fairing to it. This noise reduction, which was achieved in [22], showed that a reduction of 2 $EPNdB$ is possible on the total landing gear noise. This paper was published in 2008, meaning that the technology probably has developed itself over time to increase its efficiency. In addition to the solid fairings, research has shown that applying a cloth layer to the fairing reduces the noise with an additional 2 dB [22]. The clothed fairings will be placed on both the nose wheels and the main landing gear to reduce the noise produced by these systems. From the results of the "Joint DLR & TU Delft Aviation Noise Workshop" [55], it could be concluded that each of the aforementioned noise reduction measures can achieve a 5 dB reduction of each of these airframe components. This accumulates to an overall reduction of 6.2 dB on approach [55], leading to a PBL of 94.9 dB at the indicated measurement point. This will also reduce the Effective Perceived Noise Level, which is currently 105 $EPNdB$, exceeding the set requirement with 16%. It is not straightforward to convert dB into $EPNdb$, as this heavily relies on the frequency at which this dB reduction is achieved. Therefore, the final EPNL of the aircraft upon approach could not be calculated at this stage. However, by implementing the noise reduction technologies, the noise level, expressed in dB, was reduced with 6.1%.

11.2. Greenhouse gas emissions

The emission of greenhouse gases by the aircraft concerns both the social and environmental aspects of sustainability, as this has a large impact on the environment and the public's health. As it is expected, and almost certain, that high emission aircraft will face increased taxes,and aircraft tariffs, it therefore also influences the economical pillar of sustainability. In this section, the greenhouse gas emissions of the aircraft during operation are analysed. These are considered to be the direct aircraft's emissions.

11.2.1. NO_x

The CAEP regulations are set by the International Civil Aviation Organisation (ICAO) [65]. These regulations were installed in order to aim for an improvement of the air quality in the vicinity of airports. Therefore, the regulations were generated for emissions emitted during a reference landing and take-off (LTO) cycle below 915 m altitude (3,000 ft) [27].

The regulated CAEP/6 NO_x emission of an engine is a function of the pressure ratio and the thrust levels, expressed in g/kN. The requirement relationship for the CAEP/6 is shown in Equation 11.16. This is a function of the pressure ratio, π_{oo}, as the higher it is, the more the air is compressed within the combustion chamber. This leads to a more complete combustion, leading to a lower fuel consumption. However, an increased pressure ratio increases the amount of NO_x emissions. As the selected engine, the PW1525G, has a pressure ratio of 38.67, the maximum D_p/F_{oo} according to the CAEP/6 regulations is 76.3, which represents the total mass of NO_x in grams divided by the rated output of the engine, expressed in kN [27]. The amount of NO_x emissions was calculated using the following method: First of all, a linear trend line was generated between the fuel flow and the Emission Index of NO_x for the used engine, where the data used comes from an EASA database [25]. For

the PW1525G, this linear relationship is shown in Equation 11.17. The amount of NO_x emissions in grams can then be calculated for each of the flight phases, as shown in Equation 11.18. Lastly, the total mass of the emitted NO_x should be normalised by the maximum thrust available for take-off under normal operating conditions [27], which in case of the PW1525G is equal to 108.53 kN. This calculation is shown in Equation 11.19.

$$(D_p/F_{oo})_{CAEP/6} = -1.04 + 2\pi_{oo} \tag{11.16}$$

$$EI_{NOx} = 29.171\dot{m}_{fuel} + 3.8626 \tag{11.17}$$

$$M_{NOx} = M_{fuel} \cdot EI_{NOx} \tag{11.18}$$

$$(D_p/F_{oo})_{NOx} = M_{NOx}/T_{max} \tag{11.19}$$

Using the fuel flow and fuel mass data calculated in chapter 9, the total NO_x emissions were calculated. The results are presented below in Table 11.3. The set requirement was to reduce the NO_x emissions with 55% with respect to the CAEP/6 regulations, which in this case is not fulfilled as the maximum achieved reduction is 49.8%. This can be improved in the future under the condition that the climb and descent phases are optimised for fuel efficiency, which is currently not the case. This could lead to a significant reduction in fuel flow and mass, which leads to a reduction in NO_x emissions.

Table 11.3: NO_x emissions of the adaptive regional airliner

	M_{NO_x} [g]	D_p/F_{oo} [g/kN]	reduction wrt CAEP/6 [%]
Config. 1	4,157	38.306	49.8
Config. 2	4,573	42.136	44.7
Config. 3	4,195	38.653	49.3

Another measure which could be taken is to reduce the pressure temperature at the combustion chamber. From [57], it was found that the EI of NO_x increases with increased combustion chamber pressure and temperature. However, lowering these parameters would lead to a less complete combustion process, which would then again increase the fuel consumption of the aircraft, and thus the CO_2 footprint.

11.2.2. CO_2

CO_2 emissions are a direct result of burning kerosene. The chemical reaction of burning fuel is shown in Equation 11.20. It can be observed that the amount of CO_2 is directly related to the amount of fuel burnt during flight. Making use of the molar masses of these molecules, allows the computation of the mass of CO_2 emitted for every kg of fuel burnt. For the chosen engine PW1525G, the used fuel is Jet-A, which has an emission factor for CO_2 of 3.15 kg/kg [106][2]. Therefore, the mass of CO_2 emitted during flight can be calculated using Equation 11.21.

$$2C_{12}H_{26} + 37O_2 \rightarrow 24CO_2 + 26H_2O \tag{11.20}$$

$$M_{CO_2} = 3.15 \cdot M_{fuel} \tag{11.21}$$

It is sufficient to analyse the fuel consumption to determine the performance of the aircraft in terms of CO_2 emissions, as these are directly related to each other. In the design of the adaptive regional airliner, the fuel consumption was minimised by making use of a state-of-the-art engine, advanced composites, and the overall minimisation of weight and drag. The selected engine, the PW1525G, has a high bypass ratio of 11.05. Having a high bypass ratio lowers the fuel flow of the engine and thus fuel consumption. Additionally, the PW1525G has a high pressure ratio of 38.67. Having a high pressure ratio is beneficial, as this creates a more complete combustion cycle in the combustion chamber. This results in a higher efficiency of the combustion process and therefore less fuel is needed to deliver the same amount of thrust.

Additionally, electrical taxiing is used to reduce the fuel consumption of the adaptive regional airliner. An electrical taxiing system is currently being developed by the company *Safran*, which shows great potential to reduce aircraft emissions in the future [90]. The system uses an electrical motor on the wheels of the landing gear, which is driven by power provided by the APU of the aircraft. This system will be in service by 2022.

It is aimed to have a 30.8% reduction in CO_2 emissions in comparison to the Embraer E-1 family, as discussed in chapter 3. As mentioned before, this can be done by simply comparing the fuel consumption of the E-1 family with the values of the adaptive regional airliner. The fuel consumption of the different aircraft of the E-1 family are given in Table 11.4 [30]. The fuel consumption presented in Table 11.4 were normalised by the amount of passengers and the range flown. The single-class configuration of the aircraft were used, which resulted in 88

[2]URL: `https://www.verifavia.com/greenhouse-gas-verification/fq-how-are-aircraft-co2-emissions-calculated-11.php` [cited 3 June 2019]

passengers for the E175-E1 [8][3] and 114 for the E190-E1 [9][4]. The results are also shown Table 11.4.

Table 11.4: Fuel consumption for different missions of the ERJ175 and ERJ190 [30]

Aircraft Type	**Fuel for 500** $nm[gal]$	**Fuel for 1,000** $nm[gal]$	**Fuel for 1,500** $nm[gal]$
Embraer 175-E1	656	1,192	1,727
M_{fuel}/ N_{pax}/R $[kg/km]$	0.025	0.022	0.022
Embraer 190-E1	834	1,467	2,133
M_{fuel}/ N_{pax}/R $[kg/km]$	0.024	0.021	0.021

The fuel consumption of the design was analysed and assessed in chapter 9. The fuel consumption for nominal flight conditions, meaning without reserve fuel for redirections, was used to quantify the fuel used per passenger per kilometre. The outcomes are presented in Table 11.5. It can be observed that the requirement of a 30.8% reduction of CO_2 emissions is met for all configurations of the adaptive regional airliner. This percentage reduction was calculated using the lowest value of Table 11.4.

Table 11.5: Fuel consumption of the adaptive regional airliner

	M_{fuel}/N_{pax}/R $[kg/km]$	reduction wrt E1 family [%]
Config. 1	0.0137	34.73
Config. 2	0.01331	36.64
Config. 3	0.0130	38.06

11.3. Verification and validation

In this section the verification and validation of the noise and greenhouse gas numerical model and computations is presented.

11.3.1. Verification

In order to verify the numerical model in terms of noise and emission calculations, the approach described in chapter 5 was followed. First of all, unit testing was performed. This was done by coding the different steps needed in small functions and testing individually whether the output had the desired format. Additionally it was tested whether the functions responded correctly to a known input. For example, the function on the A-weightening correction factor was verified by plotting the applied correction factor and compare this to the reference given in [98]. This plot is shown in Figure 11.4 and it was concluded to be correct. Additionally, the influence on the PBL of the A-weightening over the different frequencies was plotted in Figure 11.5. It could be concluded that this function adopted the correction factor correctly in analogy with Figure 11.4. For the same reasons, Figure 11.6 was generated, and as the absorption coefficient increases with increasing frequency, this was concluded to be incorporated correctly. Lastly, the computations of the Strouhal number and spectrum functions for each of the airframe components were verified. Figure 11.7 shows the logarithm of both components as a function of each other. This was compared to the results presented in [98] and was concluded to be correctly implemented.

Next to unit testing, system testing was also performed. This was done on both the integration of the individual functions into one module as on the integration in the main numerical model where it is connected to the other modules. These system tests where executed in the same way. The individual functions were tested, by checking whether the output has the desired format and whether it corresponds correctly to the given input. The outputs of the individual functions inside of the integration module were checked in the same way as described with the figures above. The performed calculations on the greenhouse gas emissions of the aircraft were based on the computations performed in chapter 9. However, the same procedure described above was followed to test the functions used for computations on the greenhouse gas emissions.

[3] URL: `https://web.archive.org/web/20160304123925/http://www.embraercommercialaviation.com/AircraftPDF/E175_Cabin.pdf` [cited on 20 June 2019]

[4] URL: `https://web.archive.org/web/20140327123144/http://www.embraercommercialaviation.com/AircraftPDF/E190_Cabin.pdf` [cited 20 June 2019]

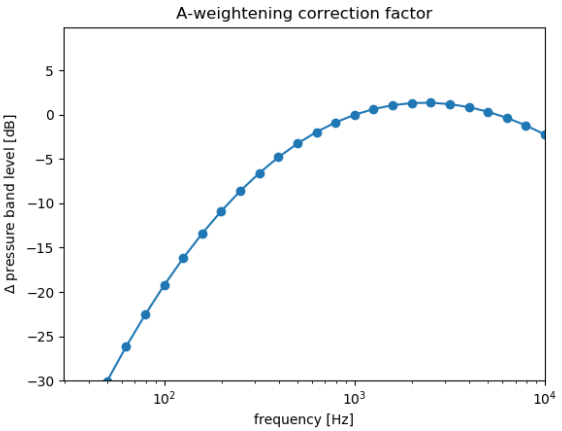

Figure 11.4: A-weightening correction factor

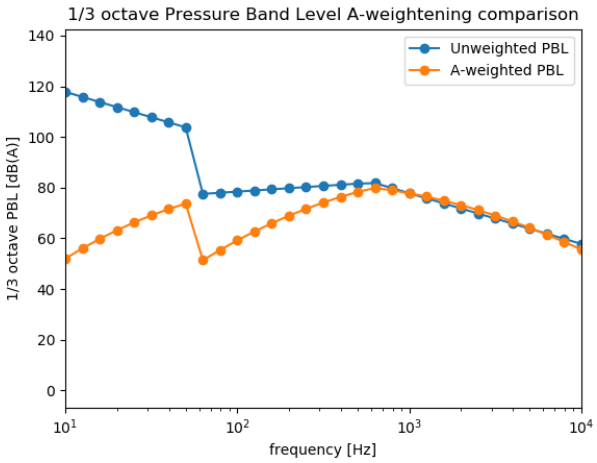

Figure 11.5: Pressure Band Level unweighted and A-weighted comparison

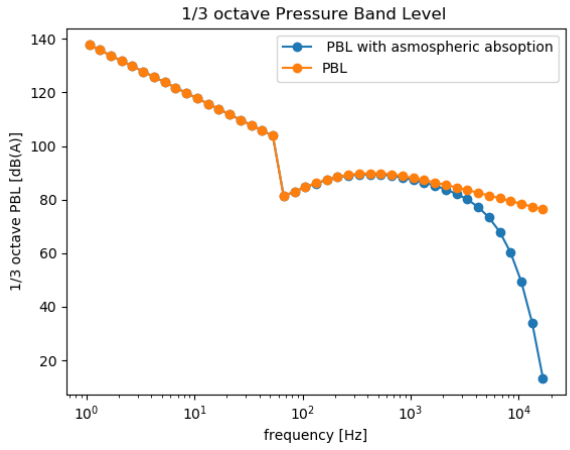

Figure 11.6: Pressure band level without and with atmospheric absorption comparison

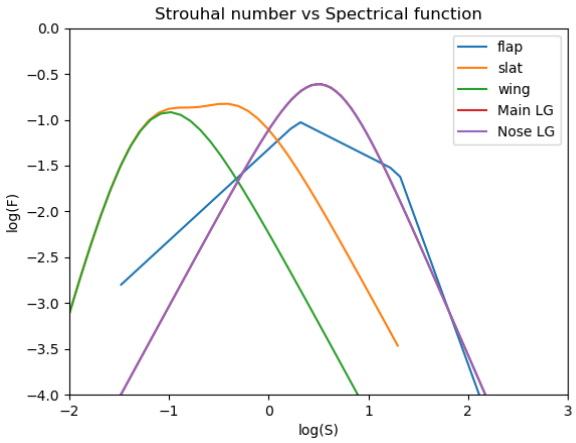

Figure 11.7: Strouhal number with spectrum function for airframe components

11.3.2. Validation

In this subsection the validation procedures and followed method are presented for the noise and greenhouse gas emissions analysis. As described in the main design methodology in chapter 5, this was done by comparing the obtained values to those of reference aircraft and other available sources on tests of the used engine.

Firstly, the noise model used to calculate the airframe noise, has to be validated. For this, experimental measurements were used, retrieved from [95]. As a reference, the Boeing 737 was used, of which the main characteristics important for noise emissions are shown and compared to those of the adaptive airliner in Table 11.6. In order to make a valid comparison, the distance of the observer and the approach speed was set to the values of the experimental measurements. Figure 11.8 and Figure 11.9 plot the PBL in dB as a function of the frequency for all the airframe components.

Table 11.6: Input values for noise validation [95]

	$r_{observer}$ $[m]$	$V_{approach}$ $[m/s]$	S $[m^2]$	b $[m]$	S_{flaps} $[m^2]$	b_{flap} $[m]$
Boeing 737	70.4	81	130	34	18	17
Adaptive airliner	70.4	81	120.46	33.83	26.06	16.5

It can be seen that the order of magnitude of the pressure band levels of both aircraft are similar. For both aircraft, the same airframe components are the most dominant, namely the flaps, slats and main landing gear. Small differences occur, however these can be explained by the (small) differences in geometry. The only significant difference is the PBL of the slat in function of the emitted frequency. For the adaptive airliner, the PBL is higher

at high frequencies, whereas this is not the case for the Boeing 737. Again, this is possibly caused by differences in the geometry.

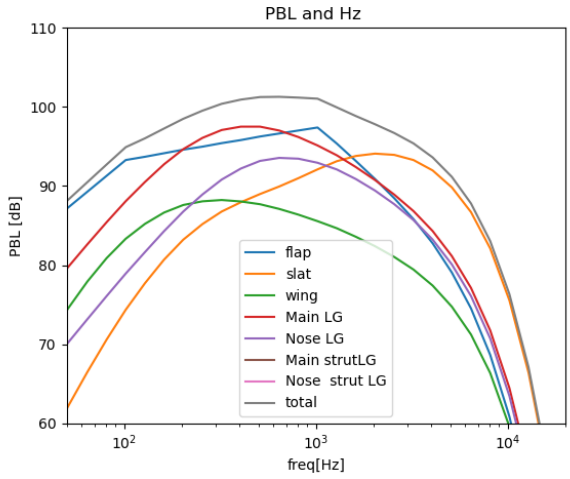

Figure 11.8: Results of noise numerical model for adaptive airliner

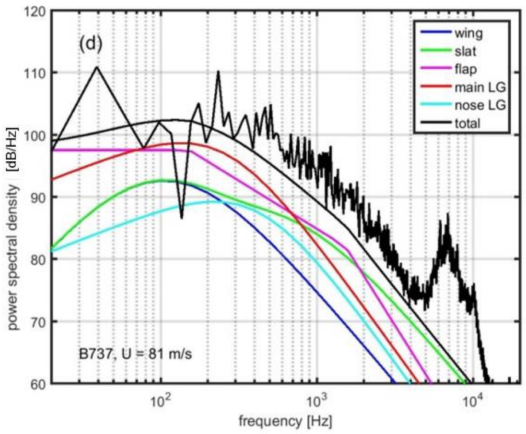

Figure 11.9: Experimental measurements airframe noise B737 at Schiphol airport [95]

In order to validate the results on the NO_x emissions of the aircraft under 3000 ft, the results of a reference LTC with the same engine were used. These results were obtained from a certification database of EASA [25]. It can be observed from Table 11.7, that the total mass of NO_x between the different configurations and the reference LTC show good consistency, which can also be concluded for the take-off and climb conditions. However, for the descent and approach phase there is a significant discrepancy between the fuel flows and emissions indexes (EI). The high fuel flow and EI during landing can be explained by the use of reverse thrust in the landing for the adaptive regional airliner, which was not taken into account in the reference cycle. Additionally, the approach phase in the reference cycle has a higher fuel flow and EI. This could be explained as the descent phase was modelled to have a constant thrust setting in chapter 9. This means that the approach phase is modelled the same as the global descent phase, which results in a lower fuel consumption than the reference cycle.

Table 11.7: Comparison values NO_x calculations with reference LTO [25]

	Fuel flow $[kg/s]$				EI_{NO_x} $[g/kg]$				M_{NO_x} $[g]$
	TO	Climb	Appr.	Landing	TO	Climb	Appr.	Landing	
Reference	0.79	0.65	0.23	0.08	28.1	21.2	11.1	6.1	4,125
Config. 1	0.765	0.698	0.056	0.349	26.23	24.23	5.5	14.04	4,157
Config. 2	0.767	0.698	0.067	0.349	26.23	24.23	5.84	14.04	4,573
Config. 3	0.767	0.698	0.067	0.349	26.23	24.23	5.84	14.04	4,195

The results on the CO_2 emission analysis were validated by comparing the nominal fuel mass per passenger and kilometre of the adaptive regional airliner with comparable and more recent aircraft than the Embraer E-1 family. The results are shown in Table 11.8 [109][5]. It can be observed that the values for the Airbus 319neo, Boeing 737-MAX-7 and the adaptive airliner are in the same order of magnitude. However, the reason that the adaptive airliner performs significantly better could be explained by the range these values are calculated for. The actual range of the Airbus 319neo & Boeing 737-MAX-7 is in reality a lot higher, which would reduce the fuel economy as take-off and climb require more thrust than the cruise phase, which would be extended in case of longer range. The same explanation holds for the Embraer E-2 family. The Antonov is most comparable to the the first configuration of the adaptive airliner, however its fuel economy is a lot higher in comparison. This can be explained by the fact that it went into service in 2010, meaning its design phase started in the early 2000's. The adaptive airliner only enters into service into 2035 and therefore uses state of the art technologies and materials.

11.4. Sensitivity analysis

In order to test the influence of the inputs on the presented results, a sensitivity analysis is performed. To comply with the conceptual design phase that the group is in, a contingency factor of 10% is used for the design [18].

[5]URL: `https://en.wikipedia.org/wiki/Fuel_economy_in_aircraft` [cited 20 June 2019]

Table 11.8: Comparison of fuel consumption of recent comparable aircraft [109]

	1st flight	N_{pax} [−]	Range [km]	$M_{fuel}/pass/km$ [kg/km]
Airbus 319neo	2015	136	1,900	0.0176
Boeing 737-MAX-7	2017	140	1,900	0.0179
Antonov An-158	2010	99	2,204	0.028
E175-E2	2020	88	1,100	0.028
E190-E2	2018	106	1,100	0.027
E195-E2	2019	132	1,100	0.023
Adaptive Airliner	2035	90-120	2,000-4,000	0.013-0.0137

For the airframe noise model, the main input variables were changed, of which the results are presented in Table 11.9. Only one of the input variables was changed at a time, in order to get the best insight on the influence. When the span of the flap or wing was adjusted, the chord remained the same and therefore also the area was adjusted with the same percentage as the span.

Table 11.9: Sensitivity analysis airframe noise model

	V_{appr} [m/s]		ϕ[°]	θ[°]		b_{flap}[m]	δ_f[°]		D_{mlg} [m]	b [m]
	+10%	-10%	45	45	135	+10 %	20	60	+10%	+10%
PBL [dB]	103.8	98.0	100.2	104.82	92.9	101.2	100.1	100.7	101.2	101.1
Δ% nominal conditions	2.67	-3.07	-0.89	3.68	-8.11	0.1	-0.99	-0.39	0.1	0

It can be observed that the approach speed has the largest influence on the noise level, as expected. In the ANOPP model, the effective acoustic pressure of the different components scales with velocity to the power 5 or 6. Furthermore do, ϕ, and especially θ, have a significant influence on the noise level. In terms of the design of the adaptive regional airliner does the geometry have a rather small influence on the emitted noise level. A change in the flap deflection settings and approach speed on the other hand would influence the emitted noise level and these parameters should be optimised in the further design phases.

Table 11.10, shows the fuel consumption per passenger and kilometre with an added 10%. It can be observed that if the fuel consumption of the aircraft would increase with this percentage, the requirement on 30.8% reduction compared to the E-1 family would only be met by the 3rd configuration. However, the reduction in fuel economy and thus CO_2 emissions is still significant. The same has been done for the NO_x emissions of the aircraft, of which the results are summarised in Table 11.11. As the requirement was not met initially, it is also not met with a contingency factor of 10%.

Table 11.10: Fuel consumption + 10%

	M_{fuel}/ N_{pax}/R [kg/km]	reduction wrt E1 family [%]
Config. 1	0.0151	28.1
Config. 2	0.0146	30.5
Config. 3	0.0143	31.9

Table 11.11: NO_x emissions + 10%

	D_p/F_{oo} [g/kN]	reduction wrt CAEP/6 [%]
Config. 1	42.14	44.77
Config. 2	46.35	39.25
Config. 3	42.52	44.27

11.5. Durability

This section will present the durability analysis of the chosen materials. This will be analysed in terms of material selection first, which is followed by the durability of the manufacturing methods. Lastly, the retirement procedure is presented.

11.5.1. Material selection

This section will present the durability of the chosen materials, presented earlier in subsection 10.1.3. The materials mentioned in that section are the result of a trade-off between the structures department and the sustainability department. For structural reasons, the most important parameters in the material selection are based on the structural performance. The sustainability department takes into account both production and disposal. However, the mass of the material and its specific properties were an important trade-off criterion for both disciplines as this would reduce the overall structural mass, which reduces fuel consumption, and the required thrust.

Minimising structural mass therefore reduces the impact of the design on all thee aspects of sustainability.

The selected materials were already discussed in chapter 10. In this section, the sustainable properties of the materials using the CES Edupack 2018 software are presented. In Figure 11.10, the water usage versus CO_2 emis-

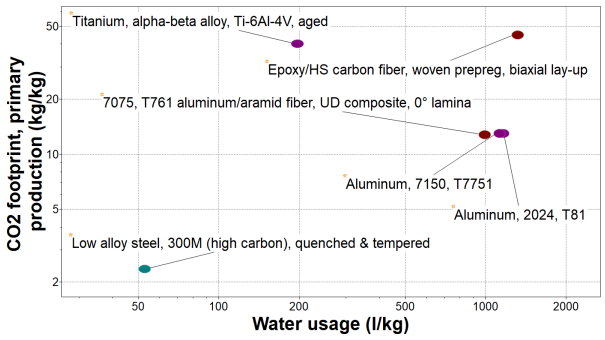

Figure 11.10: Water usage versus CO_2 emission comparison

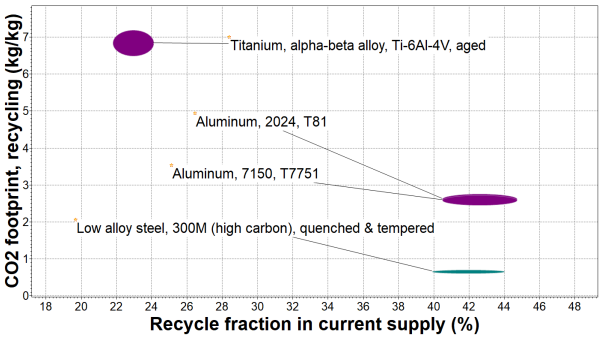

Figure 11.11: Recycling fraction versus CO_2 footprint during recycling

sion during the material production have been visualised. The most sustainable material in its production is situated in the left bottom corner, which is low alloy steel, used in the landing gear of the aircraft. The Epoxy/HS carbon fiber used in the fuselage skin, has the highest water usage and CO_2 footprint in production. This is a disadvantage of choosing this material, however it resulted in significant mass savings, which again lowers the CO_2 footprint of the aircraft in operations. The same reasoning applies to the material of the lifting surfaces, as aluminium/aramid fibres only perform slightly better than Epoxy/HS carbon fibres in terms of sustainable production.

Also the recycling properties of each of the materials were analysed, as this significantly influences the economical and environmental impact of the aircraft's disposal. In Figure 11.11, the possible recycling fraction in current society has been plotted against the CO_2 production during recycling. In this graph it is desired to have the materials positioned as far to the right bottom as possible. For this graph, it becomes again clear that low alloy steel performs the best. Also, aluminium 2024 and 7150 feature good recycling properties, however the titanium alloy used in the joints produces significantly more CO_2 during recycling. This material is only used in the joints and does not represent a large percentage of the total structure, therefore the high CO_2 footprint is deemed acceptable. The Epoxy/HS carbon fibre can unfortunately not be recycled. However, it can be used in a downcycle, which implies it can be reprocessed into a new product with a lower performance or quality. The same goes for aluminium/aramid fibre, which is also suitable for landfill purposes. Using the materials in a downcycle at the end of life is the best option for sustainable purposes.

11.5.2. Manufacturing processes

As the material selection had to be done in a sustainable manner, the same goes for the selection of the manufacturing processes. In chapter 10, these have been presented and discussed. In this section, the sustainable aspect of these processes are discussed, which was based on information available on CES Edupack 2018 software.

For the composites used in the design, lay-up is used. This manufacturing method minimises waste materials and is currently the only possible manufacturing method. However, using an advanced lay-up moulding method requires and produces approximately the same amount of water, energy, and CO_2 as the average manufacturing method for aluminium 2024-T81. For the spars and stringers, the aluminium will be processed by roll forming and extrusion. Both of these production methods require the least amount of water and energy and have a minimum CO_2 footprint compared to the other processes. Lastly, the rubber forming is used to produce the ribs, which only require one product related tool. Additionally, rubber forming is considered to be very fast and thus cost-effective.

11.5.3. Retirement strategy

After having operated the aircraft for many years, there comes a time at which the aircraft is no longer competitive with newer, more efficient technology and aircraft. Part of the sustainable approach is to develop a retirement strategy for the designed adaptive airliner.

Currently the dismantling of aircraft starts by removing items which are easily removable, such as engines and seats. From this point on the aircraft aluminium parts are shredded in smaller bits which are intended to be recycled [53][6]. The problem with this approach is that a different type of aluminium is used throughout the aircraft, resulting in a mixture of aluminium types. To transform this recycled mixture into a high quality material, many additional treatments are needed, increasing costs and environmental pollution [59].

To solve the above mentioned problem, it would be beneficial to dismantle the aircraft by material type. This would imply that all rivets need to be removed, which is a time consuming task. Removing a aluminium rivet can take up to 20 seconds, whereas removing titanium rivets can take up to 2 minutes [59]. The method of removing all rivets and sort all material types, so called 'Systematic Disassembly', is therefore deemed too time and cost consuming. The alternative, 'Shredding', in which the entire aircraft is shredded into pieces, is deemed not desired. Apart from these two extreme strategies, an intermediate strategy can be applied. By studying the time required to remove all the fasteners and trade-off whether it is beneficial, decisions can be made about the disassembly. This strategy is called 'Smart disassembly' [59].

Recycling of parts and materials can only be done if the materials used are suitable for this. The material selection presented in the previous section is revised using the CES Edupack 2018 software in terms of recycle-ability. The 7075-T761 aluminium/aramid fibre material used in the skin of the lifting surfaces is not able to be recycled. The same goes for the Epoxy/HS carbon fibre which is used in the fuselage skin. Instead of shredding these items it would therefore be desired to directly reuse these parts. It is proposed that these materials are reused in a downcycle. This can be done within the aircraft itself, where the material used in the structural components can be reused in the cabin furnishing, made from polymer matrix composites as discusses in chapter 10. The fibres from the composites in the fuselage and lifting planforms can be extracted from its matrix and reused as fillers for these polymer matrix composites.

Even at the end of life, the engines of the aircraft still have a high market value. Having these systems on a non-operating aircraft is not cost effective for the airline. Engines are therefore the most reused components of aircraft. Aircraft interior such as seats can also be reused as these are in total worth up to $5,000 [37]. Next to the engines, also the landing gears are still valuable at retirement, and out of a economical and environmental sustainable view, these items can also be reused.

[6] URL: https://www.thebalancesmb.com/airplane-recycling-and-value-extraction-2877922 [cited on 20 June 2019]

12 Operations

In this chapter, the operational side of the adaptive regional airliner is discussed. Firstly, the adaptability method is presented in detail, followed by the checking procedure. Thirdly, the required maintenance and certification process are analysed in detail. Furthermore, the verification and validation of the used methods is performed. Lastly, the sensitivity of the probability model is analysed.

12.1. Adaptability method

The challenge which was determined in the last report for this concept, was to bring down the adaptability time so that it meets the 8-hour requirement. The steps which take up significant time are determined to be the alignment of the aircraft fuselage parts and the fastening of the bolts. For that reason, most research in this phase has focused on those two aspects. First of all, the alignment of the aircraft is discussed, followed by the fastening method. Furthermore, the connector, the plug consisting of all the wires and pipes, needed to be designed in more detail. This is done in chapter 16.

Firstly, a general outline of the adaptability procedure needs to be decided. If all parts of the aircraft have been taken apart, a total of three parts is present: the nose section, the extendable fuselage section with canard, and the main fuselage including the tail. In order to facilitate the conversion method, one of these sections needs to be stationary and fixed in place. The other sections will then be attached to it. As the main fuselage section is the heaviest and most difficult to move, this section will be fixed. Whenever the extendable fuselage section is required, this will then be attached first. After this is fixed in place, the nose section will be attached last.

12.1.1. Alignment procedure

The alignment method makes sure that each time the aircraft is converted to a new configuration, the fuselage sections are aligned perfectly. The fuselage is only a few millimetre thick and the accuracy of this procedure is thus very sensitive to movement. Humans could perform this to a certain extent by visual means but the final alignment phase needs to be automated to ensure its accuracy. The first step in the procedure is thus done using the human capabilities. This is done until the parts are approximately half a meter apart. The automatic process will take over from that moment which will make use of laser transmitters and receivers. The current market allows to purchase 2D lasers systems for positioning. However, to position the fuselage in a proper position, 3D orientation is needed. Therefore, two laser transmitters will be placed in different axis orientations. First of all, the laser combination will be placed at the fuselage top. If this point is aligned, this means that the only degree of freedom of the alignment which is not fixed is pivoting around this point. To make sure this does not happen, there will be another set of two laser systems installed at the bottom of the fuselage. An overview of this is presented in Figure 12.1. As there is now a total of 4 sets of lasers present, this means that redundancy is also built in for aligning the fuselage sections. The laser transmitters will be placed on both the main fuselage section and the extendable fuselage section. Apart from these transmitters, laser receivers are placed at the canard section as well, and the nose section. The laser transmitters and receivers are placed during manufacturing with extreme precision and calibrated afterwards. The fuselage structures are placed on specially design lifts. The information about the positioning error from the lasers is constantly fed to the lift structure computer via a wireless connection. The lift support structure has a hydraulic system attached to the fuselage at standard locations. The hydraulic system allows to accurately move the fuselage section according to the input from the laser sensors.

12.1.2. Fastening method

If the fuselage sections are aligned with each other, the fastening of the two parts is performed. This is done based on the Boeing 747-4F version which has a nose door that can be opened and closed for easy cargo loading. The fastening method of the two fuselage sections will be similar to how this nose door is secured. One side of the fuselage section will contain a latch hole and the other fuselage part will contain a bolt, going through this hole. Once the bolt has successfully slid through the hole, the bolt touches upon a sensor. An operational panel is located in the aircraft which shows for all fastening locations whether the sensor has successfully been activated. After this every bolt is manually checked due to security regulations [23]. If this is all done correctly, the fastening is considered to be successful. The bolts will be operating based on electric power and will be slid through the holes all at the same time. This brings the adaptability time down significantly. In Figure 12.2, the latch hole and

bolt are presented. Also, the pressure sensor is presented at the bottom of the latch which determines whether the bolt is secured in position.

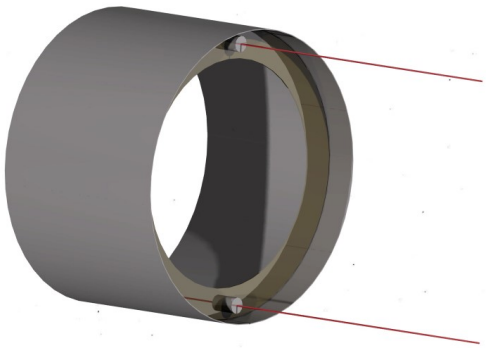

Figure 12.1: Laser positioning in fuselage cross section

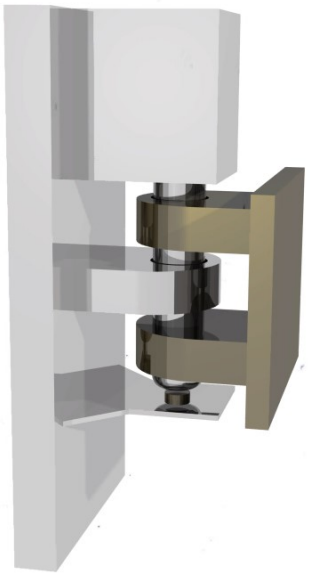

Figure 12.2: Fastening method for fuselage parts

12.1.3. Time/Cost analysis

In this subsection, the conversion is analysed in terms of time and cost. First the conversion time and man-hours are calculated using the maintenance data from the faculty of Aerospace Engineering of Delft University of Technology [15]. Using these man-hours the labour cost during conversion could be calculated.

In Appendix A, the final conversion flow diagram is presented. The boxes with a blue edge are not included in the total conversion time because these can be performed without the aircraft or are part of the checking procedure. The checking procedure was not part of the requirement of converting in under 8 hours and is therefore not accounted for in the total conversion time. The following assumptions were made during creation of the flow diagram using the maintenance data. These assumptions will be used in further analysis and are driving the analysis.

- Read component manual will always take 10 minutes per worker.
- Bring aircraft to hangar will always take 30 minutes with 3 persons.
- Bring lifts to hangar will always take 2 persons 20 minutes.
- Collect required tools to hangar will always take 2 persons 20 minutes.
- Detach or attach connector will always take 2 persons 15 minutes, this connector is designed in section 16.2.
- Detach or attach fasteners will always take 2 persons 30 minutes.
- Aligning will always take 30 minutes with 4 persons.
- Positioning of lifts will always take 30 minutes with 2 persons.
- Drive away lift will always be 15 minutes with 2 persons
- Drive in/out part 2 will always take 15 minutes with 2 persons.

Now that all steps are estimated in terms of time, the total conversion time can be calculated. This is the conversion time when everything is going right and no failures are occurring. Additionally, the total man-hours can be calculated now. From these man-hours, the labour cost can be calculated. As the estimations have been based on maintenance data, a contingency factor of 10% is added according to [18]. The contingency factor is only

added to the total man-hours and labour cost and not to the time required since the time required is analysed in detail in terms of probability in the next subsection. The labour cost is calculated by multiplying the man-hours by a $55.39/hour rate [68]. The results are shown in Table 12.1. All in all, the 8 hours conversion time requirement is met. The probability that this requirement is met is analysed in subsection 12.1.4, the cost is used in section 13.3.

Table 12.1: Conversion time and cost

Conversion type	**Total manhours** [hrs]	**Time required** [hrs]	**Labour cost [$]**
90 - 120 passengers	18.9	4,5	1,046.87
120 - 90 passengers	19.8	3.75	1,096.72

12.1.4. Probability analysis

Now that the expected conversion time is calculated, the probability that the 8 hour requirement is met is calculated. To calculate the probability, a discrete-time Markov chain is used. This Markov Chain is shown in Figure 12.3.

In the Markov chain, three types of steps are identified. Firstly, a step that can be redone or will not make it in the time set but will not cause any damage. An example of this step is step 2.7. Secondly, a step that can be redone or will not make it in the time set but can cause damage. After damage the step must be done again. An example of this step is step 3.2. Lastly, a step that can be redone or will not make it in the time set but can cause damage. After damage the next step will be performed. An example of this step is step 2.6.

In this Markov Chain a few assumptions were made using human failure data and airport delay data [70, 99, 108][1,2]. The technical failure was assumed by estimations. The following assumptions were made during the development of the probabilities of the Markov chain. Firstly, the assumption was made that the chance the aircraft is in the hangar within 30 minutes is 90%. Secondly, the chance that the positioning needs to be redone or takes longer than 30 minutes is 5%. Furthermore, the chance that the connector detachment/attachment will take longer than 15 minutes is 1%. The chance that the positioning of a lift or manoeuvring a part damages the aircraft is 0.5%. The chance that the manoeuvring of the parts will take longer than 15 minutes is set at 2.5%. The chance that the alignment of the parts will take longer than 30 minutes is set at 15%. Moreover, the chance that the repair after lift/part manoeuvring or alignment takes longer than 15 minutes is 94%. This is calculated by knowing that the average time to repair the aircraft after the damage will be 3 hours. The chance that the fasteners are not detached/attached properly is 5%. The chance that the fasteners must be fastened/detached manually is 0.5%. Lastly, the chance that the manual detachment/attachment of the fasteners will take more than 15 minutes is 96%. This is calculated by knowing that the average time will be 4 hours to manually fasten/detach the fasteners.

From the Markov Chain shown in Figure 12.3, a simulation was run. The Markov Chain was ran for 10 million times which resulted in the following 3 diagrams. Firstly, a histogram was made, secondly a probability density function and last a accumulated probability density function, all depicted in Figure 12.4 and Figure 12.5. From the accumulated probability function the chance that the requirement of 8 hours conversion was met is 95.9% for 120 to 90 passenger capacity and 90.1% for 90 to 120 passenger capacity. In the probability density function figures peaks are located. This is due to the discrete type of analysis in a Markov Chain. It takes approximately 1,000 hours for the 120 to 90 passenger configuration to converge to a probability density of 1.0 The 90 to 120 passenger conversion takes about 1,400 hours in order to converge.

12.2. Checking procedure

Whenever the conversion has been done, the aviation authorities want to see that this has been done according to the predefined manual and want to ensure that the aircraft is airworthy. In order to confirm this, aviation authorities will check the aircraft after each conversion. The time required to do this is based on provided data from the aerospace engineering faculty. In this data, all maintenance steps for an aircraft have been mentioned. All tasks which seemed relevant for the checking procedure have been summed up. In addition to that, an estimate has been made of how many people are involved in the steps in the checking procedure. From these estimates,

[1] URL: https://www.transtats.bts.gov/OT_Delay/OT_DelayCause1.asp?pn=1 [cited on 11 June 2019]
[2] URL: https://www.lifetime-reliability.com/cms/tutorials/reliability-engineering/human_error_rate_table_insights/ [cited on 11 June 2019]

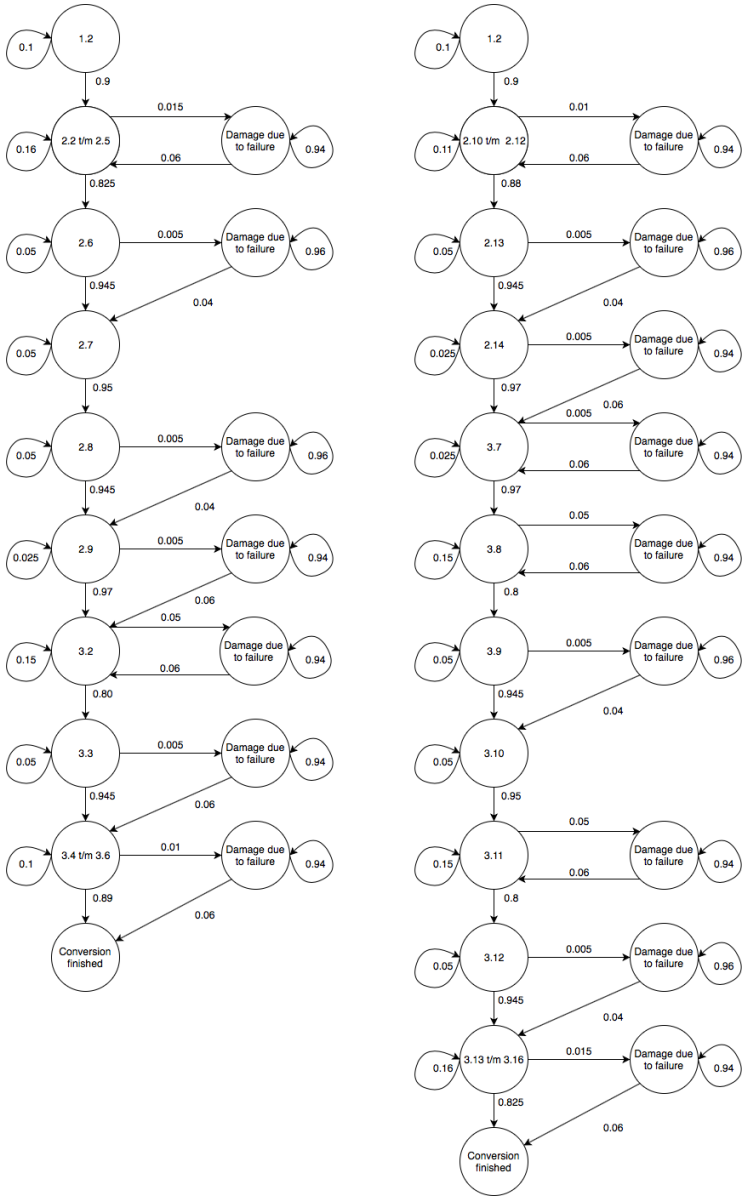

Figure 12.3: Markov chain

the total labour cost could be estimated. As the estimations have been based upon maintenance data, a contingency factor of 10% is added according to [18]. The resulting checking time is presented in Table 12.2.

Table 12.2: Checking procedure time and costs

Conversion type	**Total manhours** [hrs]	**Time required** [hrs]	**Labour cost** [$]
90 - 120 passengers	118.8	6.6	6,580
120 - 90 passengers	69.3	3.85	3,840

A remark has to be made as to why the checking time differs from the 90 to 120 configuration, compared to the 120 to 90 configuration. Whenever the aircraft is in 120 passenger configuration, this means that the fuselage needs to be fastened at two sides. Therefore, the checking of this takes more time compared to when only one fuselage cut needs to be inspected. The checking time between the two configurations is however not exactly doubled. This is due to the fact that some checking steps can only be done for the entire system and not particularly for each cut. For example: checking the fasteners/connector needs to be done for both cuts is requires thus double time. However, checking whether the air conditioning works is only done in the end for the total plane, and thus does not require double time in the 120 passenger configuration. The time required is based upon an estimate of how many workers can work at the same time during the checking, this was done by con-

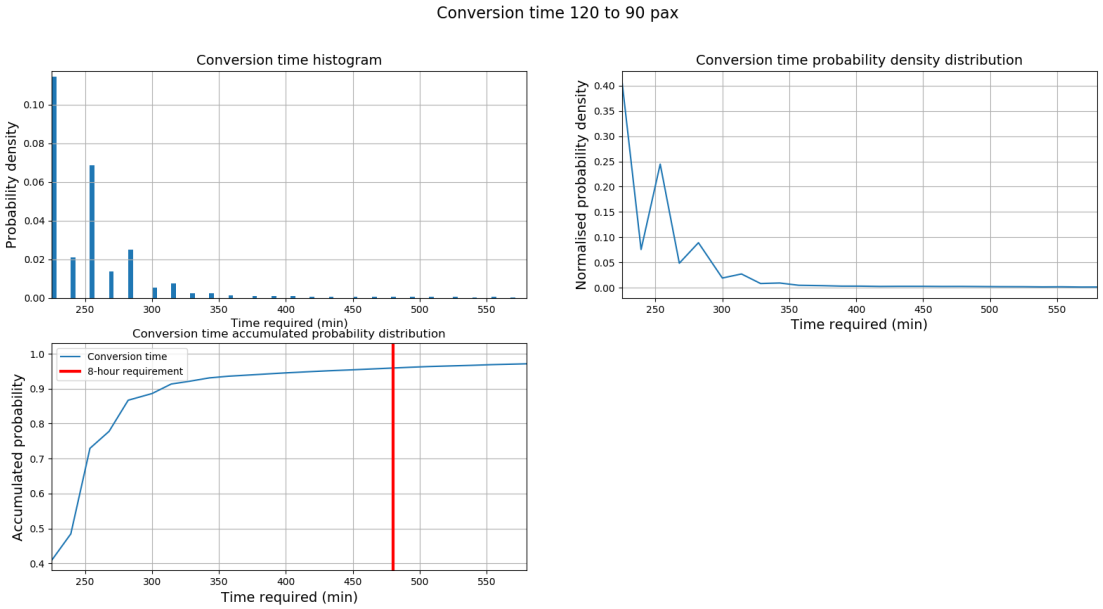

Figure 12.4: Conversion time histogram, probability density distribution and accumulated probability distribution to 90 passengers

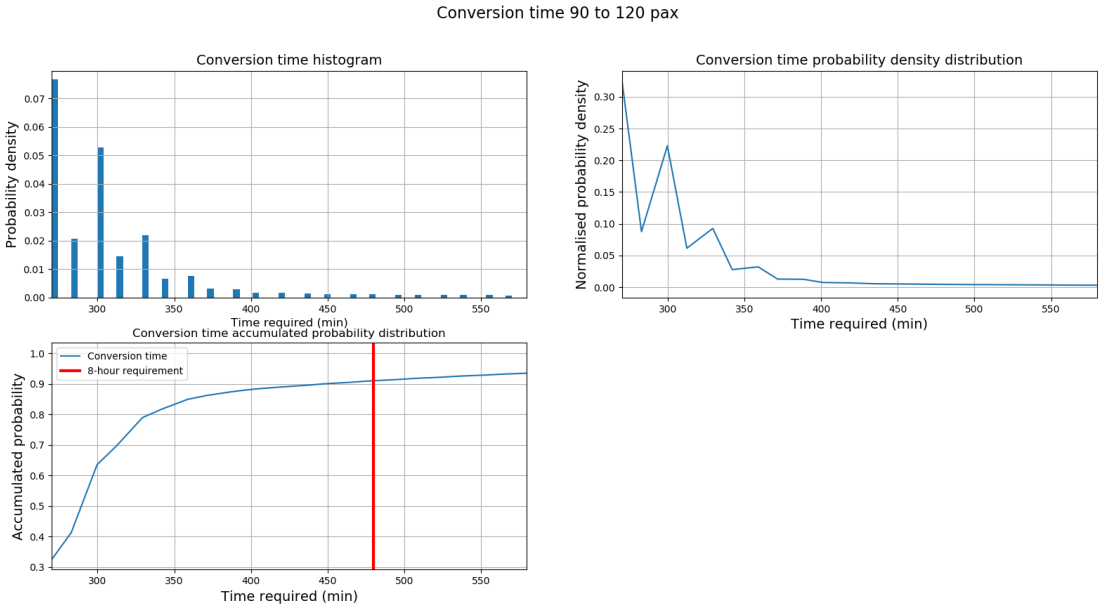

Figure 12.5: Conversion time histogram, probability density distribution and accumulated probability distribution to 120 passengers

tacting someone in the maintenance industry. The result of the checking procedure cost is incorporated in the operational cost analysis.

12.3. Maintenance

For safe operations of the aircraft, maintenance is critical. For airline operators, this however also poses a major financial setback. The airline needs to pay for the maintenance performed, but also the downtime is of major impact on the total cost. This section will present possible methods to perform maintenance and a simulation model is developed which determines which method costs the least money. The model developed in this section will function as a guideline for airlines on how to plan their maintenance. It does not present an explicit optimal maintenance method for the entire aircraft as maintenance is applied to all individual components instead of the aircraft as a whole. In the following methods, different types of replacements have been discussed. First of all, preventive repair, which means that a part is repaired without actually being broken down. The second

repair type is a corrective repair, meaning that an item is repaired once it broke down. The three maintenance methods which are considered are the following.

- **Constant interval replacement (ci)**. In this method, preventive repairs are performed in a constant interval, regardless of the last corrective repair. The disadvantage of this is that an item might undergo a preventive repair just after a corrective repair has been performed, which is not necessarily needed.
- **Age based replacement (ab)**. In order to solve the problem mentioned before, it would be beneficial to only perform preventive repairs after a predefined time, even if there is a corrective repair. Meaning that if the preventive repair was scheduled soon after a corrective repair was performed, the preventive repair is postponed.
- **Inspection based replacement (ib)**. To optimise the moment a preventive repair is performed, it might be beneficial to perform an inspection to determine whether a preventive repair is needed. Apart from the earlier mentioned preventive and corrective repair costs, now also inspection cost need to be determined.

All of the maintenance concepts mentioned above have in common that it is possible to express the total expected cost per unit time (TEC). This is done for the three different methods according to the following formulas [7].

$$TEC_{ci}(t_p) = \frac{C_p + C_c \cdot N(t_p)}{t_p} \tag{12.1}$$

$$TEC_{ab}(t_p) = \frac{C_p R(t_p) + C_c F(t_p)}{t_p R(t_p) + \int_0^{t_p} t f(t) dt} \tag{12.2}$$

$$TEC_{ib}(t_p) = \frac{\lim_{N\to\infty} \sum_{n=1}^{N} R(nt_p)\left(C_i + C_p F(t_p)\right) + C_c F(t_p)}{t_p R(t_p) + \int_0^{t_p} t f(t) dt} \tag{12.3}$$

These functions are all dependent on t_p, which is the time between two preventive repairs. From Equation 12.1 to Equation 12.3, it becomes clear that these are all highly related to probability functions. The following probability functions are distinguished. $R(t_p)$ is the reliability function, $F(t_p)$ is the failure function and $f(t)$ is the probability density function. As aircraft maintenance is not about the aircraft as a whole, but about the individual systems, these probability functions need to be determined for all subsystems. For this section, reference material was found, and the analysis was performed for a single subsystem, in this case the auxiliary power unit of a Boeing 737 [58]. APU power is the driving factor behind electric taxiing which will be implemented to save fuel, explained later in subsection 12.6.1. Failure of the APU is therefore assumed to be unwanted and will be explained in more detail in the risk analysis. The APU failure is modelled with a Weibull distribution as presented in Equation 12.4.

$$f_{Weibull}(x, \alpha, \beta) = \frac{\alpha}{\beta^{\alpha}} \cdot x^{\beta - 1} \exp^{-\left(\frac{x}{\beta}\right)^{\alpha}} \tag{12.4}$$

From the reference data, α equals 1.263 and β is equal to 3,868, approximately. The Weibull distribution allows for easy converting the $f(t)$ to $F(t_p)$ and $R(t_p)$. In order to plot the maintenance methods, it is needed to determine the C_c, C_p and C_i. As reference material on these costs could not be found and estimating would be highly subjective, ratios are used instead. It was assumed that preventive repair has a base costs of 1. Then, corrective repair is determined to be 30 times as expensive as preventive repair, this is justified by reference [58] which plots these ratios from 6 till 50. As a result, a ratio of 30 was therefore assumed to be reasonable. Finally, inspection costs are established to be equal to 1/5 of preventive repair costs. As the costs have been estimated using a ratio, the graph will not be outputting actual cost values, but only a ratio compared to each other. In Figure 12.6, the three maintenance strategies have been plotted.

In this graph, the most optimal point is the point where the total expected costs per unit time are the lowest. From this, also the optimal time between two preventive repairs can be determined. From Figure 12.6 it is thus concluded that age based replacement with a time between preventive repair of approximately 800 hours is optimal. The program is capable of automatically putting out the exact optimal time and maintenance strategy. For other components, the airline only needs to change the input values for the probability distribution. In order to determine the exact cost values, the airline needs to input actual costs of preventive, corrective repairs and inspections. With this more accurate information, airlines can determine specifically what the best maintenance

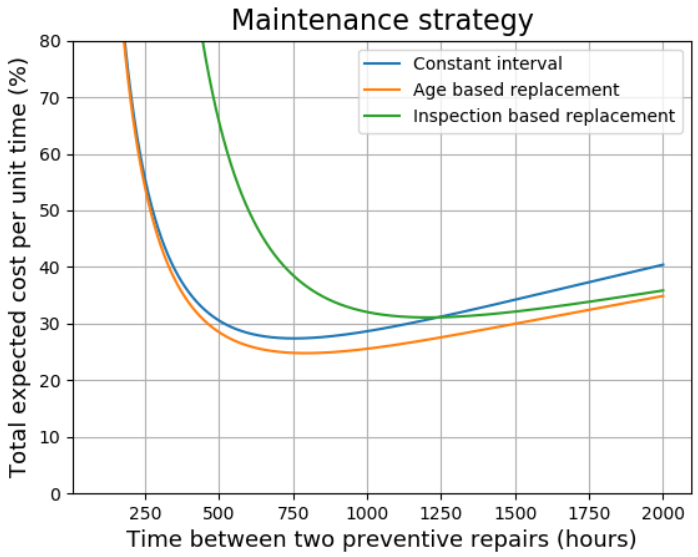

Figure 12.6: Maintenance strategies with their relative total expected cost for APU reference material

strategy would be for each individual component.

Above described procedure is not especially related to the adaptability features of the aircraft. However, systems such as the fastening structure and connector will most likely have a probability density function which is shifted such that failures occur earlier due to its complexity and possibilities of fatigue in the adaptable aircraft. A probability which is shifted towards the left, results in the fact that the time between preventive repair should be shorter. This is intuitively correct and is confirmed by the program. While running different simulations it was also found that the type of maintenance strategy, which is optimal, changed if the probability density function is changed.

Maintenance of the adaptability features of the aircraft will be dedicated mostly to the connection points. The joints have to be regularly checked and so have the automatic bolts which slide in. Any fatigue or cracks in these items might have a catastrophic consequences. In addition to that, the connector, which will be discussed later in more detail, is subjected to fatigue as it has to be attached and detached every time the conversion is performed.

12.4. Certification

Newly developed aircraft are only allowed to start operating after they have been successfully certified. The certification process is performed by the authority which is responsible for the country in which the aircraft is manufactured. For that reason, it is assumed that the certification is performed by EASA, which is responsible for the European Union [3][3]. This certification process is specific to a type certification of a conventional aircraft. The adaptive aircraft however entails a more detailed certification procedure which does not currently exist. Therefore, a new certification program has been set up by the team which will be presented to EASA for their approval. The new certification procedure will consist of the following steps: type certification, conversion certification, and finally, the conversion checking certification.

12.4.1. Type certification

The type certification procedure which EASA handles consists of four phases. To acquire the type certificate, all of these phases have to be successfully passed. The steps presented below are all taken from EASA [3].

- Whenever the design is considered to have potential and reached a sufficient degree of maturity, the first certification step is taken. In this step, the certification basis is determined. This includes rules which are specifically related to this aircraft type.
- Once the requirements are determined in the certification bases, it is important to determine how the aircraft manufacturer can demonstrate compliance with these. In this phase, it is also determined to what

[3]URL: `https://www.easa.europa.eu/easa-and-you/aircraft-products/aircraft-certification` [cited on 14 June 2019]

extent EASA is involved in the certification process.

- Subsequently, it is determined how the aircraft manufacturer should demonstrate compliance with the requirements. In this phase, the aircraft manufacturer executes these tests. EASA checks whether the tests are performed as planned, by examinating of the review documents produced by the manufacturers and visual inspection of the tests.
- The last step in the type certification procedure, EASA grants the certificate for the aircraft and the aircraft is allowed to fly in the European Union. Now authorities from foreign countries will evaluate the certificate granted by EASA. After this has been completed, the aircraft can fly in all countries in which the certificate is approved.

The above described procedure holds for all type certificates. Regulations state that it is needed to re-certify the aircraft in case major external changes have been implemented [20]. The adaptive aircraft will be mainly in two different configuration, namely the 90 and 120 passenger configuration and these changes are considered as major external changes. Both of these configurations need to go through the entire procedure which is mentioned above. During the certification of the 120 passenger configuration, the authorities will pay special attention to the canard. The canard will have a significant influence on the stability and control of the aircraft and special attention needs to be payed to this. For both configurations, special focus will also be on the structural connections of the aircraft. These attention points will be determined in a collaboration between EASA and the aircraft manufacturer in the first and second phase of the type certification procedure presented above.

12.4.2. Conversion certification

As mentioned, the procedure above will be related to gathering the type certificate of all different aircraft configurations. As the aircraft is adaptive, this leaves margin for error in the conversion method and the authorities would like to have confirmation that the conversion is done properly each time it has been performed. For that reason, two additional certification steps have been developed. The first step is the conversion certification.

The conversion certification is dedicated to the method which is used to perform the conversion. During the aircraft development, a detailed conversion method is established. This presents the steps which must be taken and in detail how they must be done. The manual contains specific focus on the critical regions of the conversions, such as the fastening method and connector. As soon as the manual has been set up by the manufacturer, EASA needs to agree upon this manual. At that point, the conversion procedure is also certified. With this manual, the technical personnel can look up what is expected from them. For the technical personnel which performs the conversion, it is very important that the conversion is always performed as mentioned in the manual. Whenever deviations from the manual are made, this implies that the conversion is not certified which results in an aircraft that is not allowed to fly. In order to check whether the personnel works according to the manual, unannounced or incognito visits from the authorities are advised.

12.4.3. Conversion checking certification

The last step in the certification procedure is to confirm that the conversion is done properly. This step needs to be performed each time after a conversion has been performed. This step is also referred to as ‘checking’ in section 12.2. In that section, the time and cost have been discussed. In the first and second phase of the type certificate procedure, critical places have been identified for all different configurations. The list with critical points will be checked upon by representatives of the aviation authorities. If all requirements which are listed are met, the aircraft is fully certified and ready to enter service.

12.5. Logistic concept

The operational concept is used for airlines as guideline how to operate the aircraft over its lifetime. One of the most important aspects of the adaptive airliner is related to the adaptability and the conversion method used. For airlines the downtime is typically of major importance since this reduces revenues. For that reason the adaptability needs to be elaborated upon in detail. This has been done extensively in Figure A.1 in Appendix A. The remaining aspect in which the adaptive aircraft will differ from regular aircraft, is the logistic and operational procedure with respect to ground operations. Currently, aircraft are parked at airports according to their specific type. For each type or series, specific places have been designated where the aircraft should park to safely attach the gate to the aircraft doors. Each commercial aircraft is equipped with a transponder which contains data such as the aircraft identification, altitude and aircraft type [31]. The latter is especially relevant for the adaptive airliner. As discussed in the certification of the aircraft, there will be different type certificates. One which is related

to the 90 passenger configuration and another one with the extendable fuselage part attached which accommodates 120 passengers. These configuration will also be used for the transponder input. Whenever the aircraft is in its large configuration, the transponder will display the 'EXT' (extended) abbreviation. This way, airports know that the aircraft is flying in the 120 passenger configuration and can take this into consideration when allocating gates. Whenever the aircraft is flying in its baseline configuration (90 passengers), the 'EXT' abbreviation will disappear from the transponder data.

The most forward door of the aircraft will always be at the same position, irrespective of the 90 or 120 configuration. For that reason, to attach the jet bridge to the aircraft for boarding and deboarding, the stopping lines does not needs to be changed. However, the canard in the large configuration poses a problem as it could interfere with ground objects. Therefore each airport needs to research whether the canard poses a problem in terms of ground object clearance. Whenever this is the case, the stopping lines of the aircraft should be different compared to the small configuration.

Apart from passengers boarding and disembarking, aircraft service vehicles also need to be able to access the aircraft. This includes for example: fuel trucks, cleaning staff, toilet disposal, galley supply, and cargo/luggage loading trucks. All mentioned trucks of personnel will not experience any problems with the adaptive aircraft. Fuel is loaded in the main wing and vehicles can be positioned there without any problems. The same goes for the cleaning staff, toilet disposal, galley and cargo trucks. These will all be located to a specific place, mostly at the back of the aircraft, which is not influenced by the extendable fuselage or canard.

12.6. Turnaround time

For airliners the turnaround time should be as small as possible to maximise their profit. It was therefore determined what the turnaround time for the adaptive aircraft will be. The assumption was made that no additional time is required for turnaround specifically because the aircraft is adaptive. Any additional time coming from the adaptability is already covered in the conversion time. The turnaround time is a result of a sequence of steps taken on the ground, in order to be ready to depart again. The steps which have been considered in this analysis are the following. Once the plane arrives at the gate, disembarking of the passengers will be performed. After that, the aircraft needs to be cleaned, the catering needs to be refilled, and fuel needs to be refilled to the aircraft. At last, the passengers should board the aircraft. It was assumed that the tasks: cleaning, catering and refuelling can be done in parallel. These tasks are then performed in series with disembarking and boarding.

In order to get an estimate of the time required for these tasks, a literature study was performed on the duration of previously mentioned tasks. From [93] and [94] it was concluded that the different tasks in the turnaround process have their specific duration distribution. These distribution are according to the Weibull distribution, which is presented in Equation 12.4 and the gamma distribution, presented in Equation 12.5. These distribution types are chosen as they allow to easily mimic behaviour and are often used.

$$f_{Gamma}(x,\alpha,\beta) = \frac{1}{\beta^{\alpha}\Gamma(\alpha)} x^{\alpha-1} \exp^{-\left(\frac{x}{\beta}\right)} \tag{12.5}$$

For previous mentioned equations, the values of α and β have been determined in the reference papers [93, 94]. For all tasks, the probability density function is set up as a function of time. After this is done, the individual density function should be combined towards a total turnaround time figure. This is done by determining all possible combinations between the individual tasks and determine their probability. As mentioned earlier, some steps have been performed in parallel and could not be modelled in series. In order to determine the most realistic output, three simulations have been run.

- Disembarking - Cleaning - Boarding
- Disembarking - Catering - Boarding
- Disembarking - Refuelling - Boarding

From these three simulations, the most limiting case was taken, which turned out to be the case in which refuelling is performed. As this is the limiting case and the tasks can be performed in parallel, it was assumed that cleaning and catering can also be done in the time span of refuelling and will not delay the turnaround.

The resulting probability density function and accumulated probability function are presented in Figure 12.7 and Figure 12.8 respectively. An overview of the used values and probability function type is presented in Table 12.3.

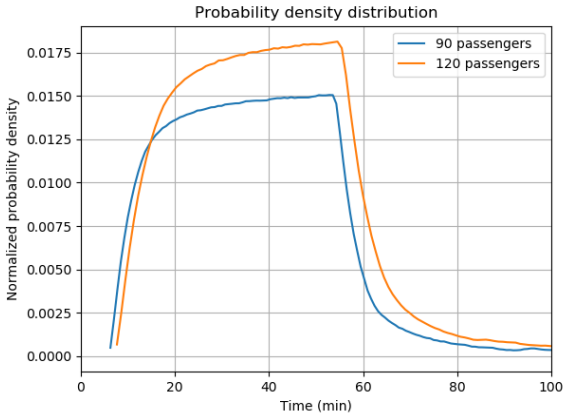

Figure 12.7: Turnaround time probability density function

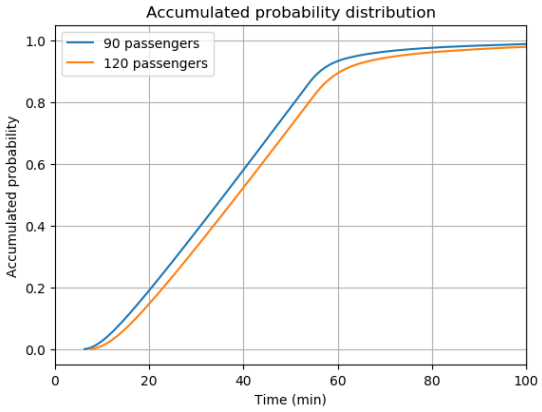

Figure 12.8: Turnaround time accumulated probability density function

Table 12.3: Task probability specifications

Task	α [−]	β [−]	**Offset**	**Distribution type**
Disembarking (pax/min)	2.23619	19.2339	10	Weibull
Cleaning	2.16	6.76	5	Weibull
Catering	2.18	17.37	0	Weibull
Refuelling	1.64	9.12	2	Gamma
Boarding (pax/min)	2.29263	19.5224	0	Weibull

The difference in turnaround time in the turnaround time figure is caused by the disembarking and boarding tasks. In Table 12.3 it is stated that disembarking and boarding are given in the probability function as a function of passengers per minute. With this data, the probability is transferred to the two different configurations in terms of passenger capacity.

12.6.1. Electrical taxiing

It is proposed that the aircraft will use electrical taxiing. Currently, a system is in development by the company *Safran*, and is estimated to enter into service by the year 2022. By doing this, the aircraft can save 4% of its total fuel consumption, which directly reduces the carbon emissions by 4%. It would make the pushback and taxiing of the aircraft completely independent of ground infrastructure, which can increase the flight punctuality and the turnaround time of the aircraft [90]. The electrical taxiing system works by installing a motor in the landing gear at the wheels. The motor would be driven by power generated by the APU.

12.7. Verification and validation

Verification and validation of the models developed is an important aspect in order to verify their correctness. Verification is applied to the code developed to generate the probability functions for the adaptability time. This is done to determine whether the code performs the desired steps. Ideally, the code should also be validated to see if the numeric output values correspond with real data. As the adaptive airliner is a new concept and no conversion time data is available, validation cannot be performed. Firstly, the adaptability probability distribution is verified and secondly the maintenance model is verified.

Verification of the adaptability probability distribution is performed by running unit tests and system tests. First of all, unit tests were set up to determine if the output values in each definition are as desired. For example, functions were set up in which the amount of iterations which the program should do are used as input. In order to check whether the program works as desired, it was checked whether the amount of output values equals the amount of iterations performed. The system tests are performed to see if individual codes work together and present the required output. For example, the generated data of the required conversion time is stored in a list with 10 million iterations. This is then plotted in a histogram which is converted to a probability density density function. This function is integrated to get the accumulated probability. In these steps, some coding errors can easily be made. For that reason, all diagrams should be checked whether they are correct. The histogram is checked to see whether the width of all bars multiplied with the height of the respective bar sums to one. For the

probability density function it was checked whether adding up the probability of all points equals one. Finally, the accumulated probability density function should converge over time to a accumulated probability of one. Once these were all checked and confirmed, a final check was performed. A simple piece of code was written which counts the amount of times the conversion time is longer than the 8-hour requirement. This is then divided over the total amount of iterations to determine the probability of a delay. This value is compared to the accumulated probability density function to see if these are the same. Initially this turned out to be different and the code in the error was found. Running another test resulted in the system passing this test positively. It was then established that the code was verified.

The maintenance model developed should also be verified and validated where possible. Verification is done by performing smaller unit tests. The reference used for the APU data also provides the probability function, failure rate, failure function and reliability function in terms of the Weibull distribution parameters. These functions could therefore easily be implemented. Simple test were performed such as plotting the failure function in the same figure as the reliability function. These two functions should mirror each other in which the reliability function goes to zero if time goes up and the failure function should limit to one for large values of time. The model could not be verified in terms of total expected cost per unit time as the input values have been takes as a percentage relative to each other. The time between corrective maintenance can also not be validated precisely. It can only be determined whether the values seem reasonable. The probability density function is plotted and from this, it was assumed that the time between corrective repair of approximately 800 is reasonable.

The turnaround time is based upon a Python simulation which means that the code should be verified and then validated. Unit tests have been performed in the entire coding process. For example, two different distribution types have been used; Weibull and Gamma. These could be entered into Python manually as a formula with variables, but also as a predefined Python function. If was checked whether these were coherent to ensure that the coding has been done properly. Apart from these simple unit tests, more advanced system tests were performed. Again, it was for example checked if the probability density function equals one if it is integrated. In addition to that, the accumulated probability function should limit to one over time.

Validation has been performed where possible. In [47], the probability density functions for most steps are presented graphically. These graphs have been checked whether they are coherent with the developed probability density function from the Python model. In addition to that, validation of the entire system can also be performed. From Figure 12.8 it is concluded that the turnaround time will be roughly between 20 and 80 minutes. The model developed in [94] uses a schedule turnaround time of less than 75 minutes, which is in accordance with the results of the analysis.

12.8. Sensitivity analysis

In this section a sensitivity analysis is performed on the probability analysis of the conversion time since a lot of assumptions are made here. The strategy during the sensitivity analysis was to add a contingency factor to all the probabilities. However, the probability of failure repair of damage in 15 minutes is calculated by estimating the average repair time. Therefore, the new probability of repair of damage is calculated differently. The contingency factor is added to the time and the new probability is calculated as explained in subsection 12.1.4. A contingency factor of 30% was chosen since the probabilities are assumptions [18].

After adding the contingency factor, the new probability of meeting the requirement of 8 hours conversion time was for the conversion from 120 to 90 passengers 94.5% and for the conversion from 90 to 120 passengers 87.8%. Comparing these to the original values respectively 95.9% and 90.1%, the shift in probability is relatively low and acceptable. A probability of 87.8% is still acceptable comparing to an average chance of delay of 80.2% [70]. Therefore, it can be stated that the requirement of 8 hours conversion time is met.

Performing a sensitivity analysis for the turnaround time and maintenance strategy is not as straight forwards as adding a contingency factor to some parameters and comparing the results. The basis of this analysis lies within the probability density functions (pdf). Changing the pdf input values result in different output values. The best sensitivity analysis is therefore to compare pdf parameters values from different airlines and compare these to each other. As this would be too detailed for this project, this has not been done.

13 Cost Analysis

In this chapter, the costs associated with the development, manufacturing, and operation of the adaptive regional airliner are calculated and presented. After calculating all the costs, and finding the predicted market share the return on investment is calculated. The costs to be calculated and their constituent parts are presented in the cost breakdown structure in Figure 13.1.

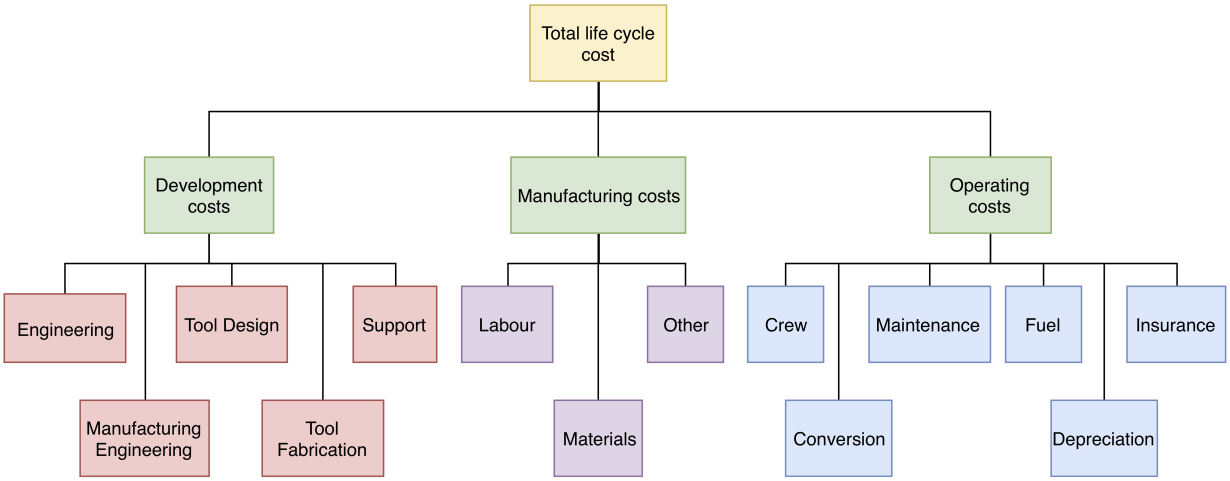

Figure 13.1: Cost breakdown structure

13.1. Development cost

The development of a new aircraft is a long and costly procedure, especially for a revolutionary aircraft like an adaptive regional aircraft. In this section, an estimate of the development costs is calculated. The first main driver of the relatively high development cost is the Technology Readiness Level (TRL), which indicates how ready the technology is.

The total development cost was calculated using the DAPCA IV model provided in Raymer [80]. Next, the total cost was divided into different component groups. For every top-level component in the aircraft, a cost per kilo was provided, based on statistical data [60]. The costs are divided into 5 main processes of development: Engineering, Manufacturing Engineering, Tool Design, Tool Fabrication, and Support. To calculate the total development cost of every component, the weight is multiplied by the cost per kilo. This cost is first adjusted for inflation. For components that are expected to require extra development efforts due to their low TRL, a factor is added to the costs, in the relevant departments, to account for that. The final results are displayed in Table 13.1.

Table 13.1: Development cost

Part	Engineering	Mfg. Eng.	Tool Design	Tool Fab	Support	Total
Wing	$124,592 K	$31,148 K	$32,705 K	$108,395 K	$14,640 K	$311,480 K
Empennage	$49,663 K	$12,416 K	$13,036 K	$43,206 K	$5,835 K	$124,156 K
Fuselage	$385,728 K	$96,432 K	$101,254 K	$335,584 K	$45,323 K	$964,321 K
Landing Gear	$7,290 K	$1,823 K	$1,914 K	$6,343 K	$857 K	$18,226 K
Engines	$47,638 K	$11,909 K	$12,505 K	$41,445 K	$5,597 K	$119,095 K
Systems	$227,850 K	$56,962 K	$59,811 K	$198,229 K	$26,772 K	$569,625 K
Payloads	$55,498 K	$13,874 K	$14,568 K	$48,283 K	$6,521 K	$138,744 K
Total	$898,259 K	$224,565 K	$235,793 K	$781,485 K	$105,545 K	**$2,245,648 K**

The three groups that were expected to require extra development efforts are the fuselage, empennage, and systems. The fuselage structure is expected to be more complicated than that to be found in an conventional aircraft, due to the adaptability feature. The section to be attached would disrupt the fuselage structure and

would thus require the placement of joints that were never used in that manner before. This is rated at a TRL of 2, because it has only been discussed in research papers before, but the method was never experimentally analysed [105]. The section connections also represent a critical point of failure, hence it is required that further research goes into the development of that part. Secondly, the empennage is also expected to require more development due to the introduction of the canard. The canard poses a difficulty in design, as no three-surface aircraft were ever developed for commercial transport, although the concept has been applied in private and fighter jets, such as the Piaggio P180 Avanti. Therefore it was rated at a TRL of 7. Finally, the systems were set at a TRL of 2, because some of the systems required for the adaptive aircraft have never been used before for that purpose or will require extra modifications. For example, the alignment system to be used to align the fuselage sections, will work in a closed feedback loop with the lifts to precisely align the sections. This system will have to be developed specifically for that purpose, although all of its components already commercially exist. Furthermore, all other system connections will have to be modified to cope with the adaptation. Some systems, such as the hydraulics, will have to be easily detachable at the cut section to facilitate the conversions. The other remaining components, such as the landing gear, engines, payloads, and wings, will have no extra modifications and will be mostly conventional. It was decided that for every component that has a TRL below 9, a 5% factor will be applied to the development costs, per TRL, to account for the extra development costs[18]. For example, a TRL of 2 will be reflected by having an increase of 35% in development costs[18].

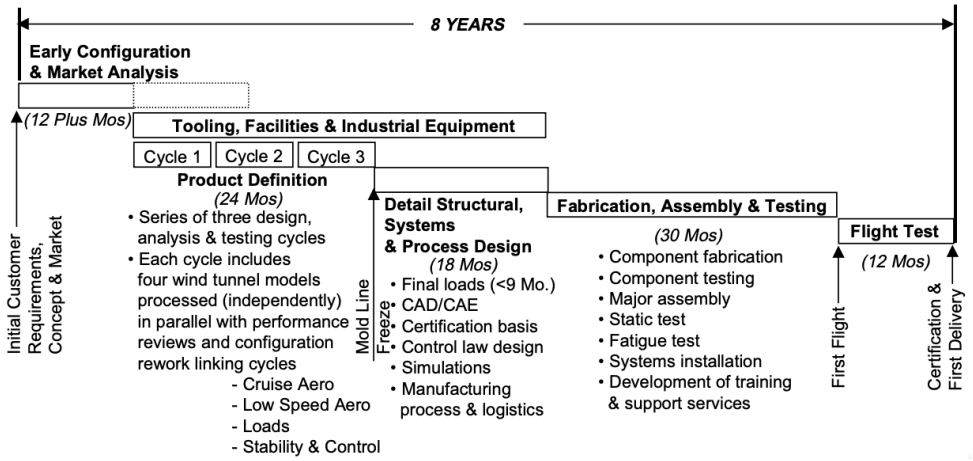

Figure 13.2: 1990 State-of-the-art airframe development cycle

With the total cost calculated, it was found to be helpful to divide the development costs over the timeline of development. The timeline was divided according to a NASA model of a typical airframe development cycle. The different phases of this model are outlined in Figure 13.2 [111]. The timeline was divided between the five processes, with some of them starting later than others, and with varying durations. The cost profile for each process was modelled using Equation 13.1, using the method outlined by Markish [60].

$$c(t) = K \cdot t^{\alpha-1} \cdot (1-t)^{\beta-1} \tag{13.1}$$

Here, α and β are constants that were provided from literature [60]. The constant K was altered till the area under the graph of each process represented the fraction of cost that each process contributed, to stay consistent with the initial cost division. All the different processes were added to each other, to get a cost profile of the whole development process. This aimed to produce a non-dimensionalised model of cost against time. The model represents the cost divisions, visualised in Figure 13.3.

Using this model, it was possible to find the area under the curve between any two points in time to find the expected cost fraction of that duration. The "Early Configuration and Market Analysis" phase is expected to have a cost of $\$69.2$ million. The "Product Definition" phase along with part of the "Tooling, Facilities & Industrial Equipment" development and manufacturing phase are expected to have a cost of $\$552.6$ million. The "Detail Structural, Systems & Process Design" phase, along with the rest of the tooling development and fabrication are expected to cost $\$1.013$ billion. The "Fabrication, Assembly & Testing" phase is expected to have a cost of $\$593.5$ million. Finally, the "Flight Testing" phase is expected to have a cost of $\$15.3$ million.

After adding a 10% contingency factor, the development cost total becomes $\$2.47$ billion. Finally, it is worth noting that compared to the previously expected budget of $\$2.54$ billion, the new estimated cost is still within budget and is lower than was expected.

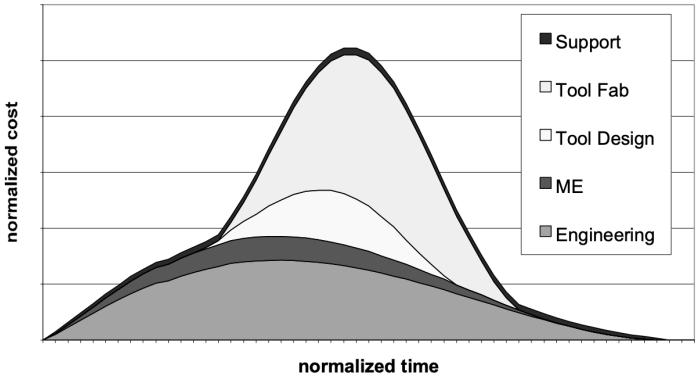

Figure 13.3: Non-recurring hours for a commercial aircraft project [60]

13.2. Manufacturing cost

As was done with the development cost, the manufacturing cost is also calculated based on the same assumption of a linear relationship between mass and cost. This relationship is found from literature, based on statistical data [60]. This is also done on a cost per part basis. The costs are then added up to find the Theoretical First Unit (TFU) cost. These are then divided into different production cost aspects, and a learning curve is applied to each of these aspects, to find the production cost of each aircraft during the first five years of production.

Firstly, based on component cost per kilo, an estimate of the cost of the aircraft is produced. This data is based on statistical data found in Markish [60]. The values are also divided into three aspects of production: labour, materials, and others. The "other" category includes processes such as quality assurance, recurring engineering, and recurring tooling [60]. However, some adjustments had to be made to these values. Firstly, since the data used dates back to 2002, all the costs presented had to be adjusted for inflation first. Secondly, since in some components, different materials are used than what was normally found in aircraft at that time, as outlined in section 10.1, this had to be accounted for. In the material cost component of every part where another material is used, the cost is multiplied by a ratio of the price per kilo of the new material to that of Aluminium. The resulting costs are shown in Table 13.2.

Table 13.2: Recurring cost breakdown

Part	Labour	Materials	Other	Total
Wing	$10,698 K	$13,146 K	$1,546 K	$25,390 K
Empennage	$3,842 K	$4,226 K	$555 K	$8,623 K
Fuselage	$20,402 K	$15,375 K	$2,945 K	$38,722 K
Landing Gear	$780 K	$715 K	$117 K	$1,612 K
Installed Engines	$3,398 K	$1,247 K	$493 K	$5,139 K
Systems	$5,230 K	$1,511 K	$764 K	$7,505 K
Payloads	$5,221 K	$1,289 K	$761 K	$7,270 K
Final Assembly	$5,828 K	$402 K	$301 K	$6,532 K
Total	$55,401 K	$37,910 K	$7,481 K	**$100,792 K**

Finally, all of the costs are added up to obtain an estimate of the TFU cost. However, since production is a recurring process, it is therefore subject to a learning curve. A learning curve reflects the decrease in cost of a recurring process, due to the workers becoming more experienced, and able to facilitate production more quickly. The learning curve was applied using Equation 13.2, provided by Fabrycky [33].

$$Cost_n = TFU \cdot n^{ln(s)/ln(2)} \tag{13.2}$$

Where $Cost_n$ is the cost of production of the nth aircraft, and s is the slope of the learning curve. The three different production aspects are also associated with different learning curve slopes and were calculated separately. The values of these slopes were found in literature to be 95% for materials and others, and 85% for labour [60]. This is expected, since labour is the aspect where the learning effect is most prominent and where the greatest reduction of cost is expected to be noticed. The learning curve was then applied to the costs of the first 200 units, which is the number of units expected to be sold in the first five years of production, as is explained in further

detail in subsection 13.4.1. The results are shown in Figure 13.4. These values will later be used to calculate the ROI in section 13.4.

13.3. Operational cost

To make sure the adaptive regional airliner is competitive on the market, it should be more profitable for airlines to operate. Therefore, in this section a first estimate of the operational cost is calculated and compared to competitors. To compare the data properly, it was decided to compare the operational cost in cost per block hour, which is the cost per hour of flight. This is a common parameter in the aviation industry.

The operational cost consists of the following cost elements: crew cost, conversion cost, maintenance cost, depreciation, fuel cost, and insurance. Airport tax, overhead, and sales are not included, because these are not heavily dependent on aircraft type. For example, airport tax will be comparable for same sized aircraft. Overhead and sales will be heavily dependent on airline and not on aircraft type.

First, the crew cost will be calculated. The crew cost is difficult to estimate specifically for the adaptive regional airliner. Since airliners differ heavily in amount of crew and cost per hour, the average of the large regional airline market is taken, which is $371 per block hour [112][1]. Because this crew cost was calculated in 2011, inflation is factored in at 2% per year [41] over 8 years. The results can be seen in Table 13.3.

Table 13.3: Operational cost per block hour.

	Cost
Crew	$434.69 /hr
Fuel configuration 1	$585.84 /hr
Fuel configuration 2/3	$634.94 /hr
Insurance	$7.03 /hr
Conversion	$6.53 /hr
Maintenance	$452.26 /hr
Depreciation	$242.13 /hr
Total configuration 1	$1,901.31 /hr
CRJ 900	$1,673.13 /hr
Total configuration 2/3	$1,955.33 /hr
Embrear 190	$3,005.31 /hr

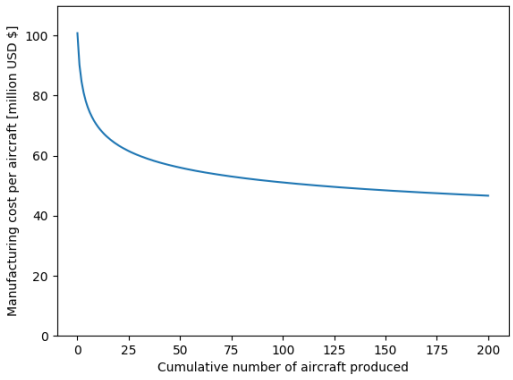

Figure 13.4: Cost of producing each aircraft against aircraft number

Secondly, the fuel cost is calculated. Here a distinction is made between the configuration with 90 passengers and 120 passengers, since the fuel consumption would be different. The fuel consumption was calculated to be on average 0.274 kg/s for the 90 passenger configuration, as calculated in chapter 9. For the 120 passenger configuration, the fuel consumption was calculated to be on average 0.297 kg/s. The price per barrel was $75.49 at the 14th of June [39][2], this kerosene price was used in further analysis and comparisons. This resulted in a total fuel cost of $585.84 per block hour for the 90 passenger configuration, and a total fuel cost of $634.94 per block hour for the 120 passenger configuration.

Thirdly, the insurance cost will be analysed. The insurance cost analysis is mainly based on reference aircraft. The insurance costs are estimated to be higher because the adaptive regional airliner is a new concept. Therefore, the insurance cost of narrow body aircraft (e.g. 737, A320) is used to take this into account. All in all, the insurance cost was set at $6 per block hour in 2011 [112]. Since the insurance cost needs to be known in 2019 again an inflation of 2% is added over 8 years [41].

Furthermore, the conversion cost will be analysed. The conversion cost was already analysed in chapter 12. The labour cost of the actual conversion and checking was calculated there. It is assumed that this is the main cost and the other costs will be neglected as for example the hangar is already present for the maintenance. The labour cost of the checking and conversion was calculated in the case of 4 conversions from 120 passengers to 90 passengers and 4 conversions from 90 to 120 passengers as was analysed in chapter 2. The total labour cost was multiplied by 30 because the lifetime of the aircraft was assumed to be 30 years. This was divided by the total life

[1]URL: `http://m.aviationweek.com/site-files/aviationweek.com/files/archive/cmsfiles/media/pdf/ad_pdf/2011/11/21/avd_11_21_2011_cht1.pdf` [cited on 21 June 2019]
[2]URL: `https://www.iata.org/publications/economics/fuel-monitor/Pages/index.aspx` [cited on 21 June 2019]

cycle hours. The conversion came out to be $6.53 per block hour when converting 4 times from configuration 1 to configuration 2/3 and converting 4 times from configuration 2/3 to 1.

Moreover, the maintenance needs to be analysed. The maintenance cost is analysed by looking at reference data. Again the assumption was made that the cut section will be more expensive. Therefore, the maintenance cost of a narrow body (e.g. 737, A320) was used to take into account the extra cost of the adaptability. This was set at $386 per block hour [112]. However, this was the maintenance cost in 2011. Therefore, an inflation of 2% per year was added over 8 years to take this into account [41]. In the end the maintenance cost came out to be $452.26 per block hour.

Lastly, the depreciation was calculated. A linear depreciation was set as this is usually the case in the aviation industry [50][3]. Furthermore, residual value was set at 10% of the unit cost as this is mostly the case in the aviation industry [50]. Dividing the total depreciation by the total amount of flight hours results in the depreciation per block hour. This is calculated to be $242.13.

All in all, the average operating cost was calculated to be $1,728.47 per block hour for configuration 1. For configuration 2/3 the average operating cost was calculated to be $1,777.57 per block hour. This is presented in Table 13.3. Since this is an estimate and a few assumptions were made a contingency factor of 10% was added [18]. To conclude if the aircraft is competitive, a comparison with the competitors in operational cost is made. The average operating cost per block hour of the CRJ900 and Embraer 190 were found [112]. The CRJ900 could be compared with the 90 passenger configuration and the Embraer 190 with the 120 passenger configuration. These costs were corrected by inflation by adding 2% over 8 years for applicable categories [41]. Also the fuel costs were corrected by the current kerosene price [39]. This resulted in the numbers shown in Table 13.3. It can be seen that the first configuration is 12% more expensive compared to the reference CRJ900. However, the CRJ900 is slightly smaller than the adaptive regional airliner. Moreover, the adaptive regional airliner is easier to adapt to the market demand in a certain time. Therefore, the profit airliners make can still be higher. Furthermore, the average hour operating cost is without contingency factor nearly the same as the CRJ900. Therefore, in further analysis the operational cost of the small configuration needs to be optimised to be competitive with the CRJ900. For the 120 passenger configuration the adaptive regional airliner is 53% more cost effective than the competitor, the Embraer 190. Furthermore, the adaptive regional airliner will be easier to adapt to the market demand and therefore make more profit for airliners. To conclude, the adaptive regional airliner has a price of one large regional airliner but provides 2 aircraft at the same time, operating at a lower cost.

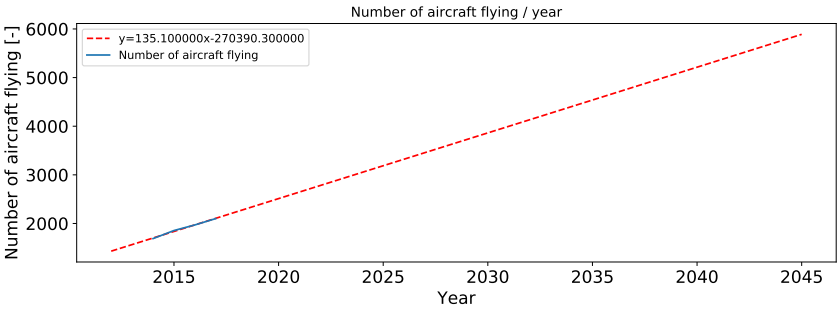

Figure 13.6: Projected market size of regional jets

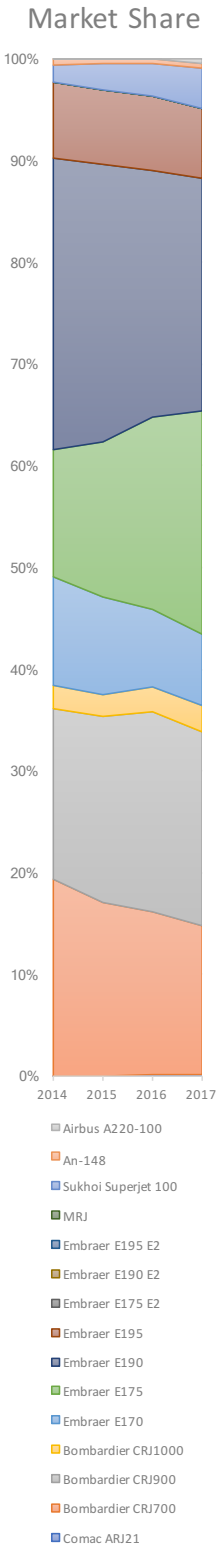

Figure 13.5: Market share of different regional airliners

[3]URL: https://www.iata.org/publications/Documents/Airline-Disclosure-Guide-aircraft-acquisition.pdf [cited on 21 June 2019]

13.4. Return on investment

In this section the return on investment will be calculated. Firstly, the amount of sold aircraft is found in subsection 13.4.1. Secondly, the price of the aircraft is found in subsection 13.4.2. Lastly, final calculations are performed to find the return on investment.

13.4.1. Predicted market share

Predicting a market share is important for any new product. It enables the manufacturer to predict the number of units that would be sold, and enables estimating a Return on Investment (ROI). For the 'adaptive regional airliner', the market targeted, and analysed, is that of regional airliners with a seating capacity between 70 and 140 passengers. First, the market size was linearised, to determine the market size in 2035, which is when the aircraft is planned to enter service, and in 2040, which is the 5 year period over which the ROI will be analysed. Using a linear regression, the market size was estimated at 4,335 flying aircraft in 2035, and at 5,010 in 2040, as can be seen in Figure 13.6.

Next, the market division between different aircraft was analysed for several consecutive years, to be able to analyse the growth trends in new aircraft, and to visualise the competition present in the market. It was determined that the Sukhoi Superjet 100 is a good example, and represents a similar aircraft program. This is because the Sukhoi Superjet was the first regional airliner developed by Sukhoi, and it represented a penetration into a completely new market for them, which is also the case for the adaptive regional airliner. Furthermore, the Sukhoi Superjet faced some problems entering the market. Therefore, it was seen as a conservative approach. The Sukhoi Superjet was able to attain a 3.9% market share within 6 years of being in service, as can be seen in Figure 13.5. This was used because airlines may be hesitant at first to adopt the new concept of the adaptive aircraft. However, it is expected that the adaptive regional airliner would be able to attain a remarkably larger market share, as it is a revolutionary concept, and it also covers a number of aircraft configurations rather than just one. Therefore, it is assumed that a similar market share to the Sukhoi Superjet could be attained within the 5 year period, that being 4% of the market at that time. This means that by 2040, it is expected that there will be 200 units of the adaptive regional airliner flying.

13.4.2. Predicted unit cost

The predicted price was modelled as a function of variables representing an aircraft's value to its operator. The model, made by Jacob Markish, was used to predict the unit price [60]. Equation 13.3 was used to model the price. In Table 13.4 the model parameters for narrow body airplanes were found. Furthermore, the reference parameters of the Sukhoi Superjet were used. Since in subsection 13.4.1, the quantity of sold airplanes was found based on the Sukhoi Superjet, it was also used here as the reference to model the price. That is because the quantity of sold airplanes and the price of the aircraft is heavily interrelated.

$$Price = (k_1(\frac{Seats}{Seats_{ref}})^{\alpha} + k_2(\frac{Range}{Range_{ref}})Price_{ref}) - \Delta(LC) \tag{13.3}$$

Table 13.4: CAROC-neutral price regression parameters [60]

	Narrow body aircraft	Wide body aircraft
k_1	0.735	0.508
k_2	0.427	0.697
α	1.910	2.760

To calculate the last parameter of Equation 13.3, $\Delta(LC)$, Equation 13.4 was used. This parameter takes the profitable from an airline perspective of the aircraft, this of course has an influence on the final market price. The annual utilisation, trip length and lifetime were taken from Table 13.5. $\Delta(CAROC)$ was calculated by the equation from Figure 13.7.

$$\Delta(LC) = (\Delta(CAROC) \cdot (Seats) \cdot (AnnualUtilization) \cdot (TripLength))Lifetime \tag{13.4}$$

All in all, the final unit cost was calculated at $62.15 million when selling the aircraft in 2019 (without inflation). The initial requirement was set at $60 million. Therefore, the requirement is not met. However, the unit cost is calculated by using the current market trend. This unit cost was set in order to have the highest revenue possible.

Table 13.5: Lifecycle cost increment parameters.[60]

	Narrow body aircraft	Wide body aircraft
Annual utilization (trips/year)	2120	590
Average trip length[30] (nm/trip)	500	3000
Service lifetime[31] (years)	27	27
Operator discount rate	12%	12%

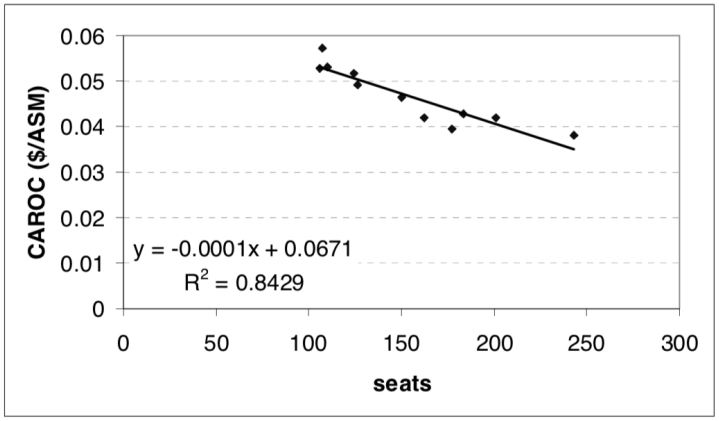

Figure 13.7: CAROC trend as a function of seat count for narrow body aircraft.

13.4.3. Final calculations

To calculate the final return on investment after 5 years the manufacturing cost, development cost, quantity of sold airplanes and unit cost are needed. These were all calculated previously. To calculate the total profit made after 5 years of production, inflation needs to be taken into account when calculating manufacturing cost and unit price. Since the aircraft will be in service in 2035 the inflation has a big factor. It was found that the average inflation was ideally 2% [41][4]. To simplify the calculations it was assumed that the 200 airplanes produced in the first 5 years were divided equally over the 5 years, at a rate of 40 airplanes every year. Taking into account the learning curve and the inflation, the return on investment is calculated at 8.63% after 5 years. Therefore, the requirement of a return on investment after 5 years of 5% is achieved.

13.5. Verification and validation

The cost model generated a cost profile. This cost profile was plotted, and compared to the profile found in literature. This is visualised in Figure 13.8 and Figure 13.9. It can be seen that both profiles show the same outline of the total cost and the same shape.

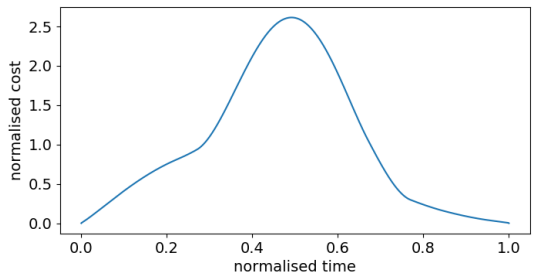

Figure 13.8: Generated cost profile model

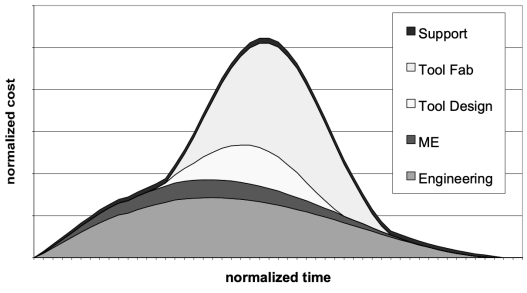

Figure 13.9: Cost profile model from literature [60]

It was supposed that an integration of the curve to find the area under the graph, should result in a precise value of 1. The area under the generated graph was found to be equal to 1.000056, which was deemed close enough to verify the model. Additionally the original model found in literature was already validated using data from Boeing about a development project. The figure including the data from Boeing is shown in Figure 13.10. It can

[4]URL: https://www.ing.com/Newsroom/All-news/Features/Features-old/What-is...-inflation.htm [cited on 18 June 2019]

also be noted that the outline of the figure matches both models and the model is deemed as valid.

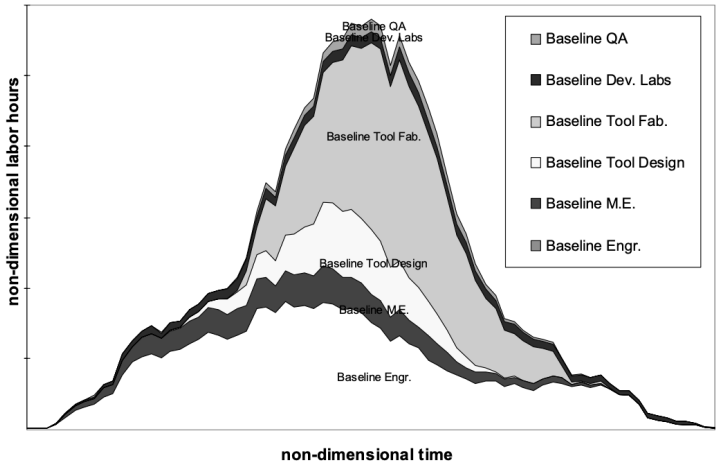

Figure 13.10: Non-recurring hours for a commercial aircraft project [60]

13.6. Sensitivity analysis

First a sensitivity analysis of the development and manufacturing costs will be performed, to measure the effect of their change on meeting the ROI requirement. Next, the sensitivity of the operational cost will be analysed.

The method used to calculate both the development cost and the manufacturing cost is totally dependent on the component weights of the aircraft. Hence, to analyse whether a change in design parameters would cause a negative effect in terms of cost, the masses used in the calculations were increased by a factor of 10%. This was done first for the development cost. This led to a development cost of $2.47 billion. With the new development cost, and the same previous unit cost, the program was able to show an ROI of -1.24%, over the same five-year period, which does not meet the set requirement. When increasing the manufacturing cost instead, the program showed an ROI of -59.55%. This indicates that the ROI is substantially more sensitive to a change in manufacturing cost, rather than development cost.

In terms of operational cost, three parameters influence the operational cost heavily. Firstly, the crew cost is changing per region and increasing in time. For example, the crew cost is in western countries a driving factor of operational cost compared to other countries. Therefore, an average is taken but still has a big influence on the final cost. Secondly, the fuel cost is changing over time. In the analysis this is corrected. However, per region there is a major difference. For example, in the middle east the fuel cost is less important in terms of operational cost. Lastly, the maintenance cost, this is also heavily changing per region and therefore changing per airliner. Because of these changing parameters a contingency factor of 10% is added to the operational cost. However, still the operational cost will be changing in different regions and different carriers (low-cost and Full-service carriers).

14 Technical Risk Assessment

The aviation industry is one of the safest industries in the world. One of the reasons for this is the large implications accidents have on society. Therefore, it is of utmost importance to design the aircraft to be as safe as possible. In order to properly assess the risk, the aircraft is divided into systems. These systems are, in turn, divided into subsystems. If applicable, the subsystems are divided into subsubsystems, also called assemblies. In order to properly address the risk of the system, a failure modes, effects, and criticality analysis (FMEA) is performed. During this analysis, the failure modes of a (sub)system are identified, investigated, and analysis on the countermeasures for the failure modes is performed. It also addresses the criticality (i.e. risk) of individual failures. The failure modes and effects analysis is shown in Appendix D. The risk codes associated with the FMEA are displayed in Table 14.1, Table 14.2 and are listed below [19].

Table 14.1: Severity of consequence

Category	Personnel illness / injury	Product loss ($)	Down time	Environmental effects
I Catastrophic	Death	>1M	>4 months	Long-term (>5 yrs) damage
II Critical	Severe injury or occupational illness	250K - 1M	2 weeks to 4 months	Medium-term (1-5 yrs) damage
III Marginal	Minor injury or occupational illness	1K - 250K	1 day to 2 weeks	Short-term (<1 yrs) damage
IV Negligible	No injury or illness	<1K	<1 day	Minor damage

Table 14.2: Probability of occurrence

Level	Descriptive word	Definition
A	Frequent	Likely to occur repeatedly in system life cycle
B	Probable	Likely to occur several times in system life cycle
C	Occasional	Likely to occur sometime in system life cycle
D	Remote	Not likely to occur in system life cycle, but possible
E	Improbable	Probability of occurrence cannot be distinguished from zero
F	Impossible	Physically impossible to occur

Risk levels:

1. Unacceptable: Severity I and probability A,B, or C, and severity II and probability A or B.
2. Provisionally acceptable: Severity I and probability D, severity II and probability C, or severity III and probability A or B.
3. Acceptable: Any other combination

The sections below describe the risk analysis of the subsystems. The systems analysed are the connection of the sections, the aircraft structure, the flight control system, the electrical system, the hydraulic system, the fuel system, the engines, the landing gear, the communication system, the air conditioning system, and finally, the water system. Only the most important risks will be highlighted, as they are a result of the adaptability and change in skin material.

14.1. Connection of the sections

The connection between the fuselage sections is the first system investigated. It is divided into the connectors, the airseal, the fastening method and the alignment system. The connectors and the airseal are highlighted below.

Connectors

As the entire fuselage is cut through at the section, the cockpit wires and hydraulics are separated from the main fuselage. These have to be connected by the connectors. The systems which have to be connected are the hydraulic, the flight control, the electrical, and the water system. These systems have 1 to 2 redundant systems, which increases the amount of connectors. The probability of failure of the connections is assumed to be occasional, as the system is at a lower technological readiness level. The probability of failure can be lowered by adding redundancy to the system. Therefore, there will be 3 connectors per cable for fly-by-wire, for hydraulics also 3 connectors for the 2 systems, to make sure the critical flight systems do not fail.

Another risk, specifically for the hydraulic system, is that the hydraulic lines become dirty, leaving particles in the hydraulic fluid which can damage the system. As the hydraulic system has at least 1 redundant system, the severity of this risk is assumed to be marginal. The probability is assumed to be occasional, as it is normal to replace hydraulic lines during maintenance.

The risk of not connecting systems properly is also applicable to the electrical system and the flight control system. The connectors (or plugs) can be installed to the wrong system, or in the wrong way, causing short circuit in the system. According to Wash-1400 [108], the human error rate for a routine repetitive task is between $3 \cdot 10^{-3}$ and $1 \cdot 10^{-2}$ per individual operation. This means that for every thousand operations, 3 - 10 mistakes will be made. Therefore, the probability of mishap during adaptation is probable. From the FMEA, it is found that this risk is marginally acceptable. By designing plugs which only fit one connector in one way, it will become improbable to connect the wrong wires, or to connect them the wrong way. This significantly lowers the risk to an acceptable level. Furthermore, there will be checking done after adaptation in order to reduce the probability of failure even more.

Airseal

If the airseal fails, this might lead to severe injury of the passengers on board, as the cabin can depressurise. The airseals of the fuselage door and cargo door of normal aircraft rarely fail. However, the scale of these air seals is much smaller than the airseal of an entire fuselage section. On the other hand, there is no loss of a Boeing 747 freighter due to failure of its nose door [110][1]. Further investigation and testing of the airseal is advised for the detailed design phase. For now, it is assumed that the probability of failure of the airseal is occasional. This leads to an unacceptable risk, which can be lowered by sufficient inspection procedures and early replacement of the airseal.

14.2. Aircraft structure

The other system which is different from regular aircraft is the structure of the aircraft. It consists of every structural element of the aircraft. Examples are spars, ribs, rivets, stringers, spars, and the skin. The structures system is divided in the wing, the fuselage, and the joints subsystems. These are, in turn, divided into assemblies.

The structure of the aircraft is rather similar to regular aircraft. The connection of the sections is the main difference, as discussed before. However, in order to save more weight and become more efficient, it is chosen that the skin will be made out of Epoxy/HS carbon. The FMEA shows the risk analysis for this. It can be seen that the corrosion for this material is different from normal aluminium aircraft. Whenever aluminium and this Epoxy/HS carbon are in contact with each other, it will become a dielectric cell which can cause Galvanic corrosion [67]. The risk this poses is unacceptable without mitigation. However, the risk can easily be mitigated. During the manufacturing process, a layer of carbon-fibre epoxy will be placed between these layers, which will prevent the contact between both materials. In this way, the materials will not form a dielectric cell and the risk is mitigated and brought back to an acceptable level.

The other risk associated with the Epoxy/HS carbon, is that the detection of cracks in the structure is much more difficult than for aluminium. Fatigue damage inspection is often not needed for composites, since designs are usually based on the no-damage-growth philosophy. Also environmental damage is much less of a problem for non-metals, if proper design precautions are taken. Furthermore, large size damage due to foreign object damage, bird strikes, or major collision with ground equipment will be easily detectable in most cases. However, low-velocity large-mass impact may lead to internal damage in the structure, which might not be seen from the outside [11]. That is why this risk is mitigated by immediate, thorough inspection after collisions.

[1] URL: `https://en.wikipedia.org/wiki/Boeing_747_hull_losses` [cited 19-06-2019]

Low-energy impacts usually cause so-called non-visible impact damage (NVID) or barely visible impact damage (BVID). These impacts can usually be attributed to hailstone strikes and foreign object damage (FOD) such as runway debris. Impact induced damage, which may be undetectable by visual inspection, can have a significant effect on the strength, durability, and stability of the structure. Existing inspection methods for these kinds of damage consist of, but is not limited to Detailed Visual Inspection, General visual inspection, and automated visual NDT, which is also referred to as "enhanced visual inspection" [11].

The final form of testing is the non-visual testing. Examples are tap testing, which can be used for testing delamination of the skin; thermography, which uses temperature differences to test the skin for cracks and flaws; acoustic emission, which can be used to find cracks in the fuselage skin; and ultrasonic detection, which is widely used for the quality control of aircraft skins [11]. All the aforementioned inspection methods should make the early detection of cracks possible and prevent the skin from failing.

14.3. Other systems

The remaining systems are mostly similar to regular aircraft. It is therefore assumed that these systems all have a probability of failure of improbable. Some of these systems attain this level of probability after mitigation. For instance the electrical, hydraulic, and flight control systems all have sufficient redundancy in order to have a probability level of improbable. The fuel system is designed with a high enough safety factor in order to lower the probability of failure.

The landing gear only has a provisionally acceptable risk associated with the strut. It is therefore advised to design the strut with a high safety factor in order to prevent it from failure during landing. Furthermore, the communications system has a provisionally acceptable risk associated with the communication to the ground. In order to lower this risk, it is advised to have a back-up system working on the APU, which is a redundant system. This lowers the probability of failure and thus lowers the risk.

It can be concluded that the adaptive airliner has risk similar to regular aircraft, except for the Epoxy/HS carbon skin and the connection between the sections. These risks can be mitigated by adding redundancy, designing the systems with a large enough safety factor, and Epoxy/HS carbon specific mitigations. All the risks before mitigation have been visualised in the risk map in Table 14.3, which uses the numbering from Appendix D and the risk codes from Table 14.1 and Table 14.2.

In Table 14.3 it can be seen that there are risks identified as unacceptable. After risk mitigation it was made sure that all these risks were mitigated into the acceptable region. The risk map associated with the mitigated risk is presented in Table 14.4.

Table 14.3: Riskmap following from the FMEA

Probability of mishap	IV: Negligible	III: Marginal	II: Critical	I: Catastrophic
A: Frequent				
B: Probable			1.1.2, 1.1.5, 2.1	
C: Occasional		1.1, 1.1.1, 1.1.3, 1.1.4, 1.3, 1.3.2, 1.4, 8.2	1.2	2.3, 5.1
D: Remote	9.2, 11.2	4.1, 4.3, 8.1, 9.3, 11.1	2, 3.2, 8.6, 10, 11.3	1.3.1, 2.1.1, 2.1.2, 2.2, 2.2.1, 2.2.2, 2.2.3, 2.2.4, 3.1, 3.3, 4, 4.2, 5.2, 5.3, 6.1, 6.2, 6.3, 7, 8.5, 9.1
E: Improbable		8.4	8.3	
F: Impossible				

Severity of consequences

1: Unacceptable
2: Provisionally acceptable
3: Acceptable

Table 14.4: Riskmap after mitigation following from the FMEA

Probability of mishap	IV: Negligible	III: Marginal	II: Critical	I: Catastrophic
A: Frequent				
B: Probable				
C: Occasional	1.3.2,	1.3, 8.2		
D: Remote	9.2, 11.2	1.1, 1.1.1, 1.1.3, 1.1.4, 1.4, 4.1, 4.3, 8.1, 10, 11.1, 11.3	1.2, 2	
E: Improbable		8.4, 9.3	1.1.2, 1.1.5, 2.1, 2.1.1, 3.2, 8.2, 8.6	1.3.1, 2.1.2, 2.2, 2.2.1, 2.2.2, 2.2.3, 2.2.4, 2.3, 3.1, 3.3, 4, 4.2, 5.1, 5.2, 5.3, 6.1, 6.2, 6.3, 7, 8.5, 9.1
F: Impossible				

Severity of consequences

1: Unacceptable
2: Provisionally acceptable
3: Acceptable

15 Final Design

In this chapter, the final design as a result of the detailed design process and iterations is presented. This includes variations of the design parameters over the different iterations, as well as the main final parameters of the design. This is followed by the presentation of the internal and external layout. Finally, the requirement compliance matrix is included in this chapter.

15.1. Results through iterations

As discussed in chapter 5, the design of the adaptive regional airliner is an iterative process. In this section the OEM and $MTOM$ variations of the design in function of the performed iterations are presented and discussed. In Figure 15.1 and Figure 15.2 the variations of these two parameters are illustrated.

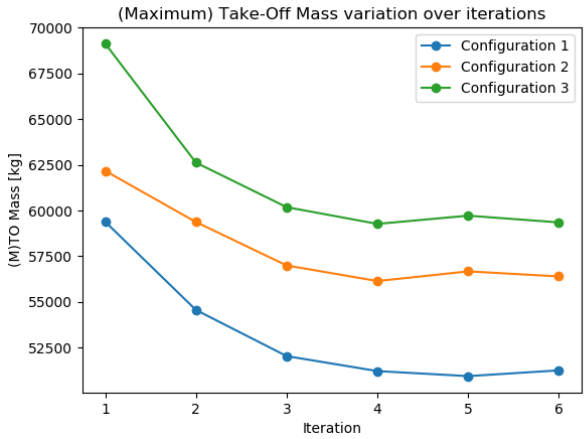

Figure 15.1: Variation of $(M)TOM$ over the iterations

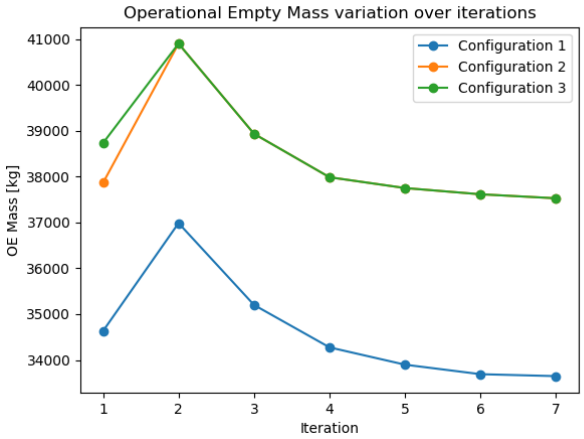

Figure 15.2: Variation of the OEM over the iterations

In the first iteration, the OEM was based on the class-I estimate. However, during the first iteration a class-II mass estimation was performed, which resulted in a higher value of the OEM, which can be clearly seen on Figure 15.2. The $MTOM$, which was based on the class-I OEM and fuel fractions, was estimated too high initially, as seen on Figure 15.1. Although the OEM went up, the $MTOM$ went down between the first and second iteration. This is explained by the fact that the estimated fuel fractions were highly overestimated in the class-I estimation. By performing a more detailed analysis on the fuel consumption with the selected engine, these could be reduced significantly. Additionally, it can be observed that in the first iteration the OEM of configuration 2 differed from configuration 3. This can be explained as initially a detachable canard was considered, however for stability and control purposes it was found that this was not desirable. Therefore, the OEM of both configurations were the same for the rest of the iterations. The iterative process had to be executed until the design parameters converged to a final value. It can be seen from the plots that this indeed occurred at the final iterations performed. The difference between the input and output of iteration 6 in terms of OEM was 0.13% and 0.23% respectively for configuration 1 and 3. Therefore, iteration 6 was the last iteration performed.

15.2. Final design parameters

In this section, the main final parameters are presented as a result of the final design phase of this project and the performed iterations.

Table 15.1: Final design main parameters

	T/W [–]	W/S$[N/m^2]$	OEM $[kg]$	$(M)TOM$ $[kg]$	$S[m^2]$	$S_h[m^2]$	$S_v[m^2]$	$S_c[m^2]$	$X_{lemac}[m]$	$L_{cutout}[m]$
Config. 1	0.288	4,173	33,649.12	51,213.9	120.5	29	26.5	0	14.1	0
Config. 2	0.2995	4,173	37,526.3	56,301.0	120.5	29	26.5	37.1	19.8	5.7
Config. 3	0.2995	4,173	37,526.3	59,249.3	120.5	29	26.5	37.1	19.8	5.7

It can be observed that the initial proposal to make the canard detachable for configuration 2 and 3 was not desirable. The canard could not be smaller for the second configuration for stability and control purposes, as discussed in chapter 8. Additionally it was found that no external fuel tanks were necessary as the main wing has enough storage capacity. Therefore, configuration two resulted to be the same configuration as the third one, only loaded with less fuel. Therefore, when $MTOM$ is mentioned, this is denoted as the $(M)TOM$ as for configuration 2 the actual $MTOM$ is higher than its actual TOM. This was not aimed to be the outcome when these design points were identified. Therefore, it is recommended that this will be further investigated in the more detailed design phases.

15.3. Internal layout

Figure F.1 and Figure F.2 in Appendix F, show the internal configurations of configuration 1 and configuration 2 & 3, respectively. This includes the placement of two galleys and two lavatories. They are sized based on comparable aircraft lavatories and galleys [82]. The seat pitch used in both configurations is 0.813 metres (32 inches), however more space is added at the cut sections in order to make the conversion easier. Additional space was also included at the two emergency exits above the wings as is required by the CS-25 regulations [23]. These regulations were also used for the sizing of the doors. Doors 1L and 3L are used for boarding of passengers and are therefore the largest doors on the aircraft and are of type-I. The doors 1R and 3R are also of type-I as is required by the CS-25 regulations, however they are smaller as only catering resupply operations will be conducted using these doors. For the emergency exits over the wings type-II doors are used.

15.4. External layout

Also in Appendix F, the external layout of configuration 1 and configuration 2/3 is shown. In these drawings, the aircraft are drawn with the correct parameters (dimensions in metres) for the fuselage, wing, canard, landing gear and empennage. The dimensions in the figure are in metres. Furthermore an exploded view is included to give an impression on how the modular section would be fitted into the extended configurations. These drawings intent to give a first impression of the aircraft. More details regarding the values can be found in the previous chapters on detailed design.

15.5. Requirement compliance matrix

In order to visualise clearly whether all requirements which have been presented in section 3.5 are met, a requirement compliance matrix is set up. This is presented in Table 15.3. As the table needs some clarification in terms of symbols used, a legend is presented in Table 15.2.

Table 15.2: Requirement compliance matrix legend

Symbol	Meaning
√	Requirement is met
X	Requirement is not met
~	Requirement was set too detailed and could not be evaluated in the DSE timespan
...[1]	Remark needed for clarification

The remarks made in Table 15.3 are explained below.

1. All the requirements related to CS-25 which are analysed are met. The other CS-25 requirement are too detailed and will be analysed in a later stage of the design.
2. These sustainable requirements have not been met and recommendations on improving this will be explained in chapter 17.
3. The unit cost will be $62.15 million which is more than the requirement of $60 million. However, after performing a more in depth price analysis a price of $62.15 million is optimal and will result in more profit.
4. These requirements are set too detailed and will be researched in a later design phase.
5. This requirement is set too detailed, the exact layout of the cockpit will not be determined in this stage.
6. These requirements need to be fulfilled but are too detailed for this phase. These will be investigated in a more detailed design.

7. These values have not been explicitly calculated. The control system is however a fly-by-wire system meaning that this can be programmed, installed and designed such that these requirements will always be met.

8. The aircraft is able to maintain stability when the aircraft's centre of gravity is most aft or forward, however the vertical c.g. was not taken into account until this phase of analysis. The longitudinal vertical tail is designed such that it can withstand the one engine inoperative case at the critical point during flight, which is considered the most critical condition regarding lateral stability. This is during take-off. For other events such as sideslip/gusts the aircraft will be kept stable by the use of its advanced fly-by-wire system. Therefore, this part of the requirement is assumed to be fulfilled.

9. Locking devices for the removable fasteners at the fuselage joints are not investigated in this phase of the project as it is only relevant in more detailed design of the aircraft. The design of an automated locking mechanism is too detailed in this phase.

Table 15.3: Requirement compliance matrix

Requirement ID	*Check?*	*Requirement ID*	*Check?*	*Requirement ID*	*Check?*
Customer		**Passenger**		**CS-25**	
SYS-MI-CU-01	√	SYS-MI-PA-01	√	SYS-MI-CU-09-01	√
SYS-MI-CU-02	√	SYS-MI-PA-02	$\sim^{5}$	SYS-MI-CU-09-02	√
SYS-MI-CU-03	√	**Cabin environment**		SYS-MI-CU-09-03	√
SYS-MI-CU-04	√	SYS-CE-01	√	SYS-MI-CU-09-04	√
SYS-MI-CU-05	√	**Flight control**		SYS-MI-CU-09-05	$\sim^{6}$
SYS-MI-CU-06	√	SYS-FC-01	√	SYS-MI-CU-09-06	$\sim^{6}$
SYS-MI-CU-07	√	**Electronics**		SYS-MI-CU-09-07	√
SYS-MI-CU-08	√	SYS-EL-01	√	SYS-MI-CU-09-08	$\sim^{6}$
SYS-MI-CU-09	$\sqrt{}^{1}$	**Fuel system**		SYS-MI-CU-09-09	$\sim^{6}$
SYS-MI-CU-10	√	SYS-FS-01	√	SYS-MI-CU-09-10	√
SYS-MI-CU-11	X^{2}	SYS-FS-02	√	SYS-MI-CU-09-11	√
SYS-MI-CU-12	X^{2}	**Guidance, navigation and control**		SYS-MI-CU-09-12	√
SYS-MI-CU-13	√	SYS-GNC-01	√	SYS-MI-CU-09-13	√
SYS-MI-CU-14	X^{3}	**Hydraulic**		SYS-MI-CU-09-14	√
SYS-MI-CU-15	√	SYS-HD-01	√	SYS-MI-CU-09-15	$\sim^{7}$
SYS-MI-CU-16	√	**Ice protection**		SYS-MI-CU-09-16	$\sim^{7}$
SYS-MI-CU-17	√	SYS-IP-01	√	SYS-MI-CU-09-17	$\sim^{7}$
SYS-MI-CU-18	√	**Landing gear**		SYS-MI-CU-09-18	$\sim^{7}$
Structures		SYS-LG-01	√	SYS-MI-CU-09-19	$\sim^{7}$
SYS-ST-01	√	SYS-LG-02	√	SYS-MI-CU-09-20	$\sim^{7}$
Auxiliary power unit		SYS-LG-03	√	SYS-MI-CU-09-21	√
SYS-APU-01	√	SYS-LG-04	√	SYS-MI-CU-09-22	√
SYS-APU-02	√	SYS-LG-05	√	SYS-MI-CU-09-23	$\sim^{8}$
SYS-APU-03	√	**Avionics**		SYS-MI-CU-09-24	$\sim^{9}$
SYS-APU-04	√	SYS-AV-01	√	SYS-MI-CU-09-25	√
System		SYS-AV-02	√	SYS-MI-CU-09-26	√
SYS-S-01	√	SYS-AV-03	√	SYS-MI-CU-09-27	√
SYS-S-02	√	SYS-AV-04	√	SYS-MI-CU-09-28	√
SYS-S-03	√	SYS-AV-05	√	SYS-MI-CU-09-29	√
SYS-S-04	√	SYS-AV-06	√	SYS-MI-CU-09-30	√
SYS-S-05	√	SYS-AV-07	√		
SYS-S-06	$\sim^{4}$	SYS-AV-08	√		
SYS-S-07	$\sim^{4}$	SYS-AV-09	√		
SYS-S-08	$\sim^{4}$				

15.6. Resource allocation

This section will reflect upon the resource allocation which is performed in the baseline report and will expand it for further development after the DSE project. The two aspects which were considered in the baseline report were the mass of the aircraft and the thrust force. The maximum take-off mass was at that moment assumed to

be 44,100 kg. The required thrust was estimated by applying a linear regression with respect to reference aircraft, resulting in approximately 160 kN. To these values, a contingency factor of 30% should be applied since this was a very first estimate [18]. After the last iteration, the final output values for these parameters are 51,300 kg and 145 kN for the base configuration. These values are again used as input for an update of the resource allocation for the preliminary design, this time with a contingency factor of 10%. In addition to that, an estimate has been made for the detailed design in which a contingency factor of 5% is used. An overview of the development over the design phases can be seen in Figure 15.3 and Figure 15.4.

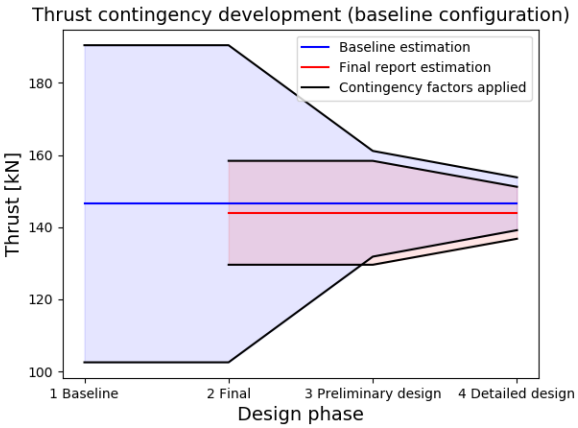

Figure 15.3: Thrust contingency development

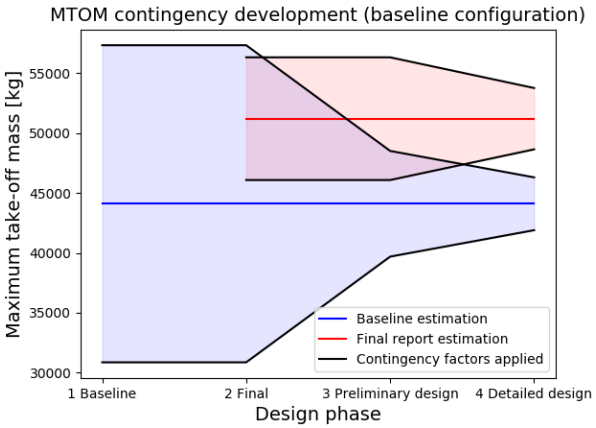

Figure 15.4: Maximum take-off mass contingency development

In these figures, the blue filled area is the contingency region allowed from the baseline report. From these figures it can be concluded that both the thrust and the maximum take-off mass calculations performed in the final iteration are within the contingency margin of the baseline report. In this report and design phase, a more detailed analysis is performed which means a new contingency estimate can be made for the next phases, presented in the red area in the graphs. The graph is constructed for the numerical values of the baseline configuration as this configuration was used in the baseline report. The maximum take-off mass and thrust required for the other configurations are however higher, thus these are not the maximum budgeted values. The same graph can be produced for the other configurations but this is not done as it was considered that this does not have specific additional value.

15.7. Budget breakdown

The budget breakdown presented below will be related to the operational empty mass and take-off mass. In this way the distinction between different components can be made visible the best. An overview of the budget breakdown for the OEM is presented in Table 15.4. From the table it can be seen that the structural component mass does not considerably change within the different configurations. The largest difference in percentage is the powerplant mass, caused by the decision to have the same engine for all configurations. Table 15.5 presents the breakdown of the $MTOM$ and TOM in case of configuration 2.

Table 15.4: Budget breakdown empty operational mass

	Configuration 1	*Configuration 2*	*Configuration 3*
Structural mass [kg/%]	20,886.4 (62.0%)	23,450.8 (62.5%)	23,450.8 (62.5%)
Powerplant mass [kg/%]	4,828.4 (14.4%)	4,837.2 (12.9%)	4,837.2 (12.9%)
Fixed equipment mass [kg/%]	7,934.3 (23.6%)	9,238.3 (24.6%)	9,238.3 (24.6%)
Empty Operational Mass [kg/%]	33,649.1 (100%)	37,526.3 (100%)	37,526.3 (100%)

Table 15.5: Budget breakdown take-off mass

	Configuration 1	*Configuration 2*	*Configuration 3*
$M_{payload}$ [kg/%]	10,306.4 (20.1%)	13,575.5 (24.1%)	13,575.5 (22.9%)
M_{fuel} [kg/%]	7,258.4 (14.2%)	5,199.2 (9.2%)	8,147.51 (13.8%)
OEM [kg/%]	33,649.1 (65.7%)	37,526.3 (66.7%)	37,526.3 (63.3%)
$(M)TOM$ **[kg/%]**	51,213.9 (100%)	56,301.0 (100%)	59,249.8 (100%)

16 System Characteristics

In this chapter the subsystems of the aircraft are pointed out. The systems which are discussed are the hydraulic system, the electrical system, the control lines, the air conditioning system, the fuel system, the water and waste system, the auxiliary power unit, the communication system, the braking system, and the landing gear retracting system. After that, as it is an important part of the adaptive design, the connection of the systems at the cut out are discussed in section 16.2. To give a final overview of the systems and their interfaces, a hardware and software diagram are presented in section 16.3. The chapter concludes with a data handling diagram in section 16.4.

16.1. Subsystem design

In this section the different subsystems are mentioned and where possible visualised.

16.1.1. Hydraulic system

Hydraulics are required to ensure that the pilot is able to exert the required force on the control surfaces and other aircraft systems such as landing gear and HLDs. Most hydraulic systems are located in the back of the aircraft. Here the ailerons, main landing gear, spoilers, high lift devices, aft cargo door, rudder, and tail control surfaces are positioned which require hydraulic power. Apart from this, the nose wheel and front cargo door also require hydraulics. As most hydraulic systems are located behind the removable fuselage section of the aircraft, it was determined that the central hydraulic distribution system will be position behind the removable fuselage section. This ensures that only one hydraulic line per system is going through the extendable fuselage section.

The hydraulic system consists of 3 different systems pressurised by three different reservoirs. The first system is powered by the Auxiliary Power Unit (APU) as shown in Figure 16.1. The second system is powered by the left engine as shown in Figure 16.2. The third system is powered by the right engine as shown in Figure 16.3. All systems are serviceable at the service panel, also a hand pump is available here to pressurise the system manually. Three types of hydraulic users are served. Firstly, a system that only is needed at the ground and does not need redundancy. Secondly, a system that is used during flight and where failure is not catastrophic. This system has been designed in single redundancy. Thirdly, a system that is used during flight and failure is catastrophic. This system is served by all three systems. To design the layout of the hydraulic systems, the hydraulic layout of an A320 is used [10]. The auxiliary power unit serves all systems, because in a total engine failure, the control surfaces are still controllable. Furthermore, the systems that are only needed on the ground are served only by the apu. Because, these systems still need the hydraulic system when the engines are turned off but don't need hydraulics during flight. The following systems have a single redundancy build in: horizontal tail control surfaces, spoilers ,and landing gear. The following systems have a redundancy of two: rudder, ailerons and high lift devices.

16.1.2. Electrical system

Electrical power is required for a lot of systems of an aircraft. Modern planes make use of alternating current instead of direct current. Alternating current is preferred as it has economical benefits over direct current. The technology is lighter, requires less space and requires less maintenance [47][1], [61][2]. For that reason, it was decided that the electrical systems in the designed aircraft will also be using alternating current. Furthermore, having one type of power ensures that only one electrical connection type is required. The electricity in an aircraft is generated via the rotating engines and the auxiliary power unit. Every engine consists of two variable-frequency starter generators and the auxiliary power unit consists of two starter generators. This power is then distributed via cables to all systems in the aircraft as can been seen in Figure 16.4. The equipment bay is located differently compared to "conventional" airplanes. The equipment bay is located at the height of the engine. The advantage of this location is the amount of wiring, which reduces due to this location. Furthermore, less wiring is required crossing the cuts. This layout is used in newer types of aircraft such as the Boeing 787 [1][3]. The complete flow of the electrical system can be seen in Figure 16.5.

[1] URL: https://www.skybrary.aero/index.php/Aircraft_Electrical_Systems [cited 11 June 2019]
[2] URL: http://www.flight-mechanic.com/alternating-current-ac-introduction/ [cited 11 June 2019]
[3] https://787updates.newairplane.com/787-Electrical-Systems/787-Electrical-System [cited 17 June 2019]

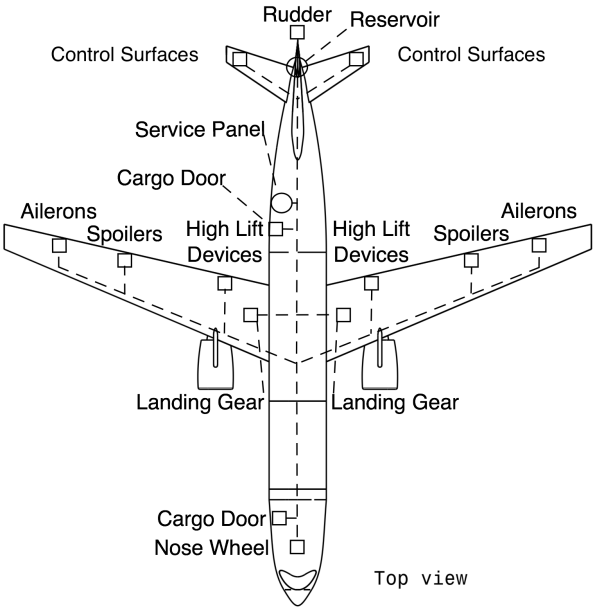

Figure 16.1: Hydraulic system 1.

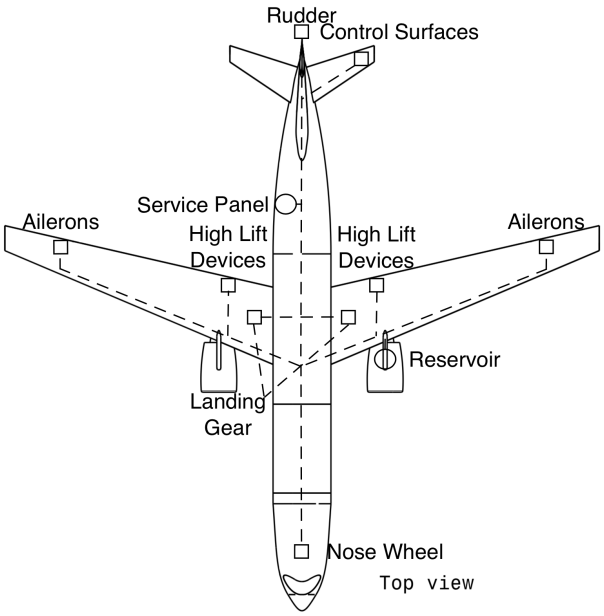

Figure 16.2: Hydraulic system 2.

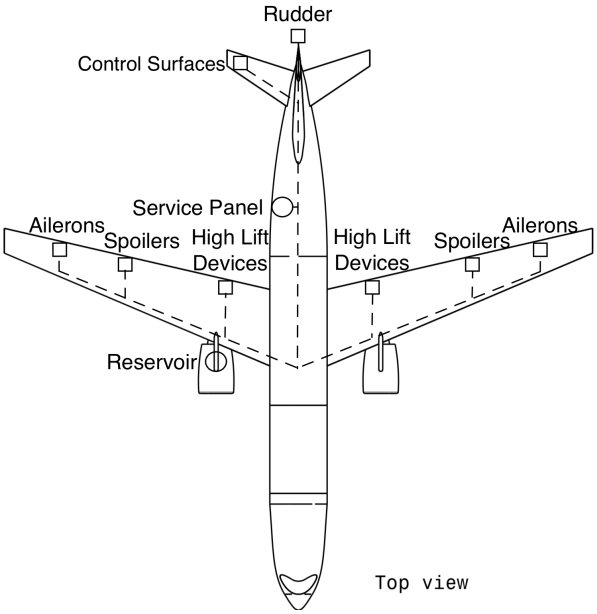

Figure 16.3: Hydraulic system 3.

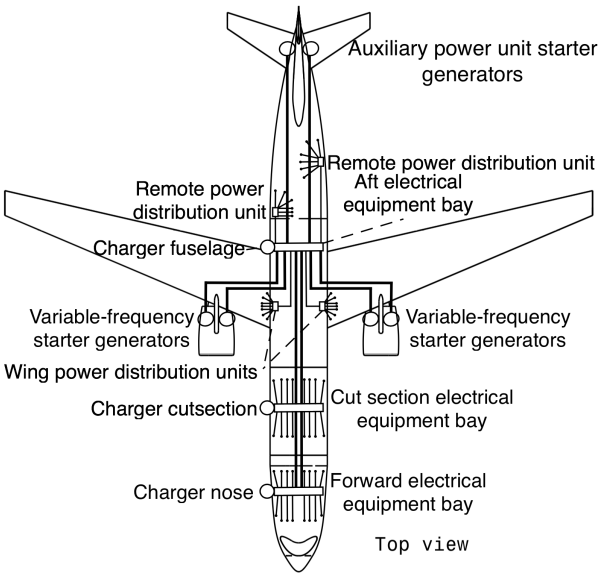

Figure 16.4: Electrical system.

16.1.3. Control lines

The system will be flown by the pilot using a fly-by-wire system. This control system is for pilots convenient as no significant manual force is required. In addition to that, the control system can be modelled in the flight computer such that it allows for easy use by the pilots [104] [4]. Different control lines come together to the flight computer which processes all inputs. As with most systems described, most connections are positioned in the back of the aircraft and thus the flight computer will also be positioned behind the removable fuselage section. The canard will not contain any control surfaces, so no additional control lines need to be connected to these. The flight computer needs to be connected with the control stick of the pilots, the rudder pedals and the airdata [104]. This results in a total of three control lines, since this is a critical system and failure would be catastrophic, a double redundancy is build in. Therefore a total of nine control lines will run through the removable fuselage section to the flight computer as can been seen in Figure 16.6.

[4] URL: https://www.aopa.org/news-and-media/all-news/2017/july/flight-training-magazine/fly-by-wire [cited 20 June 2019]

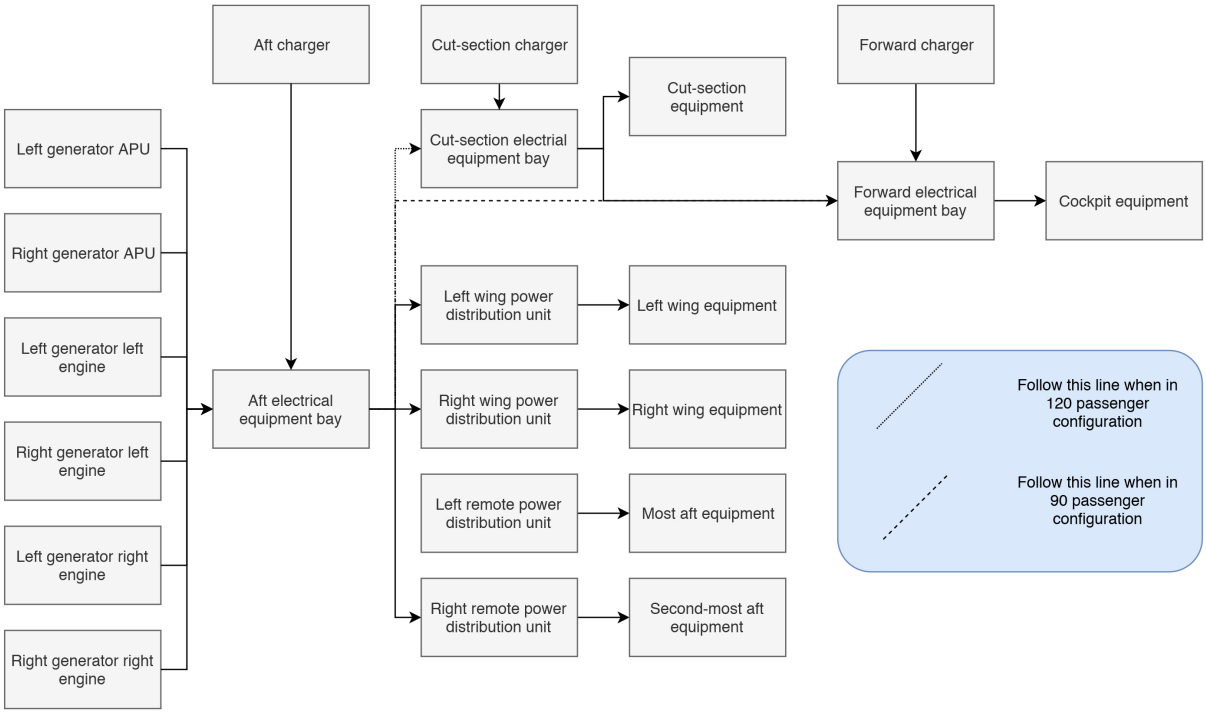

Figure 16.5: Overview of electrical flow system.

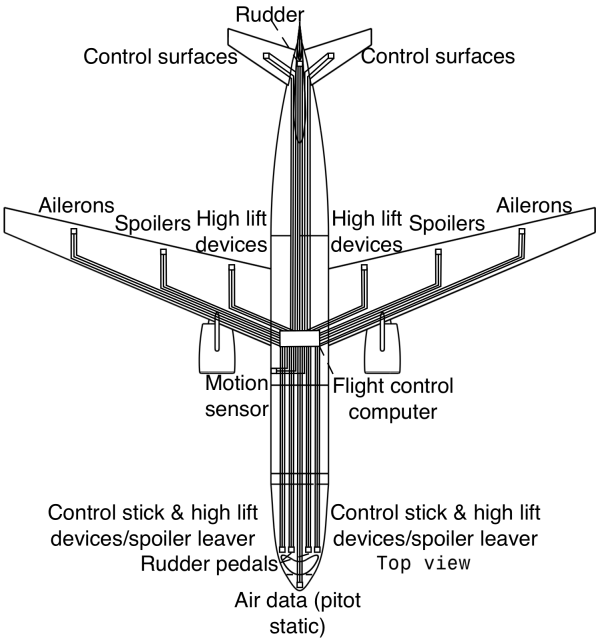

Figure 16.6: Fly-by-wire layout.

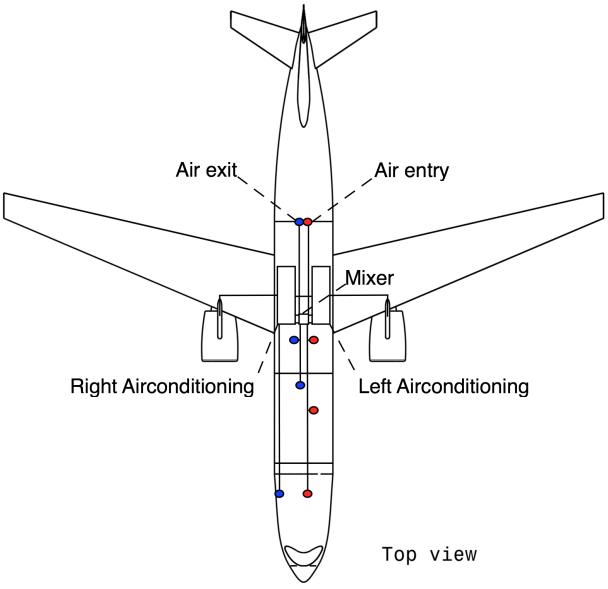

Figure 16.7: Environmental control system.

16.1.4. Environmental control system

The environmental control system operates by using the engines and auxiliary power unit. The bleed air from the engines is cooled down, pressured and used for the cabin [66][5]. For that reason the air conditioning is positioned in the middle of the fuselage as can be seen in Figure 16.7. The system has 4 zones: aft section, mid section, cut section and cockpit section. The air of the first 3 zones comes from the mixer. This air consist of old recycled air and new air from the air conditioning systems. However, the cockpit is only provided by fresh air and not by recycled air (due to regulations) as can be seen in Figure 16.7. As a result a total of 3 air conditioning pipes will be needed at the connector.

[5]URL: https://www.linkedin.com/pulse/back-basics-aircraft-systems-air-conditioning-paulo-neto [cited 20 June 2019]

16.1.5. Fuel system

The fuel system has three functions. Firstly, it needs to transport the fuel from the fuel tanks to the engine. Secondly, it needs to jettison the fuel if needed. Lastly, it needs to equalise the fuel mass across the aircraft to keep the centre of gravity constant. In Figure 16.8, the fuel system layout is shown. The valves are located such to keep the fuel in the right tank. For example, the jettison fuelling valves prevent the fuel to exit the aircraft with a redundancy of one. The equaliser will keep the centre of gravity at the right spot. The pump and valve located at the fuel tanks will pump the fuel through the whole system and will provide fuel to the engines and APU.

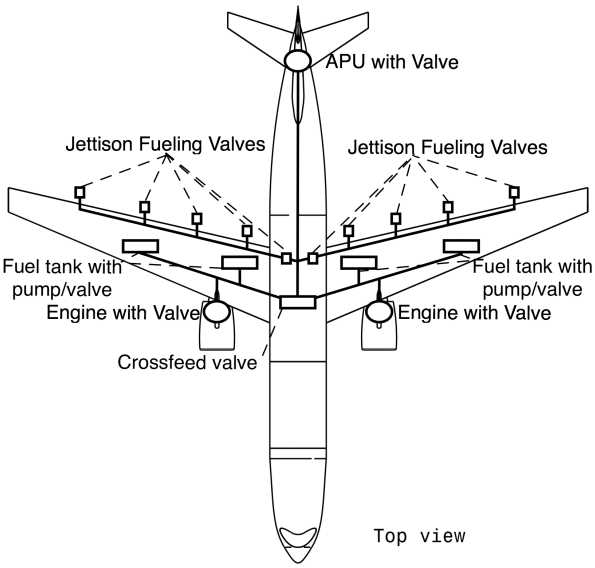

Figure 16.8: Fuel system.

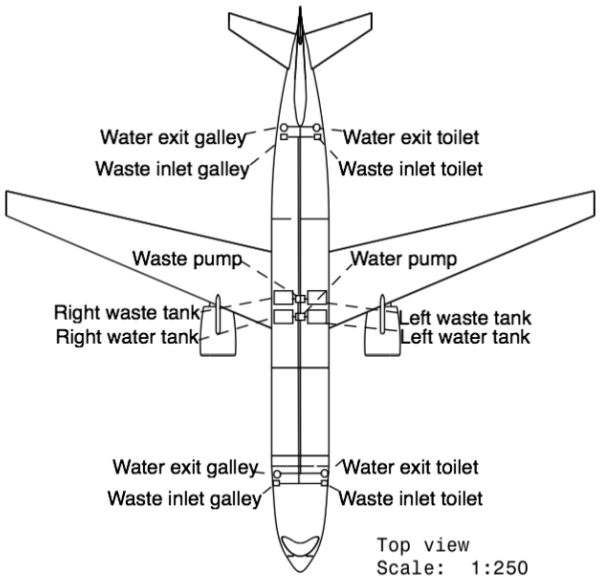

Figure 16.9: Water and waste system

16.1.6. Water and waste system.

The aircraft will have two lavatories, one positioned at the nose section and one after the passenger cabin. The lavatories require a supply of water and possibility to dispose their waste. This can be done in two ways, first of all, two water tanks and two waste tanks can be installed. This means that no internal connection is required between the front and back lavatory. The main disadvantage of this is that the turn around time at airports becomes longer and/or expensive as the water supply/disposal truck has to dock at two positions. In order to prevent this, a water pipe between the front and back will be installed. This will ensure that fresh and waste water can be transported through the plane. There will be only one water tank and the water supply/disposal truck only needs to attach to one place to the aircraft. The water connections will therefore be as follows. There will be one pipe running from the fresh water tank to the front lavatory. In addition, there will be a separate water pipe from the front lavatory to the back waste tank. Therefore, two water pipes need to be fastened in case the aircraft undergoes a conversion to a different configuration as can be seen in Figure 16.9.

16.1.7. Auxiliary power unit

Every commercial aircraft needs an Auxiliary Power Unit (APU) to provide all the systems electricity when the engines are not running or when the generators in the engine do not provide enough power. The trend in aviation is the increasing amount of electrical systems in commercial airplanes [76][6]. Therefore, bigger APU's are needed to provide enough power. In the large regional aircraft segment the APU's are also innovating and increasing in efficiency and size. Therefore, it is difficult to find the right APU at this moment in time since the aircraft will enter service in 2035. Furthermore, an electrical taxiing system is used of which it is unknown how much power is needed during manoeuvring the aircraft.

To make a first choice on the APU, reference aircraft were used. It was found that the newest generation of large regional jets (Embreaer E2 family, Mitsubishi 90, COMAC ARJ) uses the Pratt & Whitney APS2600 [76][7]. The Pratt

[6]URL: https://www.pwc.ca/en/products-and-services/products/auxiliary-power-units [cited 17 June 2019]
[7]URL: https://www.pwc.ca/en/products-and-services/products/auxiliary-power-units [cited 17 June 2019]

& Whitney APS2600 has a power of 40 kVA (kilo Volt Ampere) and has a weight of 104 kg [75][8]. The Pratt & Whitney APS2600 is the second generation of the APS2000 family and is the successor of the Pratt & Whitney APS2300 which was used by the first generation E-jet family. Therefore, when the adaptive regional aircraft will enter service a third generation APS2000 family will be developed, the more efficient and a more powerful APU will be developed again as a successor of the Pratt & Whitney APS2600. This is also needed to cope with new systems such as the electrical taxiing system.

16.1.8. Communication flow diagram

Another subsystem is the communication system. In Figure 16.10 an overview of the communication flow is presented.

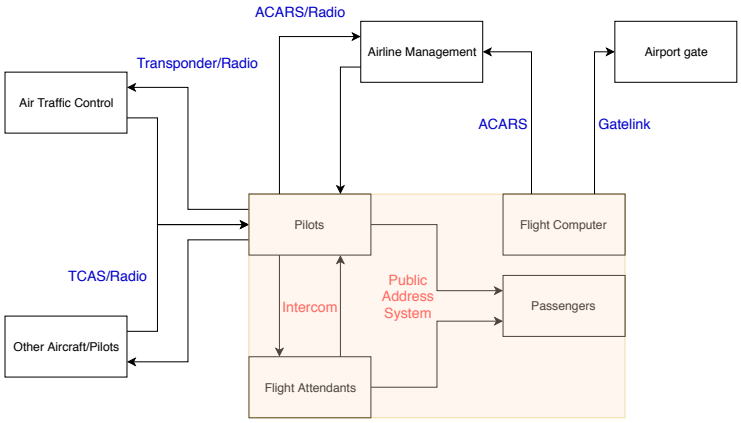

Figure 16.10: Overview of communication flow system

In the figure, a separation has been made for internal and external communication. Any boxes which are related to external communication are presented with blue text explanation.

Internal communication is about the communication between the pilots, flight attendants and the passengers. Pilots can have a private line with the flight attendants using the intercom. Whenever pilots or flight attendants would like to inform the passengers, the public address system is used.

External communication can be done by the flight crew manually but is also done automatically. The flight computer automatically sends data to the airline management using the ACARS system (Aircraft Communications Addressing and Reporting System) [17]. This system can also be used by the pilots to send data to the airline management. Contact with the airline management can also be made using a radio connection. The pilots can talk to air traffic control using the radio as well. The frequency band which is used is between 108 and 137 MHz [17]. In order to have build in redundancy, multiple radio's should be made available and the APU power should also be able to power the radio's. The aircraft also contains a transponder which contains data to reduce the verbal communication flow between the pilots and air traffic control. Communication to pilots from other aircraft can also be done by the radio. In addition to that, the aircraft will be equipped with the TCAS system (Traffic Collision Avoidance System) [96]. This ensures that the pilots are warned in case of an approaching collision with another aircraft.

Aircraft are collecting more and more data during flight and this needs to be uploaded to their management and or maintenance department. As the size of data is getting outside current capabilities of transferring this, 'gatelink' has been designed. This is a system in which collected data can be send via a wireless connection from the aircraft to the terminal. Apart from uploading data to the terminal, data can also be downloaded from the terminal to the aircraft [52][9].

16.1.9. Braking system

The brake system was selected to be a carbon brake system. A carbon braking system has a higher energy absorption and thus a better performance. Additionally these types of brake have a faster cool down time than

[8] URL: `http://pwaeropower.com/en/apu-engine-center/our-products` [cited 17 June 2019]
[9] URL: `https://www.flightglobal.com/news/articles/arinc-launches-common-use-wireless-gatelink-system-214660/` [cited on 21 June 2019]

other brake systems, due to its increased ventilation. This reduces the turnaround time without the use of brake cooler. It additionally features a reduction in weight and has enhanced reliability [89].
The carbon brake SEPCARBIII OR, design by *Safran* and used on the Airbus A320neo was selected as the braking system for the adaptive regional airliner [89]. This was done for the aforementioned reasons, as well as the sustainable aspect of the system as it is free of toxic materials and chemicals. Additionally it has been treated to be oxidation and corrosion resistant to ensure a longer lifetime.

16.1.10. Landing gear retracting system

As presented in section 16.1, the hydraulic system will be connected to both the main and nose landing gear. This ensures that the landing gear is retractable using hydraulic power. The retraction of the landing gear is of major importance to decrease the drag in-flight. As all systems which have been discussed have a form of redundancy build in, this should also be incorporated in the landing gear. Redundancy can be build in for retracting the landing gear, but also for lowering the landing gear. Retracting the landing gear is not assumed to be critical for safety. Whenever the retraction of the landing gear has failed after take-off, multiple new attempts can be made. If it turns out that the hydraulic retraction has completely failed, an emergency landing can be made without any consequences for safety. Lowering the landing gear is however more critical as this subsystem is essential for a safe landing. For that reason it was determined that a backup system should be made available for the nose and main landing gear in case of hydraulic failure. Aircraft might might use a backup system which uses gravity to lower the gear in case of hydraulic failure [113]. This system will be implemented for both the nose wheel and the main landing gear.

16.2. Fuselage connector

As the removable fuselage section poses a problem for any connections it is required to research this extensively. Connections going through the fuselage are: electrical cables, water pipes, hydraulics, air conditioning and control lines. All these cables need to be fastened whenever the aircraft undergoes a conversion. In addition to that, it is vital to have redundancy build in, in case of emergency. This section will first discuss the redundancy. Secondly, the certification is discussed. Lastly, the cables per connector will be described.

In order to have an easy connection method, it was determined that the connection lines and pipes will be placed in a large connector. The connector sides will be made such that the extendable fuselage can always fit in between the fuselage sections, and that the connector also works in case the extendable fuselage is not implemented. As the connector should not be interfering with the passenger compartment, it was decided to place the connector in the cargo hold of the aircraft. For all mentioned wire connections it is important to have redundancy build in. In case of structural failure of the bottom side of the aircraft, this would imply that all connection lines are cut. In order to prevent this, a second connector is placed on the left side of the fuselage, just below the passenger floor. A third connector is placed on the right side of the fuselage, also just under the passenger floor. This allows redundancy in fuselage width location and fuselage height. As redundancy also means additional weight, it was considered which systems should be placed in single and/or double redundancy. First of all, the electrical cables, hydraulics and control lines will be placed in double redundancy. These components are critical for flight control operations and failure of those systems might lead to catastrophic failure of the aircraft. The air conditioning will only be placed in a single redundancy system. Failure of the main system would be dangerous for the passengers and thus a back-up system is required. Double redundancy is however not deemed to be needed as this will only be used in case of a major structural failure. This would imply loss of cabin pressure, meaning that the air conditioning system would not help. The aircraft will in that case make an emergency decent towards breathable air to ensure the safety of the passengers. At last, the water pipes have not been placed in any redundancy. This is due the heavy weight of the water pipes for both fresh water and waste. In addition to that, a failure of the water system does not create a dangerous situation for passengers or crew, it is only inconvenient. The flight can continue without problems and the failure can be repaired once the aircraft is landed.

Furthermore, the certification of these connectors during the design is checked. A few rules are set about distances between types of cables in an aircraft. Firstly, there must be 2 inch between the signal(fly-by-wire) and fluid wires(hydraulics, water, waste) [103][10]. Secondly, there must be 1 inch between power wires and fluid wires. This is taken into account during the design of the connector [103].
All in all, the following cables and wires are present. In the first connector the following cables and pipes are present: 3 hydraulic pipes, 2 electrical wires, 15 control lines, 2 air conditioning pipes ,and 2 water/waste pipes. In the second connector the following cables and pipes are present: 3 hydraulic pipes, 2 electrical wires, 15

[10]URL: `https://www.assemblymag.com/articles/93379-rules-for-routing-aircraft-wiring` [cited 20 June 2019]

control lines ,and 2 air conditioning pipes. In the third connector the following cables and pipes are present: 3 hydraulic pipes, 2 electrical wires, and 15 control lines.

16.3. Hardware & software interface

Next to focusing on the different subsystems, it is also needed to look at the interfaces between them. The relationship between them gives insight in how the subsystems should be connected and what specific tasks the different subsystem must fulfil. Especially in the adaptive design, it is important to see what connections must be made after every conversion. To visualise this in a clear and concise way, it was chosen to put this in an N2 chart, as can be seen in Figure 16.11. In this chart, the control lines were split into fly-by-wire system and control surfaces. Furthermore, the braking system and landing gear retraction system were combined into landing gear.

Communi-cation & Naviagation					Heading / route					
Power distribution	**Electronics**	Power distribution	Power distribution	Power distribution	Power distribution		Power distribution	Power distribution	Power distribution	Power distribution
		Hydraulics				Control exerted force				Control exerted force
	Power generation		**APU**							
			Providing fuel	**Fuel System**			Providing fuel			
					Control system	Control movement				
						Control surfaces				
	Power generation						**Engine**			
Cooling	Cooling	Cooling	Cooling	Cooling	Cooling		Cooling	**Aircon-ditioning system**		
									Water / waste system	
										Landing gear

Figure 16.11: Interfaces between different aircraft subsystems

Lastly, the software of the aircraft was checked. Here, the different systems that were distinguished are the autopilot, flight control system, collision avoidance system, (bad) weather detection, flight recorder, fuel indication system and communication and navigation system [21][11]. For some of the software, an adaptive aircraft will not have an influence. However, for the autopilot, flight control system, communication and navigation system and collision avoidance system this will have consequences. To avoid control inputs that are too big or small, both the autopilot and flight control system need to know the configuration settings, as the larger aircraft must be controlled differently. For communication and navigation, the system must know the configuration as well, such that the transponder can send the correct information about the aircraft to the airports, as mentioned in section 12.5. The collision avoidance system must know the exact length of the aircraft to determine the distance

[11] URL: `https://www.nap.edu/read/2035/chapter/12` [cited on 21 June 2019]

between different aircraft, so this system has to know the configuration settings as well. A software diagram is shown in Figure 16.12.

16.4. Data handling

During flight an aircraft receives lots of data. This mainly comes from the sensors located inside or outside the aircraft. The sensors include for example angle of attack sensors, pitot tubes, engine sensors, etc. Some measurements give information needed in order to fly, like altitude, angle of attack and airspeed. Additional sensors measure the air or fuel temperature, the amount of fuel in the tanks and pressure sensors which determine the pressure of for instance the hydraulic fluids and cabin pressure. Some sensors are used for safety, like a fire sensor and carbon dioxide and oxygen sensors. Furthermore, sensors are also used for the health monitoring system. This is a system that is responsible for in flight failure detection and identifying its cause [48][12]. This information will be transferred to the airport and aircraft manufacturer by the ACARS, as mentioned in subsection 16.1.8. An overview of this data handling can be seen in Figure 16.13.

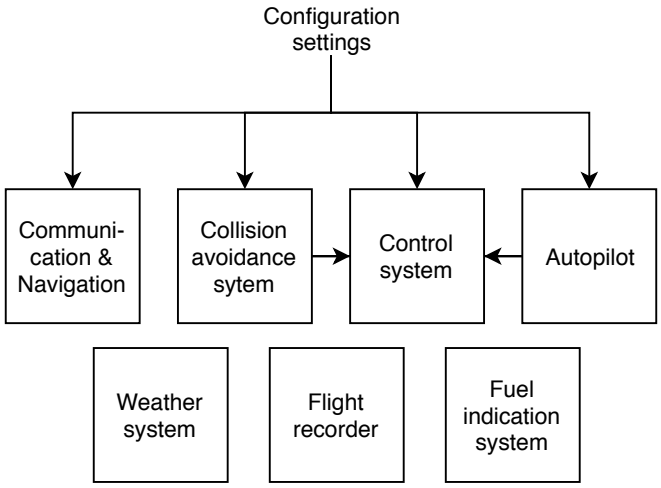

Figure 16.12: The different software subsystems and their dependency on the configuration

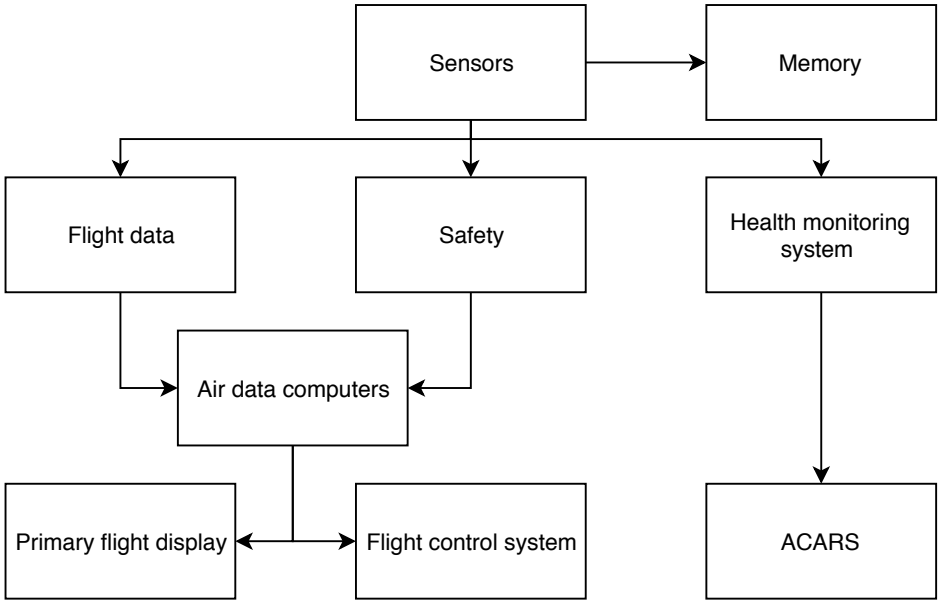

Figure 16.13: The data handling diagram which shows some paths the sensor signals can follow

[12]URL: https://pdfs.semanticscholar.org/8c12/93ee4a8c93197409fda1263380a96c4569f1.pdf [cited on 21 June 2019]

17 Post-DSE Activities

This chapter is set up to present the activities which will be performed after the DSE has been completed. The build up of this chapter is as follows: First, in section 17.1 the post-DSE activities are presented in a logical order. After which, the project Gantt chart is presented in section 17.2.

17.1. Project design and development logic

Aircraft design consist of three phases: the conceptual design, preliminary design and finally; the detailed design. The steps are presented in Figure 17.1.

In this phase of the DSE, the conceptual design has been finished. A few preliminary design aspects have also been performed, but this phase is not completed yet. The post-DSE activities will consist of finishing the preliminary design and detailed design. It will also contain the actual production and testing of the aircraft. These steps are all visualised in the work flow diagram, presented in Figure C.1. In this flow diagram the last step is the delivery of the aircraft. Manufacturer's support during the operational life time has not been documented as this falls outside the scope of this project.

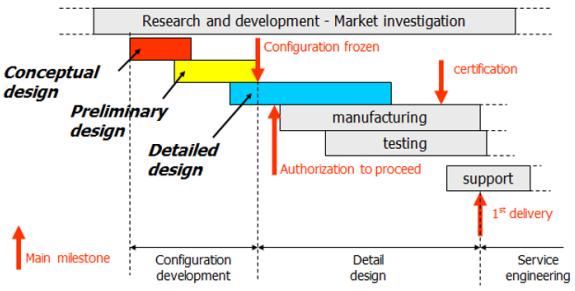

Figure 17.1: Aircraft design process visualisation [79]

As mentioned in this report, the canard poses a challenge in terms of stability and control. To ensure proper functioning of the canard, the lift coefficient should be higher that what currently seems realistic. For that reason, the post-DSE activities will be related to finding new technologies which increase the lift coefficient of the canard. These technologies will then be implemented to ensure a stable and controllable aircraft. In addition to that, the airflow interference of the canard with respect to the main wing, horizontal tail, and engines have not been extensively researched yet. These aspects can be researched by more detailed aerodynamic analysis and by wind tunnel testing. Also the use of sophisticated simulation software will result in more detailed prediction of airflow wake effects.

The wing does currently not include any type of winglets, since these have not been researched within the scope of the past weeks. The use of these winglets might however be beneficial in reducing the induced drag and thus leading to reduced fuel consumption [77].

The maintenance strategy is currently dependent on the probability distribution input parameters. For now, the APU data has been used, as this system is critical for the electric taxiing. For an airline it would, however, be interesting to know the maintenance strategy for all the important systems. Therefore, in the next DSE phase, probability density functions related to failure should be determined for all systems. This allows the manufacturer to present the airline with a more detailed maintenance strategy.

More research should also be done into whether it would be economically beneficial to have an adaptive airliner instead of having two separate aircraft flying. The additional costs of the adaptability should be calculated and it should be compared to having multiple aircraft flying in different configurations. If it turns out that the aircraft is economically not profitable, the aircraft will never be successful.

In the design, the change in lift for the flaps in take-off configuration is not accurately determined. For now, an average is taken between the clean configuration and the configuration where the flaps are fully extended. Furthermore, a more detailed design of the flaps should be performed, as they are only designed based upon statistical relationships.

With current input values all configurations are over-designed for take-off, next iterations should address this, by lowering take-off lift and/or selecting a less powerful engine. In addition to that, more detailed design of thrust

reversers and brakes should be done in order to more accurately estimate landing performance.

The effects of derated engine use should be assessed, especially since no engine adaptations are made between configurations, and two configurations will hence fly with an overly powerful engine and thus at derated thrust setting. As a result, the engine wear might be reduced.

Velocity effects on thrust should also be estimated. More detailed engine specifications on internal mass flows must be requested from the manufacturer.

The flight profile should be optimised, saving fuel mass. As every flight phase is interdependent, this requires investigation into the fields of optimal control theory, and calculus of variations.

In the aspect of structure, there are no ready sources available that can be used to validate the stresses. One recommendation is to create a FEM model to validate the analysis. Structural life estimation is extensive in the phase of the project. One recommendation is to use Palmgren Miner method of analysis to predict the maximum number of flights the aircraft can perform [67]. Locking devices and self-locking nut for the fuselage extension joints should also be investigated.

In the design process of the canard a process extrapolated from the empennage design is used. The same holds for the elevator trim curve, which has a negative angle of attack for the trim point. It is therefore recommended to further investigate the stability, controllability, sizing for the canard, and the elevator trim curve in the next phase of the design. Another recommendation would be to perform scaled wind tunnel tests and perform CFD analysis on the model to investigate the stability and controllability of the complete aircraft. Finally, in order to fit the c.g. range of configuration 2 and 3 in the stable and controllable region of the scissor plot, a high lift coefficient was required, which need more investigation as already mentioned above.
The canard is currently placed in such a way that the airflow around it might interfere with the engines. The engine performance is therefore affected. This interference should be researched and different canard placements should be considered. The canard could also be placed on top of the fuselage instead of below. In this case, structural reinforcement of the fuselage top is needed, introducing additional weight here.

Finally it can also be considered to discard the canard option to solve previous mentioned problem. In order to fly efficient and provide enough lift, extendable wingtips can be installed. Research needs to be done to determine the most beneficial method.

17.2. Project Gantt chart

From the flow diagram presented in Figure C.1, a project Gantt chart can be made. This includes all tasks but also the time allocated to each of the tasks. It is assumed that the first task starts at January 1st 2020. As stated in the requirements, the aircraft shall enter into service in 2035. Therefore, the Gantt chart is scheduled up to the market entry of the first aircraft, on January 1st 2035. The Gantt chart is presented in Figure C.2. No specific persons are allocated to the Gantt chart since the determination of the time required for each tasks is still relatively generic.

18 Conclusion and Recommendations

The purpose of this report was to provide the reader with a complete overview of the project tackled by the group. The goal of this project was to develop an aircraft, which is capable of adapting within an 8-hour maintenance check. The demand for this aircraft type originates from aircraft not being utilised optimally for their specific design point, in terms of range and passenger capacity. In addition to that, airlines need to buy multiple aircraft to serve a range of operational profiles. The adaptive regional airliner should prevent this, and have efficient performance in different configurations.

The market analysis which is performed determines the design points for the aircraft. It was concluded that the following points will be designed for.

- Configuration 1: 90 passengers over a range of 4,000 km (base configuration)
- Configuration 2: 120 passengers over a range of 2,000 km
- Configuration 3: 120 passengers over a range of 4,000 km

With these design points in mind, different conceptual ideas were set up. In this project, three concepts have been discussed and analysed. From the discipline analysis, it was determined that the first concept performs the best in the sustainability aspect. The second concept scored best for operations. The third concept was discarded after the trade-off was performed, since it ended up with the overall lowest score. As efficient operation in terms of sustainability of the aircraft was assumed to be the most important aspect of the adaptive aircraft, the first concept was chosen to be analysed in more detail in the final project phase.

The basis of this concept is a fuselage which contains 90 seats. Whenever the conversion to 120 passengers is required, a prebuilt fuselage part is installed between the nose section and the main cabin. This fuselage part was initially designed to contain a removable canard wing which lifts the additional mass introduced by the extended fuselage. With the use of the canard, the main wing is not overdesigned in case the aircraft is flying in its base configuration.

From the initial analysis of the three concepts, the main objection against the first concept was the adaptability time. A new method had to be developed, so that the aircraft meets the 8-hour requirement set by the customer. The adaptability time consists of performing the alignment of the two fuselage structures followed by the fastening of the sections together. To have a fast, safe, and accurate alignment procedure, it was decided to use laser guidance. The high accuracy of lasers allows the positioning of the fuselage section with 0.05 mm precision, which should be enough to successfully perform the alignment. The new fastening method makes use of automatic bolts which lock into place. Whenever locked in place, a confirmation signal is given that the fastening has been successful.

The detailed design of the aircraft is done within all disciplines and is eventually combined in a programming environment. This way iterations can be performed easily and the outputs of the iterations over time can be tracked. It was determined to stop iterating when the difference between the input and output of an iteration was less then 1%. During iterations the design of the canard is also updated to have it placed and sized optimally. The sustainability aspect of this project has been incorporated by the sustainable development department with close collaboration of the structures department. Aspects such as material selection, manufacturing processes, and a retirement strategy have been extensively monitored to ensure a sustainable design.

As the adaptive airliner introduces a full cut in the fuselage, research has been done on the connectors of all lines and wires running through the fuselage. In order to have an efficient connection procedure, a connector has been designed which can be easily clicked in, between different fuselage parts. This connector will house all control lines, hydraulics, air conditioning, and water pipes which are running through the cut. In order to ensure redundancy of the system, the connector will be installed in triplex. Each connector will be placed on another height and width in the fuselage cross-section. This ensures that in case of local damage, there is always a connector operable.

From the performance analysis, it turned out that no additional external fuel tanks were required, as all fuel could be stored in the wings. The removable canard option is also discarded. The added efficiency of a reduced canard size between configuration two and three is not out weighted by the disadvantages of the aerodynamic, operational and structural complications of such option. This results in the same aircraft for configurations two and three. The only difference is the amount of fuel carried by the aircraft.

The final design iteration output parameters allow to perform a detailed cost analysis of the development program of the adaptive airliner. It is concluded, that a production rate of 40 aircraft per year is achievable, which results in a return on investment of 8.63% after five years. In terms of operational costs, the first configuration is 12% more expensive compared to the reference CRJ900. In the 120 passenger configuration, the aircraft's operation costs 53% less, compared to the reference Embraer 190.

In addition to the cost analysis, a risk analysis is performed to determine and mitigate unacceptable risks. Concluding from this, it was determined that most risks arise from the adaptability of the aircraft, in terms of structural components, the fastening of the two fuselages, and the connector. In structural components, the skin made of epoxy/HS carbon imposes a high risk as cracks are hard to locate.

With the design finalised, it is possible to check the requirement compliance matrix. The important requirements regarding the adaptability time, CS-25 regulations, CO_2 emission, return on investment, and take-off noise, have been met. Most additional subsystem requirements, have been met as well and some particular requirements were set too detailed to be analysed during the DSE's time-span, and have therefore not been analysed, but included as further recommendations. In total, three requirements are not met, and will be explained below.

- SYS-MI-CU-11. The aircraft's NO_x emissions could not meet the set requirement, within the current design approach. Recommendations for this are provided later in this chapter.
- SYS-MI-CU-12. The aircraft's approach noise currently exceeds the requirements set. Recommendations for this are provided later in this chapter.
- SYS-MI-CU-14. The aircraft unit cost slightly exceeded the $60 million budget. This happened due to the method used to determine the unit price. It has not been calculated according to the actual production costs of a single aircraft, but was done by optimising the total revenues for the aircraft manufacturer. The production costs are however taken into consideration in the return on investment to ensure profit for the manufacturer. In addition to that, the customer gets an adaptable aircraft, that is able to serve the functionality of two aircraft for the price of a single aircraft, increasing the economic benefit.

Combining the obstacles encountered in the detailed analysis with the requirements which have not been met, recommendations for research after the DSE project have been identified. First of all, the canard's stability and control needs further research. The current canard needs a lift coefficient which cannot be achieved with current technology. Furthermore, it has a negative trim point. Therefore, more research needs to be done on the lifting technology of canards but also on the general approach for designing a three surface lifting aircraft. Apart from that, configurations two and three have the same layout. In order to increase efficiency of the two separate configurations, more research should be dedicated to canard sizing.

As mentioned in this conclusion, the requirement regarding NO_x emissions, is currently not met. In order to meet this requirement, the climb and descent phase should be optimised for fuel efficiency, which is currently not done. This could lead to a significant reduction in fuel flow and mass, leading to a reduction in NO_x emissions. The noise reduction requirement during approach is also not met at this stage of the design. Numerous measures have been researched to reduce the noise emissions of the aircraft. In the post-DSE phase, these techniques have to be worked out in more detailed and fine tuned to meet the ambitious noise requirements.

The canard currently poses a problem as it is interfering with the airflow reaching the engine. The canard might also be placed at the fuselage top to avoid the previously mentioned problem. In the next phase of the DSE the disadvantages of different canard location placements are researched. In addition to that, research is needed to determine whether the canard is the optimal solution to increase the lifting capacities of the aircraft. It might also be possible to have extendable or removable wings, which might be easier to design for control and stability. The post-DSE activities have been documented in a flow diagram. The requirements state that the first aircraft should go into service in 2035. By allocating time to all tasks pointed out in the post-DSE work flow, a planning can be made towards the first delivery. This has been documented in the project Gantt chart to visualise and track this planning. It was determined that it was possible to deliver the first aircraft in 2035.

Bibliography

[1] 787updates. 787 electrical system. newairplane.com, 2011.
[2] MTU aero engines. Gtf engine family, April 2019.
[3] European Union Aviation Safety Agency. Aircraft certification, 2019.
[4] Airbus. Global market forecast: Global networks, global citizens 2018-2037. Technical report, 2017.
[5] AirInsight. *Embraer E-jets E2; Building on Success*. 2016.
[6] Ambri and Ramandeep Kaur. Spars and stringers- function and designing. *International Journal of Aerospace and Mechanical Engineering*, 1(1), September 2014.
[7] Ehsan Arzaghi. Scada, pm modelling & logistic delays. Asset Management Minor Offshore Wind Energy 2018.
[8] Embraer Commercial Aviation. Embraer 175 cabin, June 2013.
[9] Embraer Commercial Aviation. Embraer 190 cabin, June 2013.
[10] D. Metzler B. Hauber. Assessment of electromechanical flight control actuators with regard to direct operating costs. *Institute of Aerospace Systems, RWTH Aachen University*, 2016.
[11] Jens Baaran. Visual inspection of composite structures. *EASA-Research Project/2007/3*, March 2007.
[12] Boeing. Commercial market outlook 2018-2037. Technical report, 2017.
[13] E.F. Bruhn. *Analysis and Design of Flight Vehicle Structures*. Tri-State Offset Company, 1973.
[14] Butterworth-Heinemann. Civil jet aircraft design - aircraft data file. Elsevier, - 2001.
[15] Henry Canaday. Narrowbody mro costs averaged $828 per flight hour in 2017, December 2018. Source based on Maintenance Cost Task Force survey 2017.
[16] William M. Humphreys-Jr. Casey L. Burley, Thomas F. Brooks and Jr John W. Rawls. Anopp landing-gear noise prediction with comparison to model-scale data. *International journal of aeroacoustics*, 8(5):445–476, 2009.
[17] Wind River Aerospace & Defense Chip Downing. An introduction to airline communication types, 2016.
[18] Peter Christensen and Larry R. Dysert. Cost estimate classification system – as applied in engineering, procurement, and construction for the process industries. *AACE International Recommended Practice No. 18R-97*, 2005.
[19] Pat L. Clemens and Rodney J. Simmons. *System Safety and Risk Management; A Guide for Engineering Educators*. U.S. Department of Health and Human Services, March 1998.
[20] Joint Aviation Authorities Committee. *JAR-21 Certification Procedures for Aircraft and Related Products and Parts*. Westward Digital, 1997.
[21] National Research Council. *Aeronautical Technologies for the Twenty-First Century*. National Academy Press, 1st edition, September 1992.
[22] Werner Dobrzynski. Almost 40 years of airframe noise research – what did we achieve? *Aeroacoustics Conference*, 14, May 2008. Institute of Aerodynamics and Flow Technology.
[23] EASA. Certification specifications for large aeroplanes cs-25 / amendment 22, November 2018.
[24] EASA. Type-certificate data sheet for pw1500g series engines. Technical report, EASA, 2018.
[25] EASA. Icao aircraft engine emissions databank, May 2018. Accessed Emissions Databank (05/2018).
[26] EASA. Easa certification noise levels, November 2018. Accessed Jet aeroplanes noise database.
[27] EASA. Introduction to the icao engine emissions databank, May 2019.
[28] Embraer. Market outlook 2018-2037. Technical report, 2017.
[29] MTU Aero Engines. Pratt & whitney gtf™ engines, April 2019.
[30] Dr. A.M. Schonland E.S. Arvai. *Embraer E-jets E2; Building on Success*. AirInsight, 2016.
[31] Eurocontrol. Transponders in aviation. *NETALERT - the Safety Nets newsletter*, 19, May 2014.
[32] ExxonMobil. Jet a/jet a-1, June 2019.
[33] Wolt Fabrycky. Life cycle cost and economic analysis. *Virginia Polytechnic Institute and State University*, 1991.
[34] Group23. Baseline report adaptive regional airliner. Brightspace TU Delft, May 2019. Previous report.
[35] Group23. Midterm report, June 2019. Midterm report Design Synthesis exercise Group 23.
[36] L.B. Vogelesang & J.W. Gunnink. Arall: A material challenge for the next generation of aircraft. *Material & Design*, 7(6):287, December 1986.
[37] Matt Hardigree. How to recycle an airplane, June 2010.
[38] Alan Hiken. The evolution of the composite fuselage: A manufacturing perspective, July 2018.
[39] IATA. Aircraft operating costs and statistics. iata.org, June 2019.

[40] ICAO. Icao engine exhaust emissions data bank - subsonic engines - pw1525g, November 2016.
[41] ING. What is... inflation?, 2019.
[42] Dr. Ir. M. Voskuijl Ir. P.C. Roling. Flight & orbital mechanics – ae2230-i, 2017. Lecture notes on airfield performance.
[43] Dr. Ir. M. Voskuijl Ir. P.C. Roling. Flight & orbital mechanics – ae2230-i, 2017. Lecture notes on longitudinal derivation of equations of motion.
[44] Albert E. von Doenhoff Ira H. Abbott. *Theory of Wing Sections*. Dover Publications, Inc., 1959.
[45] Scott Jackson. *Systems Engineering for Commercial Aircraft*. Ashgate Publishing Limited, 1997.
[46] Joost Ellerbroek Junzi Sun, Jacco M. Hoekstra. Aircraft drag polar estimation based on a stochastic hierarchical model, December 2018.
[47] Jithin Mohan K. Basic electrical system of aircraft, January 2016.
[48] John Vian Gary Mansouri K. Wojtek Przytula, David Allen. Health monitoring for commercial aircraft systems, 2008.
[49] Andrew Kempton. Acoustic liners for modern aero-engines. *Chief Noise Specialist, Rolls-Royce*, 2011.
[50] KPMG. Aircraft acquisition cost and depreciation. International Air Transport Association, 2016.
[51] Gianfranco La Rocca. personal communication.
[52] David Learmount. Arinc launches common-use wireless gatelink system, June 2007. SOURCE: FLIGHT INTERNATIONAL.
[53] Rick Leblanc. Airplane recycling and value extraction. METAL RECYCLING, November 2018. The Balance Small Business.
[54] Jr Loftin, Lawrence K. Quest for performance: the evolution of modern aircraft, 1985.
[55] Bertsch Lothar, Simons Dick, and Snellen Mirjam. Aircraft noise: The major sources, modelling capabilities, and reduction possibilities. Technical report, Delft University of Technology & DLR, 2015.
[56] Mirjam Snellen Lothar Bertsch, Dick G. Simons. Aircraft noise: The major sources, modelling capabilities, and reduction possibilities. *Deutsches Zentrum Für Luft- und Raumfahrt*, March 2015.
[57] Lecht M and Dopelheuer A. Influence of engine performance on emission characteristics. *Symposium of the applied vehicle Technology Pane-Gas Turbine Engine Combustion, Emissions and alternative fuels*, October 1998.
[58] A. M. Al-Garni M. Tozan, A. Z. Al-Garni and A. Jamal. Failure data analysis for aircraft maintenance planning. King Fahd University of Petroleum and Minerals, December 2004. Aerospace Department.
[59] Christian Mascle Pierre Baptiste Mahdi Sabaghia, Yongliang Cai. Towards a sustainable disassembly/dismantling in aerospace industry. *Global Conference on Sustainable Manufacturing - Decoupling Growth from Resource Use*, 13, 2016.
[60] Jacob Markish. Valuation techniques for commercial aircraft program design. Master's thesis, Massachusetts Institute of Technology, June 2002.
[61] Flight Mechanics.com. Alternating current (ac) introduction in aircraft electrical system, 2017.
[62] David Megginson. Ourairports: Airport database. ourairports.com, June 2019.
[63] T.H.G. Megson. *Aircraft Structures for Engineering Students*. Elsevier Ltd, fourth edition, 2007.
[64] Ulf Michel. Noise reduction by aircraft innovations. *German Aerospace Center (DLR)*, June 2010. Institute of Propulsion Technology, Engine Acoustics Department, Berlin.
[65] Emily S. Nelson and D.R. Reddy. *Green Aviation: Reduction of Environmental Impact Through Aircraft Technology and Alternative Fuels*. CRC Press, 1st edition, September 2017.
[66] Paulo Neto. Back to basics - aircraft systems - air conditioning, July 2016.
[67] Michael C. Y. NIU. *Airframe Structural Design*. Conmilit Press Ltd., Hong Kong, 9th edition, May 1997.
[68] US Bureau of Labor Statistics. Aerospace engineers, April 2019.
[69] U.S. Department of Transportation. U.s. air carriertraffic statistic. website, March 2019.
[70] Bureau of Transportation Statistics. Airline on-time statistics and delay causes. Website Bureau of Transportation Statistics, April 2019.
[71] C.A.J.R. Vermeeren O.K. Bergsma, J. Sinke. *Materials and Manufacturing 2*. Faculty of Aerospace Engineering, 3rd edition, August 2006. Course AE2600.
[72] Dr. Fabrizio Oliviero. Aerospace design and systems engineering elements ii – ae2111-ii, 2017. Lecture notes on Aircraft aerodynamic analysis – Mobile surfaces of the wing.
[73] International Civil Aviation Organization. Environmental protection: Annex 16 aircraft noise. I, July 2008.
[74] International Civil Aviation Organization. Standards and recommended practices: Annex 6. 2010.
[75] Pratt&Whitney. Our products. Website Pratt& Whitney, 2016.
[76] Pratt&Whitney. Auxiliary power units. Website Pratt& Whitney, 2018.
[77] Prasetyo Edi A.A. Jaafar-Thamir S. Younis M. Saleem Prithvi Raj Arora, A. Hossain. Drag reduction in aircraft model using elliptical winglet. *The Institution of Engineers, Malaysia*, 66(4):8, December 2005.

[78] Prof.dr. E.K.A. Gill, S.S. Mestry, Dr. F. Oliviero and Dr.ir. W.J.C. Verhagen . Slides ae3122-i systems engineering and aerospace design, February 2019.
[79] B.T.C. Zandbergen R. Vos, J.A. Melkert. Aerospace design and systems engineering, introduction and organization, 2017.
[80] Daniel P. Raymer. *Aircraft Design: A Conceptual Approach*. AIAA (American Institute of Aeronautics & Astronautics), 1999.
[81] Eric Rosen. The 2019 list of busiest airline routes in the world. Forbes, April 2019.
[82] Jan Roskam. *Airplane Design Part III: Layout design of cockpit, fuselage, wing, and empennage: cutaways and inboard profiles*, volume 3. DARcorporation, 1986.
[83] Jan Roskam. *Airplane Design Part VI: Preliminary Calculation of Aerodynamic Thrust and Power Characteristics*, volume 6. DARcorporation, 1990.
[84] Jan Roskam. *Airplane Design Part II: Preliminary Configuration Design and Integration of the Propulsion System*, volume 2. DARcorporation, 1997.
[85] Jan Roskam. *Airplane Design Part V: Component Weight Estimation*, volume 5. DARcorporation, 1999.
[86] Jan Roskam. *Airplane Design Part I: Preliminary Sizing or Airplanes*, volume 1. DARcorporation, 2003.
[87] Jan Roskam. *Airplane Design Part IV: Layout of Landing Gear and Systems*, volume 1. DARcorporation, 2003.
[88] Ger J.J. Ruijgrok. *Elements of airplane performance*. Delft Academic Press, 2nd edition, 2009.
[89] Safran. airbus a320neo carbon brake, September 2016.
[90] Safran. Electric taxiing by safran, May 2017.
[91] Mary Schlangenstein and Rachel Layne. Jetblue picks pratt over cfm for engines valued at $1.03 billion. Bloomberg, December 2011.
[92] Prof. Dr.-Ing. Dieter Scholz. Aircraft design - 11 aircraft design. website, 2015.
[93] Hartmut Fricke & Michael Schultz. Improving aircraft turn around reliability specific aircraft body design parts hamper ground handling and airport performance. *THIRD INTERNATIONAL CONFERENCE ON RESEARCH IN AIR TRANSPORTATION*, June 2008.
[94] Hartmut Fricke & Michael Schultz. Delay impacts onto turnaround performance, optimal time buffering for minimizing delay propagation. *Europe Air Traffic Management Research and Development Seminar*, 2009.
[95] Merino Martinez Roberto Simons Dick, Snellen Mirjam and Malgoezar Anwar. Noise breakdown of landing aircraft using a microphone array and an airframe noise model. . *In Proceedings of the 46th International Congress and Exposition on Noise Control Engineering Taming Noise and Moving Quiet: Taming Noise and Moving Quiet*, pages 4361–4372, August 2017.
[96] EUROCONTROL SKYbrary. Airborne collision avoidance system (acas), January 2019.
[97] Howards Slutsken. How airlines make big bucks from cargo. the Points Guy, August 2018.
[98] Dr. Mirjam Snellen and Dr. D. G. Simons. Lecture slides ae4463-17 advanced noise modeling and measurement, March 2019.
[99] Mike Sondalini. Unearth the answers and solve the causes of human error in your company by understanding the hidden truths in human error rate tables. lifetime reliability, 2019.
[100] Piaggio Aero Industries SpA. Avanti p180 ii specification and description. Smartcockpit, January 2005.
[101] thwink.org. The three pillars of sustainability.
[102] Egbert Torenbeek. *Synthesis of Subsonic Airplane Design*. Delft University Press, 1982.
[103] Michael Traskos. Rules for routing aircraft wiring. Website assemblymag, April 2016.
[104] Ian J. Twombly. How it works: Fly-by-wire the computer takes control, July 2017.
[105] Q.P.D. van Keymeulen. Design of a modular fuselage for commercial aircraft. Master's thesis, Delft University of Technology, September 2015.
[106] Verifavia. Greenhouse gas emissions verification, July 2017.
[107] R. Vos and J. A. Melkert. Aerospace design and systems engineering elements i – ae1222-ii, Februari 2017. Lecture notes on A/C Preliminary Sizing (class I weight estimation method).
[108] (NUREG)-75/014) Wash-1400. *Reactor Safety Study – An Assessment of Accident Risks in U.S. Commercial Nuclear Power Plants*. United States Nuclear Regulatory Commission, October 1975.
[109] Wikipedia. Fuel economy in aircraft, June 2019.
[110] Wikipedia. Boeing 747 hull losses, May 2019.
[111] Richard Golaszewski William Spitz and Frank Berardino. Development cycle time simulation for civil aircraft. Technical report, NASA, 2001.
[112] Oliver Wyman. Aircraft operating costs and statistics. planestats.com, March 2011.
[113] Wei Xiaohui Chen Heng Yin Yin, Nie Hong and Zhang Ming. Fault analysis and solution of an airplane nose landing gear's emergency lowering. *Journal of Aircraft*, May 2016. Version 2.5.
[114] Y Zhou. *Microjoining and nanojoining*. Woodhead publishing limited, 2008. p.758-785.

A Conversion flow diagram

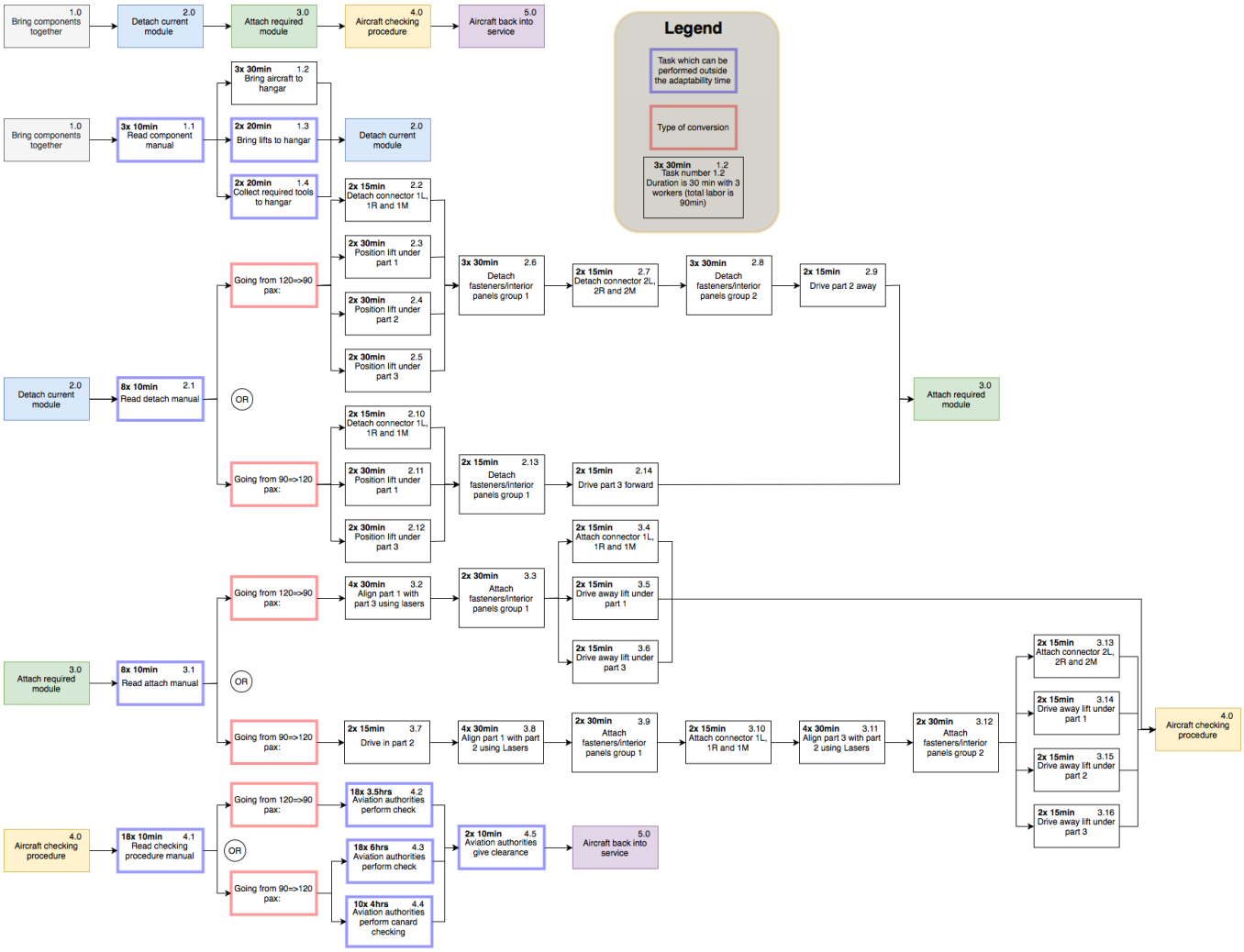

Figure A.1: Conversion flow diagram

B Assembly line stations overview

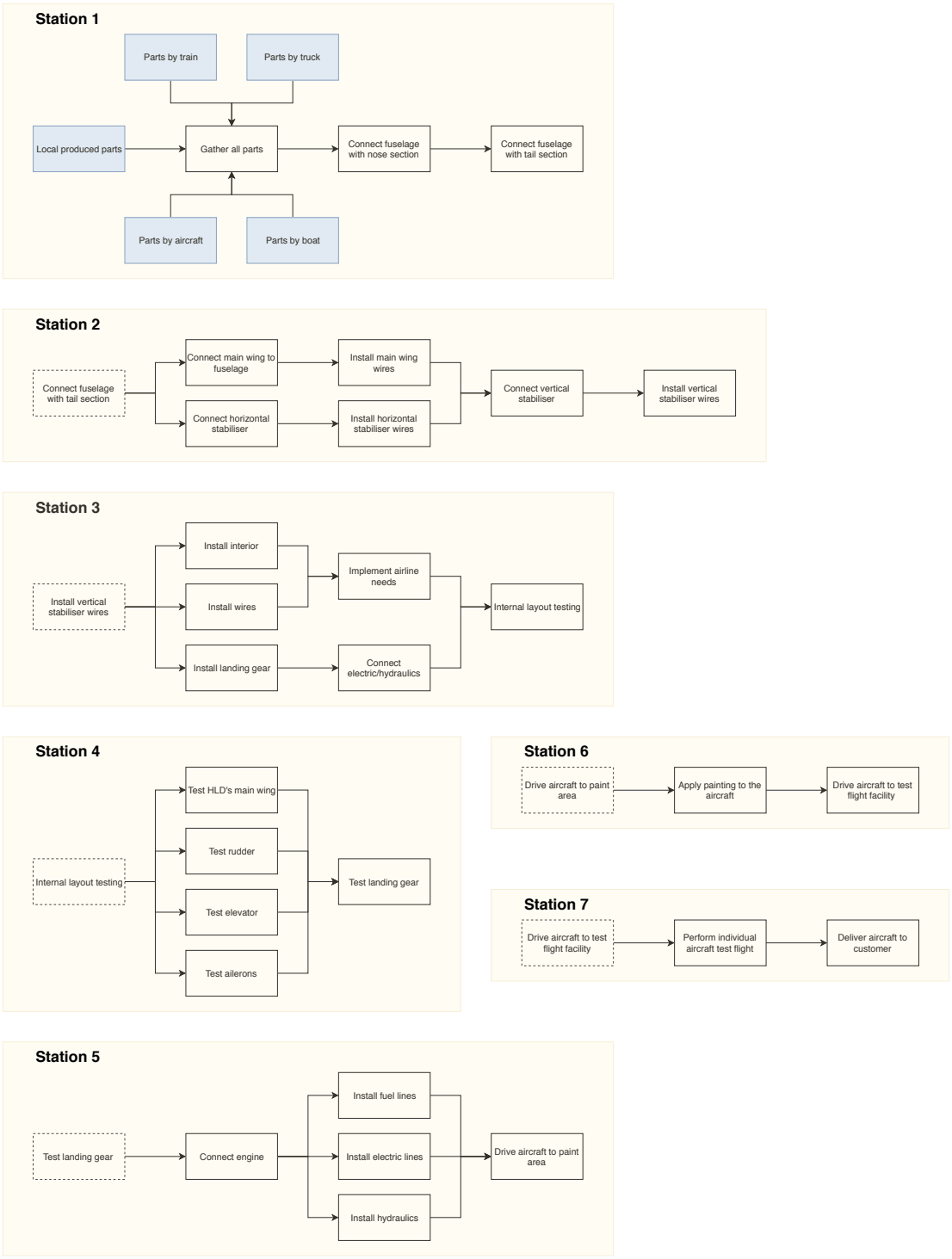

Figure B.1: Station lay out overview

C Post-DSE analysis

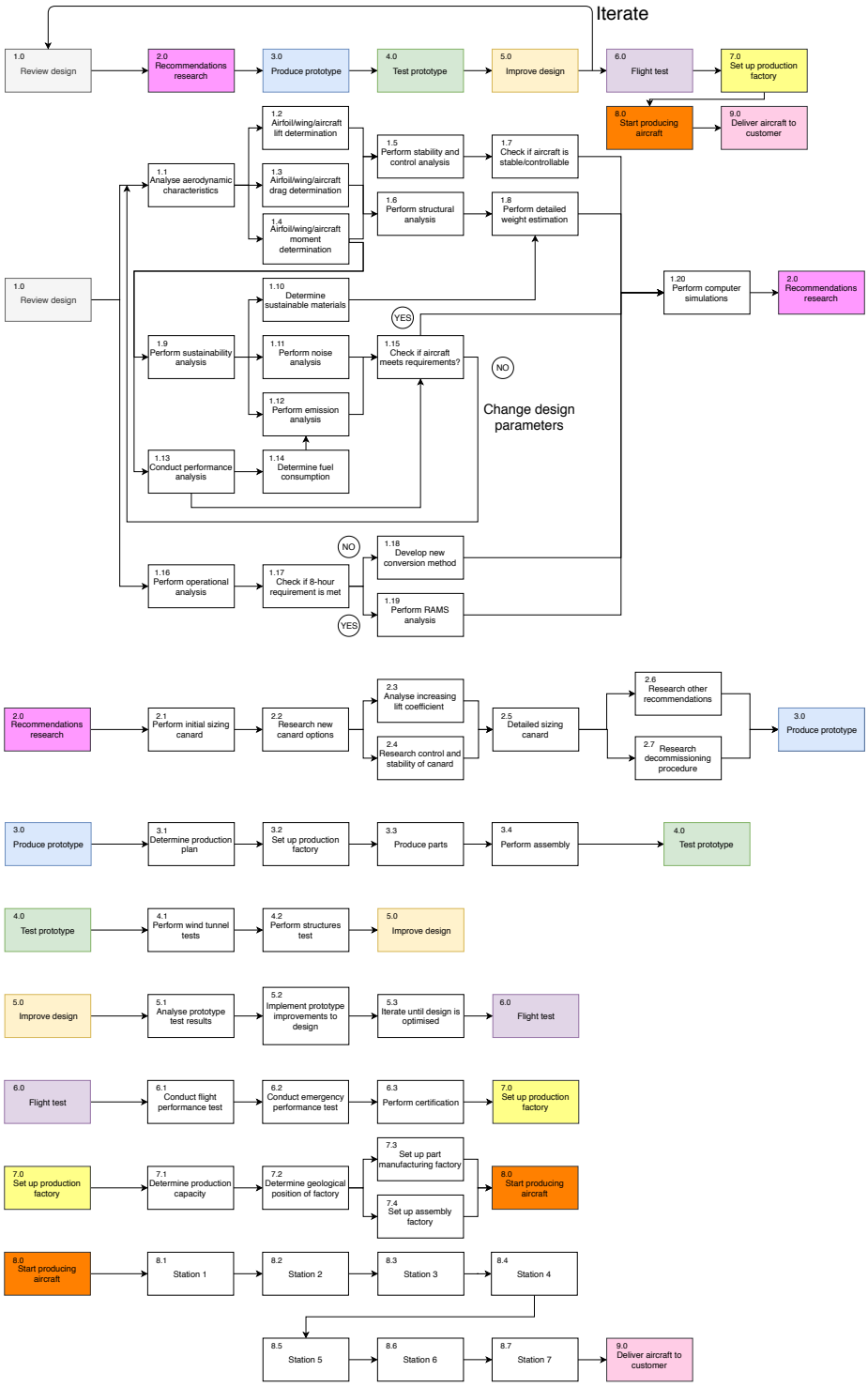

Figure C.1: Flow diagram post-DSE activities

ID	WBS	Task Name	Duration	Start	Finish	Predecessors
1	**1**	**Review Design**	**800 days**	**Wed 01-01-20**	**Tue 24-01-23**	
2	1.1	Analyse aerodynamic characteristics	150 days	Wed 01-01-20	Tue 28-07-20	
3	1.2	Airfoil/wing/aircraft lift determination	150 days	Wed 29-07-20	Tue 23-02-21	2
4	1.3	Airfoil/wing/aircraft drag determination	150 days	Wed 29-07-20	Tue 23-02-21	2
5	1.4	Airfoil/wing/aircraft moment determination	150 days	Wed 29-07-20	Tue 23-02-21	2
6	1.5	Perform stability and control analysis	150 days	Wed 24-02-21	Tue 21-09-21	3,5
7	1.6	Perform structural analysis	150 days	Wed 24-02-21	Tue 21-09-21	3,5
8	1.7	Check if aircraft is stable/controllable	100 days	Wed 22-09-21	Tue 08-02-22	6
9	1.8	Perform detailed weight estimation	200 days	Wed 22-09-21	Tue 28-06-22	7
10	1.9	Perform sustainable analysis	100 days	Wed 24-02-21	Tue 13-07-21	3,5
11	1.10	Determine sustainable materials	100 days	Wed 14-07-21	Tue 30-11-21	10
12	1.11	Perform noise analysis	100 days	Wed 14-07-21	Tue 30-11-21	10
13	1.12	Perform emission analysis	100 days	Wed 14-07-21	Tue 30-11-21	10
14	1.13	Conduct performance analysis	100 days	Wed 24-02-21	Tue 13-07-21	3,5
15	1.14	Determine fuel flow consumption	120 days	Wed 14-07-21	Tue 28-12-21	14
16	1.15	Check if aircraft meets requirements?	50 days	Wed 01-12-21	Tue 08-02-22	11,12,14
17	1.16	Perform operational analysis	150 days	Wed 01-01-20	Tue 28-07-20	
18	1.17	Check if 8-hour requirement is met	100 days	Wed 29-07-20	Tue 15-12-20	17
19	1.18	Develop new conversion method	150 days	Wed 16-12-20	Tue 13-07-21	18
20	1.19	Perform RAMS analysis	150 days	Wed 16-12-20	Tue 13-07-21	18
21	1.20	Perform computer simulation	150 days	Wed 29-06-22	Tue 24-01-23	8,9,16,19,20
22	**2**	**Recommendations research**	**800 days**	**Wed 25-01-23**	**Tue 17-02-26**	**1**
23	2.1	Perform initial sizing canard	200 days	Wed 25-01-23	Tue 31-10-23	
24	2.2	Research new canard options	150 days	Wed 01-11-23	Tue 28-05-24	23
25	2.3	Analyse increasing lift coefficient	100 days	Wed 29-05-24	Tue 15-10-24	24
26	2.4	Research control and stability of canard	100 days	Wed 29-05-24	Tue 15-10-24	24
27	2.5	Detailed sizing canard	125 days	Wed 16-10-24	Tue 08-04-25	25,26
28	2.6	Research other recommendations	225 days	Wed 09-04-25	Tue 17-02-26	27
29	2.7	Research decomissioning procedure	225 days	Wed 09-04-25	Tue 17-02-26	27
30	**3**	**Produce prototype**	**330 days**	**Wed 18-02-26**	**Tue 25-05-27**	**22**
31	3.1	Determine production plan	100 days	Wed 18-02-26	Tue 07-07-26	
32	3.2	Set up production method	100 days	Wed 08-07-26	Tue 24-11-26	31
33	3.3	Produce parts	100 days	Wed 25-11-26	Tue 13-04-27	32
34	3.4	Perform assembly	30 days	Wed 14-04-27	Tue 25-05-27	33
35	**4**	**Test prototype**	**200 days**	**Wed 26-05-27**	**Tue 29-02-28**	**30**
36	4.1	Perform wind tunnel tests	100 days	Wed 26-05-27	Tue 12-10-27	
37	4.2	Perform structures test	100 days	Wed 13-10-27	Tue 29-02-28	36
38	**5**	**Improve design**	**500 days**	**Wed 01-03-28**	**Tue 29-01-30**	**35**
39	5.1	Analyse prototype test results	100 days	Wed 01-03-28	Tue 18-07-28	
40	5.2	Implement prototype improvements to design	200 days	Wed 19-07-28	Tue 24-04-29	39
41	5.3	Iterate until design is optimised	200 days	Wed 25-04-29	Tue 29-01-30	40
42	**6**	**Flight test**	**400 days**	**Wed 30-01-30**	**Tue 12-08-31**	**38**
43	6.1	Conduct flight performance test	100 days	Wed 30-01-30	Tue 18-06-30	
44	6.2	Conduct emergency performance test	150 days	Wed 19-06-30	Tue 14-01-31	43
45	6.3	Perform certification	150 days	Wed 15-01-31	Tue 12-08-31	44
46	**7**	**Set up production factory**	**825 days**	**Wed 13-08-31**	**Tue 10-10-34**	**42**
47	7.1	Determine production capacity	275 days	Wed 13-08-31	Tue 31-08-32	
48	7.2	Determine geological position of factory	50 days	Wed 01-09-32	Tue 09-11-32	47
49	7.3	Set up part manufacturing factory	500 days	Wed 10-11-32	Tue 10-10-34	48
50	7.4	Set up assembly factory	500 days	Wed 10-11-32	Tue 10-10-34	48
51	**8**	**Start producing aircraft**	**35 days**	**Wed 11-10-34**	**Tue 28-11-34**	**49,50**
52	8.1	Station 1	5 days	Wed 11-10-34	Tue 17-10-34	
53	8.2	Station 2	5 days	Wed 18-10-34	Tue 24-10-34	52
54	8.3	Station3	5 days	Wed 25-10-34	Tue 31-10-34	53
55	8.4	Station 4	5 days	Wed 01-11-34	Tue 07-11-34	54
56	8.5	Station 5	5 days	Wed 08-11-34	Tue 14-11-34	55
57	8.6	Station 6	5 days	Wed 15-11-34	Tue 21-11-34	56
58	8.7	Station 7	5 days	Wed 22-11-34	Tue 28-11-34	57
59	9	Deliver aircraft to customer	24 days	Wed 29-11-34	Mon 01-01-35	51

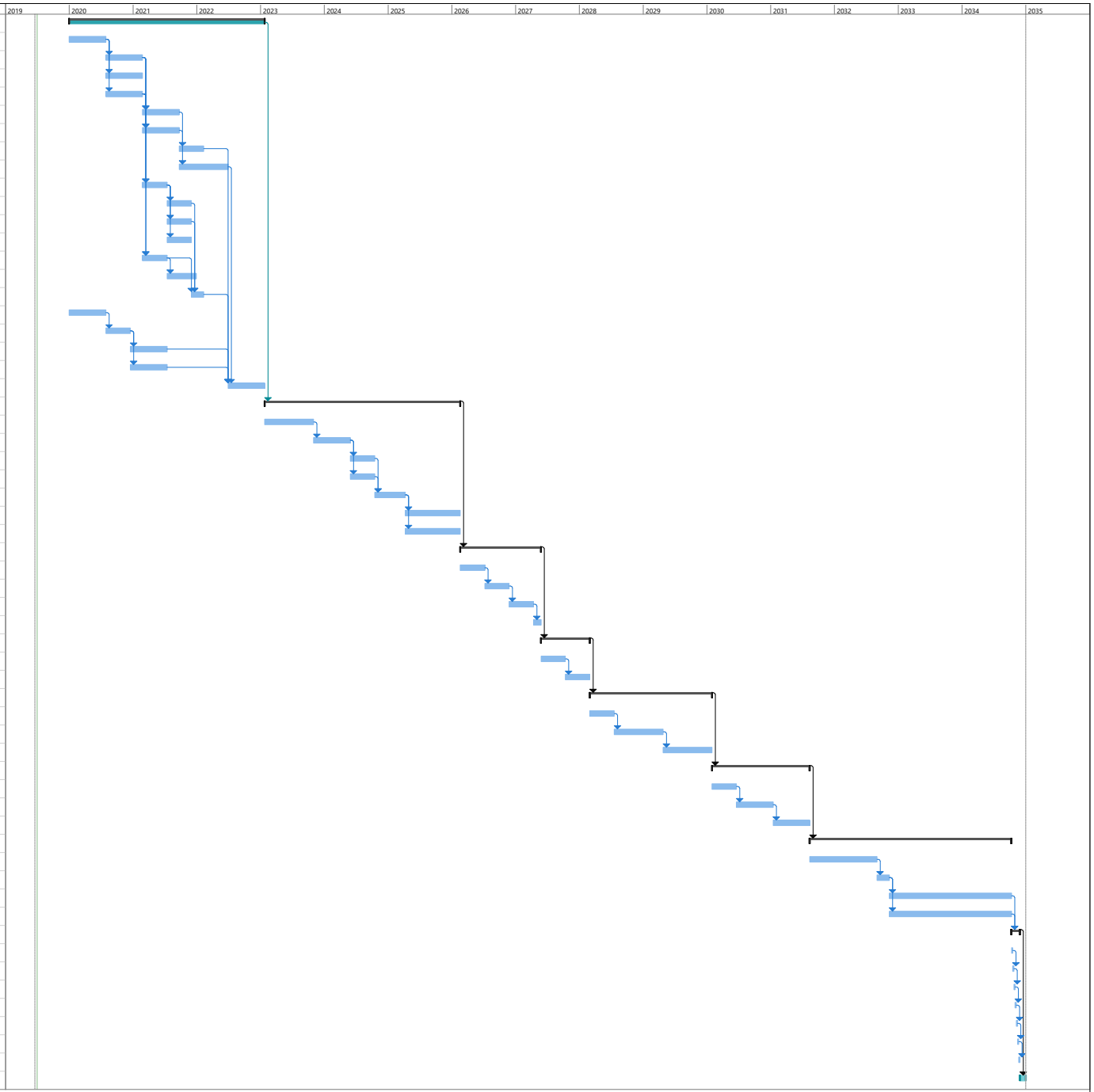

Project: Post-DSE gannt
Date: Mon 01-07-19

Task, Split, Milestone, Summary, Project Summary, Inactive Task, Inactive Milestone, Inactive Summary, Manual Task, Duration-only, Manual Summary Rollup, Manual Summary, Start-only, Finish-only, External Tasks, External Milestone, Deadline, Progress, Manual Progress

Figure C.2: Gantt chart post-DSE activities

D Failure Mode and Effects Analysis

Project No.: DSE 23 System: Concept 1 Probability Interval: Lifetime Operational Phase(s): Normal operation	Failure Modes & Effects Analysis FMEA No.: 2	Sheet 1 Date: 25/06/2019 Prep. by: Sybren Rev. by: Niels Approved by: DSE group 23

IDENT. No.	ITEM/ FUNCTIONAL IDENT.	FAILURE MODE	FAILURE CAUSE	FAILURE EFFECT	TARGET	RISK ASSESSMENT			ACTION REQUIRED / REMARKS	RISK ASSESSMENT		
						SEV	PROB	Risk Code		SEV	PROB	Risk Code
Sys 1	Connection of the sections											
Sys 1.1	Connectors	Connectors cannot connect to each other	Connector production has not been done accurately enough and lines/pipes do not align	Connectors cannot be connected, meaning that the aircraft cannot be delivered to the client or cannot take-off	PTR	III	C	3	Perform proper quality control of all connectors produced to ensure their accuracy, add redundant connectors	III	D	3
Sys 1.1.1	Hydraulic connector	Clogged hydraulic line in connector	Sand particles, dirtiness come into contact with connector	Hydraulics not capable of applying pressure throughout connector	TR	III	C	3	Clear connector lines each time before connecting it	III	D	3
Sys 1.1.2	Electric connector	Short circuit in connector	Connector not placed accurately. Electric lines which are not supposed to come into contant with each other do constantly now	Short circuit/damage in the connector. Electricity is not transferred through the connector	TR	II	B	1	Proper education of the workers to make sure the allignment will be done accurately, redesign the connection	II	E	3
Sys 1.1.3	Water connector	Leakage in connector	Tearing of the water line connector	Short circuit/damage in the connector	TRV	III	C	3	Regularly check the water lines and inspect for any damage	III	D	3
Sys 1.1.4	Air conditioning	Corrosion of airseal in connector	Air conditioning pipe airseal is damaged	Fresh air for passengers is not transferred efficently through the connector	TRV	III	C	3	Regulary replace airseal rubbers in the connector	III	D	3
Sys 1.1.5	Control system connector	Control lines are not properly connected	Allignment of the connector is not done accurately	Control inputs from flight deck are not transferred through the connector	TR	II	B	1	Same as Sys 1.1.2	II	E	3
Sys 1.2	Airseal	Airseal corrosion	Rubber airseal has been dried out and does not seal fuselage properly	Breathable air escapes the cabin and slowly depressurizes the cabin	TRV	II	C	2	Install oxygen indicators and regularly inspect and replace the rubber airseals.	II	D	3
Sys 1.3	Fastening method	Fastening procedure failed	Allignment not done properly	Bolts do not slide through the latches, redo the alignment procedure	PTR	III	C	3				
Sys 1.3.1	Locking mechanism	Bolt failure	Overloading, fatigue of the bolt	Catastrophic failure of the aircraft	TRV	I	D	2	Regular inspection of the locking mechanism structure, adding reduncancy	I	E	3
Sys 1.3.2	Bolt sensor	Faulty sensor	Short circuit in the sensors	System displays that locking procedure is not succesfull although it might be succesfull	PTR	III	C	3	Add possibility to physically check if the locking bolt is in place	IV	C	3
Sys 1.4	Alignment system	Sensor failure	Faulty sensor, sensor blocked by sand/dirt	Alignment cannot be performed accurately	PET	III	C	3	Build in redundancy in the sensors	III	D	3

Sys 2	Aircraft structure	Corrosion	Due to the lack of oxygen, there are not enough oxides to form the protective layer. Difference in thermal expansion may cause internal stresses in the structure	Quick degradation of the structure, expensive maintenance needed	T R V	II	D	3				
Sys 2.1	Fuselage	Galvanic corrosion	Direct connection between the carbon fibre skin and the aluminium stringers will create a dielectric cell	Aluminium will corrode	T R V	II	B	1	A layer of carbon-fibre epoxy between the two materials will prevent contact	II	E	3
Sys 2.1.1	Frames / stringers	Failure due to fatigue, failure due to corrosion	Pressurisation cycles will cause the fatigue, residual water in the bottom of the aircraft will cause the corrosion	The frames and stringers will become less strong and might fail during normal operation, reduced residual strength	T R V	I	D	2	Add sufficient redundancy, design drainage to prevent water from accumulating in the belly of the aircraft	II	E	3
Sys 2.1.2	Skin	Failure due to cracks, delamination of the skin	Pressurisation cycles, ground handeling operations, foreign object damage, uncontrolled production/fabrication techniques	Catastrophic failure of the skin, explosive decompression of cabin	T R V	I	D	2	Regulary inspect for cracks, immediately inspect the plane for cracks after foreign object damage	I	E	3
Sys 2.2	Lifting surfaces	Failure due to corrosion	Corrosion caused by the residual fuel	Failure of the lifting surface, catastrophic failure of the aircraft	T R V	I	D	2	Design material such that is has a protective layer against corrosion	I	E	3
Sys 2.2.1	Ribs	Cracks propagate and tear out	Crack initiation at the holes	Ribs detach from the spars and skin, wing skin might buckle	T R V	I	D	2	Design ribs with safety factor, add extra material at the connection points	I	E	3
Sys 2.2.2	Skin	Cracks, buckling, delamination of the skin	Ground handeling operations, foreign object damage, load factor is too high, so the limit load is exceeded, improper fabrication/production methods	Rivets shear out, skin shear out, change in load distribution, skin detached from wing	T R V	I	D	2	Design the connections with extra redundancy and with a safety factor	I	E	3
Sys 2.2.3	Spars	Failure due to fatigue, failure due to corrosion	Loading cycles will cause the fatigue, residual fuel in the wing will cause the corrosion	Bending of the spar can go further than predicted, resulting in skin buckling, failure of the entire spar	T R V	I	D	2	Design the spar with a safety factor, add protective layer against corrosion	I	E	3
Sys 2.2.4	Stringers	Failure due to fatigue, failure due to corrosion	Loading cycles will cause the fatigue, residual fuel in the wing will cause the corrosion	Early skin buckling, more drag and less lift produced, which may result in an unstable aircraft	T R V	I	D	2	Design the stringer with a safety factor, add protective layer against corrosion	I	E	3
Sys 2.3	Joints	Failure due to fatigue, shear out of the joints, stress corrosion	Flight cycles, loading and unloading the aircraft, fuelling cause the fatigue, heavy impact during landing might cause the shear out, stress corrosion is caused by the combination of stresses during loading and the corrosion of the joints	Failure of the joints lead to a failure of the system which is joined together, which might cause the aircraft to fall apart mid-air	T R V	I	C	1	Design the joints with a safety factor, add redundant joints to the connection, early replacement of the joints during maintenance	I	E	3
Sys 3	Flight control system											
Sys 3.1	Flight computer	Unexpected behaviour	Coding error/bug in flight computer software	Potentially catastrophic failure (737MAX)	P T R V	I	D	2	Extensive verification, validation, certification of the flight computer	I	E	3

Figure D.1: FMEA of the concept

Sys 3.2	Cockpit controls	Jammed control column	Internal blocking of the control column	Not able to input any controls or constantly inputting wrong controls	TRV	II	D	3	Have control system of the pilot and copilot seperately connected and have option to disable one of them	II	E	3
Sys 3.3	Control surface operating system	Short circuit of the system, loss of power	Internal defect, improper wiring, leaking hydraulic connection	Not able to operate the control surfaces	TRV	I	D	2	Build in redundancy of control lines	I	E	3
Sys 4	Electrical system	Short circuit of the system	Failure of the subsystems, short circuit in the subsytems	No electricity in (part of) the aircraft, no hydraulic power, control screens in the cockpit switch off	TRV	I	D	2	Build in redundancy electric wires, have back-up power generator (APU and ram air turbine)	I	E	3
Sys 4.1	APU	Malfunctioning of the APU, shut down of the APU	Debris or other particles in the APU	No hydraulics, airconditioning, and electronic cockpit displays when on the ground, no electric taxiing	TRV	III	D	3	Use an outside energy source for cabin air conditioning and electricity			
Sys 4.2	Electrical wires	Failure of the electrical wires	Damage from the outside, short circuit of the electrical system, failure of the connections between the wires	No electricity in (part of) the aircraft, no hydraulic power, control screens in the cockpit switch off	TRV	I	D	2	Build in redundancy electric wires	I	E	3
Sys 4.3	Generators	Engine generator failure	Engine failure, failure of connection between engine and generator	No electricity from the engine(s), APU provides redundancy to important systems, non essential systems fall out due to power loss	TRV	III	D	3	Use the APU for backup power. Repair needed during turn around			
Sys 5	Hydraulics											
Sys 5.1	Pipes	Cracks in the pipes, rupture of the pipes	Overpressurisation, improper production, damage from the outside	Loss of hydraulic fluid, potentially damaging other systems, loss of hydraulic power, loss of control systems	TRV	I	C	1	Build in redundant hydraulic system	I	E	3
Sys 5.2	Pumps	Failure of the pumps	No power to the pumps, internal defect	No hydraulic power	TRV	I	D	2	Having multiple hydraulic systems to avoid single point failure	I	E	3
Sys 5.3	Reservoirs	Leakage of the reservoirs	Cracks in the reservoir, failure of the connection between the reservoir and the system	No hydraulic power	TRV	I	D	2	Have redundant reservoirs, have multiple hydraulic systems be dependent on different reservoirs	I	E	3
Sys 6	Fuel system											
Sys 6.1	Fuel tanks	Leaks in the tanks	Failure due to fatigue (pressurisation of the fueltanks), failure because of corrosion	Loss of fuel, potential fire hazard	TRV	I	D	2	Shut down unneeded electrical systems. Immidiate emergency landing, add safety factor to design	I	E	3
Sys 6.2	Fuel pipes	Leaks in the fuel pipes	Impact damage to the fuel pipes	Engines receive less fuel then needed, reduced power. Potential fire hazard.	TRV	I	D	2	Immidiate emergency landing, add safety factor in design	I	E	3
Sys 6.3	Fuel pumps	Blockage in fuel pump, overworking of the pump	Contaminated fuel, not switching off	Fuel pumps not able to deliver fuel to engines, no power from engines, fuel gets pumped to one side of the aircraft which might make it unstable	TRV	I	D	2	Fuel quality control at airport	I	E	3
Sys 7	Engines	Object collision	Bird stike or foreign objects come into contact with operating engine	Complete failure of the engine. Aborted take of or emergency landing	TRV	I	D	2	Regular runway inspection	I	E	3
Sys 8	Landing gear											
Sys 8.1	Brakes	Melting of the brakes, failure due to fatigue	No hydraulics, high temperature due to friction while braking	Aircraft having to brake with the thrust reversers only	TRV	III	D	3	Sufficient redundancy due to other braking mechanisms such as aerobrakes and thrust reversers			

Figure D.2: FMEA of the concept

Sys 8.2	Electric taxiing motor	Failure of the motor, internal short circuit	No electrical power, internal defect	Aircraft needs to taxi using its engines. Increased fuel consumption	T R V	III	C	3	Repair the system during the next turnaround procedure			
Sys 8.3	Retracting mechanism	Malfunctioning of the retracting mechanism	No hydraulics	Flying with high drag, higher fuel usage. Not able to fly at high speeds	T R V	II	E	3	Having a manual system to retract landing gear. Make emergency landing			
Sys 8.4	Steering mechanism	Nose gear control loss	No hydraulics, failure of the control mechanism	Inability to steer the plane at low speeds, grounding of the plane, delays in the flight schedule	T R V	III	E	3	At higher speeds on the ground, the plane can steer with its rudder			
Sys 8.5	Strut	Compression or lateral failure	High impact loads in downward direction or in lateral direction	Landing gear collapses, the fuselage might hit the ground during landing and get heavily damaged	T R V	I	D	2	System which warns for too high vertical/horizontal speeds. Apply safety factor in design	I	E	3
Sys 8.6	Wheels	Tire rupture	Debris on the runway, too much tire pressure, high impact during landing	Damage to the internal structure of the tire, damage to the strut, damage to the brakes	T R V	II	D	3	Regular runway inspection, adding safety factor during landing gear design	II	E	3
Sys 9	Communication system											
Sys 9.1	Communication to the ground	Radio connection lost	Failure of the radio system due to electrical malfunctioning	Unable to contact ground to ask landing clearance or flying directions and commands.	P T R V	I	D	2	Have backup radio working on APU	I	E	3
Sys 9.2	Intercom failure	Internal aircraft communication lost	Short circuit in one of the aircraft contact systems	Unable to contact flight attendants from the cockpit.	T R V	IV	D	3				
Sys 9.3	Public address system failure	Communication to passengers lost	Short circuit in the aircraft intercom system	Unable to inform passengers (during emergency)	T R V	III	D	3	Have backup manual speakers to communicate to passengers	III	E	3
Sys 10	Air conditioning system	Short circuit of the system, shut down of the system	Internal defect, failure of the power supply	No cooled cabin	T R V	II	D	3	Emergency landing to repair air conditioning system	III	D	3
Sys 11	Water system											
Sys 11.1	Water reservoir	Leaks in the reservoir	Failure due to pressurisation, cracks because of fatigue	Water in the bottom of the aircraft, damage to the cargo	T R V	III	D	3	Clean up emerged water, repair during next turn around			
Sys 11.2	Water pumps	Malfunctioning of the pumps	Internal defect, failure of the power supply	No water for the toilet	T R V	IV	D	3	Repair during next turn around			
Sys 11.3	Water pipes	Leaks in the pipes	Failure due to pressurisation, cracks because of fatigue	Water in the bottom of the aircraft, damage to the cargo, no water for the toilets	T R V	II	D	3	Repair during next turn around, isolate the water pipes such that water will not damage the cargo	III	D	3

P:Personnel / E:Equipment / T:Downtime / R:Product / V:Environment

Figure D.3: FMEA of the concept

E Functional Analysis

Figure E.1: Functional flow diagram

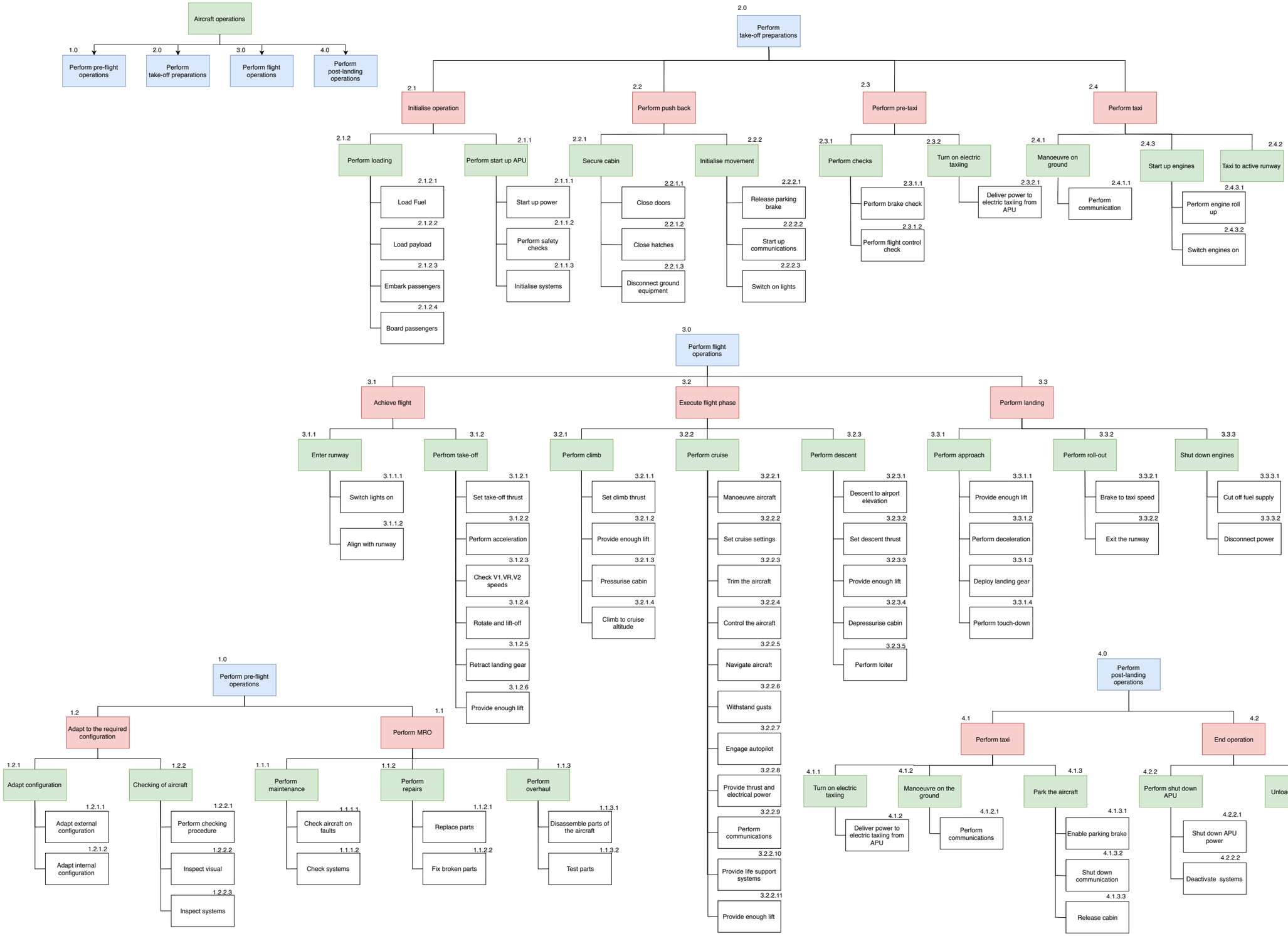

Figure E.2: Functional break-down structure

F Internal/External lay-out

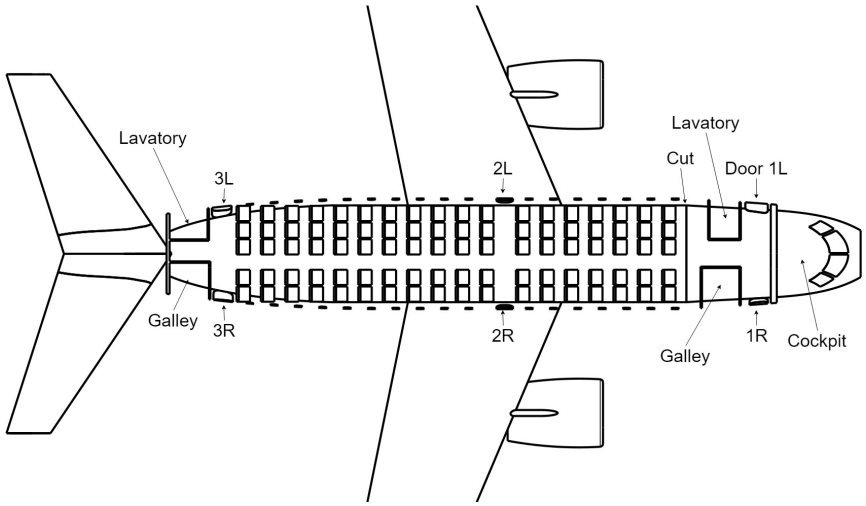

Figure F.1: Internal lay-out configuration 1

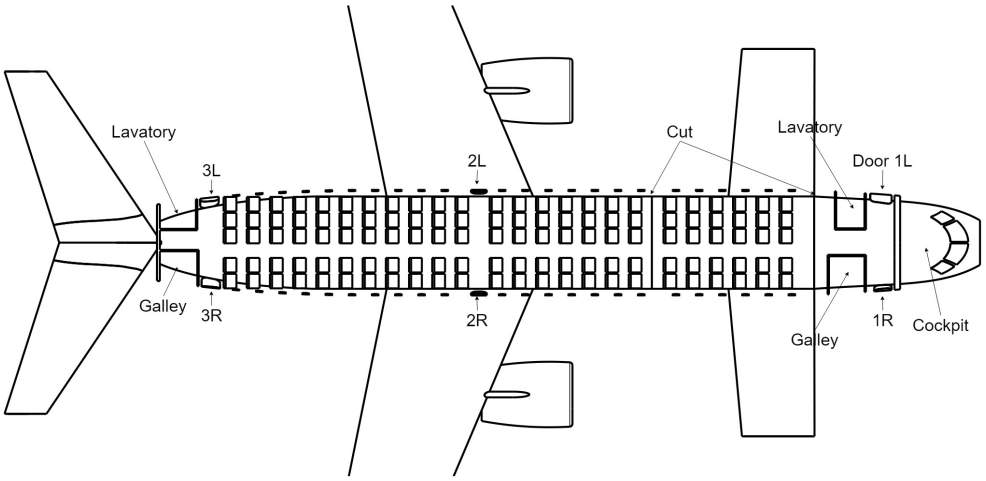

Figure F.2: Internal lay-out configuration 2 & 3

Isometric view
Scale: 1:350

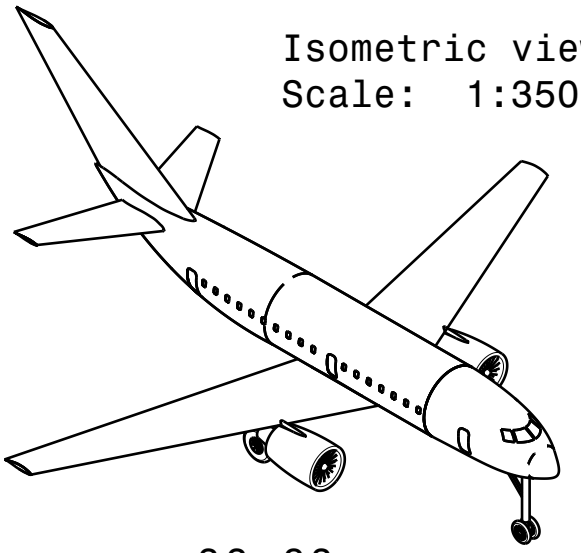

Isometric view
Scale: 1:350

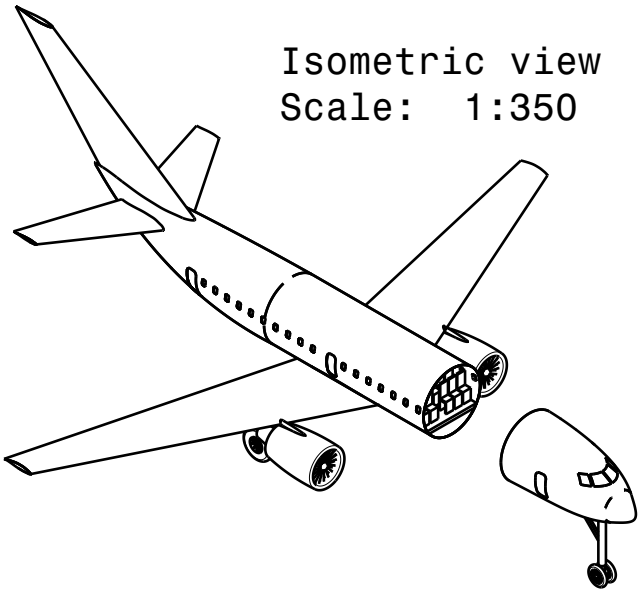

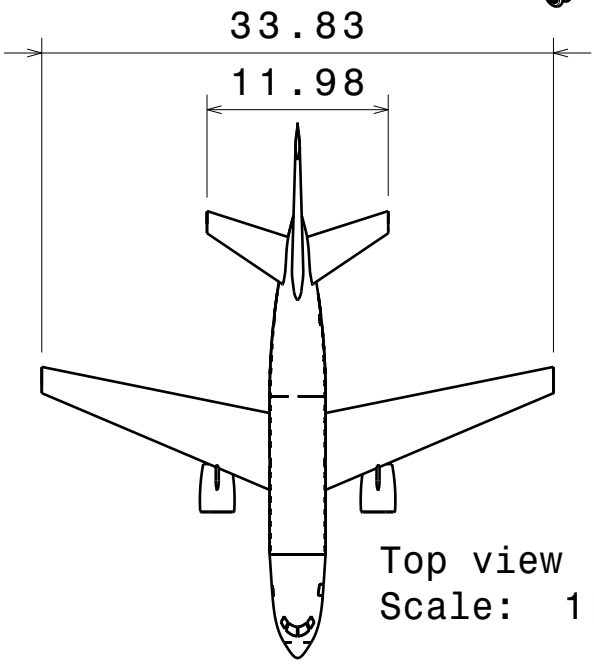

Top view
Scale: 1:500

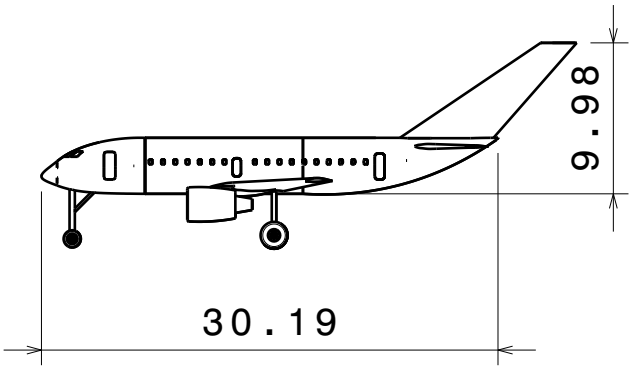

Right view
Scale: 1:500

Front view
Scale: 1:300

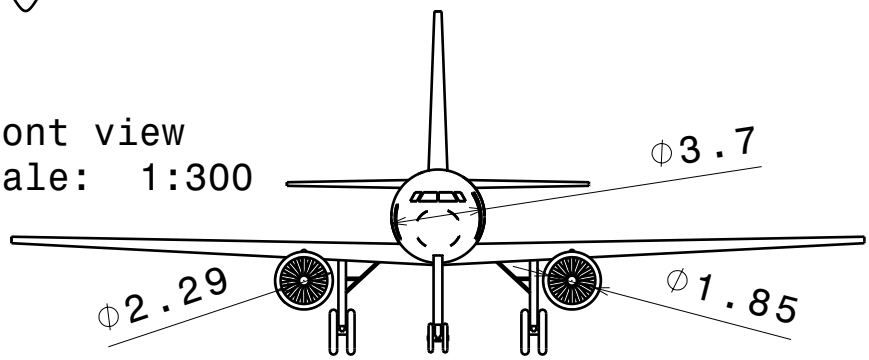

TU Delft

DRAWN BY: DSE Group 23	DATE: 18-6-2019	DRAWING TITLE: Configuration 1		
CHECKED BY: XXX	DATE: XXX	SIZE: A4	DRAWING NUMBER: AE3200-A1	REV: X
DESIGNED BY: XXX	DATE: XXX	SCALE 1:500	WEIGHT(kg) 34,632	SHEET 1/1

Isometric view
Scale: 1:350

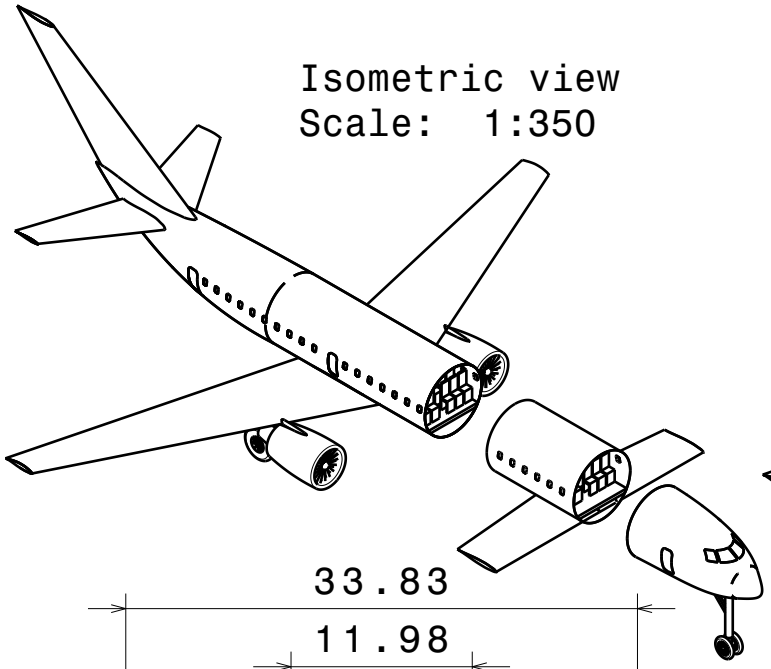

Isometric view
Scale: 1:350

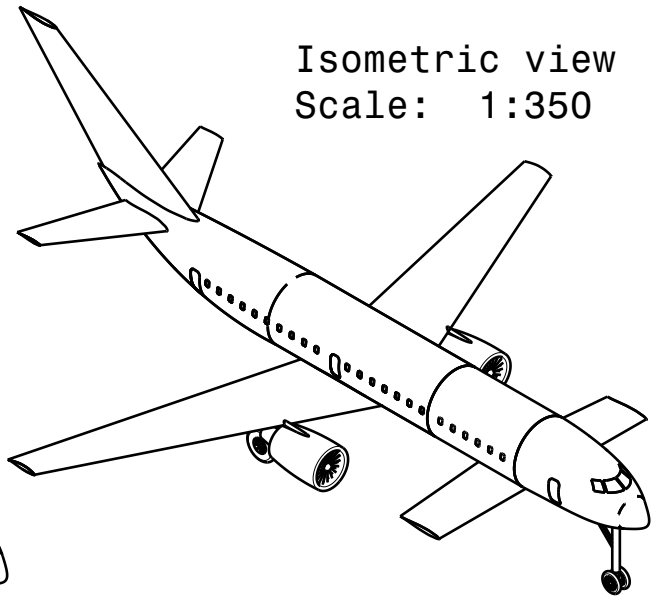

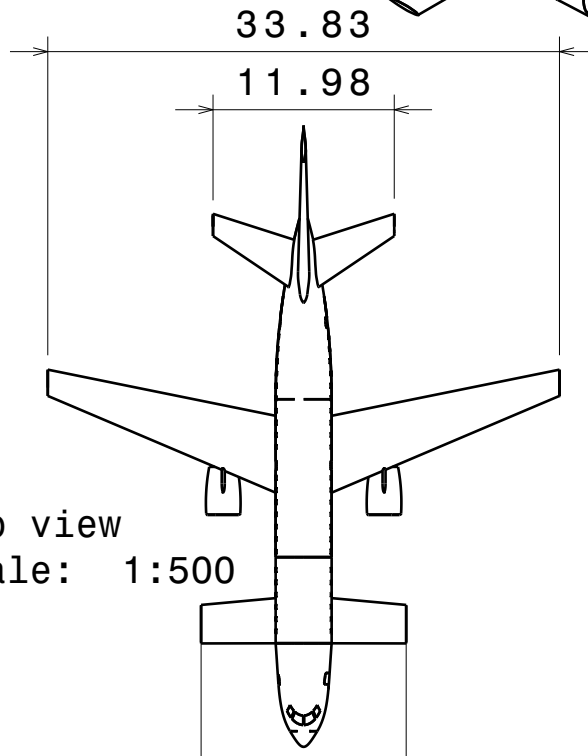

Top view
Scale: 1:500

Right view
Scale: 1:500

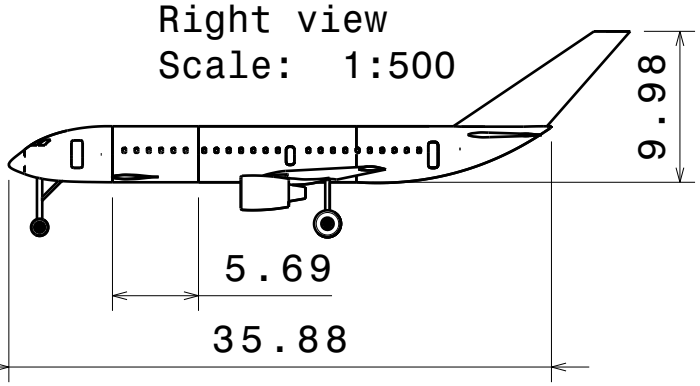

Front view
Scale: 1:300

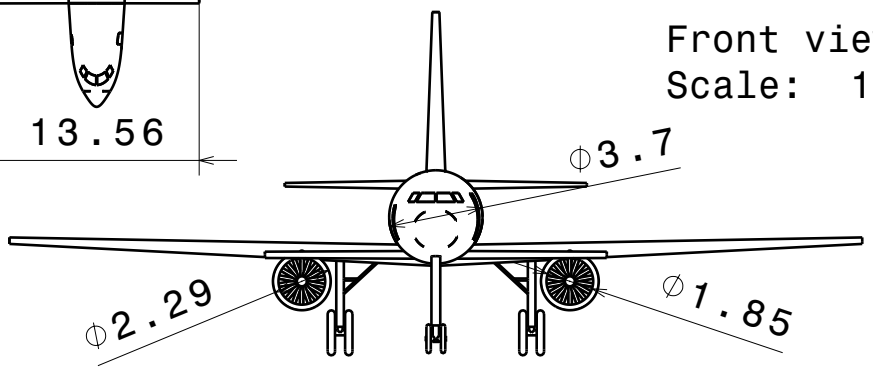

TU Delft

DRAWN BY: DSE Group 23	DATE: 18-6-2019	DRAWING TITLE: Configuration 2&3			
CHECKED BY: XXX	DATE: XXX	SIZE: A4	DRAWING NUMBER: AE3200-A2		REV: X
DESIGNED BY: XXX	DATE: XXX	SCALE 1:500	WEIGHT(kg) 38,730		SHEET 1/1